FORECASTING LONG-TERM SEDIMENT YIELD FROM THE UPPER NORTH FORK TOUTLE RIVER, MOUNT ST HELENS, USA

TIM MEADOWS, BSc., MSc.

Thesis submitted to the University of Nottingham
for the degree of Doctor of Philosophy

NOVEMBER 2014

ABSTRACT

The Toutle-Cowlitz River system experienced dramatic landscape disturbance during the catastrophic eruption of Mount St Helens on May 18, 1980. The eruption was triggered by a 2.5 km^3 debris avalanche which buried the upper 60 km^2 of the North Fork Toutle River catchment to an average depth of 45 m and obliterated the surface drainage network. Subsequent channel response on the debris avalanche, dominated by incision and widening, has delivered significant quantities of sediment to downstream reaches where resultant deposition has reduced channel capacity and heightened flood risk. Estimates of future sediment yield from the upper North Fork Toutle River are therefore required to inform development of sustainable options for long-term flood risk mitigation. Previous estimates have been based on extrapolation of post-eruption trends in sediment yield and channel network evolution, but the divergent predictions reported in a number of studies have clouded effective decision-making regarding long-term sediment management. This study therefore uses a numerical, landscape evolution model (CAESAR-Lisflood) to make long-term forecasts of sediment yield based on process simulation rather than extrapolation. A suite of forecasts of cumulative catchment sediment yields up to 2100 are produced using scenario-based model runs designed to account for uncertainty associated with the hydrological impacts of climate change and the model coefficient for lateral mobility. The forecasts fall in a narrow band +/-20% of the mean that lies between two previous estimates derived from the extrapolation of post-eruption trends. Importantly, predicted trends in future annual sediment yield are predominantly linear, although some limited decay is evident for runs in which modelled channel lateral mobility is lower. Sustained sediment production in the upper North Fork Toutle River is found to result from persistent bank erosion and channel widening. These findings cast doubt on the applicability of negative exponential decay functions based on the rate law to characterise post-disturbance sediment yield when lateral rather than vertical adjustments dominate channel evolution. Moreover, forecast trends in future sediment yield suggest that it may not be possible to manage future sediment-related flood risk along the lower Cowlitz solely by retaining sediment in the upper North Fork Toutle River catchment.

ACKNOWLEDGEMENTS

This research was supported by a three-year studentship from the School of Geography, University of Nottingham. Additional financial support for field work and equipment purchases was provided by the Flood Risk Management Research Consortium (www.floodrisk.org.uk), which is funded by the UK Engineering and Physical Sciences Research Council (EPSRC).

I would like to express my gratitude to Professor Colin Thorne for providing me with the opportunity to work on such an interesting and challenging project, for introducing me to so many fascinating and genuinely helpful people, and for bringing his wealth of knowledge and experience to this thesis. I would also like to extend my thanks to Dr Nick Mount who has provided invaluable technical advice and thought-provoking discussions across a broad range of issues, and has been enthusiastic, supportive and encouraging throughout. I am also very grateful to Dr Gary Priestnall for the many helpful suggestions and insights he has provided at each of our annual review meetings.

This research would not have been possible without the help of a substantial number of people from outside the University of Nottingham. I would particularly like to thank Professor Tom Coulthard (University of Hull) for his patient explanations of CAESAR-Lisflood, for his help in making modifications to the model, and for his enthusiasm and insights during our field work in 2011. I would also like to express my gratitude to Chris Nygaard and Paul Sclafani (US Army Corps of Engineers, Portland District) for sharing their knowledge of the Toutle-Cowlitz River system and for providing data sets that were vital to this research. Invaluable data sets, photographs, first-hand knowledge of the area and assistance with field work were also provided by Jon Major, Kurt Spicer and Adam Mosbrucker (US Geological Survey, Cascades Volcano Observatory), to whom I am extremely grateful.

I would also like to thank: John Milner (University of Nottingham) for providing computer resources and IT support; Ingrid Tohver (Climate Impacts Group, University of Washington) for explaining various aspects of the

Columbia Basin Climate Change Scenarios Project; Ken Stone (Cowlitz County, Washington) for sharing his practical experiences of flood risk management in the lower Cowlitz River; Peter Frenzen (Mount St Helens National Volcanic Monument) for his cooperation regarding access to Administratively Closed Areas at Mount St Helens; Hillsboro Aviation for their provision of helicopter support during field work; and Shan Zheng (Tsinghau University, Beijing) for her assistance in the field. I am also very grateful for the warm hospitality provided by Emily Forsyth and Janine Castro during trips to Washington State in 2011 and 2012.

Completing this thesis has also been made possible by the support I have received from my friends and family. In particular, I would like to thank my parents and my sister for their help and encouragement, and Darren, Heather and Sam for keeping me going through the more difficult times.

CONTENTS

LIST OF FIGURES

LIST OF TABLES

CHAPTER 1 INTRODUCTION

1.1 LONG-TERM RECOVERY OF FLUVIAL SYSTEMS DISTURBED BY LARGE-SCALE SEDIMENT LOADING

The disturbance of otherwise stable fluvial systems by heavy sediment loading is a common phenomenon, particularly in mountainous areas (Pitlick, 1993; Rathburn et al., 2013), and may result from both natural and anthropogenic processes (Gran and Montgomery, 2005). Disturbances such as landslides (e.g. Hicks et al., 2000; Glade, 2003; Koi et al., 2008), dam-break floods (e.g. Bathurst et al., 1990; Pitlick, 1993; Major et al., 2012), volcanic eruptions (e.g. Major et al., 2000; Gran and Montgomery, 2005; Pierson et al., 2011; Pierson and Major, 2014), hydraulic mining (e.g. Gilbert, 1917), and land use changes (e.g. Gaillard et al., 1991; Trimble, 2009) result in heavy sediment loading and typically have widespread impacts on the interrelated hydrologic and geomorphic (hydrogeomorphic) components of the affected catchments (Pierson and Major, 2014).

Elevated post-disturbance sediment yields are common following the variety of sediment loading events cited above, predominantly due to increased availability of source material and hydrological changes that result in higher peak floods, although explosive volcanic eruptions often have the greatest impact. Indeed, some of the highest specific sediment yields have been recorded in mountain rivers disturbed by volcanic eruptions, with transport rates that exceed the 99^{th} percentile of historic sediment yields reported in undisturbed catchments (Korup, 2012). However, the longer-term patterns of sediment yield are not well understood because most studies last only a few years post-eruption and rarely focus on the later stages of response in which sediment transport is dominated by fluvial processes rather than eruption-triggered mudflows (commonly known as lahars) (Gran and Montgomery, 2005; Swanson and Major, 2005; Gran et al., 2011). Moreover, in a recent review of hydrogeomorphic effects of explosive eruptions on drainage basins, Pierson and Major (2014, p. 498), found that “definitive documentation of full

geomorphic recovery of volcanically disturbed basins remains elusive, at least for recent eruptions".

Where long-term recovery trends from explosive eruptions have been monitored, the results often indicate that sediment yields can remain elevated for decades, centuries or even millennia (Pierson and Major, 2014). The hydrogeomorphic effects of the 1980 eruption of Mount St Helens, Washington State, USA, remain the most thoroughly studied record of long-term landscape impact following a voluminous explosive eruption (e.g. Pearson, 1984; Meyer and Dodge, 1987; Meyer and Martinson, 1989; Simon and Thorne, 1996; Simon, 1999; Major et al., 2000; Major, 2004; Major and Mark, 2006; Zheng et al., 2014), while the effects of the 1991 eruption of Mount Pinatubo, Philippines, on the surrounding river basins have also received considerable attention (e.g. Pierson et al., 1992; Hayes, 2002; Gran and Montgomery, 2005; Gran et al., 2011; Gran, 2012), albeit over a shorter timeframe.

At both Mount St Helens and Mount Pinatubo, similar post-event trajectories of sediment yield have been identified from empirical data in which the response consists of two distinct phases of erosion and sediment export (Major et al., 2000; Gran et al., 2011). The first phase is characterised by extraordinarily high sediment yields that decline exponentially over the first decade as hillslope tephra is rapidly eroded, the frequency of debris flows decreases, and the rate of channel network reintegration slows. The second phase is dominated by continued valley widening and fluvial instability that maintain significantly elevated sediment yields for at least several decades (Major et al., 2000; Gran et al., 2011). At Mount St Helens, annual sediment yields during the second phase have remained up to an order of magnitude greater than pre-disturbance values for more than 20 years, while yields are still elevated 2 to 10 times above estimated background levels at Mount Pinatubo (Pierson and Major, 2014).

Geologic studies of older eruptions also suggest that complete geomorphic recovery can take at least several decades and possibly millennia. For instance, Manville et al. (2009) found that fluvial conditions took between two and three

decades to stabilise to background levels following the 1.8 ka Taupo eruption, New Zealand. Similarly, channel incision on the Sandy River continued for more than half a century following sediment loading during the Old Maid eruptive period of Mount Hood, Oregon, USA, during the late 18th century (Pierson et al., 2011). Moreover, modern sediment input rates to the Sandy River are thought to remain higher than pre-eruption rates, and recent evidence suggests that the channel is still more unstable than similarly sized rivers in adjacent drainage basins (Pierson et al., 2011; Pierson and Major, 2014). The longest post-eruption recovery period, however, has been documented following the 26.5 ka Oruanui eruption, New Zealand, which is thought to be one of the largest known eruptions of the last 250,000 years (Wilson, 2001) and resulted in continued fluvial instability and elevated sediment yields for more than 10,000 years (Manville and Wilson, 2004).

Recovery periods of decades to centuries have also been documented in basins heavily loaded by sediment from a range of other disturbance events. For instance, Koi et al. (2008) found that a landslide generated by the 1923 Kanto earthquake, Japan, has affected sediment discharge for over 80 years, while Korup (2005) pointed out that the geomorphic effects of large coseismic landslides in South Westland, New Zealand, can persist for at least a century. Studies conducted on the Roaring River, Colorado, USA, in the aftermath of the 1982 Lawn Lake Dam failure also hint at prolonged recovery periods following extreme sediment loading events (Bathurst et al., 1990; Pitlick, 1993). Elevated sediment yields were found to persist for the first five years after the dam-break flood, with average bedload transport rates at least 100 times greater than pre-disturbance rates (Bathurst et al., 1990; Pitlick, 1993). Despite the short monitoring period, it was concluded that sediment yields of the affected channels were likely to remain high "for the foreseeable future" (Bathurst et al., 1990, p. 287).

Long recovery periods have also been observed following large-scale sediment loading of river basins by anthropogenic activities. For instance, one of the most influential early studies of channel morphological response to sedimentation was undertaken by Gilbert (1917) following the introduction of

approximately 1 km^3 of hydraulic mining debris into the Sacramento River, USA. Gilbert (1917) observed that low-flow bed elevation changes, which were assumed to be synchronised with bed material sediment yield, were symmetrical in time and he subsequently proposed a symmetrical wave model to describe the passage of sediment out of the Sacramento River basin. Although Gilbert's model implied that sediment yields would decline to pre-disturbance values relatively rapidly (within 50 years) following cessation of mining activities at the end of the 19^{th} century, later analyses prove that yields actually remained elevated for over a century (e.g. James, 1989; James, 1997; James, 1999; Cui and Parker, 2005). Results based on hindcasting in these more recent studies show that Gilbert's symmetrical sediment wave model was inappropriate in fluvial systems where sediment is stored in sites with the potential for long-term residence and protracted release through time, and that it cannot be assumed that sediment yields are linearly related to changes in bed elevations measured during periods of low-flow (James, 1997; James, 1999).

The examples cited above demonstrate that recovery of fluvial systems heavily loaded with sediment derived from natural and anthropogenic disturbances to the catchment or fluvial system takes place over periods extending from decades to millennia. However, it is also evident that recovery trajectories vary substantially (Korup, 2012) because they are influenced by a number of important factors. In the context of large, explosive volcanic eruptions, for instance, Manville and Wilson (2004) identified two broad categories of variables that influence post-disturbance response:

1. general controls, which include the volume, nature and distribution of the emplaced material; and
2. local controls, which include the regional climate, pre-eruption topography and basement geology of the impacted area.

The number and range of controlling variables means that predicting long-term response in disturbed fluvial systems with heavy sediment loadings and relating these responses to causal factors that could be mitigated against, is a major challenge – particularly following large, explosive volcanic eruptions

(Manville and Wilson, 2004; Manville et al., 2009). However, it is important that this challenge is addressed because the socio-economic consequences of post-disturbance responses are certainly longer-lasting, usually more widespread and potentially more damaging than the direct impacts of the disturbance itself (Pierson and Major, 2014).

Despite the importance of this task, fluvial geomorphologists and river managers have until recently lacked the tools with which to make predictions over the large spatial and long temporal scales that are necessary to understand the response of fluvial systems to large sediment loading events. Empirical approaches, which involve the extrapolation of observed post-disturbance trends, are hampered by their over-reliance on expert interpretation and data that are, usually, inadequate for the purpose, incomplete and highly variable. Similarly, it is unclear whether the conventionally applied theory of the rate law (which postulates that rates of adjustment decline exponentially with time after a disturbance from the point of maximum disturbance) is applicable in all cases (Gran et al., 2011). Moreover, traditional numerical models are equally unsuited to this task given that their computational complexity generally restricts their application to short time periods and/or small areas. The high computational demand of such models also prohibits their implementation in ensemble-based predictions, which are essential given the need to incorporate uncertainties associated with model parameterisation and future climatic changes.

Recent advances in numerical modelling techniques, however, offer new opportunities to develop quantitative, physically-based predictions of fluvial system recovery following disturbance that has generated an excessively large pulse in large sediment loading. Reduced complexity, landscape evolution models are explicitly designed to operate at low computational cost, thereby allowing multiple simulations to be conducted over long time periods and at the scale of whole river catchments. Although such models appear capable of filling a significant gap in the toolbox available for fluvial geomorphologists to use in seeking to understand, explain and predict the response of the fluvial

system to disturbance at the catchment scale, they have rarely been employed in this context.

The research presented in this thesis therefore investigates whether a reduced complexity, landscape evolution model can be used to develop quantitative, long-term forecasts of sediment yields generated in basins disturbed by major perturbations. This investigation is performed in the specific context of the upper North Fork Toutle River catchment, Washington State, USA, which was severely disturbed during and following the May 18, 1980 eruption of Mount St Helens. The upper North Fork Toutle River catchment was chosen because its post-disturbance recovery trajectory remains contested despite over three decades of intensive monitoring and research, and because elevated sediment yields continue to pose a significant flood-related hazard to downstream communities.

1.2 RESEARCH QUESTION AND OBJECTIVES

The key research question that this thesis aims to answer is:

To what extent can reduced complexity, landscape evolution modelling be used to support quantitative, long-term forecasting of sediment yields generated in the volcanically disturbed upper North Fork Toutle River catchment, Washington State, USA?

Answering this research question required that eight specific research objectives be achieved. These are to:

1. Explain the practical need to forecast future long-term sediment yield from the upper North Fork Toutle River catchment.
2. Establish the feasibility of modelling of geomorphological change at large space and timescales as an approach to predicting future sediment yields.
3. Identify the most appropriate model available for simulating geomorphological change at large space and timescales.

4. Assess data requirements for model set-up and parameterisation, and assemble the data sets for the study catchment necessary to apply the most appropriate model.
5. Evaluate model outputs by comparison with observed data during a data-rich period through model hindcasting, in order to:
    i. establish how well the model is able to replicate observed historical changes; and
    ii. calibrate model parameters.
6. Use the calibrated models to make ensemble predictions of long-term sediment yield in the upper North Fork Toutle River catchment, explicitly accounting for the main sources of model uncertainty and incorporating potential changes in climate during the forecast period.
7. Assess trends in future sediment yields forecast by the model, compare them with the results of predictions made in previous studies, and relate the forecast trends to changes in the climatic and geomorphic drivers of sediment production, so gaining insights into modelled processes responsible for long-term, post-disturbance relaxation in the fluvial system.
8. Evaluate the applicability of reduced complexity modelling and interpret the research findings in the context of future long-term sediment management in the upper North Fork Toutle River and the broader Toutle-Cowlitz River system.

1.3 THESIS STRUCTURE AND METHODOLOGICAL APPROACH

The structure of this thesis is designed to address each of the eight research objectives in turn, and is depicted schematically in Figure 1.1.

Chapter 2 outlines the context and rationale of the research presented in the Chapters that follow and is, therefore, concerned predominantly with objective 1. The 1980 eruption of Mount St Helens and the impact it had on the catchment and drainage network of the upper North Fork Toutle River are introduced in the first part of the Chapter. The Chapter then goes on to describe the post-disturbance evolution of the fluvial system and how elevated sediment

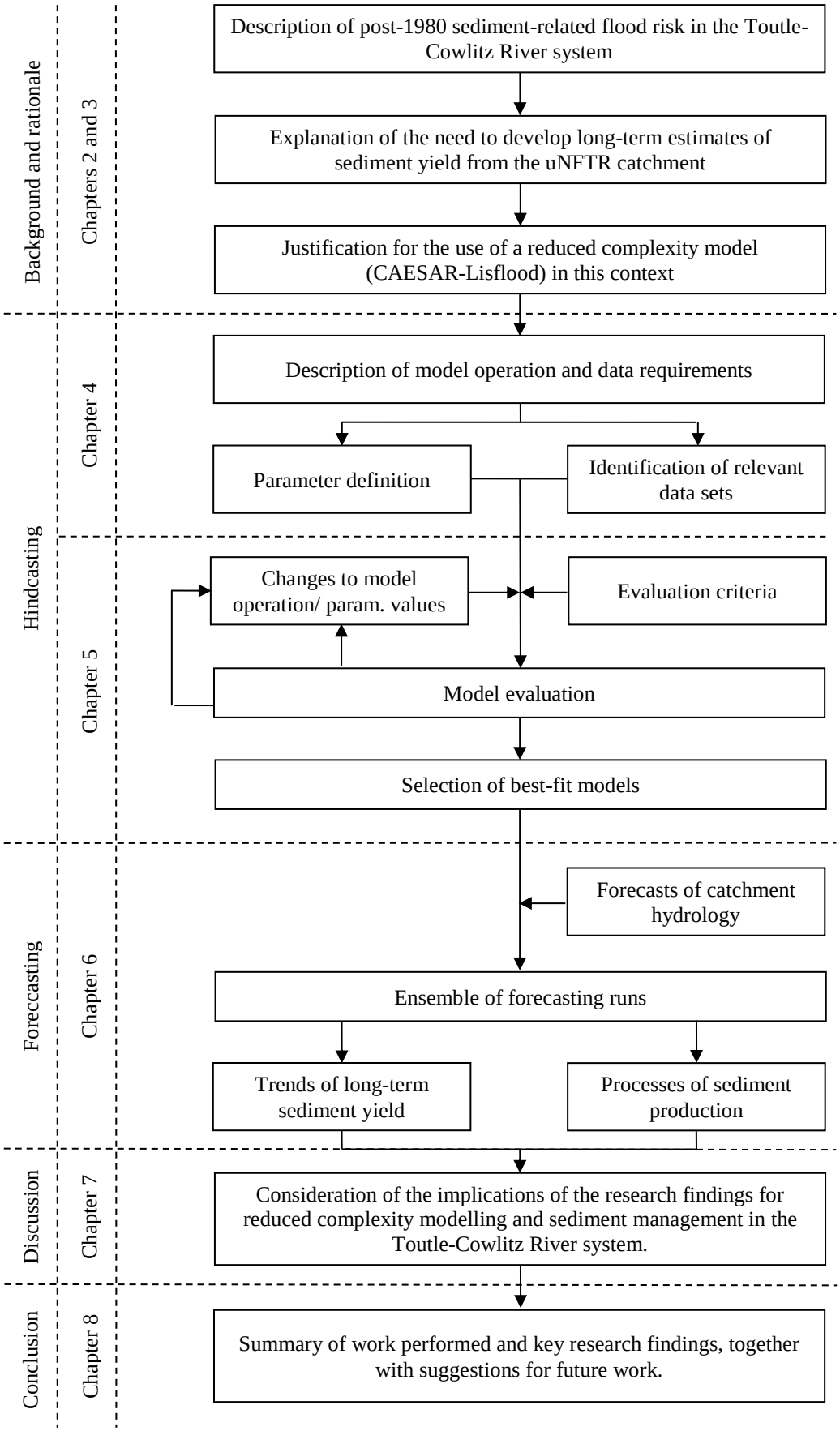

Figure 1.1 Thesis structure.

yields from the Toutle River catchment increased flood risk in communities along the Cowlitz River further downstream. This account establishes the need for long-term forecasts of geomorphological change in the catchment to inform decision-making regarding sustainable sediment management.

Chapter 3 addresses objectives 2 and 3 by considering the different modelling approaches that could be used to develop such forecasts and then selecting the most appropriate technique. The Chapter begins by summarising previous work that has been undertaken to establish long-term forecasts of sediment yield from the upper North Fork Toutle River based on extrapolation of post-eruption trends. The limitations and resulting uncertainties associated with this technique are then discussed, before alternative approaches based on numerical modelling are considered. Subsequently, a reduced complexity landscape evolution model, specifically CAESAR-Lisflood (C-L), is identified as the most appropriate tool.

Based on the modelling approach justified in Chapter 3, the remainder of the thesis is divided into two sections: model hindcasting (Chapters 4 and 5) and model forecasting (Chapter 6). Hindcasting is the process by which model performance is assessed in the context of recent historical observations, while forecasting refers to the development of long-term estimates of future sediment yield.

The process of hindcasting is recounted in Chapters 4 and 5. Chapter 4 addresses objective 4 by first establishing the basic configuration of the model. This includes summarising the operation of CAESAR-Lisflood, introducing and describing the initial specification of key model parameters, and identifying requisite input data sets. This Chapter explains how this process facilitated definition of the period over which hindcasting was conducted and also provides valuable insights into the applicability of CAESAR-Lisflood, not only in the context of the upper North Toutle River catchment but also more generally.

The second step in hindcasting, as specified in objective 5, was to compare model outputs with historical observations (evaluation) and refine model parameters based on this evaluation (calibration). These procedures are reported in Chapter 5, which starts by explaining the need to evaluate model performance, particularly when the aim of the study is to make predictions, and then highlights the lack of documented examples of evaluation in the context of data-rich case studies. Chapter 5 goes on to identify data sets that can be used for model evaluation in the study catchment and defines appropriate criteria for the assessment of model performance.

The research revealed both the strengths and weaknesses of the CAESAR-Lisflood model, and a number of modifications made to improve the model's representation of catchment hydrology are described. The final part of Chapter 5 explains how a sub-set of models was selected for use in forecasting. A novel procedure was developed to select (from a suite of 126 hindcasting runs) the two models most suited to forecasting. Selection was based on the need to identify models that produced the best fit to the observed data while accounting for uncertainty in a key model parameter representing lateral channel erosion. The new selection method combines four physically-based performance criteria and two statistical goodness-of-fit metrics.

Chapter 6 addresses objective 6 by reporting how the models selected in Chapter 5 were used to make long-term forecasts of sediment yield in the upper North Fork Toutle River catchment. The Chapter begins by identifying data sets capable of representing possible future hydrological regimes for the river in the study catchment as it responds to climatic change, before describing how these data sets were implemented within CAESAR-Lisflood. The remainder of the Chapter presents the results of 36 forecasting run, each beginning in 2009 (that is the end of the hindcasting period) and extending to the end of the 21st century. Model outputs (cumulative volumes, trends and sources of sediment yield) are compared with previous predictions and causal links are made to changes in the climatic and geomorphic drivers of sediment production. This assessment addresses objective 7 and provides insights into modelled processes responsible for long-term, post-disturbance relaxation in the fluvial system.

Chapter 7 is concerned with objective 8 and therefore discusses the implications of the results presented in the preceding Chapters for a number of important aspects. The Chapter begins by evaluating the realism of model outputs, before attempting to explain how this research could add to understanding regarding erosion processes in mountainous catchments that have been severely disturbed by large-scale sediment inundation. The implications of the results for sediment management in the Toutle-Cowlitz River system are then discussed, before some reflections are made on the applicability of reduced complexity landscape evolution modelling, and in particular CAESAR-Lisflood, for making quantitative predictions of long-term change in complex fluvial geomorphological settings.

Finally, Chapter 8 summarises the keys findings of this research and its principal contributions, as well as providing some recommendations for further work.

CHAPTER 2 THE TOUTLE-COWLITZ RIVER SYSTEM: LANDSCAPE DISTURBANCE, GEOMORPHIC RESPONSE AND FLOOD RISK

2.1 GEOGRAPHICAL SETTING

The Cowlitz River and its principal tributary, the Toutle River, are located in southwest Washington State (WA) in the Pacific Northwest of the USA. The rivers drain a combined area of 6,420 km^2 to the west of the volcanically-active Cascade Range, a north-south aligned orogenic-belt that extends from northern California to British Columbia. Both the Cowlitz and Toutle Rivers have their headwaters on the slopes of Cascade Range mountains: the Cowlitz drains both Mount Ranier and Mount Adams, while the Toutle predominantly drains the northern and western slopes of Mount St Helens. The Toutle River receives flow from three major tributaries, specifically the North and South Fork Toutle Rivers and the Green River, all of which flow from east to west and deliver water and sediment to the Cowlitz. Below its confluence with the Toutle, the lower Cowlitz River flows for approximately 32 km past the cities of Castle Rock (population 1,982), Kelso (population 11,925) and Longview (population 36,648), WA, before entering the Columbia River (Figure 2.1 and Figure 2.2) (population data from US Census Bureau and correct as of April 1, 2010).

2.2 THE 1980 ERUPTION OF MOUNT ST HELENS

The Toutle-Cowlitz River system experienced dramatic landscape disturbance during the eruption of Mount St Helens on May 18, 1980. Mount St Helens has been characterised by intermittent explosive behaviour throughout the course of its 300,000 year history, and nine periods of extended volcanism separated by apparent dormant intervals have been identified (Mullineaux and Crandell, 1981; Clynne et al., 2008). However, the pre-1980 volcano, which was as large as or larger than at any previous time in its development, was predominantly built during four eruptive periods within the last 2,500 years (Mullineaux and Crandell, 1981). The final period of volcanic activity and dome growth ended in 1857 and preceded 123 years of dormancy before renewed seismic activity

in the spring of 1980 signalled the beginning of a new and consequently destructive period of volcanism. The following Sections detail the events and processes of the May 18, 1980 eruption of Mount St Helens which removed the top 450 m of the formerly symmetrical cone and formed a 600 m deep north-facing amphitheatre-shaped crater (Simon, 1999) (Figure 2.3). The impacts that the eruption had on the Toutle-Cowlitz River system are also discussed, and are summarised in Table 2.1.

2.2.1 Pre-May 18 activity

The 1980 activity of Mount St Helens began on March 20 with an intensifying series of earthquakes that reached a climax on March 25, when 24 earthquakes of magnitude 4 or greater occurred during an eight-hour period (Christiansen and Peterson, 1981). The first steam-blast eruption, two days later, was associated with the formation of a summit crater and the emergence of a newly uplifted block, or bulge, on the north flank of the volcano (Christiansen and Peterson, 1981). The bulge, which grew northwards at a rate of between 1.5 and 2.5 m day^{-1} from late-April to mid-May (Lipman et al., 1981), was caused by the emplacement and expansion of a shallow magma intrusion, or cryptodome, beneath the summit and north flank of the mountain (Moore and Albee, 1981). It is thought that the deformation was localised on the north side of the mountain due to the occurrence of thinly bedded lava flows in the southern part which may have buttressed the south flank and made it structurally more stable (Hoblitt et al., 1981). The growth of the bulge over-steepened and subsequently destabilised the north flank of Mount St Helens, rendering it vulnerable to gravitational failures and landsliding (Lipman et al., 1981; Simon, 1999).

2.2.2 Rockslide-debris avalanche

At 08:32 Pacific Daylight Time on May 18, an earthquake of magnitude 5 or greater opened up a 1.5 km long fracture across the volcano's north slope, approximately along the apex of the cryptodome bulge. This new fracture

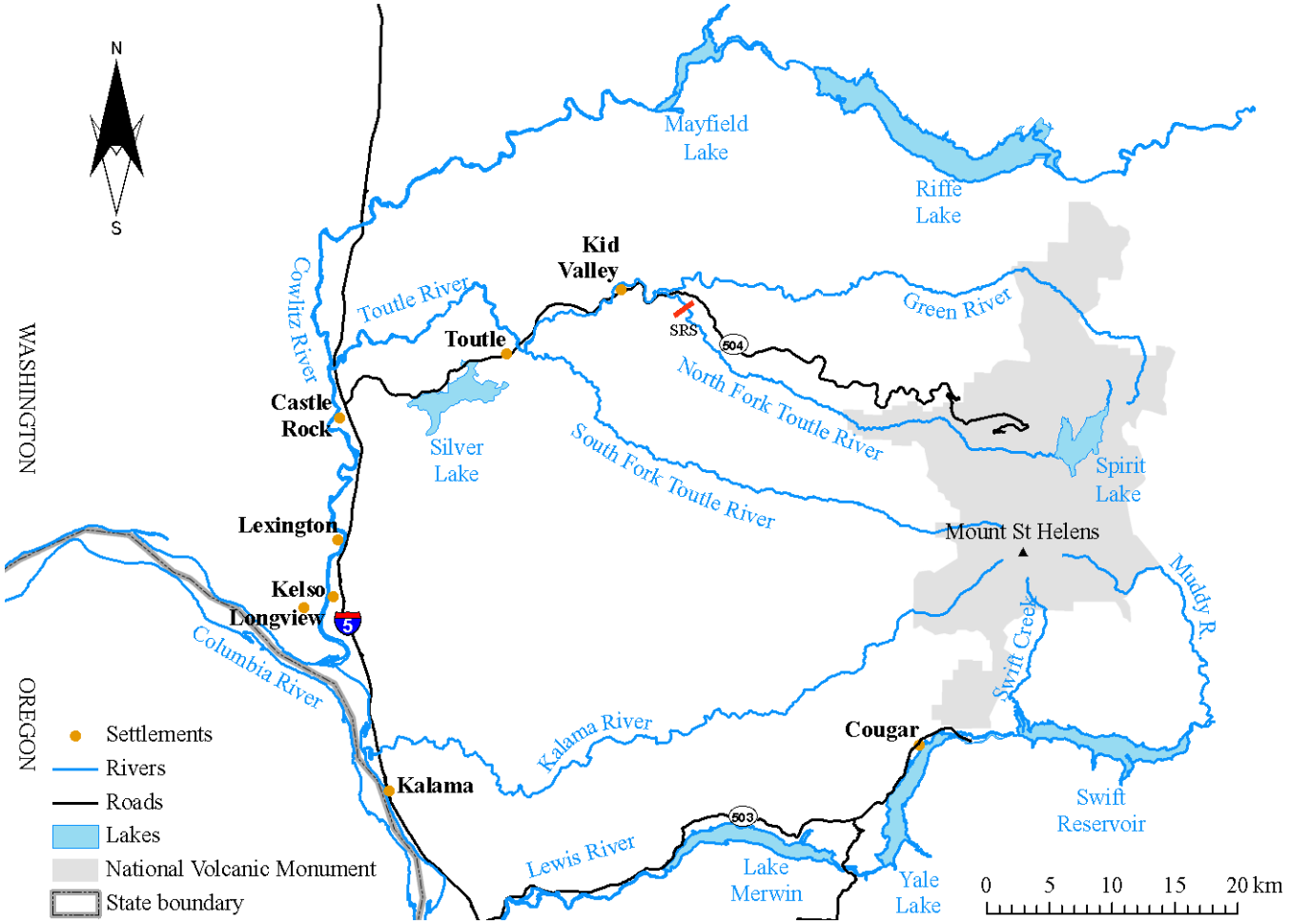

Figure 2.1 Map of Toutle-Cowlitz River system. Data from Washington State Geospatial Data Archive.

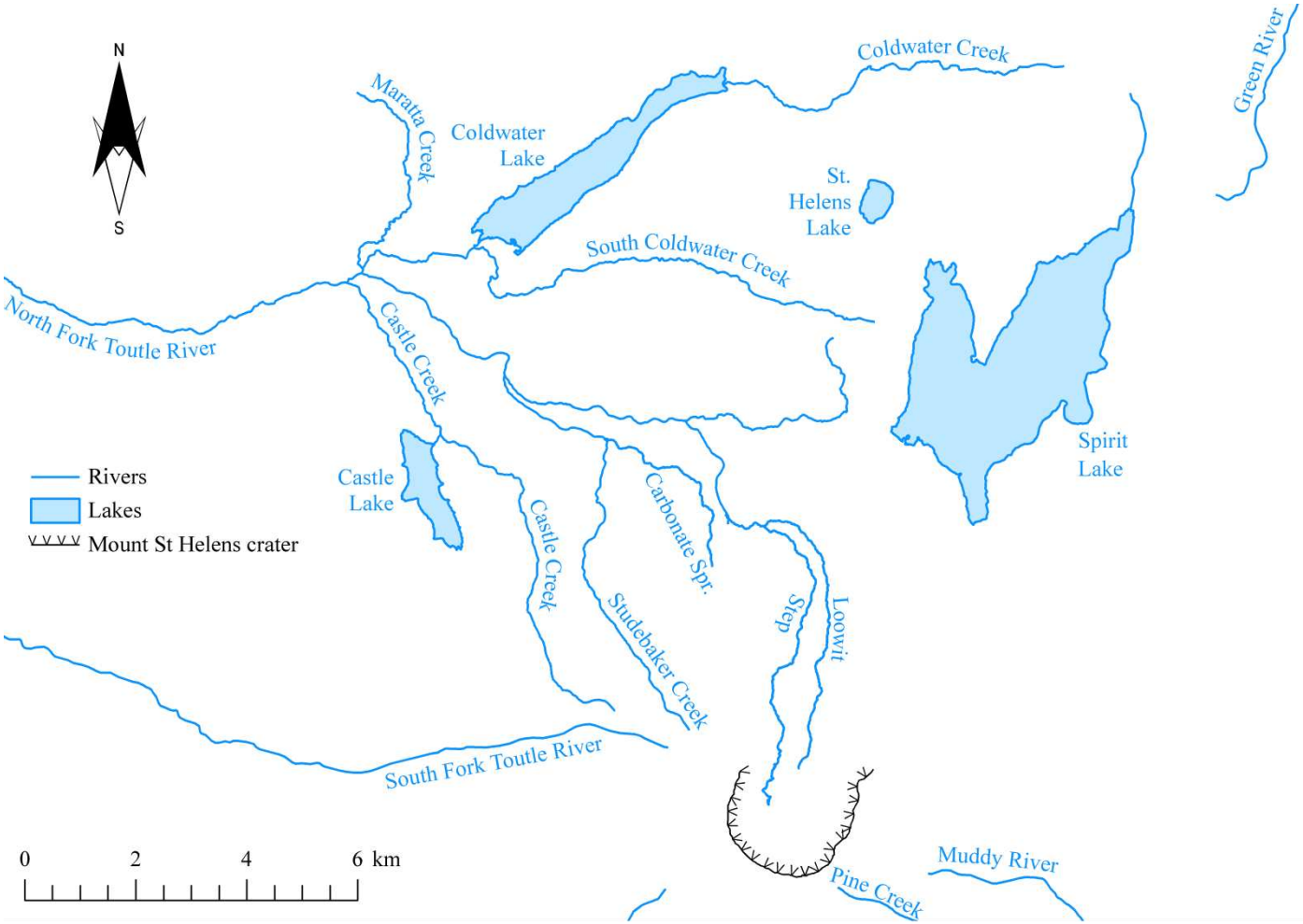

Figure 2.2 Map of the upper North Fork Toutle River catchment. Data from Washington State Geospatial Data Archive.

Figure 2.3 Pre- (top) and post-eruption images of Mount St Helens. Photographs by US Geological Survey, Cascades Volcano Observatory (USGS CVO) (1980).

Table 2.1 Characteristics and impacts of deposits associated with the May 18, 1980 eruption of Mount St Helens. Data taken from Lipman and Mullineaux (1981).

Deposit/process	**Volume of material (km^3)**	**Deposit thickness (m)**	**Affected area (km^2)**	**Affected basins**	**Major impacts**
Debris avalanche	2.5	10 – 195	64	Upper NF Toutle	Obliteration of drainage network Increased channel slopes
Directed blast	0.19	0.01 – 1	600	Upper NF Toutle SF Toutle Green	Removal and/or scorching of vegetation Removal of soil within 10km due north Reduction of infiltration capacity
Pyroclastic flows	0.12	0.25 – 40	15.5	Upper NF Toutle	Local burial of channels on the pumice plain
Lahars	0.05	> 5	50	Lower NF Toutle SF Toutle Toutle Lower Cowlitz	Reduction of channel carrying capacity Hydraulic smoothing of channels caused by the removal of riparian vegetation, channel straightening and the deposition of sand-sized material

NF = North Fork; SF = South Fork

system set the stage for the largest mass movement event in recorded history, as the entire north side of the mountain collapsed in a succession of multiple, retrogressive, slope failures, collectively termed a rockslide-debris avalanche (referred to hereafter as the debris avalanche). The debris avalanche deposited approximately 2.5 km^3 of material over an area of 64 km^2 to the north and northwest of the mountain in around 10 minutes (Voight et al., 1981; Glicken, 1996). The spatial distribution of this deposition was heavily influenced by local topography, which split the downslope flow of the debris avalanche into three main units (Voight et al., 1981). The majority of the material, approximately 2 km^3, was deposited into the upper 23 km of the North Fork Toutle River valley (Christiansen and Peterson, 1981; Voight et al., 1981).

The deposit consisted of unconsolidated, poorly sorted volcaniclastic debris (Figure 2.4) which buried the North Fork Toutle River valley to an average depth of 45 m and was locally as much as 200 m thick (Voight et al., 1981). The deposit was also characterised by irregular hummocks that had as much as 75 m of relief, as well as levees up to 30 m high which formed against valley walls (Glicken, 1996). A further 0.43 km^3 of material moved to the northeast and into Spirit Lake, causing a 260 m high seiche, or oscillating standing wave, to develop on the lake and raising the bed in its southern part by about 60 m (Voight et al., 1981; Glicken, 1996). The remaining 0.06 km^3 of material travelled predominantly north before crossing Johnston Ridge and being deposited into the valley of South Coldwater Creek (Glicken, 1996).

The debris avalanche obliterated the surface drainage network of the North Fork Toutle River valley and left a devastated landscape devoid of stream channels and with little or no through-going flow (Meyer and Martinson, 1989; Simon and Thorne, 1996; Major and Mark, 2006). Moreover, three major and nine minor tributaries with a combined drainage area of 225 km^2 were dammed by the deposit (Meyer and Martinson, 1989; Simon, 1999). Deposition of the debris avalanche also increased the potential energy of the North Fork Toutle River by raising surface elevations in the valley by an average of around 10% (Simon, 1992). Stream gradients were concurrently increased from the pre-eruption average of 0.027 m m^{-1} to 0.030 m m^{-1} (USACE, 1984).

2.2.3 Directed blast

The initial stages of the debris avalanche rapidly removed pre-existing rock material from the top and sides of the crypotodome and the associated hydrothermal system that it had developed since March 1980 (Moore and Sisson, 1981; Waitt, 1981). The resultant release of pressure enabled volatile gases to expand rapidly, to produce numerous explosions in the steep headwall that had been exposed by the landslide.

Explosions were also generated by the flashing of superheated ground water to steam, and the heating of steam, air and other gases by contact with hot rock fragments (Moore and Sisson, 1981). These explosions swiftly coalesced to form a single, huge explosion and a subsequent ground-hugging, northward-directed blast that moved off the volcano with an initial velocity of 250 m s^{-1} and temperatures in excess of 350º ± 50ºC (Moore and Albee, 1981; Moore and Sisson, 1981; Voight, 1981). The directed blast, which was a turbulent mixture of expanding gases and pyroclastic debris, followed local topography and was predominantly funnelled down the valleys of Smith Creek, the upper Green River and the North Fork Toutle River (Hoblitt et al., 1981; Waitt, 1981).

The devastated area extended in a broad arc from northwest to northeast of the volcano and included 600 km^2 of rugged and predominantly forested terrain (Moore and Sisson, 1981). Trees within 25 km of the crater were blown down by the blast (Figure 2.5), while those within 12 km were uprooted and carried away (Waitt, 1981). At the outer limit of the blast-affected area, beyond the blowdown zone was a ring 0.3 to 3 km wide in which every tree was scorched and many were killed, but all remained standing (Hoblitt et al., 1981; Simon, 1999). Temperatures within this scorch zone were estimated at between 50º and 250ºC (Winner and Casadevall, 1981).

Fine ash was lifted more than 6 km above the moving blast cloud by convective currents and later fell as tephra, including accretionary lapilli which formed as ash particles adhered to water droplets in the atmosphere (Moore and Sisson, 1981). The directed blast and its attendant airfall emplaced approximately 0.19 km^3 of unconsolidated material throughout the 600 km^2

Figure 2.4 Hummocky debris avalanche deposit filling the upper North Fork Toutle River valley and blocking Coldwater and South Coldwater Creeks. Photograph by USGS CVO (1984). View northeast (upstream).

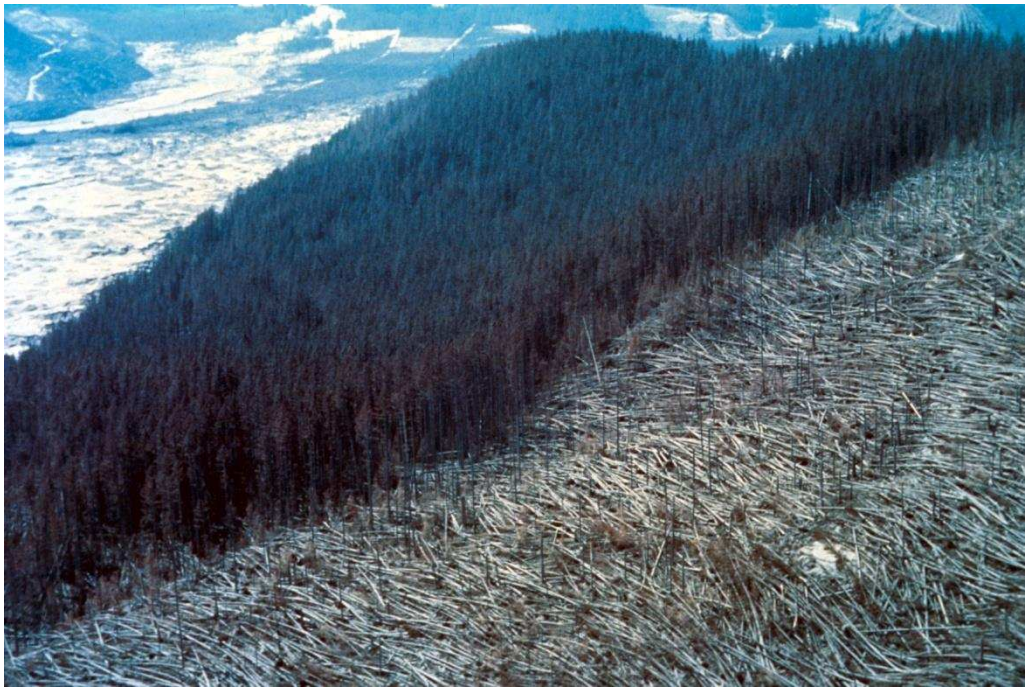

Figure 2.5 Tree blow down near the edge of the blast zone. Note scorch zone between downed and standing trees. Photograph by USGS CVO (1980).

devastated area (Moore and Sisson, 1981). This deposit was relatively thin and depth generally decreased from 1 m or less near the source to 0.01 m at the edge of the scorch zone (Hoblitt et al., 1981; Moore and Sisson, 1981). However, local variability was largely due to topographic effects and deposition was consistently thinner on slopes and ridge crests than it was in topographic hollows at any given distance from the volcano (Hoblitt et al., 1981; Waitt, 1981).

2.2.4 Plinian eruption and pyroclastic flows

The directed blast and continued collapse of the north flank caused further unloading of magma in the cryptodome and exposed the main volcanic conduit to a depth of more than 1 km (Moore and Albee, 1981). The resultant pressure reduction triggered a vertical (Plinian) eruption column that reached a height of 20 km within 10 minutes of the initial blast and continued for the next nine hours (Christiansen and Peterson, 1981; Waitt and Dzurisin, 1981). The ash plume was swept east-northeastward by a prevailing westerly wind and produced heavy ash fall over a large area to the east of the volcano that included Washington, northern Idaho and western Montana (Sarna-Wojcicki et al., 1981). Areas upwind of the mountain, including the majority of the Toutle-Cowlitz River system, received very little ash fall from the Plinian phase of the eruption (Waitt and Dzurisin, 1981).

Numerous pyroclastic flows (Figure 2.6) were generated from the eruption column as bulbous masses of ash, lapilli and blocks erupted to a height of no more than a few hundred metres before collapsing and plunging down the slopes of the volcano (Rowley et al., 1981). Most of the pyroclastic flows were directed north from the vent and produced a fan of pumiceous material, known as the ‘pumice plain’, on top of the debris avalanche and blast deposits that extended from the base of the volcano to as far north as Spirit Lake (Christiansen and Peterson, 1981; Rowley et al., 1981; Glicken, 1996). Although depths were generally less than several metres, the deposit thickened with distance from the vent as the flows banked against Johnston Ridge and pooled in the valley, and local accumulations of up to 40 m were observed in

the northern part of the pumice plain (Banks and Hoblitt, 1981; Rowley et al., 1981). The pyroclastic flow deposits emplaced on the northern flank of the mountain during the May 18 eruption were estimated to have a volume of around 0.12 km^3 (Rowley et al., 1981).

2.2.5 Lahars

Rapid water-saturated flows of volcanic debris, known as lahars (Crandell, 1971), developed on many streams draining the cone of Mount St Helens within minutes of the beginning of the eruption and continued throughout the afternoon of May 18. Relatively minor lahars were generated on the upper east and west slopes of the volcano in the headwaters of Pine, Smith and Swift Creeks and Muddy and Kalama Rivers as hot pyroclastic debris melted snow and glacial ice (Janda et al., 1981; Meyer and Martinson, 1989).

A more significant lahar originated in the South Fork Toutle River valley by swift snowmelt at the base of the hot and relatively dry pyroclastic flow described in sub-section 2.2.4 above (Waitt, 1989). The channel of the South Fork Toutle River was substantially modified by the passage of the lahar in a number of ways. In the upper reaches of the catchment deposition was generally less than 1.0 – 1.5 m, although up to 4 m of incision occurred into the May 18 and older lahar deposits during the recessional phase of the flow (Janda et al., 1981; Simon, 1999). Conversely, deposition was dominant in broad alluvial reaches farther downstream on the South Fork Toutle River, where fill was between 2 and 4 m thick (Janda et al., 1981; Simon, 1999). Although the passage of the South Fork lahar was recorded at Castle Rock on the lower Cowlitz River, this lahar was responsible for very little deposition below the confluence with the North Fork (Janda et al., 1981).

The most substantial lahar, however, was generated in the North Fork Toutle River valley (Figure 2.7) by local liquefaction and subsequent flowing of water-saturated parts of the debris avalanche which was emplaced during the early stages of the eruption (Janda et al., 1981; Meyer and Martinson, 1989). With an estimated volume of 0.14 km^3, the North Fork Toutle River lahar was

at least ten times larger than any other lahar that occurred at Mount St Helens on May 18 (Major et al., 2005). The lahar incised channels up to 30 m deep and 70 m wide on the lower part of the debris avalanche (Fairchild, 1985 cited in Simon, 1999, p. 18) before inundating 120 km of channel along the lower North Fork Toutle, Toutle and Cowlitz Rivers (Janda et al., 1981) as shown in Figure 2.7. The passage of the lahar raised the elevation of the water surface on the Cowlitz River at Castle Rock by 5.8 m, to overtop flood walls in this and numerous other locations along the Toutle and Cowlitz Rivers (Lombard et al., 1981).

The depth of lahar deposits varied locally, although up to 5 m of fill occurred in wide alluvial reaches along all affected channels (Janda et al., 1981; Simon, 1999). In total, the North and South Fork Toutle River lahars deposited 0.025 km^3 of sediment along the forks and mainstem of the Toutle River (Fairchild and Wigmosta, 1983 cited in Simon, 1999, p. 11), while 0.023 km^3 of deposition in the channel and on the floodplain of the Cowlitz River reduced the carrying capacity of the channel by 90% and increased the potential for severe flooding during subsequent high flows (Lombard et al., 1981; Meier et al., 1981). For example, following passage of the lahar, the stage elevation of a flow of 2,150 $m^3 s^{-1}$ (the pre-eruption bankfull discharge), was increased by 2.7 m at Castle Rock (Lombard et al., 1981).

2.3 POST-ERUPTION CHANNEL EVOLUTION AND SEDIMENT PRODUCTION IN THE TOUTLE-COWLITZ RIVER SYSTEM

The volcanic processes and deposits associated with the May 18, 1980 eruption of Mount St Helens significantly altered the hydrology, geomorphology and ecology of the Toutle-Cowlitz River system. Major modifications included: alterations to surface drainage characteristics; increased availability of easily erodible sediment in channels and on hillslopes; increased channel gradients; and the removal of vegetation (Lehre et al., 1983; Simon, 1999).

Figure 2.7 (above) Toutle River inundated by the passage of the North Fork Toutle River lahar. Photograph by Lyn Topinka (1980).

Figure 2.6 (left) Pyroclastic flow descending the north flank of Mount St Helens on August 7, 1980. Photograph by Peter Lipman (1980).

Stream channels were consequently destabilised and rapid processes of channel adjustment, development and recovery resulted in erosion and deposition throughout the catchment on a scale rarely witnessed (Lehre et al., 1983; Meyer and Dodge, 1987; Meyer and Martinson, 1989). Sediment production was significantly elevated above pre-eruption levels in all the basins impacted by the eruption, although the magnitude and persistence of heightened sediment yields varied according to the type and severity of volcanic disturbance (Simon, 1999; Major et al., 2000). The primary impacts of the eruption and subsequent processes of geomorphological response in each of the main sub-catchments of the Toutle River are summarised in Table 2.2.

Table 2.2 Primary impacts of the 1980 eruption of Mount St Helens on the main basins in the Toutle-Cowlitz River system and the processes of geomorphological response (Lehre et al., 1983; Meyer and Martinson, 1989; Simon, 1999; Major et al., 2000).

	Upper North Fork Toutle River	Green River	South Fork, Lower North Fork and mainstem Toutle Rivers
Primary eruption impact/s	Debris avalanche deposition	Lateral blast and associated airfall deposits	Lahars
Processes of geomorphological response	Filling and spilling of lakes followed by channel network development dominated by lateral erosion	Hillslope erosion by sheet wash, rilling and gullying	Incision followed by lateral erosion of lahar and older deposits
Relative magnitude of sediment yield and explanation	High Large volumes of poorly sorted and unconsolidated material deposited. Increases in mean channel gradient and stream energy	Low Least amount of modification and sediment yields subdued by trees felled within stream channels	Intermediate Smaller volume of sediment deposited, lower proportion of sand-sized material and smaller increases in stream energy than upper NFTR

Table 2.3 and Figure 2.8 summarise the values and trends of annual specific sediment yields from the four major basins impacted by the eruption and its associated deposits. It is evident that the dominant source of sediment in the Toutle-Cowlitz River system has been erosion of the debris avalanche in the

upper North Fork Toutle River valley, which resulted in average annual sediment yields of 11.64 x 10^3 Mg km^{-2} between 1982 and 1994 which delivered up to 3 x 10^7 m^3 of material annually between 1980 and 1986 (Lehre et al., 1983; Meyer and Martinson, 1989). Conversely, the channels of the blast-affected Green River basin have transported the least sediment since the eruption, contributing less than 1% of the suspended-sediment load recorded in the Toutle River between 1982 and 1994 (Major et al., 2000; Major, 2004). Sediment yields from the South Fork Toutle River, which was affected predominantly by lahar deposition, were intermediate between that of the upper North Fork and Green Rivers, contributing approximately 10% of the total suspended sediment load of the Toutle River between 1982 and 1999 (Simon, 1999; Major et al., 2000).

2.3.1 The upper North Fork Toutle River

Channel response in the upper North Fork Toutle River valley was dominated by the initiation, evolution and reintegration of a through-flowing drainage network on the surface of the debris avalanche (Lehre et al., 1983). This process began with filling and spilling of small, isolated water bodies that formed on or adjacent to the debris avalanche deposit (Simon and Thorne, 1996). Formation of these water bodies was facilitated by the topographically irregular nature of the deposit that resulted from subsidence and differential compaction, together with the prevalence of phreatic explosion pits caused by the expulsion of superheated pockets of groundwater (Simon, 1999). Lakes also formed along the margins of the deposit where tributary channels had been blocked and runoff impounded (Simon and Thorne, 1996).

The water bodies filled, breached and spilled down valley (Meyer and Martinson, 1989) resulting in rapid channel incision which cut steep-walled, trapezoidal channels and gullies up to 50 m deep and 120 m wide (Lehre et al., 1983). Lateral erosion through the failure of saturated banks and streamside hummocks dominated the latter stages of the evolution of these newly cut channels, with mean annual rates of channel widening as high as 200 m yr^{-1} (Meyer and Martinson, 1989; Simon, 1992; Simon and Thorne, 1996).

Table 2.3 Average annual specific suspended sediment yields between 1980 and 2000 from basins affected by the 1980 eruption of Mount St Helens. Data from Major et al. (2000).

Average annual specific suspended sediment yields (Mg km^{-2} x 10^3)			
North Fork Toutle River	South Fork Toutle River	Toutle River mainstem	Green River
11.64	2.68	7.29	0.33

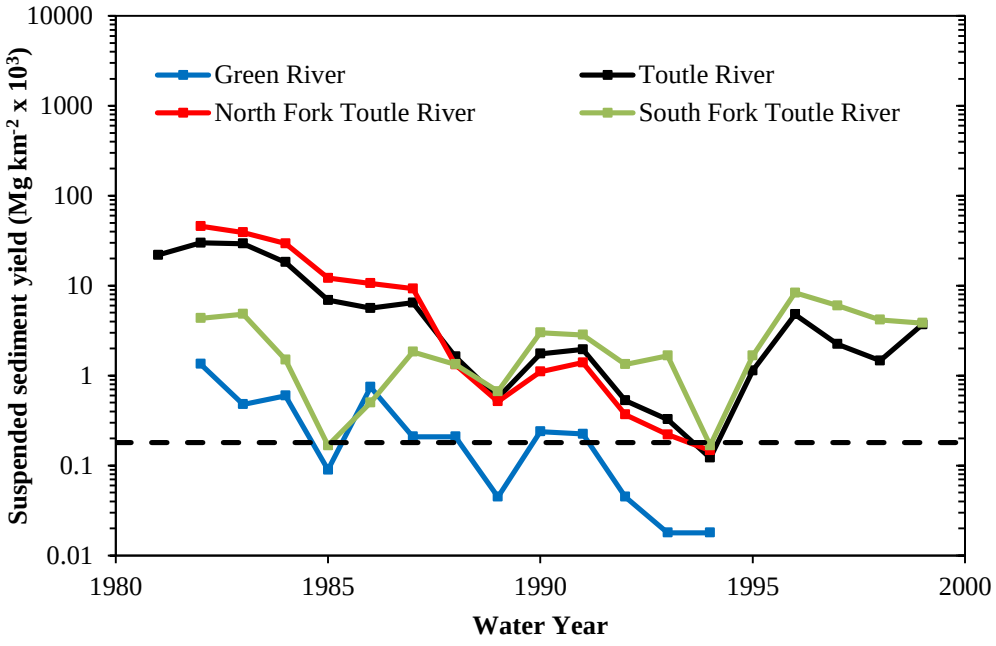

Figure 2.8 Annual post-eruption specific suspended sediment yields at gauging stations within the Toutle-Cowlitz River system. Dashed line represents the mean value of average annual sediment yields for selected Western Cascade Range rivers. Adapted from Major et al. (2000, p. 821).

The process of erosion by natural lake-breakout was supplemented by controlled releases of clear water from the engineered outlets of Castle, Coldwater and Spirit Lakes (Simon, 1999) (see Figure 2.2 for locations of lakes).

Channel adjustment on the debris avalanche followed a four-step sequence (Meyer and Martinson, 1989):

1. channel formation by the filling and spilling of water bodies;
2. channel incision;
3. channel widening and aggradation; and,
4. channel widening with bed scour and fill but little net change in channel elevation.

Reintegration of the drainage network through natural and artificial lake breaches within the upper North Fork Toutle River valley restored the contributing drainage area above the toe of the avalanche deposit from 80 km^2 on May 18, 1980 to its pre-eruption value of 282 km^2 by November 3, 1982 (Meyer and Dodge, 1987; Simon and Thorne, 1996). During this early period of drainage system evolution, specific yields of suspended sediment in the North Fork Toutle River at the Kid Valley gauging station were initially as much as 500 times greater than levels typical for western Cascade Range streams, peaking in 1982 at 46,000 Mg km^{-2} (Meyer and Martinson, 1989; Major et al., 2000).

Sediment supply from the debris avalanche naturally declined in the decades following the eruption as widening channels and coarsening bed material acted to reduce excess stream power and therefore sediment transport capacity (Simon and Thorne, 1996). However, this decline was not an indication of sediment source depletion but rather of sediment sequestration (Dinehart, 1998). Indeed, in 2000, Major et al. estimated that only 12% of the debris avalanche deposit had been eroded between 1980 and 1999 indicating that a vast quantity of material at that time remained stored in the upper North Fork Toutle River valley.

Since 2000, channel adjustments on the debris avalanche have persisted, especially in the steeper upstream reaches, and sediment yields from these reaches have remained elevated (Pierson and Major, 2014). Continued bank retreat and valley widening, particularly during high flows, will therefore continue to provide abundant sediment to the channels and sustain the high rates of sediment discharge that have been recorded since the eruption (Simon, 1999; Major et al., 2000; Major, 2004). In this context, it is important to note that the rapid decline in suspended sediment yield after 1987 evident in Figure 2.8 results from construction of the Sediment Retention Structure (SRS) on the North Fork Toutle River, which is discussed further in Section 2.5.2 and shown in Figure 2.1.

In summary, the upper North Fork Toutle River has been transformed from a predominantly alluvial, gravel-bed, pool-riffle channel with a sinuous planform bounded by a densely vegetated riparian corridor prior to the eruption, to a fully alluvial, mixed sand and gravel-bed stream with a wandering/braided planform flowing through and continuously reworking a wide braid plain that lacks riparian vegetation (Major et al., 2009). Contemporary photographs of the upper North Fork Toutle River catchment are shown in Figure 2.9.

2.3.2 The Green River

Sediment production from the Green River basin, which was affected solely by the lateral blast (Major et al., 2000), initially occurred through rapid sheet, rill and gully erosion from hillslopes covered with deposits associated with the directed blast (Lehre et al., 1983; Collins and Dunne, 1986). Erosion through modifications to channel morphology was limited in this catchment (Meyer and Martinson, 1989; Simon, 1999). The dominance of hillslope processes was enhanced by the removal of vegetation and the impervious nature of the blast deposits, which together markedly increased surface runoff in the years immediately following the eruption (Major and Mark, 2006).

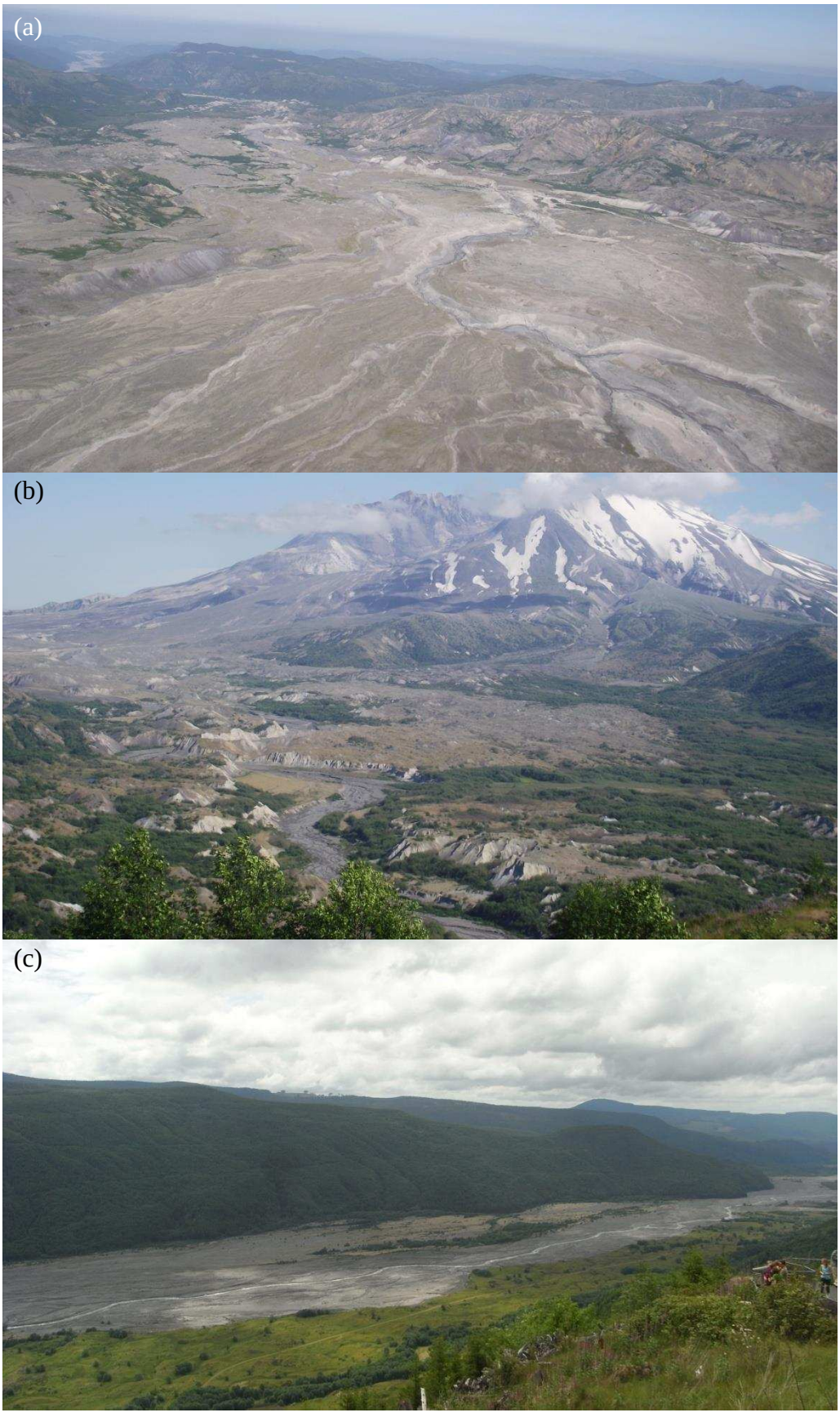

Figure 2.9 Photographs of the upper North Fork Toutle River catchment showing: (a) headwaters (view upstream); (b) upper reaches; (c) lower reaches (view downstream). Photographs (a) and (b) by author (2011); photograph (c) by Tom Roworth (2012).

However, hillslope erosion generally declined as a stable rill network developed and more permeable and less erodible substrates were exposed or created (Collins and Dunne, 1986). The occurrence of woody debris felled into or adjacent to stream channels further subdued sediment yields from the Green River by increasing hydraulic roughness, decreasing flow velocities, restricting bank erosion and providing sediment storage sites (Meyer and Martinson, 1989; Simon, 1999). The Green River transported the least amount of sediment carried by the four streams impacted by the May 1980 eruption of Mount St Helens and the annual specific suspended sediment yield peaked at 1,300 Mg km^{-2} in 1982, before declining monotonically and returning to background levels within 5 years (Major et al., 2000).

2.3.3 The lower North Fork Toutle, South Fork Toutle and Toutle Rivers

In contrast to basins that were predominantly blast-affected, channel adjustments in lahar-affected basins were pronounced and resultant sediment yields were, therefore, significantly greater. Extensive widening (on the order of tens of metres) was evident, principally through high-flow bank erosion along the channels of the South Fork and lower North Fork Toutle Rivers (below the toe of the debris avalanche deposit) and on the mainstem of the Toutle River in the first year following the eruption (Lehre et al., 1983; Meyer and Martinson, 1989; Simon, 1999). These adjustments released sediment not only from May 18 lahar deposits, but also from older channel banks and terraces that had been stable prior to the eruption (Janda et al., 1981; Meyer and Martinson, 1989).

However, sediment production from bank erosion and channel widening in lahar-affected channels was significantly lower than that resulting from reintegration of the drainage network on the debris avalanche surface. For example, the South Fork Toutle River, which was predominantly impacted by the passage of a lahar, contributed only approximately 2,676 Mg km^{-2} yr^{-1} between 1982 and 1999 (compared with 46,000 Mg km^{-2} yr^{-1} from channels of the debris avalanche). This difference has been attributed to three main factors (Simon, 1999):

1. much less sediment was available from lahar deposits than from the debris avalanche;
2. lahar deposits contained a lower proportion of fine-grained material; and,
3. increases in excess stream power were smaller in these streams.

In fact, the lahar-affected reaches of the lower North Fork Toutle River and Toutle River mainstem widened primarily in response to bar building and bed accretion by flows over-ladened with sediment derived from extensive erosion of the debris avalanche upstream (Meyer and Martinson, 1989).

2.4 CLIMATE AND LAND USE OF THE TOUTLE-COWLITZ RIVER SYSTEM

2.4.1 Climate

The Toutle-Cowlitz River system has a typical mid-latitude, west coast marine climate (WEST, 2002) which is characterised by cool, wet winters and warm, dry summers (Major and Mark, 2006). Precipitation is predominantly marine in origin due to prevailing westerly air currents and the close proximity of the Pacific Ocean (approximately 145 km west) (Uhrich, 1990). Around 75% of annual precipitation occurs during a six-month period that begins in October and reaches a monthly maximum in December (Collins and Dunne, 1986), and 40% occurs between November and January (Uhrich, 1990). Over longer timescales, interdecadal precipitation variations are related to climate shifts associated with interdecadal variations in sea surface temperature referred to as the Pacific Decadal Oscillation (PDO) (Mantua et al., 1997; Major, 2004). This climate pattern results in periods of greater-than-average and lower-than-average values of a range of variables in the North Pacific basin including land surface temperatures, precipitation and streamflow (Mantua et al., 1997).

Elevations within the catchment vary from 3 m at the confluence of the Cowlitz and Columbia Rivers to 2,550 m at the summit of Mount St Helens. Annual precipitation follows a strong west-northwest to east-southeast

orographic gradient (Collins and Dunne, 1986) and total annual precipitation ranges from 1,140 mm near the Columbia River to 3,200 mm on the upper slopes of Mount St Helens (Meyer and Martinson, 1989; Simon, 1999). Below ~600 m elevation, precipitation generally falls as rain, although elevations between 200 m and 1,000 m are within the transient snow zone. A seasonal snowpack accumulates over 1,000 m, and snowpack of more than 3 m is common and can persist into July above 1,200 m (Major and Mark, 2006). Snowpack accumulations in areas affected by the eruption of Mount St Helens may be less than pre-1980 averages due to increased wind speeds and higher ground temperatures that have resulted from the removal of the original vegetation cover (Pearson, 1984; Uhrich, 1990; Simon, 1999).

Short-term rainfall intensity is low and periods of rain generally occur continuously over a period of time rather than falling as short, heavy downpours (Meyer and Martinson, 1989; Uhrich, 1990). The seasonal hydrograph is largely driven by these prolonged, low-intensity rainfall events that occur predominantly in autumn and winter, although spring melt of high elevation snowpack makes a significant contribution to streamflow (Major and Mark, 2006). This is particularly the case in the upper North Fork Toutle River catchment where streamflows are heavily augmented by spring- and lake-fed runoff, as well as runoff from the now permanent glacier that has developed in the north-facing, amphitheatre-shaped crater of Mount St Helens (Walder et al., 2007) (Figure 2.10). Maximum streamflows in the wet season are usually the result of warm rain falling on thick, saturated snowpack (Meyer and Martinson, 1989; Uhrich, 1990; Major and Mark, 2006).

2.4.2 Land use

Prior to the 1980 eruption of Mount St Helens, the Toutle River basin was dominated by Douglas fir (*Pseudotsuga menziesii*), Western hemlock (*Tsuga heterophylla*) and Western red cedar (*Thuja plicata*) below an elevation of ~900 m, and by true firs (*Abies* sp.) at higher elevations (Collins and Dunne, 1986). These forests were intensively logged which produced a network of unimproved roads and a patchwork of forested and clearcut land in varying

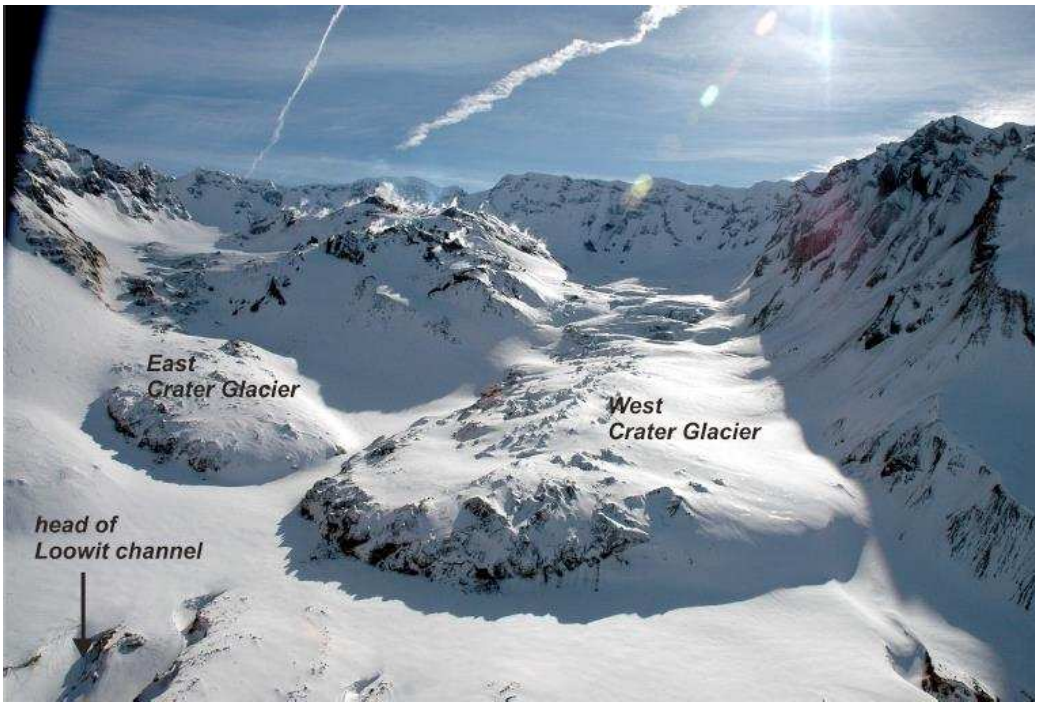

Figure 2.10 The Mount St Helens crater glacier. Taken from Walder et al. (2010, p. 24); photograph by Eugene Iwatsubo (2008).

stages of succession (Collins and Dunne, 1986; Simon, 1999; Dale and Adams, 2003). However, as discussed in previous Sections, the eruption killed the above-ground portions of nearly all plants within a 600 km^2 area (Collins and Dunne, 1986) and left a barren landscape devoid of vegetation and soil (del Moral and Lacher, 2005).

In August 1982, the US Congress established a 44,000-ha National Volcanic Monument (referred to hereafter as the Monument) in the devastated area surrounding Mount St Helens (the boundary is mapped in Figure 2.1) where natural processes of ecological recovery were allowed to dominate (Dale et al., 2005; Lawrence, 2005). Specifically, the US Forest Service was directed to protect the geologic, ecologic, and cultural resources within the Monument, and to allow geologic forces and ecologic succession to continue substantially unimpeded (Franklin et al., 1988). The rate of ecological succession within the Monument has varied spatially in relation to the type of volcanic disturbance and the life form of species present before the eruption, and this has resulted in a unique pattern of plant survival and reestablishment (Dale and Adams, 2003). On the debris avalanche and pyroclastic flow deposits, vegetation is lush

around ponds and wetlands, but sparse herb and shrub cover characterises upland areas and actively eroding sites (Dale et al., 2005). Outside the Monument, land has predominantly been planted with commercial conifer species, mainly Douglas fir (Pseudotsuga menziesii) (Lawrence, 2005), and logging operations have resumed.

2.5 SEDIMENT-RELATED FLOOD RISK AND ENGINEERING RESPONSES

Emplacement of volcanic debris on May 18, and its subsequent erosion by fluvial and hillslope processes in the years following the eruption, have presented significant and persistent flood risk management problems in the Toutle-Cowlitz River system. Investigations performed soon after the eruption predicted that approximately 420 million m^3 of sediment could be eroded from the debris avalanche between 1986 and 2035 (USACE, 1984, 1985). It was thought that this sediment would be transported out of the Toutle River system and deposited along the lower Cowlitz River where it would reduce the conveyance capacity of the channel and increase flood elevations.

Responsibility for controlling the predicted transfer of sediment through the river system in order to maintain acceptable levels of flood protection along the lower Cowlitz River rests with the Portland District, US Army Corps of Engineers (USACE). In exercising its responsibility, the Corps has implemented a number of sediment management actions on the channels affected by the eruption. These measures have attempted to control sedimentation in the lower Cowlitz in three main ways:

1. retaining sediment in the Toutle basin;
2. dredging to maintain or enlarge the flood conveyance capacities of channels with flood control functions;
3. improving flood defences protecting urbanised areas (USACE, 1985).

The locations of major engineering works implemented in the Toutle-Cowlitz River system between May 1980 and November 1987 are mapped in Figure 2.11.

2.5.1 Emergency measures (May 18, 1980 – September 1986)

Initial, emergency responses focused on restoring the flood conveyance capacity of the Toutle and Cowlitz Rivers, which had been significantly reduced principally by the impacts of the North Fork and South Fork Toutle River lahars (Section 2.2.5). To this end, dredging began almost immediately along reaches affected by sedimentation throughout the basin (Simon, 1999). By the end of November 1980, the conveyance capacity of the Cowlitz River had been restored from its post-eruption value of 368 $m^3 s^{-1}$ to 1,416 $m^3 s^{-1}$ so that the channel could convey typical storm flows expected that winter (USACE, 1983). Dredging continued until mid-May 1981, by which time nearly 10 and 43 million m^3 of sediment had been removed from the Toutle and Cowlitz Rivers, respectively (USACE, 1982). Emergency dredging was supplemented by raising the crests of existing flood defences along approximately 3.8 km of the lower Cowlitz River at Castle Rock, Lexington, Kelso and Longview, while 3.4 km of new flood defences were also constructed at Kelso (USACE, 1983).

Initial attempts to reduce flood risk by retaining sediment in the Toutle catchment were made using two approaches. The first was to construct temporary Debris Retaining Structures (DRS) on the North and South Fork Toutle Rivers (USACE, 1983; Simon, 1999). The larger DRS (N-1), with a capacity of 4.6 million m^3 (USACE, 1982), was built between July and September 1980 at the toe of the debris avalanche deposit on the North Fork (Figure 2.11). The South Fork DRS (S-1) (Figure 2.11) had a sediment storage capacity of approximately 0.46 million m^3 (USACE, 1982). Both structures accumulated material rapidly and continual dredging (at rates of up to 11,500 $m^3 day^{-1}$) was required to maintain their storage capacities (USACE, 1982, 1983). The DRSs were, however, only ever intended to provide a temporary solution and once maintenance dredging ceased in September 1981 they

quickly filled to capacity (USACE, 1983). The S-1 structure was removed in November 1982, and while the N-1 structure remains in place, it has been breached in two places, largely buried, and is no longer functional (USACE, 1983) (Figure 2.12).

The second means by which engineers attempted to retain sediment in the Toutle River catchment was through excavation of eight sediment basins: three on the lower Toutle (LT1 to 3) and five on the North Fork (NF1 to 5) (USACE, 1983). The locations of these basins are mapped in Figure 2.11. The basins were created by widening and deepening selected reaches to reduce velocities and encourage sediment deposition (USACE, 1985). Approximately 5.73 million m^3 of sediment was trapped in the basins and then mechanically removed from the Toutle River system while they were operational between December 1981 and May 1982 (USACE, 1983). However, lateral shifting of the river subsequently re-eroded thick piles of dredge spoil placed adjacent to the channel, and it has been estimated that as much as 80% of the material stored in these spoil piles had been remobilised by the end of 1982 (Simon, 1999). Due to continued sedimentation problems in the lower Cowlitz, the sediment basin nearest the mouth of the Toutle River (LT1) was reactivated during the winters of 1982-1983 and 1983-1984, with an additional 2.29 and 3.44 million m^3 excavated during these two periods, respectively (USACE, 2010).

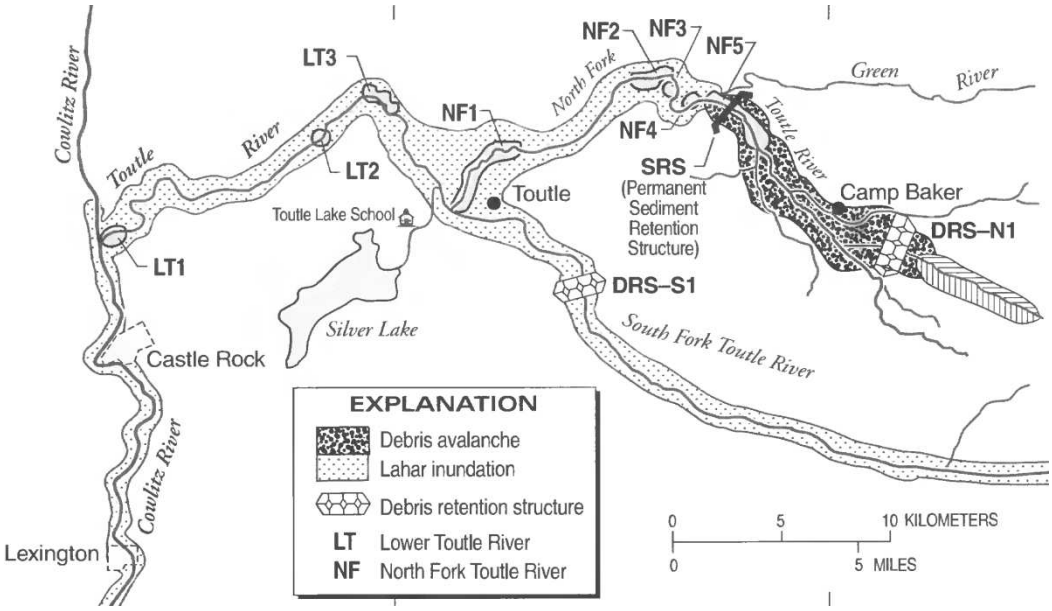

Figure 2.11 Locations of debris retaining structures, sediment stabilisation basins and a permanent sediment retention structure in the Toutle-Cowlitz River system. Taken from Simon (1999, p. 29).

Figure 2.12 Present condition of the N1-DRS on the North Fork Toutle River. Photograph by author (2011).

2.5.2 Sediment Retention Structure (SRS) on the North Fork Toutle River

i. SRS conception (1981-1985)

The emergency measures undertaken by the Corps of Engineers described above were effective in preventing flooding along urbanised reaches of the lower Cowlitz River in the years immediately following the eruption. However, the need for a long term solution to the sediment management problem in the Toutle-Cowlitz River system was soon recognised, and a number of options were proposed in the Corps of Engineers' Comprehensive Plan (USACE, 1983). Four options were selected for deep analysis (USACE, 1983):

1. evacuation of the Cowlitz River floodplain upstream of Longview and Kelso;
2. continued excavation of sediment stabilisation basins in the Toutle River;
3. construction of multiple, small sediment retention structures;
4. construction of a single, large sediment retention structure.

These options were then analysed in terms of their engineering feasibility, cost-effectiveness and environmental impact in the context of the forecast made at the time, that a total of 420 million m^3 of sediment would be eroded from the debris avalanche during the next 50 years – that is up to 2035 (USACE, 1984, 1985).

Following these analyses, option 4, for a single sediment retention structure (SRS) on the North Fork Toutle River upstream of the confluence with the Green River, together with minimal levee improvements along the Cowlitz River, was identified as the preferred solution (USACE, 1985). It was predicted that these measures would protect Castle Rock, Lexington, Kelso and Longview (see Figure 2.1 for locations) against floods with return periods of 167, 143, 167, and 118 years, respectively (USACE, 1985).

In 1985, the US Congress directed the Corps of Engineers to ensure that these Levels of Protection (LoP) were achieved. The Water Resources Development

Act of 2000 subsequently authorised the Corps of Engineers to maintain these LoPs through to 2035, which was then, and still remains, the end of the Mount St Helens project planning period (USACE, 2010).

ii. SRS operation: Phase 1 (October 1986 – April 1998)

Construction of the SRS began in October 1986 and, although not fully completed until 1990, the structure began trapping sediment as early as November 1987 (Simon, 1999; Biedenharn Group, 2010). The SRS consists of an embankment dam approximately 500 m long and 40 m high which has a storage capacity of around 200 million m^3 (USACE, 2002, 2010), as shown in Figure 2.13. During the initial phase of SRS operation (Phase 1), all flow passed through an array of thirty, 1 m diameter pipes, arranged in six rows of five, with each row closing progressively as sediment accumulated behind the dam (Simon, 1999). While operating in this initial state, the SRS had a trap efficiency of at least 90% meaning that sediment transfer from the upper North Fork Toutle River to the Cowlitz River was substantially reduced (Major et al., 2000; Major, 2004). By this criterion, construction of the SRS was effective in delivering flood risk reduction benefits and maintaining the specified LoPs within the congressionally authorised, protected areas (USACE, 2010).

iii. SRS operation: Phase 2 (April 1998 – August 2012)

In April 1998 the upper row of outlet pipes was buried by sediment accumulation upstream of the SRS. At that point, the structure became a run-of-the-river project with no settling pool and all flow passing over the spillway to the right of the embankment (WEST, 2002; USACE, 2010), as shown in Figure 2.14. During this Phase 2 operating period, the trap efficiency of the SRS has declined, perhaps to as little as 31% (Figure 2.15), meaning that the rate of sediment transfer to the Cowlitz River has increased markedly compared with that during Phase 1 (USACE, 2012). Moreover, there is evidence to suggest that in its current Phase 2 condition, the SRS is acting as a source for sand and a sink for gravel. This is particularly problematic given that it is the deposition of sand-sized sediment in the lower Cowlitz that is primarily

responsible for reducing channel capacity and increasing flood risk (USACE, 2010).

Consequently, concerns have been raised regarding the potential impact of increased sedimentation in the Cowlitz River on LoPs at Congressionally authorised communities. Indeed, calculated LoPs were shown to decrease at all four authorised locations between 1996 and 2007 as a consequence of the shift in the operating state of the SRS from Phase 1 to Phase 2 (Figure 2.16). Emergency dredging was necessary in 2007 and 2008, following heavy sedimentation in the lower 9.2 km of the Cowlitz River, in order to prevent the LoPs at Lexington, Kelso and Longview from falling below authorised levels (Figure 2.16). The benefits of these dredging operations did not extend upstream to Castle Rock where, in 2009, the LoP was judged to have fallen below 100 years (Figure 2.16). Subsequent improvements to Castle Rock's flood defences at the end of 2009 restored the LoP to the authorised level of 118 years or longer (USACE, 2010).

Despite these interim measures, probabilistic estimates made in 2009 suggested that unless further sediment management measures were taken, LoPs for each of the four communities would consistently decrease during the Congressionally mandated period up to 2035 (Figure 2.17), with resulting increases in flood risk (USACE, 2012). These predictions prompted further research to identify a long-term, sediment management plan to maintain the congressionally authorised LoPs and to continue to deliver flood risk reduction benefits along the lower Cowlitz (USACE, 2010).

The 1985 Decision Document (USACE, 1985) that recommended construction of the SRS, identified dredging downstream of the structure as a long-term solution to the problem of aggradation in the lower Cowlitz River once operation of the SRS entered Phase 2. However, this is no longer a viable option due to increasingly stringent restrictions associated with recently introduced environmental legislation, particularly the Endangered Species Act (ESA; Title 16 United States Code, Sections 1531-1544) (USACE, 2010). Significantly, the lower Toutle and Cowlitz Rivers were designated as critical

Figure 2.13 North Fork Toutle River Sediment Retention Structure in its initial Phase 1 operation condition, November 1987. Note the pool behind the dam and the flow of water through the structure. Photograph by Bill Johnson (1987).

Figure 2.14 North Fork Toutle River Sediment Retention Structure in its Phase 2 operating condition, May 2009. Note the lack of settling pool and the flow passing over the spillway to the left of the structure. Photograph by Colin Thorne (2009).

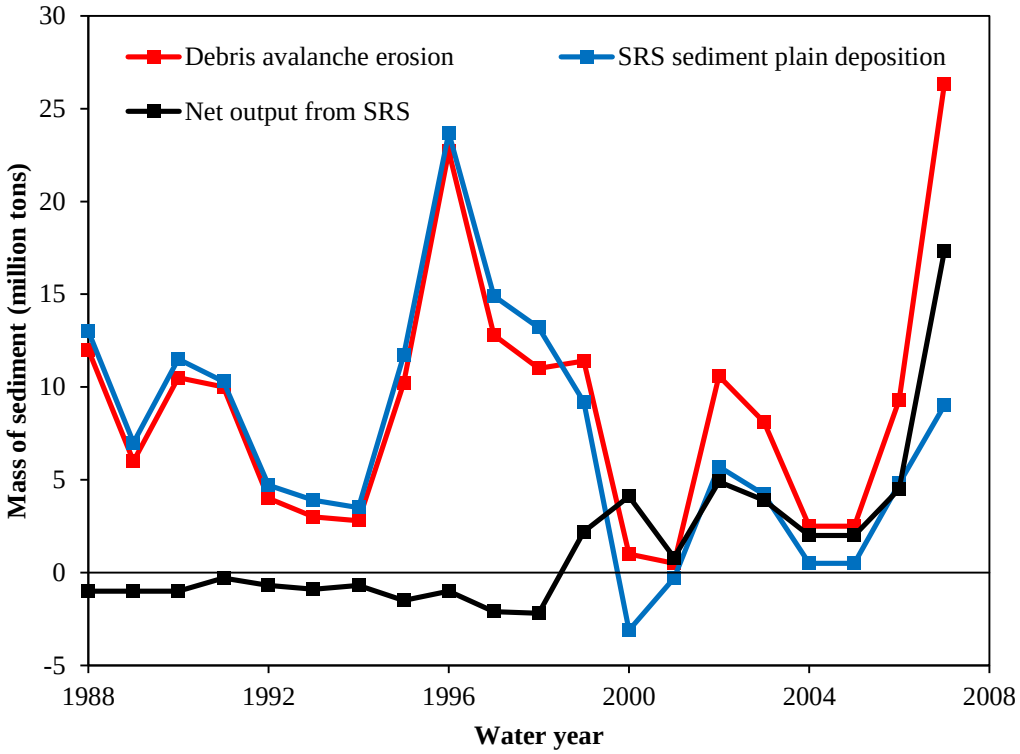

Figure 2.15 Annual estimates of debris avalanche erosion and SRS deposition between water years 1988 and 2007. Adapted from Biedenharn Group (2010, p. 88).

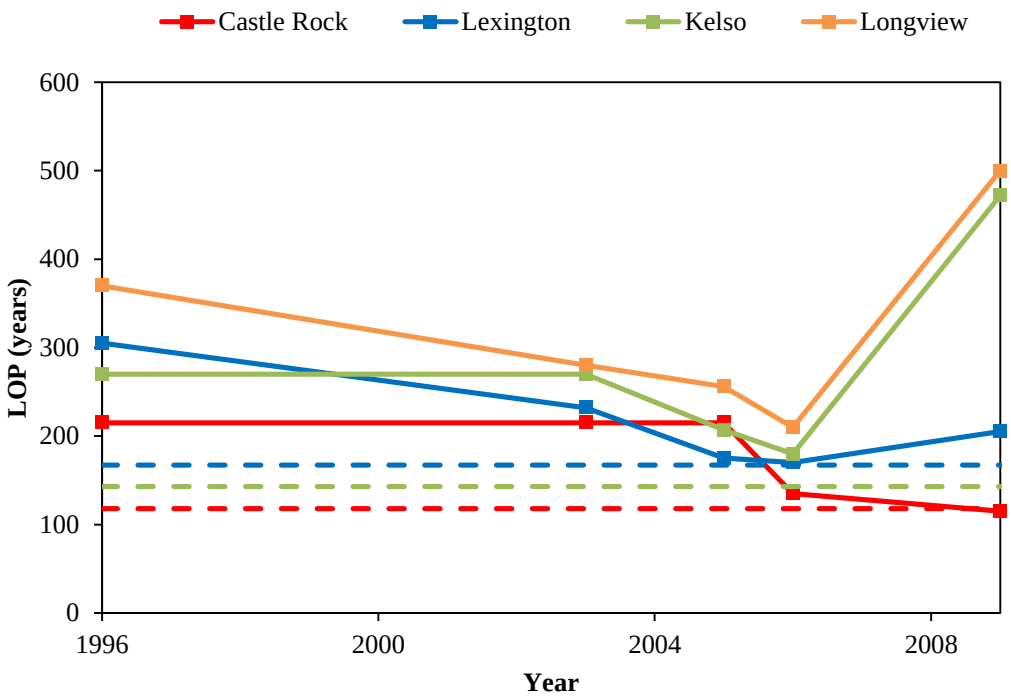

Figure 2.16 Level of Protection (LoP) history of flood defences along the Cowlitz River. Red, green and blue dashed lines represent the 118, 143 and 167 year authorised LoPs, respectively. Adapted from USACE (2010, p. 14).

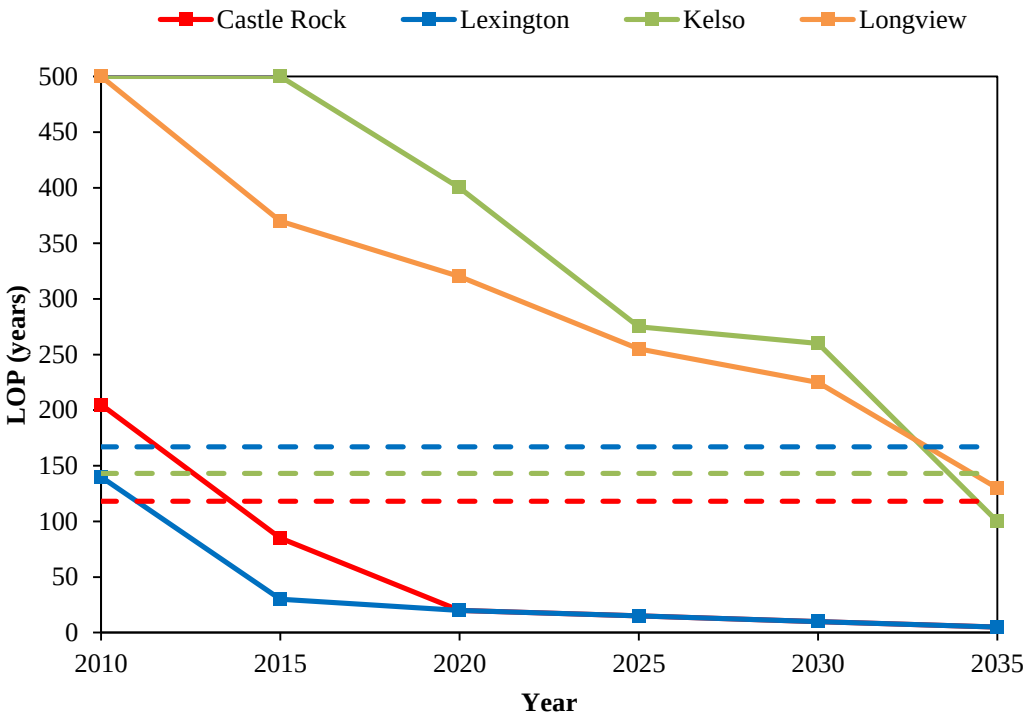

Figure 2.17 Probabilistic forecasts of LoPs at authorised communities on the Cowlitz River. Red, green and blue dashed lines represent the 118, 143 and 167 year authorised LoPs respectively. Adapted from USACE (2012, p. 4).

habitat for Pacific Eulachon or Smelt (Thaleichthys pacificus) in October 2011 (76 FR 65323) after the species was listed as threatened under the ESA in March 2010 (75 FR 13012). The Toutle River system has also historically supported populations of several salmon species currently listed as threatened under the ESA including winter steelhead (Oncorhynchus mykiss), coho salmon (Oncorhynchus kisutch), spring and fall Chinook salmon (Oncorhynchus tshawytscha) and chum salmon (Oncorhynchus keta) (USACE, 2007). Under the ESA, federally funded, constructed, permitted or licensed projects must take into account potential impacts on species listed as either threatened or endangered (USACE, 2010). Therefore, these designations and their associated regulations pose a significant challenge to continuation of long-term dredging operations downstream of the SRS as a sediment management measure (USACE, 2012).

A number of alternative solutions for reducing the rate of sediment supply to the lower Cowlitz were therefore considered at an expert workshop in May

2009 (USACE, 2010), and two of the measures identified at that workshop have recently been implemented. The first measure was construction of engineered log jams and grade-building structures on the sediment plain upstream of the SRS, designed to increase sediment (and especially sand) retention on the sediment plain by roughening it and prompting its evolution from an unvegetated braid plain to a channel-floodplain system with a floodplain featuring mixed wetlands and woodlands (USACE, 2010). The engineered log jams and grade-building structures were built in 2010 as a pilot project under funding from the economic stimulus package, and an on-going monitoring programme is currently underway to evaluate their effectiveness and to assess whether they could play a significant role in long-term sediment management (USACE, 2012).

The second measure designed to temporarily increase the trap efficiency of the SRS and add to its sediment storage capacity was initiated in 2012 when the elevation of the SRS spillway was raised by 10 feet (approximately 3 m) (USACE, 2012). This modification is allowable because improved modelling has reduced the discharge of the maximum probable flood (actually a lahar) that the spillway must be able to convey safely. It will provide an additional 1.5 million m^3 of storage capacity as well as reducing the average slope of the sediment plain as the pool upstream of the spillway fills with sediment. This measure is anticipated to deliver flood risk reduction benefits to communities along the lower Cowlitz River for 5 to 10 years (USACE, 2012).

2.6 SUMMARY

The eruption of Mount St Helens on May 18, 1980 transfigured hundreds of square kilometres of landscape and deposited approximately 2.9 km^3 of explosively generated volcanic material in a broad arc from northwest to northeast of the volcano. Channels of the Toutle-Cowlitz River system were severely affected by the eruption, although deposition of a 2.5 km^3 debris avalanche into the upper 64 km^2 of the North Fork Toutle River catchment had the greatest impact on fluvial geomorphological processes. The debris avalanche obliterated the surface drainage network, increased stream gradients

and supplied channels with a large volume of easily erodible volcaniclastic debris.

Geomorphological response in the upper North Fork Toutle River catchment was dominated by drainage network reintegration initiated by the filling-and-spilling of lakes that formed on the hummocky debris avalanche surface. Rapid channel incision downstream of lake breaches cut steep-walled trapezoidal channels and gullies. Stream bed elevations then began to stabilise and lateral erosion through the failure of saturated banks and streamside hummocks became the primary process of channel adjustment. These processes resulted in sediment yields that were significantly elevated relative to pre-eruption levels and far greater than those from basins affected solely by the lateral blast (Green River) or lahars (South Fork Toutle River). Although sediment supply from the upper North Fork Toutle River has naturally declined in the years following the eruption, a vast quantity of material remains stored in the valley and persistent channel adjustments by bank retreat and valley widening continue to provide abundant sediment to stream channels.

Elevated sediment yields from the upper North Fork Toutle River increased flood risk to downstream communities along the lower Cowlitz River (Castle Rock, Kelso and Longview) where sediment deposition reduced the conveyance capacity of the channel. Following emergency measures in the early 1980s, including dredging and raising flood embankments, the US Army Corps of Engineers constructed a 40 m high Sediment Retention Structure (SRS) with a capacity of 200 million m^3 on the North Fork Toutle River. Between 1986 and 1998, the SRS had a trap efficiency of at least 90% and therefore substantially reduced sediment transfer to the Cowlitz. However, since the SRS became a run-of-the river project in 1998, trap efficiency has reduced to perhaps as little as 31% meaning that the problem of sediment accumulation in the lower Cowlitz has been renewed. Although interim measures have recently been put in place to reduce the immediate risk of flooding at Castle Rock, Lexington, Kelso and Longview, long-term alternatives are required to ensure that these communities receive acceptable levels of flood protection into the future.

CHAPTER 3 MODELLING LONG-TERM SEDIMENT YIELD FROM THE UPPER NORTH FORK TOUTLE RIVER: PREVIOUS WORK AND ALTERNATIVE OPTIONS

3.1 INTRODUCTION

Development of long-term alternatives for managing sediment within the Toutle-Cowlitz River system up to and beyond the end of the project planning period in 2035 is currently in progress. Options under consideration include:

1. additional, further incremental raising of the SRS spillway by up to 20 feet (approximately 6 m);
2. installing more engineered log jams and grade-building structures on the sediment plain;
3. raising the entire SRS structure (dam and spillway) by about 43 feet (approximately 13 m) (USACE, 2010, 2012).

Alternatives analysis will be performed for these options, with selection of the preferred solution(s) dependent on revised predictions of future sediment yields and, particularly, on the rate at which sediment load in the upper North Fork Toutle River will relax back towards its pre-disturbance value (USACE, 2010). These predictions are essential to provide the basis from which to estimate with confidence the total volume of sediment that must be managed and the period of time over which the project must remain operationally effective.

As discussed in the Introduction to this thesis (Chapter 1), a number of studies have demonstrated that recovery of fluvial systems heavily loaded with sediment derived from natural and anthropogenic disturbances takes place over periods extending from decades to millennia (e.g. James, 1989; Manville and Wilson, 2004; Gran and Montgomery, 2005; Korup, 2005; Koi et al., 2008; Manville et al., 2009; Pierson et al., 2011; Pierson and Major, 2014). Although such studies provide useful insights into possible recovery trajectories at Mount St Helens, the range of variables that control long-term response (e.g. Manville and Wilson, 2004; Manville et al., 2009) limits the extent to which

observations can be transferred from different disturbances in different catchments. As such, site-specific, applied research is necessary to inform long-term sediment management in the Toutle-Cowlitz River system.

Similarly, historic eruptions of Mount St Helens provide little information regarding possible recovery trajectories of the affected catchments. For instance, the most recent volcanic activity prior to the 1980 eruption, which occurred between 1800 and 1857 during the Goat Rocks eruptive period (Mullineaux and Crandell, 1981), had very little impact on the surrounding landscape. The Goat Rocks period was initiated in 1800 by an explosive eruption that emplaced a small (approximately 0.1 km^3) tephra layer thinly spread over a large area that extended up to 525 km northwest of the volcano (Crandell, 1987; Clynne et al., 2005).

The next recorded eruption of that period produced a lava flow on the northwest flank of the mountain, followed by the extrusion of the Goat Rocks magma dome during the 1840s and 1850s. The lava flow extended no more than 5 km from the vent, and was between 0.2 and 0.7 km wide (Crandell, 1987). The growth of the Goat Rocks dome was also associated with the emplacement of a small fan of volcanic debris on the volcano's northwest flank (Mullineaux and Crandell, 1981; Clynne et al., 2005). The last significant eruption of the Goat Rocks period was in 1857, although no depositional units have been associated with this event (Mullineaux and Crandell, 1981; Crandell, 1987). Moreover, no lahars large enough to inundate flood plains a significant distance from the volcano have been recognised from the Goat Rocks eruptive period (Scott, 1989).

It is therefore evident that volcanic activity during the youngest of the pre-1980 eruptive periods did not have any significant impacts on the fluvial system of the upper North Fork Toutle River catchment. Furthermore, fluvial recovery following older, larger eruptions of Mount St Helens has not been explicitly documented or studied. However, Scott (1989) notes that the volcanically dormant interval of approximately 300 years after the emplacement of a huge volume of sediment by lahars during the Pine Creek eruptive period

approximately 2,500 years ago was characterised by extensive reworking of lahar-emplaced sediment. Scott (1989) also suggests that the sediment transport regime in the Toutle River period during this dormant interval was probably one of rapidly migrating braided channels, in which the vast influx of laharic sediment was reworked. Arguably, these findings suggest that previous sediment loading of the Toutle River system by volcanic eruptions has resulted in possibly several centuries of fluvial instability.

3.2 PREVIOUS WORK: EMPIRICAL ANALYSES AND CURVE EXTRAPOLATION

Since the SRS entered its current, Phase 2 operating condition, the Corps of Engineers has commissioned three separate investigations intended to inform long-term sediment management, principally by predicting future volumes of sediment delivery from the debris avalanche to the SRS. These investigations led to reports submitted to the Corps by WEST Consultants (WEST, 2002), the Biedenharn Group (Biedenharn Group, 2010) and the USDA Agricultural Research Service (ARS) National Sedimentation Laboratory (Simon and Klimetz, 2012). All three studies took a similar approach whereby historical trends of change during the post-eruption period were established empirically and then extrapolated to predict future rates of sediment supply to the SRS. However, methodologies and data sets varied between the reports, and these differences are described, together with pertinent results and conclusions, in the following sub-sections.

3.2.1 Mount St Helens Engineering Reanalysis (WEST, 2002)

The study undertaken by WEST Consultants generated a time series of annual sediment yield from the debris avalanche for the seventeen year period from 1982 to 1998 based on a combination of suspended sediment data and SRS deposition volumes. Prior to closure of the SRS in 1988, debris avalanche sediment yield was estimated indirectly, using measured suspended sediment yields recorded at the Tower Road gauging station on the Toutle River mainstem, which is located approximately 54 km downstream of the debris avalanche itself (Figure 3.1). Between 1988 and 1998, however, sediment yield

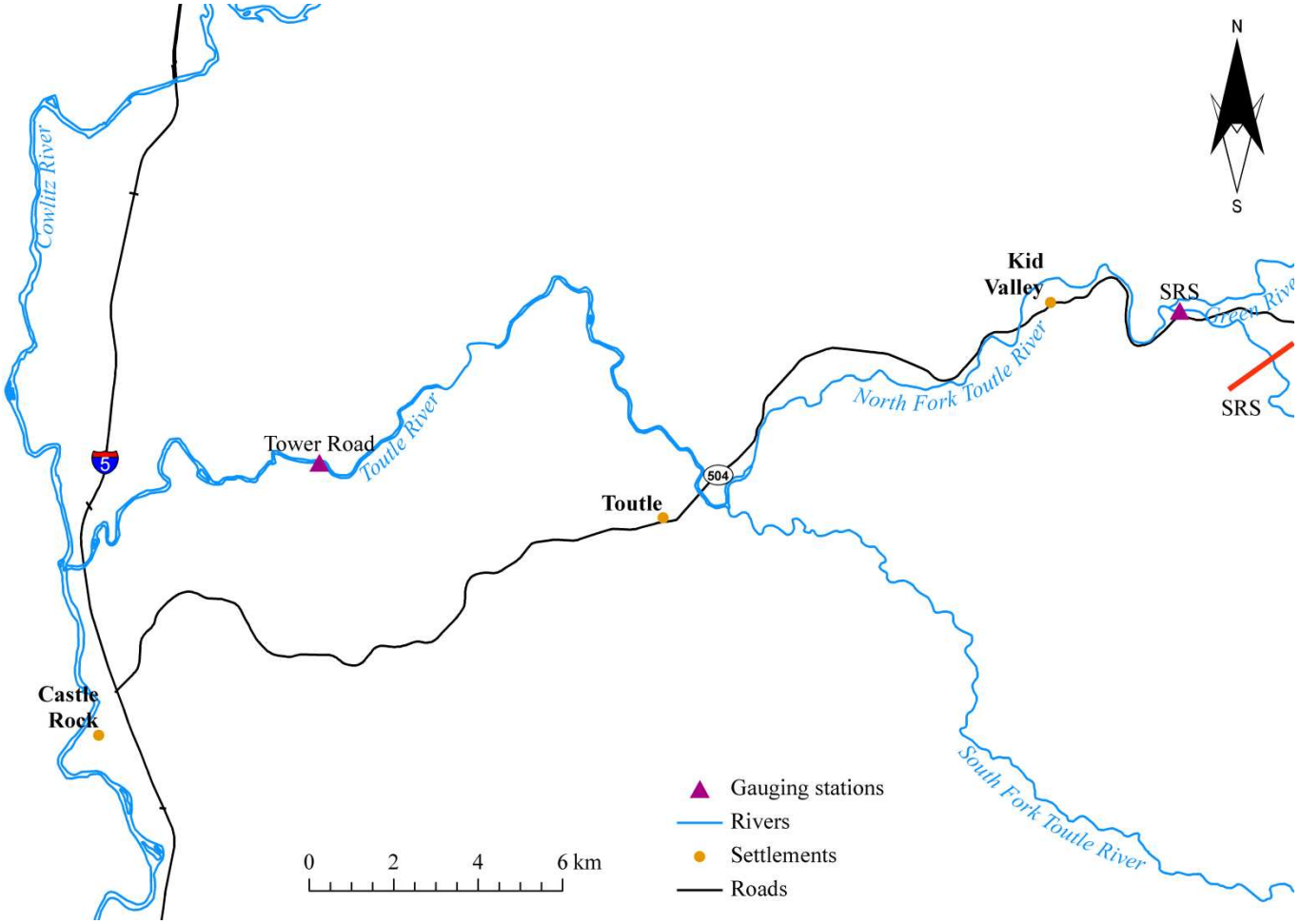

Figure 3.1 Locations of USGS Tower Road and SRS gauging stations. Data from Washington State Geospatial Data Archive and USGS.

could be calculated by combining the Tower Road suspended sediment record with measured volumes of sediment deposition behind the SRS obtained from ground-based surveys. Acknowledging that sediment yield is strongly dependent on hydrology, the annual sediment yield was divided by the annual runoff to determine average sediment concentration (yield of sediment per unit volume of runoff). The normalised concentrations were then accumulated on an annual basis and plotted to reveal a decreasing trend in annual sediment concentrations over time.

A power function was fitted to the data to develop a cumulative sediment concentration decay curve that could be extrapolated to predict future annual sediment concentrations through to 2035. Predicted annual sediment concentrations derived from the curve were multiplied by the average annual runoff for the period of record at Tower Road (1931 to 1998) to convert annual concentrations to volumetric annual sediment yields. The results suggested that 163 million m^3 of sediment had been delivered to the SRS between 1982 and 1999, and that a further 153 million m^3 would be supplied between 1999 and 2035. Total sediment yield from the debris avalanche between 1982 and 2035 was, therefore, estimated to be 316 million m^3. Annual sediment yields were predicted to decrease from 5.28 million $m^3 yr^{-1}$ in 1999, to 3.44 million $m^3 yr^{-1}$ in 2035, a reduction of approximately 35%.

3.2.2 Toutle-Cowlitz River Sediment Budget (Biedenharn Group, 2010)

The Biedenharn Group utilised Digital Elevation Models (DEM) produced from remotely sensed survey data to identify trends in sediment yield from the debris avalanche between 1984 and 2007. Total net change in volume was calculated by differencing the DEMs for selected years, and this was done for three periods: 1984 to 1987; 1987 to 1999; and 1999 to 2007. These periods were defined by the availability of DEMs with sufficient spatial coverage to enable volume change calculations to be made for the entire debris avalanche upstream of the N1-DRS. The results suggested a significant reduction in average annual sediment yield from the debris avalanche between the first two periods, and a slight reduction between the second and third periods (Table 3.1).

Although these results could be interpreted as evidence of decay in post-eruption sediment yield, the report authors suggested that hydrological variability prevented such a conclusion from being drawn with any confidence. Specifically, total runoff gauged at Tower Road was approximately 40% lower between 1999 and 2007 than it had been between 1987 and 1999. Consequently, the Biedenharn Group argued that the relative drought experienced during the third period may have been responsible for the observed reduction in annual sediment yield, and that this reduction could not be taken to indicate that the rate of erosion due to channel adjustments on the debris avalanche was slowing significantly. As no significant decay had been detected, the annual sediment yield of 4.51 million m^3 yr^{-1} obtained between 1999 and 2007 was extrapolated linearly to predict that the total sediment yield between 2008 and 2035 would be 126 million m^3. When combined with the estimated sediment yield between 1981 and 2007 (424 million m^3), the Biedenharn Group concluded that by 2035 a total of 558 million m^3 will have been eroded from the 1980 debris avalanche and transported to the N1-DRS.

Table 3.1 Debris avalanche erosion, 1984 to 2007.
Modified from Biedenharn Group (2010, p. 64).

Surface differencing period	Debris avalanche erosion	
	Total (10^6 m^3)	Annual Yield (10^6 m^3 yr^{-1})
1984-1987	182.88	60.94
1987-1999	68.96	5.73
1999-2007	35.93	4.51

3.2.3 Analysis of Long-Term Sediment Loadings from the Upper North Fork Toutle River System, Mount St Helens, Washington (Simon and Klimetz, 2012)

The study conducted by Dr Andrew Simon (then a research leader at the ARS National Sedimentation Laboratory) analysed cross-sectional changes at monumented cross-sections with long records of repeat surveys to establish how channel dimensions and geometries have evolved since the eruption.

Following the eruption of Mount St Helens in 1980, scientists at the USGS Cascades Volcano Observatory established an extensive network of monumented cross-sections in the North Fork Toutle River catchment in order to monitor the post-disturbance response of the channels draining the mountain. Seventy cross-sections were initially set-up on the debris avalanche, and these have been re-surveyed at various times since 1980 to provide a record of post-eruption channel change.

Although repeat surveys at some locations were infrequent, Dr Simon and his team were able to increase the temporal resolution of the data by extracting cross-sections from DEMs produced in 1980, 1987, 1990, 2003, 2006, 2007 and 2009, in combination with additional, ground-based surveys undertaken in 2009 and 2010. Successive surveys at monumented cross-sections were overlain so that the net change in cross-sectional area could be calculated. This process was repeated for all available cross-sections to build up a record of channel changes throughout the drainage network on the debris avalanche. The cumulative data were found to reveal decreasing trends in rates of channel change through time at all cross-sections, which could be represented by a nonlinear (logarithmic) decay function (see Figure 3.2 for an example).

To estimate annual change in channel cross-sectional area during the period of interest, the nonlinear regression equation for each cross-section was then solved for every year between 1980 and 2035. The equations were also used to predict channel change by the years 2050, 2070, 2090 and 2110 for each cross-section. The methodology described above produced estimated values of change in area at individual cross-sections distributed throughout the drainage network on the debris avalanche. The next step was to convert these to net change in volume. Conversion to volumetric change was achieved by multiplying the change in area at each cross-section by the length of the reach between that cross-section and the next cross-section downstream. The resultant volumes for each reach were then summed to produce a series of annual volumes for the debris avalanche as a whole. These annual volumes may be accumulated to estimate the total sediment yield for any selected period since 1980.

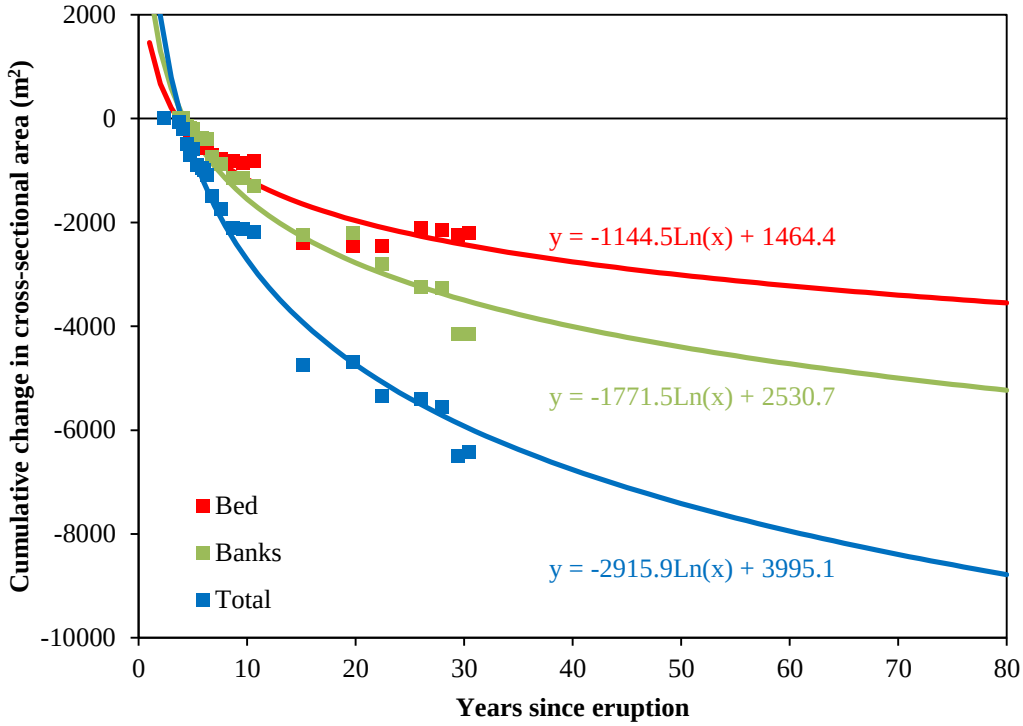

Figure 3.2 Example of logarithmic regression curves developed from cumulative cross-sectional area data. Adapted from Simon and Klimetz (2012, p. 40).

The resulting, estimated sediment yield between 1980 and 2010 was 290 million m^3, while total sediment yield by 2035 was predicted to reach 331 million m^3. The average annual rate of sediment yield was expected to decline from 1.68 million m^3 yr^{-1} in 2010 to 0.98 million m^3 yr^{-1} in 2035, a reduction of approximately 42%. The observed trend was also extrapolated to 2110 to predict that 389 million m^3 will have been delivered from the debris avalanche to the N1-DRS by that date. It should be noted that remarkably similar results were obtained by Simon and Klimetz (2012) using the mechanistic Bank-Stability and Toe Erosion Model (BSTEM; Simon et al. (2000)).

3.3 CRITIQUE OF THE CURVE EXTRAPOLATION TECHNIQUE

The three studies discussed in the preceding sub-sections all attempted to estimate long-term sediment yield from the debris avalanche based on hindcasting to derive empirical trends from observed data and extrapolating those trends into the future. However, each study used different historical data, analysed different time periods, and implemented different methodological

approaches to quantify temporal changes in the annual sediment yield since the eruption. These variations resulted in significant differences in sediment yield from the debris avalanche during the period of observation, as well as large differences in the yields predicted to 2035 (Table 3.2 and Figure 3.3). Taking the year 1999 as a benchmark at which all of the three studies had estimated post-eruption sediment yield from observed data, these discrepancies become obvious. Table 3.2 reveals a difference of 227.58 million m^3 between the highest (Biedenharn Group, 2010) and the lowest (WEST, 2002) estimates of sediment yield over the first 19 post-eruption years.

Of potentially greater significance to decision-making on sediment management are marked discrepancies between the temporal trends in annual sediment production and delivery to the SRS during the period of observations. WEST (2002) and Simon and Klimetz (2012) both identified decreasing trends in annual sediment yields, but the Biedenharn Group (2010) concluded that the evidence for a decaying trend was weak and suggested that post-1999 the rate of erosion had been effectively constant. Moreover, WEST (2002) and Simon and Klimetz (2012) fitted contrasting functions to describe the trend for decay in post-eruption sediment yields.

Specifically, the logarithmic trend fitted by Dr Simon (Simon and Klimetz, 2012) indicated that average annual sediment yield declined by approximately 93% between 1980 and 1999, while the power function fitted by WEST indicated a significantly lower reduction of 79% during the same period. The fitted curves not only produce different rates of change in past erosion and sediment delivery, they also reveal fundamental differences between the ways that the studies conceptualise the processes driving channel change and evolution of the fluvial system on the debris avalanche.

The variations in the volumes and trends of sediment yield estimated by the three studies during the period of measured data are exaggerated by subsequent temporal extrapolation and explain the discrepancies between the long-term estimates of sediment yield evident in Table 3.2 and Figure 3.3. Coincidentally, curves fitted to the cumulative sediment yield data analysed by WEST (2002)

Table 3.2 Key findings of the empirical analyses of sediment yield from the upper North Fork Toutle River debris avalanche.

	WEST (2002)	Biedenharn Group (2010)	Simon and Klimetz (2012)
Empirical data used	Suspended sediment records and estimates of sediment deposition behind SRS	Volumes calculated from DEM differencing	Change in cross-sectional area derived from repeat cross-sectional surveys, DEMs and fieldwork
Period of observed data	1982 – 1999	1984 – 2007	1980 – 2010
Estimated cumulative sediment yield in 1999 (million m^3)	168.20	395.78	257.40
Predicted sediment yield up to 2035 (million m^3)	316.53	558.02	330.98
Evidence of decay identified?	Yes	No	Yes

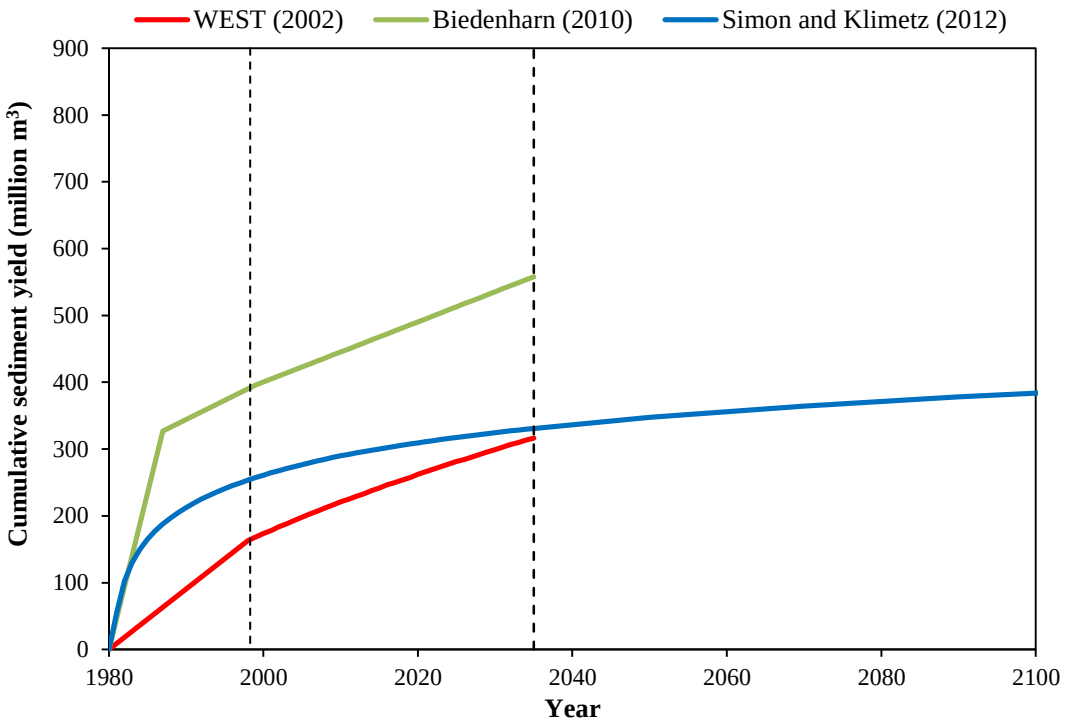

Figure 3.3 Comparison of predicted cumulative sediment yield from the debris avalanche to 2100. Dashed lines indicate the benchmark years 1999 and 2035.

and the cumulative channel change data analysed by Simon and Klimetz (2012) converge around the year 2035 so that the difference between them is only about 4% at that time (Table 3.2; Figure 3.3). That said, the curves have markedly different trajectories, with contrasting implications regarding the requirement for continued sediment management to maintain minimum levels of flood protection to communities along the lower Cowlitz River beyond 2035.

It is, therefore, evident that previous research (WEST, 2002; Biedenharn Group, 2010; Simon and Klimetz, 2012) has been unable to reach a consensus on either the quantities or trends of sediment production that may be expected from the North Fork Toutle River debris avalanche up to and beyond 2035. The resulting uncertainty has hindered effective decision-making regarding long-term sediment management in the Toutle-Cowlitz River system by limiting the extent to which potential alternative options can be analysed in the context of likely future sediment yields. The lack of consensus also demonstrates the problems associated with extrapolating short-term data over long time periods based on information that is less than ideally suited to the task, being in different respects inadequate, incomplete and naturally variable.

A further limitation on the confidence that can be placed in predictions of future sediment yields and patterns of channel evolution based on extrapolation of past trends derived from historical records arises because this approach rests on the assumption that climatic and drainage basin controls on precipitation, rainfall-runoff relationships, sediment erodibility and sediment dynamics are time-invariant, or at least that past rates and trends of change in those drivers will continue (Downs and Thorne, 1996). Clearly, assumptions of driver and process stationarity must be questioned, both with respect to the periods of monitoring and prediction, and if drivers and processes are non-stationary the accuracy of the predictions made that way will suffer (Bray and Hooke, 1997). Similarly, exceptional conditions are, by definition, not covered by empirical models (Nachtergaele et al., 2001) and it is therefore difficult to extrapolate the fitted relationships beyond the range of the conditions studied (Darby and Van De Wiel, 2003). This problem is exacerbated by the importance of antecedent

conditions in that the response of a system to an imposed process event depends on the conditioning effect of previous events (Newson, 1980).

Predictions based on extrapolation of regression relationships can be classified as non-explanatory according to the definitions introduced by Sayer (1992) in that they isolate purely empirical relationships without attempting mechanistic explanation (Murray, 2007). Despite being staightforward, non-explanatory predictions that neglect physical processes face significant challenges when applied in the context of complex, open systems (Sayer, 1992). For example, Schumm (1991) identified ten problems associated with extrapolation of recently observed trends that could be assigned to three broad categories. The following summary is adapted from Beven (2009).

Problems of scale and place:

- Time (observations are only available over a particular period and time span);
- Space (observations are only available at particular scales);
- Location (observations are only available at particular locations).

Problems of cause and process:

- Convergence (the production of similar results from different processes and causes);
- Divergence (the production of different results from similar processes and causes);
- Efficiency (variable efficiency and work accomplished by a process);
- Multiplicity (effects due to multiple causes acting simultaneously).

Problems of system response:

- Singularity (natural variability among like things);
- Sensitivity (susceptibility of a system to change);
- Complexity (complex responses of a system with multiple interconnected parts).

Of particular relevance to the issue of predicting long-term sediment yield from the upper North Fork Toutle River catchment are the problems of time, divergence and complexity. In relation to time, it is questionable whether the

18, 27 and 30-year periods used in the WEST, Biedenharn Group and Simon and Klimetz studies, respectively are adequate to fully describe the range of physical processes responsible for the evolution of the drainage network in the catchment in the way necessary to support reliable predictions. Similarly, curve-extrapolation does not explicitly account for potential modification to the future hydrological regime of the catchment resulting from climate change.

As stated by Major et al. (2000), the process of channel adjustment by widening on the debris avalanche is heavily discharge-dependent and future hydrological variability and change are, therefore, likely to punctuate, or even reverse, previously well-established trends of sediment production in the upper North Fork Toutle River catchment. This limitation was acknowledged by WEST (2002) who noted that their estimates were based on average hydrological conditions that occurred between 1931 and 1998, and that different hydrological conditions could, therefore, significantly alter future rates of reduction in sediment yield from those predicted in their report.

Divergence and complexity relate to the issue of nonlinearity in fluvial geomorphic systems and can make extrapolation extremely difficult as they imply that the same driving variables can result in very different system responses (Schumm, 1991). Complexity refers predominantly to the concept of ‘complex response’ introduced by Schumm (1973), which suggests that abrupt changes in rates and directions of adjustment in the fluvial system may be caused by the crossing of geomorphic thresholds that are intrinsic to the system itself, as well as the crossing of external thresholds associated with perturbations to that system.

On this basis, Schumm argued that threshold behaviour may be inherent to development and evolution of the fluvial system (Schumm, 1973). Specifically, abrupt changes in the evolution of a drainage system are not necessarily related to external influences such as climatic, tectonic, isostatic or land use changes, but may be the result of an event which performs little of the total geomorphic work within a catchment but which triggers a complex sequence of adjustments that produce changes in the landscape that are disproportionately large, long-

lasting and significant (Schumm, 1973). This implies that landscape development may not feature progressive change, but that evolution may be characterised by relatively long periods of progressively slowing change interrupted by abrupt shifts from one state of dynamic equilibrium to another, a condition he termed dynamic, meta-stable equilibrium (Schumm, 1973).

Schumm (1973, 1979) identified the crossing of geomorphic thresholds as a key mechanism by which this complex response is initiated in geomorphic systems. Such thresholds are the result of landform change through time to a condition of incipient instability and then failure, and may lead to episodic erosion or deposition which can significantly affect sediment yields (Schumm, 1979). Phillips (2006) identified eight further sources of nonlinearity in geomorphic systems that render predictions by curve-extrapolation potentially unreliable:

1. storage effects;
2. saturation and depletion relationships;
3. self-reinforcing positive feedbacks;
4. self-limiting negative feedbacks;
5. opposing or competitive interactions;
6. multiple modes of adjustment;
7. self-organisation; and,
8. hysteresis.

It is therefore apparent from this brief account of the functioning of geomorphic systems over short periods of time (as opposed to geologic time) that the extrapolation of average rates of erosion and deposition is unlikely to reflect natural complexity in landform development over timescales relevant to planning and management (Schumm, 1979). Specifically, it is not safe to assume that future responses in a geomorphic system will be quantitatively or qualitatively similar to those evident in the historical record (Phillips, 2006).

In this context, Downs and Thorne (1996) argue that geomorphological modelling, whereby the processes and mechanisms of change are explicitly

accounted for, represents a superior approach and better facilitates prediction of channel response to changes in climate and drainage basin controls. Process-based modelling is therefore preferable if complex responses and the effects of geomorphic thresholds, together with other sources of nonlinearity, are to be incorporated into predictions, and also offers the opportunity to add explanation to otherwise non-explanatory predictions.

Given both the uncertainty surrounding previous estimates of future long-term sediment production in the upper catchment of the North Fork Toutle River and the limitations associated with the methodologies employed to date in these studies, it is evident that an alternative approach, based on geomorphic modelling, is required. Importantly, such an approach is not entirely reliant on the extrapolation of empirical trends derived from short periods of data, and should therefore be able to account for threshold behaviours and incorporate the potential impacts of hydrologic perturbations that may result from future climatic change. However, the model would need to be able to operate over the extent of the upper North Fork Toutle River catchment and over timescales of decades to centuries. These criteria form the context within which alternative options for predicting long-term sediment production and delivery to the SRS are assessed in the following Sections.

3.4 ALTERNATIVE OPTIONS: NUMERICAL MODELLING

As outlined above, the primary alternative to the empirically-based methods employed by WEST (2002), Biedenharn Group (2010) and Simon and Klimetz (2012) to make quantitative predictions of erosion and sediment yield is numerical modelling of the geomorphic system. Numerical models in geomorphology represent relevant physical processes as a set of governing equations that are ultimately solved by a numerical algorithm implemented as a computer program (Darby and Van De Wiel, 2003; Pazzaglia, 2003; Pizzuto, 2003). The use of numerical models became increasingly widespread during the last quarter of the 20th century owing, predominantly, to improved computational capability, increases in the availability and quality of terrain

data, and advances in knowledge and understanding of geomorphological processes (Martin and Church, 2004; Tucker and Hancock, 2010).

A variety of numerical models have been developed across the disciplines of fluvial geomorphology, hydrology and hydraulics that attempt to describe, explain and/or predict processes occurring in river channels and catchments at a range of spatial and temporal scales. Numerical models represent controllable virtual environments which can be analysed at any point in space and time (Van De Wiel et al., 2011), and they avoid the limitations associated with field monitoring or laboratory modelling (Cox et al., 2005). As such, computer simulation has become a widely-used framework for formulating and testing theories as well as for making practical predictions to inform decision makers (Beven, 2002).

In general, numerical models represent a river channel or basin as a grid consisting of a finite number of points which store discrete values relating to the spatially distributed physical properties of the system such as elevation, water depth, hydraulic roughness and flow velocity (Bathurst, 1986; Darby and Van De Wiel, 2003). This spatial division, or discretisation, is necessary in order to facilitate implementation of the equations used to simulate the flow of water and sediment across a topographic surface (Tucker et al., 2001; Tucker and Hancock, 2010). The governing equations are explicitly modelled at a resolution specified by the spacing of individual grid points, and this scale therefore forms the foundation for operation of the model (Van De Wiel et al., 2011). In addition to the spatial discretisation of numerical models, the time dimension is also discretised into time steps (Bathurst, 1986; Coulthard et al., 2002; Darby and Van De Wiel, 2003). At each time step, the governing equations are solved, the values held in the grid are updated, and this iterative process represents the temporal evolution of physical conditions within the system (Darby and Van De Wiel, 2003; Pazzaglia, 2003; Van De Wiel et al., 2011).

The mathematical descriptions of physical processes within a numerical model can be derived either theoretically or empirically (Abbott et al., 1986b;

Bathurst, 2002; Darby and Van De Wiel, 2003), and as such the term 'model' often refers to both the underlying hypotheses, theories and observations on which the governing equations are based, as well as the computational techniques used to calculate solutions to these equations (Willgoose, 2005; Codilean et al., 2006; Tucker and Hancock, 2010). However, exactly which processes are realised, and how this is done, largely depends on the intended purpose of the model, the level of detail required, the spatial and temporal scales under consideration and the specific aims of the particular modelling application (Darby and Van De Wiel, 2003; Martin and Church, 2004; Tucker and Hancock, 2010).

When developing a numerical model for either explanation or prediction in any discipline, therefore, the question arises of how complex the model should be in terms of process representation and the numerical implementation of these processes (Murray, 2007). Similarly, it is often necessary to strike a balance between adherence to physical realities on the one hand and computing requirements, including numerical convenience, stability and time limits, on the other (Bathurst, 1986). As a result, models generally lie somewhere on a continuum between reductionist approaches and reduced complexity approaches as the two end points (Paola, 2001; Murray, 2003). The following sub-sections describe these two alternative approaches to numerical modelling, whilst Table 3.3 summarises this discussion in terms of the key issues and also compares these approaches with empirical curve-extrapolation techniques.

3.4.1 Reductionist approaches to numerical modelling

Reductionist models attempt to include as many primary and secondary processes as possible, with simplification of the fundamental governing equations being minimised (Paola, 2001; Van De Wiel et al., 2011). Such models are designed with the aim of reproducing the behaviour of natural systems as accurately as possible (Murray, 2003; Van De Wiel et al., 2011). The reductionist approach argues that the, "understanding of complex systems can be achieved when the behaviour of the individual components are aggregated" (Harrison, 2001, p. 328). The argument for the implementation of

reductionist modelling approaches in hydrology is exemplified by Lane and Richards (1997) who suggest that short time-scale and small space-scale processes exert a critical control on larger-scale river behaviour.

Reductionist models in hydrology are therefore based on a set of partial differential equations known as the Navier-Stokes equations that govern the fundamental principles of fluid flow, specifically the conservation of mass and the conservation of momentum (Lane, 1998; Darby and Van De Wiel, 2003; Nicholas, 2005). The Navier-Stokes equations (shown in equation 3.1, below) have no analytical solution and therefore must be simplified by the omission of selected terms to obtain a solution.

$$\frac{\partial}{\partial t}(\rho u) + \frac{\partial}{\partial x}(\rho u^2) + \frac{\partial}{\partial y}(\rho uv) + \frac{\partial}{\partial z}(\rho uw) - 2\rho u\zeta \sin\Phi + \frac{\partial p}{\partial x} - \frac{\partial \tau_{xx}}{\partial x} - \frac{\partial \tau_{xy}}{\partial y} - \frac{\partial \tau_{xz}}{\partial z} = 0$$

$$\frac{\partial}{\partial t}(\rho v) + \frac{\partial}{\partial x}(\rho uv) + \frac{\partial}{\partial y}(\rho v^2) + \frac{\partial}{\partial z}(\rho vw) - 2\rho v\zeta \sin\Phi + \frac{\partial p}{\partial y} - \frac{\partial \tau_{xy}}{\partial x} - \frac{\partial \tau_{yy}}{\partial y} - \frac{\partial \tau_{yz}}{\partial z} = 0$$

$$\frac{\partial}{\partial t}(\rho w) + \frac{\partial}{\partial x}(\rho uw) + \frac{\partial}{\partial y}(\rho vw) + \frac{\partial}{\partial z}(\rho w^2) - \rho g + \frac{\partial p}{\partial z} - \frac{\partial \tau_{xz}}{\partial x} - \frac{\partial \tau_{yz}}{\partial y} - \frac{\partial \tau_{zz}}{\partial z} = 0$$

(3.1)

Where, u, v and w are the components of velocity in the x, y (planform) and z (vertical) directions, respectively; ρ = density of water; ζ = angular rotation of the earth; Φ = latitude; p = pressure; and, g = acceleration due to gravity (notation taken from Lane (1998)).

Although these equations can be solved in either one, two or three dimensions, two-dimensional solutions are of most relevance to the current study. One-dimensional models, which describe a river channel and floodplain as a series of cross sections, capture only a relatively small fraction of the active processes, while full three-dimensional solutions are difficult to construct in complex domains meaning that such models are relatively rare (Bates and De Roo, 2000; Horritt and Bates, 2001; Nelson et al., 2003).

Table 3.3 Key features of empirical (curve-extrapolation) and numerical (reductionist and reduced complexity) approaches to modelling.

	Empirical models (curve-extrapolation)	Reductionist models	Reduced complexity models
Key assumption	Stationarity of processes through time	Small-scale processes can be known and quantified	System behaviour can be represented by broad-scale approximations
Operational framework	N/A	Solution of partial differential equations	Rule-based
Representation of flow processes	No	Based on computational fluid dynamics	Cellular routing schemes
Incorporation of dynamic terrain adjustments?	No	Rarely; topographic adjustment too computationally demanding	Yes, although extent and success variable between models
Incorporation of extreme events?	No	Yes	Yes
Data requirements	Low; time series of variable to be predicted over a 'representative' timescale	Very high; high resolution terrain data and/or quantification of small-scale processes	Relatively low; terrain data (can be low resolution), sediment grain size, precipitation.
Computational demand	Low; solving regression equations	Very high; solving CFD equations	Intermediate; applying simple rules to the grid
Spatial scale of applicability	Large; dependent on extent of observed record	Short river reaches but can be catchment-scale if dynamic terrain adjustments omitted (e.g. SHETRAN)	Whole river catchments
Temporal scale of applicability	Unconstrained	Individual storm events but can be up to several decades if dynamic terrain adjustments omitted (e.g. SHETRAN)	Decades to millennia

Solution of the shallow water St Venant equations, which are derived from depth-integrating the Navier Stokes equations, in two dimensions (x and y) within computational fluid dynamics (CFD) models has traditionally underpinned numerical modelling studies of river channel hydraulics and hydrology (Brasington and Richards, 2007). This type of modelling approach has been particularly popular given its basis on fundamental equations which have been extensively validated in experiments (Bras et al., 2003; Keylock, 2007). The theory of water flow is relatively well understood at the small scale (Cox et al., 2005), and these two-dimensional solutions provide a high order representation of river hydraulics that is consistent with known processes (Bates and De Roo, 2000).

CFD models are often implemented at the reach-scale where they are primarily used for flood inundation modelling to inform floodplain management and flood risk assessment (Horritt et al., 2007; Van De Wiel et al., 2011). Model outputs have been shown to perform well when compared with inundation extents derived from remotely sensed data (e.g. Bates et al., 1997; Horritt and Bates, 2002), and the perception that such models are physically complete in the sense that their parameters have a physical meaning and can be measured in the field has led to the popularity of this modelling approach (Coulthard et al., 1998; Bathurst, 2002; Bras et al., 2003; Brasington and Richards, 2007).

The reductionist approach has also been applied at the catchment-scale and has led to the development of physically-based, spatially-distributed (PBSD) models which simulate hydrologic and sediment erosion processes for whole river basins (Abbott et al., 1986a; Takken et al., 1999). These models are physically-based because the various flow and transport processes are modelled either by finite difference equations of the partial differential equations of mass, momentum and energy conservation, or by empirical equations derived from experimental research (Bathurst, 2002). As well as benefiting from having theoretically measurable parameters, the physical basis of these models also means that parameter values can be specified for a future altered state of a basin so that the impacts of possible land use and climatic change can be simulated (Lukey et al., 2000; Bathurst, 2002).

Models that fall into the PBSD category include the SHE (Système Hydrologique Européen) (Abbott et al., 1986a; Abbott et al., 1986b) and its derivatives, (SHESED (Wicks and Bathurst, 1996), MIKE SHE (Refsgaard and Storm, 1995) and SHETRAN (Ewen et al., 2000; Bathurst, 2002)), ANSWERS (Areal Areal Non-point Source Watershed Environment Response Simulation) (e.g. Silburn and Connolly, 1995), WEPP (Water Erosion Prediction Project) (Nearing et al., 1989), EUROSEM (European Soil Erosion Model) (Morgan et al., 1998) and LISEM (Limburg Soil Erosion Model) (De Roo et al., 1996).

Of the PBSD models cited above, SHETRAN is the most comprehensive and sophisticated in that it not only simulates erosion by raindrop impact and overland flow, but it also provides a basis for simulating the sediment yield arising from gullying and landsliding (Ewen et al., 2000; Bathurst, 2002; Bathurst et al., 2004). Moreover, SHETRAN is able to simulate these processes for large river basins of up to 2,000 km^2, and for continuous periods (several decades), whereas ANSWERS, WEPP, EUROSEM and LISEM predominantly operate over much smaller spatial extents (<50 km^2) and on an event-scale. SHETRAN has also been extensively tested and has been shown to be a useful tool for predicting the impacts of changes in climate and land use on basin hydrology and sediment yield (e.g. Bathurst et al., 1996; Lukey et al., 2000; Bathurst et al., 2004; Bathurst et al., 2007).

However, SHETRAN and other similar PBSD models, suffer from a number of limitations. On a scale of complexity of hydrological models, this type of model lies at the extreme in terms of representation of physical processes (Parkin et al., 1996). Free surface flows, for instance, are modelled by a finite-difference solution of the St Venant equations, which are computationally demanding (Bathurst, 1986). Therefore, although SHETRAN is able to model large river basins, this requires a commensurate use of large grid cells which may be in the order of 500 m (e.g. Bathurst et al., 2007) to 1,350 m (e.g. Bathurst et al., 2006). Given the heavy computational requirements, Bathurst (2002) recommended that a maximum of 400 grid cells should be used for any given application of SHETRAN.

In applications of PBSD models, it is therefore necessary to lump up the small-scale physics to the larger model grid-scale (Beven, 1989). This lumping process has been described as a conceptual leap as it is necessary to assume that the same small-scale physical equations can be applied at the model grid-scale with the same parameters (Beven, 1989). However, there is no theoretical framework for carrying out this lumping, and there is no certainty that the equations will be the same at the grid-scale, nor that effective grid-scale parameters can be defined (Beven, 1989).

A further problem of PBSD models is their requirement of a large number of input parameters which are spatially and temporally variable (Bathurst, 1986; Takken et al., 1999; Bathurst, 2002). Quite often, data availability for the calibration of such parameters does not grow commensurately with increases in model complexity (Beven, 1996) and, unless small-scale processes are resolved with a high degree of accuracy, the large-scale interactions simulated in the model may not resemble those seen in nature (Murray, 2003). Specifically, when attempting to model systems with multiple, interacting processes operating over relatively large spatial and temporal scales, basing the model on the very small scales can lead to inaccurate predictions as inevitable imperfections in the small-scale model components can cascade up through the scales (Murray, 2007).

Moreover, the reductionist approach assumes that small-scale parameters are measurable in the first place. Bras et al. (2003), for instance, argue that parameters such as hydraulic conductivity, transmissivity, eddy viscosity, and roughness coefficients (e.g. Manning's n, Chezy C) are inherently unmeasurable. This data deficit leads to a situation of model over-parameterisation, and irresolvable uncertainties surrounding model outputs subsequently result (Beven, 1996; Beven, 2006).

Furthermore, although physically-based, spatially-distributed models such as SHETRAN are capable of simulating in detail a range of processes on a catchment scale, they often do not include a high-resolution representation of river and floodplain flow (Stewart et al., 1999). In the SHE and its derivatives,

for instance, the channel system is represented by a simple orthogonal system of stream links along the boundary of the grid squares (Abbott et al., 1986b; Bathurst, 1986; Bathurst, 2002).

Additionally, although sediment transport is represented within SHETRAN, the change in topography that would result from processes of erosion and deposition are not included (Wicks and Bathurst, 1996). This significantly hampers their ability to simulate geomorphological change and means that such models can provide only a snapshot of flow patterns at a specific time in the evolution of a river channel (Coulthard et al., 2007; Van De Wiel et al., 2011). Including geomorphological change would introduce the need to constantly re-size or re-define the mesh that represents channel topography which would create an additional computational overhead and reduce still further the spatial and temporal extent over which these models could be applied (Brasington and Richards, 2007; Coulthard et al., 2007).

3.4.2 Reduced complexity approaches to numerical modelling

Given the limitations of reductionist methods noted above, it is evident that a different approach is necessary for modelling at scales more pertinent to planning and management applications (Brasington and Richards, 2007; Coulthard et al., 2007). To this end, the development and application of reduced-complexity models that attempt to maximise understanding through emphasising simplicity has recently emerged as a significant research area in geomorphology (Nicholas and Quine, 2007).

Reduced complexity, or synthesist approaches contrast traditional reductionist techniques in that they aim to keep the model simple by removing as many processes as possible, or by merging their formulations in as few equations as possible (Van De Wiel et al., 2011). This approach is based on recognition that behaviour at a given level in a multi-scale system is dominated by only certain aspects of the dynamics at the level below, and that modelling should therefore only focus on those few key aspects of lower-level behaviour that actually matter (Paola, 2001). Specifically, only the effects that processes operating on

much smaller spatial and temporal scales have on the scale of interest are explicitly included in reduced complexity models (Murray, 2007).

Many reduced complexity models in geomorphology operate within a cellular framework and have evolved from earlier applications of cellular automata (CA) that were originally designed to study the formation of patterns resulting from simple, deterministic, local interactions (Murray, 2003; Brasington and Richards, 2007). The key features of CA as described by Wolfram (1984), such as the discretisation of time and space, are common to many numerical models in geomorphology.

However, it is the application of a set of laws or rules to the grid of cells, rather than physics-based parameterisations (Nicholas, 2005; Brasington and Richards, 2007; Coulthard et al., 2007; Van De Wiel et al., 2011), that distinguishes reduced-complexity cellular models from reductionist, CFD-based approaches. In this context, rules can be defined as hypothesised relationships based on less formal observations, theory, or experience that summarise the crucial dynamics of lower-level processes within a higher-level model (Paola, 2001; Murray, 2007). The development of such rules is necessary for modelling complex geomorphic systems involving a vast array of scales and processes for which an obvious set of equations based on conservation laws or analyses of smaller-scale processes is lacking (Murray, 2003; Doeschl-Wilson and Ashmore, 2005; Murray, 2007).

The braided river model of Murray and Paola (1994) is often seen as seminal in the recent development of reduced-complexity cellular models for fluvial geomorphology (Brasington and Richards, 2007). The Murray and Paola model was designed to identify the essential processes necessary to reproduce the main spatial and temporal features of braided rivers in an exploratory way. The success of the model, although later questioned by Doeschl-Wilson and Ashmore (2005), sparked a paradigm shift in the discipline by implying that the pursuit of reductionist approaches for the modelling of fluvial systems was not necessary for all modelling applications, and that models treating relatively simple, large-scale interactions could be more effective (Murray, 2007).

Later work (e.g. Coulthard et al., 2000; Thomas and Nicholas, 2002) built on the framework pioneered by Murray and Paola (1994) to develop their original exploratory model into a useful predictive tool (Murray, 2007). The advances in cellular approaches to modelling river form and process since Murray and Paola (1994) led Nicholas (2005, p. 645) to argue that the development of this technique, "represents one of the most important advances in fluvial geomorphology over the past decade".

Implementation of simplified equations and rules within reduced complexity cellular models significantly reduces computational overheads and therefore increases the speed of model operation (Brasington and Richards, 2007; Coulthard et al., 2007). This computational efficiency has two principal advantages. First, it facilitates modelling over 'useful' temporal and spatial scales, i.e. decades to centuries, and extended reaches to whole river basins (Thomas et al., 2007; Nicholas, 2009). Second, it allows for the incorporation of sediment erosion, transport and deposition by fluvial and hillslope processes as surface topography can be adjusted dynamically (Thomas and Nicholas, 2002; Coulthard et al., 2007; Tucker and Hancock, 2010; Hancock et al., 2011). The computational efficiency of reduced complexity approaches therefore provides a framework within which large catchments can be modelled holistically as coupled channel-hillslope systems, and in the context of both hydrologic and geomorphic change (Coulthard, 2001; Willgoose, 2005).

Reduced complexity, cellular models also minimise the potential propagation of errors from lower-level processes to higher-level phenomena and therefore address a significant criticism of reductionist approaches (Murray, 2003). By basing the model on large-scale interactions, observed effects which may not be captured by exact physical equations based on small-scale processes can be incorporated into the model (Doeschl-Wilson and Ashmore, 2005). In this sense, it has been suggested that empirically-based parameterisations of large-scale (general) interactions are likely to produce more numerically accurate model behaviour than parameterisations of smaller-scale (local) processes (Murray, 2003). Furthermore, the demand for high quality, high resolution data

to represent small-scale processes is also removed by formulating equations and rules at the landscape scale (Formann et al., 2007; Keylock, 2007), and this facilitates the use of reduced complexity models for a greater range of applications.

Importantly, the 'top-down' approach adopted by reduced complexity, cellular models (Murray, 2007) outlined above allows for the emergence of complex, large-scale phenomena (Dearing et al., 2006; Welsh et al., 2009) and nonlinear behaviour (Coulthard et al., 1998). The structure and operation of these models captures interactions between cells together with process-form feedbacks that control emergent properties and system response to external forcing over timescales of decades to centuries (Nicholas and Quine, 2007). Such feedbacks, as well as time-lags and -leads that result in the complex and nonlinear behaviour described by Schumm (1973; 1979; 1991), can rarely be identified through the use of reductionist models which do not explicitly allow for the evolution of emergent features (Werner, 1999; Dearing et al., 2006). Therefore, although the equations and rules used to represent relevant processes are simplified in reduced complexity models, the implementation of these equations may produce complex responses that cannot be predicted a priori (Nicholas, 2005).

Although reduced complexity, cellular models clearly have a number of features that make them well suited to simulating the long-term, catchment-scale evolution of fluvial systems, the approach is inevitably associated with certain limitations. The most significant of these relates to the simplified way in which processes are represented by approximations of the relevant physical principles rather than discretisation of the physics (Doeschl-Wilson and Ashmore, 2005; Nicholas, 2009). This has led to suggestions that reduced complexity approaches are less rigorous than reductionist models (Van De Wiel et al., 2011). The use of simple, quasi-physical rules (Brasington and Richards, 2007) is thought to introduce considerable uncertainty into the modelling process, and arguments for their use are generally heuristic owing to the lack of available evidence on which to justify their application (Keylock, 2007).

The problem of process representation is particularly pertinent to the modelling of flow hydraulics (Nicholas, 2009) where simple empirical equations and cellular routing schemes often fail to conserve fluid momentum or incorporate the terms for describing secondary circulation (Coulthard and Van De Wiel, 2006; Nicholas, 2009). Traditional, steepest-descent (e.g. Willgoose et al., 1991; Tucker and Slingerland, 1994), 'cascade' (e.g. Braun and Sambridge, 1997; Tucker et al., 2001)) or 'scanning' (e.g. Coulthard et al., 2000) flow-routing algorithms are limited in their ability to accurately represent the passage of a flood wave through a reach and, therefore, to generate realistic predictions of distributed flow and inundation patterns (Thomas and Nicholas, 2002; Coulthard et al., 2007). Inadequate representation of flow hydraulics could arguably be propagated into other model components, particularly at sub-width scales where bedload transport calculations are dependent on modelled patterns of variables such as boundary shear stress or specific stream power (Nicholas, 2009). Inaccuracies in this regard may result in unreliable rates of sedimentation and therefore unrealistic floodplain development (Coulthard et al., 2007).

3.5 SELECTION OF MODELLING APPROACH

3.5.1 Comparison of available modelling approaches in the context of the upper North Fork Toutle River catchment

Table 3.4 summarises the key features of the three available modelling techniques discussed in the preceding Sections (empirical, reductionist and reduced complexity) in relation to the requirements of the modelling problem in the upper North Fork Toutle River. Although process representation is clearly an issue in reduced-complexity modelling, this approach has numerous advantages over reductionist models in the context of generating long-term predictions of sediment production within and yield from the upper North Fork Toutle River. Specifically, greater computational efficiency increases the spatial and temporal scales over which reduced complexity models can operate. The reduced computational demand also facilitates the integration of hydrologic and geomorphic processes which is essential for the holistic assessment of catchment response to future climate change. Reduced

Table 3.4 Comparison of three available modelling techniques in the context of the requirements of research in the upper North Fork Toutle River.

Key requirement	Empirical models (curve-extrapolation)	Reductionist models	Reduced complexity models
Able to represent processes:			
Flow dynamics	✗	✓	✓
Sediment transport	✗	✓	✓
Channel-hillslope coupling	✗	✓	✓
Able to incorporate feedbacks, nonlinearity and complex response	✗	✗	✓
Able to operate over time periods of up to 100 years†	✓	✓ (e.g. SHETRAN)	✓
Able to operate on a catchment-scale (10^2 km^2)†	✓	✓ (e.g. SHETRAN)	✓
Conducive to multiple runs/scenarios†	✗	✓ (e.g. SHETRAN)	✓
Can be implemented with broad-scale secondary data sets	✓	✗	✓

†Reductionist models are only cable of operating over long temporal- and large spatial-scales if dynamic terrain adjustments are omitted and very large grid cells are used (e.g. SHETRAN).

complexity models are also less data intensive than reductionist approaches, and provide a framework for the evolution of emergent phenomena and nonlinear behaviours.

Moreover, it was stated in Simon and Klimetz (2012) that analysis of sediment production and subsequent yield from the upper North fork Toutle River must explicitly account for bank and terrace instability given that undercutting of terrace slopes and consequent mass failures continue to be important if not primary sources of sediment (Simon, 1992; Simon, 1999; Major et al., 2000). The use of reduced complexity models is arguably the only approach reviewed in this Chapter that is capable of accounting for such processes. It is increasingly acknowledged that this modelling approach can be used to inform broad management strategies relating to the response of catchments to environmental change in real-world landscapes (Brasington and Richards, 2007; Thomas et al., 2007), and consequently this methodology has been selected for use in the present study.

Of particular interest to this study is a group of reduced complexity models known as landscape evolution models. Although no clear definition of landscape evolution models is available from the current literature (Temme et al., 2011), they can be broadly considered as computer models that predict or simulate the three-dimensional development of landscapes through time (Kirkby, 1971; Ahnert, 1976). As such, these models commonly permit the effect of multiple geomorphic processes that contribute to the redistribution of mass within a catchment to be integrated together over complex topographic surfaces and extended periods of time (Pazzaglia, 2003; Martin and Church, 2004).

Landscape evolution models aim to represent the principal erosion processes operating in a catchment, which are broadly grouped into those affecting hillslopes and those operating in stream channels (Swanson et al., 1982), as shown in Figure 3.4 and discussed in detail below. In some cases, bedrock weathering and flexural isostatic uplift in response to denudation are also included (e.g. Tucker and Slingerland, 1994), although such processes are not

considered relevant over the timescales considered in the present study. Landscape evolution models mathematically describe these processes, link the mathematical descriptions together and, through many iterations of solving the equations, predict changes in cell height that mimic real time-dependent changes in landscape elevation and relief (Pazzaglia, 2003).

Hillslope processes, which play an important role in transporting material to the channel and making it accessible to fluvial processes (Bryan, 2000), include surface erosion by sheetwash and raindrop splash, soil creep, and landslides and slumps (Swanson et al., 1982; Leopold, 1994; Bryan, 2000; Aksoy and Kavvas, 2005; Kinnell, 2005). Typically, landscape evolution models collapse surface erosion and soil creep processes into one mathematical equation that treats them collectively as diffusion (Tucker and Slingerland, 1994; Pazzaglia, 2003; Coulthard and Van De Wiel, 2007), with the rate of the process characterised by a single number. This simplification is necessitated by the complexity of the processes and interactions involved in soil erodibility, which cannot readily be represented within a physically-based model (Bryan, 2000; Kinnell, 2005). Similarly, landscape evolution models commonly represent landslides by assigning a simple threshold slope angle below which sediment is transported by diffusion, and above which sediment is transported by landslides until the slope diminishes to the threshold angle (Kirkby, 1984).

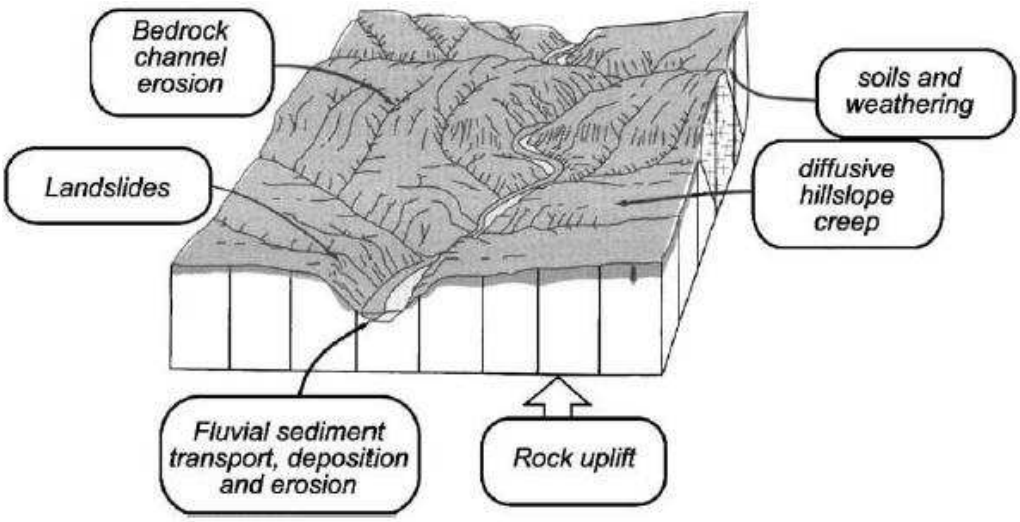

Figure 3.4 Schematic showing the principal processes that are represented mathematically in landscape evolution models. Taken from Pazzaglia (2003).

Channel processes typically represented by landscape evolution models include the lateral and vertical cutting of the stream bed and banks in alluvial channels, and the subsequent transport of eroded material as either suspended load or bedload, and stream incision into bedrock (Swanson et al., 1982; Pazzaglia, 2003). Channel processes are particularly important where terrace remnants present high banks to a channel moving laterally against them. When a river erodes a terrace that stands above the floodplain, the volume of sediment eroded per unit of lateral erosion is proportional to the height of the terrace. As such, a substantially larger volume of sediment is produced than that involved in the usual trading of material between cut bank and point bar during meander development (Leopold, 1994).

The calculation of channel processes relies on the routing of surface water through the drainage network, which is another important process common to all landscape evolution models. Both channel processes and flow routing are discussed in more detail in sub-section 3.5.2 below, as the sophistication and level of detail with which such processes are represented within contemporary landscape evolution models vary substantially.

3.5.2 Assessment of available reduced complexity landscape evolution models

The CAESAR-Lisflood landscape evolution model, referred to hereafter as C-L, has been selected as the most suitable of the currently available reduced complexity models for simulating landscape evolution in, and sediment delivery to the SRS from, the upper North Fork Toutle River catchment. While the operation and development of C-L is described in greater detail in Chapter 4, the following sub-sections summarise the key features of the model and justify its selection for the current study.

C-L is one of a suite of reduced complexity cellular models that have been developed since the original paper by Murray and Paola (1994) and that include SIBERIA (Willgoose et al., 1991), GOLEM (Tucker and Slingerland, 1994), CHILD (Tucker et al., 2001) and CASCADE (Braun and Sambridge, 1997) as reviewed by Coulthard (2001) and discussed by Fleurant et al. (2008).

In the remainder of this Chapter, these models are compared in terms of their representation of flow dynamics, sediment transport and fluvial processes, and climate. This comparison is also summarised in Table 3.5.

i. Flow dynamics

As discussed in Section 3.4, the representation of processes in reduced complexity numerical modelling, specifically flow dynamics and hydraulic routing, is a key criticism of this type of modelling approach. Such a criticism is particularly applicable to SIBERIA, GOLEM, CASCADE and CHILD which use highly simplified cellular routing schemes to simulate the flow of water across the grid (Table 3.5). Weaknesses include the steepest descent and cascade algorithms which involve moving volumes of water between adjacent cells based on elevation differences. The latest release of C-L (Coulthard et al., 2013), on the other hand, now integrates the newly developed LISFLOOD-FP equations, which were developed by Bates et al. (2010) for hydraulic routing and flood inundation modelling. LISFLOOD-FP is a raster-based, storage cell model within which each cell of the raster grid represents a storage compartment, and the mass balance for each cell is updated at each time step according to the fluxes of water into and out of each cell (Bates et al., 2010).

The LISFLOOD-FP equations are based on the momentum equation from the one-dimensional St Venant shallow water equations (shown in equation 3.2, below, taken from Bates et al. (2010)) and are designed to be solved explicitly at very low computational cost (Bates et al., 2010).

$$\frac{\partial Q}{\partial t} + \frac{\partial}{\partial x}\left[\frac{Q^2}{A}\right] + \frac{gA\partial(h+z)}{\partial x} + \frac{gn^2Q^2}{R^{4/3}A} = 0 \tag{3.2}$$

Where, Q = discharge ($m^3\ s^{-1}$); t = time (s); A = flow cross-sectional area (m^2); h = flow depth (m); z = bed elevation (m); R = hydraulic radius (m); g = acceleration due to gravity ($m\ s^{-2}$); and, n = Manning's friction coefficient.

Table 3.5 Comparison of five contemporary reduced complexity landscape evolution models indicating relevant landscape attributes represented.

	SIBERIA	GOLEM	CASCADE	CHILD	CAESAR-Lisflood
Surface erosion	Diffusion-type equation	Diffusion-type equation	Diffusion-type equation	Diffusion-type equation	Diffusion-type equation
Landsliding	No explicit representation	Slope failure threshold	No explicit representation	No explicit representation	Slope failure threshold
Erosion/deposition by channelled flow?	Yes	Yes	Yes	Yes	Yes
Flow routing algorithm	Steepest descent	Steepest descent	Cascade	Steepest descent	LISFLOOD-FP
Sediment transport equation	General sediment transport function	General sediment transport function	General sediment transport function	Einstein (1950)	Einstein (1950) or Wilcock and Crowe (2003)
Number of grain sizes	One	One	One	Two (sand and gravel)	Nine (based on size distribution)
Suspended sediment?	No	No	No	No	Yes
Inclusion of meandering and braiding?	Neither	Neither	Neither	Meandering only	Meandering and braiding
Representation of rainfall regime	Runoff constant	Runoff constant	Runoff constant	Sequence of discrete storm events	Hourly rainfall or discharge time series

Importantly, the LISFLOOD-FP equations include the inertial term from the St Venant equations which gives the water being modelled some mass (Bates et al., 2010). More details of the LISFLOOD-FP component of the C-L model are given in Chapter 4. The addition of mass via the inertial term is a key aspect of flow physics and therefore facilitates improved representation of shallow water wave propagation and floodplain inundation (Hunter et al., 2008). This is a significant benefit of C-L in comparison to other available reduced complexity models and is an important reason for the selection of C-L in this study. Inclusion of the inertial term also enables the use of much longer time steps than was possible with previous storage cell models (Bates et al., 2010) which improves computational efficiency and reduces run times.

ii. Sediment transport

Although most cellular models integrate erosion and deposition to some extent, this is often carried out in a rather basic way (Coulthard et al., 2007). For instance, SIBERIA, GOLEM and CASCADE are essentially based on a simplified relationship derived from the Einstein (1950) equation that implies that sediment transport rate increases with water discharge and slope (Henderson, 1966; Tucker and Slingerland, 1994). Within these models this relationship takes the general form:

$$q_s = \beta_1 Q^{m_1} S^{n_1} \tag{3.3}$$

where q_s = sediment transport rate per unit width ($m^3\ s^{-1}\ m^{-1}$ width); Q = water discharge per unit width ($m^3\ s^{-1}\ m^{-1}$ width); S = slope ($m\ m^{-1}$); and β_1, m_1 and n_1 are parameters (notation taken from Hancock and Willgoose, 2002).

The values of m_1 and n_1 are both set equal to 1 in GOLEM and CASCADE implying a linear relationship (Tucker and Slingerland, 1994; Braun and Sambridge, 1997), while in SIBERIA these parameters require calibration and the model therefore allows both linear and nonlinear relationships (Willgoose et al., 1991). The parameter β_1 is calibrated in all three models and represents a 'sediment transport coefficient' (Tucker and Slingerland, 1994) or a 'stream

erosion constant' (Braun and Sambridge, 1997) that controls the rate of erosion and can be scaled to match the observed erosion rate (Hancock and Willgoose, 2002).

The value of q_s calculated from equation 3.3 is used to determine the mass balance of each cell. On the basis of this calculation, the elevation of an individual cell can be adjusted and this adjustment represents the erosion or deposition of sediment within that cell (Tucker and Slingerland, 1994; Braun and Sambridge, 1997). The exact implementation of this equation for the calculation of sediment fluxes into and out of individual cells varies between models, although the simplicity of this approach is clear. The relationship is based on a number of severe approximations (Henderson, 1966) and does not include a consideration of multiple sediment-size fractions (Willgoose, 2005).

CHILD, however, utilises the complete (non-simplified) Einstein (1950) transport equation to model sediment erosion and deposition. Furthermore, representation of size-selective erosion and deposition is improved in CHILD through the use of a two-fraction (sand and gravel) approach based on Wilcock (1998), rather than treating the bed as a single size fraction (Tucker et al., 2001). A two-fraction estimate allows sand and gravel to move at different rates (Wilcock, 1998), but cannot be used for the prediction of phenomena such as bed armouring for which differences between size-related, gravel transport rates are important (Wilcock, 2001).

The most comprehensive representation of sediment heterogeneity, however, is achieved by C-L which models the erosion, transport and deposition of nine grain size fractions using either the complete (non-simplified) Einstein (1950) or Wilcock and Crowe (2003) transport equations, embedded within a three-dimensional active-layer system (Coulthard and Van De Wiel, 2007; Van De Wiel et al., 2007; Hancock et al., 2011). This detailed representation of fluvial erosion and deposition is a key advantage of C-L over other models and will be discussed further in Chapter 4. Calibration of the erosion model used within C-L is also far simpler than it is for other models (particularly SIBERIA), as it requires only a sediment size distribution, which is easy to obtain in the field.

Although the inevitable, point specific nature of the collected data is a potential problem for the representation of catchment-scale sediment transport rates (Hancock et al., 2010), the reduced data demand makes C-L far more applicable than, for instance, SIBERIA to the current study.

iii. Reach-scale fluvial processes

Of the five reduced complexity landscape evolution models considered here, only C-L and CHILD include explicit representations of local-scale geomorphic (channel) processes; specifically, lateral erosion and meandering. Although both C-L and CHILD incorporate meander models, the steepest descent flow routing algorithm employed by CHILD prevents the development of braiding. C-L, on the other hand, combines a meander model, which is described in Coulthard and Van De Wiel (2006) and will be discussed further in Chapter 4, with a discharge routing model that is able to produce both divergent and convergent flow. C-L therefore enables both meandering and braiding to be modelled simultaneously (Coulthard and Van De Wiel, 2006). This capability represents a notable advancement in reduced complexity fluvial modelling and facilitates far more detailed investigations of channel development, which can be useful in understanding processes of future landscape evolution. Moreover, unlike SIBERIA, GOLEM, CASCADE and CHILD, C-L includes suspended sediment within the sediment transport model, which facilitates much better representation of floodplain alluviation and the development of natural levees (Coulthard et al., 2007; Van De Wiel et al., 2007).

iv. Climate

Representation of climate, specifically the precipitation regime of the study catchment, within models such as SIBERIA, GOLEM and CASCADE was also found to be unsatisfactory and inappropriate for the current application. In order to facilitate long-term modelling of landscape change, these models utilise a steady, or geomorphologically effective, runoff coefficient that is designed to encapsulate the average effect of many floods over many years (Tucker and Bras, 2000). This approach fails to account for a number of factors

that are important in the development of fluvial landscapes, including specifically: the influence of intrinsic climate variability on erosion and sedimentation rates (Tucker and Bras, 2000); and the emergence of stochastic dynamics when a spectrum of events of varying magnitude and frequency acts in the presence of geomorphic and hydrologic thresholds (Tucker et al., 2001).

These limitations have been addressed in part by CHILD which models rainfall as a series of discrete random storm events which have a constant intensity throughout their duration (Tucker and Bras, 2000; Tucker et al., 2001). Representation of catchment hydrology is further enhanced in C-L because the model directly implements an hourly rainfall record (Coulthard et al., 2002) and can, therefore, capture the series of discrete storm events that drive landscape evolution. Although the use of mean discharge via runoff coefficients in models such as SIBERIA, GOLEM and CASCADE reduces computational demand and facilitates modelling over longer timescales (10^3-10^4 years), it means that processes are time-averaged and the effect of an individual flood event may be lost (Coulthard and Van De Wiel, 2012). Given that such events may be important over the timescales of the modelling application in the upper North Fork Toutle River catchment, the use of a model which incorporates daily or sub-daily precipitation data, such as C-L, is clearly beneficial.

3.6 SUMMARY

The selection of preferred solution(s) to the long-term sediment management problem in the Toutle-Cowlitz River system is dependent on estimates of future sediment yields and, particularly, on the rate at which sediment yield from the upper North Fork Toutle River will relax back towards its pre-disturbance value. Previous studies (WEST, 2002; Biedenharn Group, 2010; Simon and Klimetz, 2012) have attempted to make such estimates on the basis of hindcasting to derive empirical trends from observed data and extrapolating those trends into the future. However, these studies have been unable to agree on either the volume or, more importantly, the temporal trends in annual sediment yield to the end of the project planning period in 2035 and beyond.

It was argued in Section 3.3 that this lack of consensus, which has hindered effective decision-making regarding long-term sediment management, is likely to be the result of deficiencies in the curve-extrapolation techniques employed in these studies. Such deficiencies include: the reliance on historical data which can be inadequate, incomplete and naturally variable; the inherent assumption of driver and process stationarity; and the lack of process representation. It was subsequently proposed in Section 3.4 that numerical modelling, which does not depend on the interpretation of historical data to the same extent as curve extrapolation techniques, could be used as an alternative approach to making quantitative predictions of sediment yield from the upper North Fork Toutle River.

Two broad approaches to numerical modelling in geomorphology were identified, and these can be distinguished on the basis of the complexity with which processes are represented within the model. Reductionist models aim to reproduce the behaviour of natural systems as accurately as possible by focusing on small-scale processes and minimising simplification of the fundamental governing equations. This is a popular approach given its use of fundamental equations which have been extensively validated in experiments. However, reductionist models suffer from heavy computational requirements which restrict the spatial and temporal scales at which they can be applied, and/or necessitate the use of excessively large grid cells. Such models also require highly accurate data to define a large number of input parameters. These data are not available in many cases and may be disproportionately expensive or infeasible to collect, while it has been argued that some of the parameters that require definition are inherently immeasurable.

Reduced complexity models, on the other hand, take a ‘top-down’ approach whereby only the effects that small-scale processes have on the scale of interest are explicitly included. These models therefore remove as many processes as possible or merge their formulations into a small number of equations which are then implemented as rules in a cellular automaton (CA) framework. Although this approach has been criticised for being less physically rigorous than reductionist techniques, it is computationally more efficient and facilitates

modelling over time and space scales that are more relevant to planning and management problems. Moreover, sediment erosion, transport and deposition can be incorporated and surface topography adjusted dynamically. This allows for the emergence of complex, nonlinear behaviours that are a feature of fluvial geomorphic systems.

Following an analysis of the three approaches in the context of the upper North Fork Toutle River (sub-section 3.5.1), reduced complexity modelling was selected as the preferred approach. The key features of a range of available reduced complexity models were then discussed (sub-section 3.5.2), and it became apparent from that discussion that C-L includes the most sophisticated representation of flow hydraulics, the most detailed model of fluvial erosion and deposition (including multiple grain sizes, lateral erosion and suspended sediment) and the most comprehensive representation of catchment hydrology relative to other reduced complexity cellular models. Although C-L may suffer from slightly reduced computational efficiency and therefore increased run times in comparison to less detailed models such as SIBERIA (Hancock et al., 2010), the processing time remains sufficiently short to facilitate modelling over long temporal and large spatial-scales.

C-L has also been shown to demonstrate the complex, non-linear behaviour of fluvial systems (e.g. Coulthard et al., 1998; Coulthard and Van De Wiel, 2007) that plays an important role in long-term landscape development. For these reasons, C-L has been selected as the preferred modelling approach for making long-term predictions of erosion and sediment yield from the North Fork Toutle River. However, C-L, like other reduced complexity models, has rarely been applied to inform options appraisal with regard to sediment management alternatives, and the current study therefore provides a unique opportunity to test the capabilities of the model in this context.

CHAPTER 4 CAESAR-LISFLOOD: MODEL OPERATION, DATA REQUIREMENTS AND SET UP

4.1 INTRODUCTION

This Chapter describes the operation of the C-L model and outlines the algorithms used to determine discharge, route flow between cells and calculate the transport of sediment by fluvial and hillslope processes. Concurrently, data requirements are summarised and the availability of these requisite data sets for hindcasting in the upper North Fork Toutle River catchment is described. Next, key model parameters are introduced, explained and, where possible, values appropriate to the current application are specified. Concurrently, the implications of the algorithms used by the model for process-representation are considered throughout the Chapter. Figure 4.1 presents a simplified schematic representation of the model's operational framework.

C-L has undergone continuous development since it was first released in the late-1990s, and some of the most significant updates occurred in 2011 and 2012 with the integration of the LISFLOOD-FP code and improvements to the lateral erosion algorithm. Seven different versions of the model were released during this two-year period as errors were reported and subsequently corrected. These updates are summarised in Table 4.1. Errors in the algorithms used to calculate sediment transport were common to the first six versions of the model released between August 20, 2011 and May 31, 2012. These errors were fully resolved only in the most recent version (1.2x), released October 10, 2012 and this version was, therefore, used to conduct all model runs described in the remainder of this thesis.

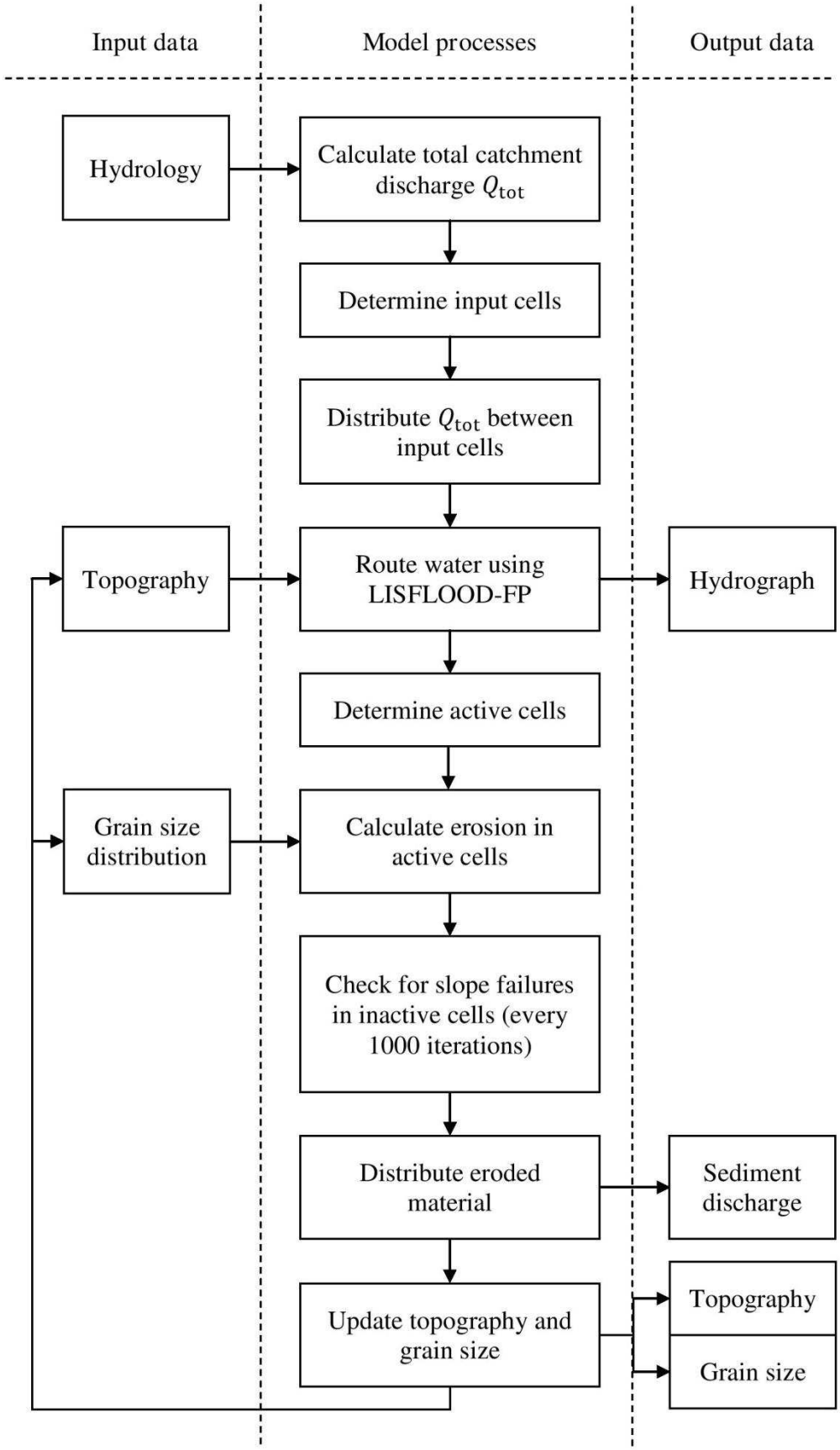

Figure 4.1 Schematic representation of C-L model operation.

Table 4.1 Updates to the C-L model made between August 2011 and October 2012. Information taken from Coulthard (2013).

Release date	**Version**	**Description of key modifications**
20/08/2011	1.0	Integration of the LISFLOOD-FP hydrodynamic flow code.
07/10/2011	1.1a	Flow routing between cells extended from four- to eight-directional to include diagonals. Inclusion of the N_{shift} parameter for the calculation of lateral erosion (see Section 4.4.1). Fix to error in the calculation of suspended sediment transportation and deposition.
20/10/2011	1.1d	Additional fix to error in the calculation of suspended sediment transportation and deposition.
21/05/2012	1.2n	Flow routing between cells limited to four-directional to prevent volumetric errors and to enhance model efficiency. Fix to error in the calculation of sediment transportation and deposition. Lateral erosion calculated according to shear stress to improve grid cell size independence. This is a significant update and required alterations to the value of Λ (see Section 4.4.1). Inclusion of $\Delta\nabla_{\text{max}}$ parameter (see Section 4.4.1).
22/05/2012	1.2o	Inclusion of a user-specified maximum Froude number to limit flow between cells (see Section 4.3.1).
31/05/2012	1.2q	Fix to error in lateral erosion algorithm which required further alterations to the value of Λ.
10/10/2012	1.2x	Fix to error in the calculation of D_{50} for the Wilcock and Crowe transport equation which impacted the volume and spatial distribution of erosion and deposition.

4.2 TERRAIN REPRESENTATION

4.2.1 Data requirements and availability

As discussed in Chapter 3, numerical models discretise physical space into a grid or mesh consisting of a finite number of points (Bathurst, 1986; Murray and Paola, 1994; Lane et al., 2004; Van De Wiel et al., 2011). The structure of this mesh varies depending on model structure and operation, with some models using triangulated irregular networks (TINs) in an attempt to improve computational efficiency (Van De Wiel et al., 2011). C-L, however, represents catchment topography using a regularly gridded, raster, digital elevation model (DEM), with model operation instead optimised temporally (see Sections 4.3 and 4.4).

Since the eruption of Mount St Helens in May 1980, the North Fork Toutle River valley has been the subject of a number of topographic mapping efforts as well as aerial reconnaissance missions that have acquired either stereoscopic photography or LiDAR data. DEMs derived from each of these data sources were obtained from the USACE Portland District and the USGS Cascades Volcano Observatory, for the post-eruption years 1980, 1987, 1999, 2003, 2006, 2007 and 2009 (Table 4.2).

However, the spatial resolutions and aerial extents of these surfaces are highly varied, with few covering the entire catchment area of the North Fork Toutle River (Figure 4.2). All of the DEMs, with the exception of the one derived from aerial LiDAR surveys conducted in September and October 2003, exclude significant areas of the headwater catchments (Loowit and Step Creeks) as well as providing only partial coverage of the catchments of Castle and Coldwater Creeks. Given that the 2003 DEM provides full coverage of the catchment above the confluence of Castle and Coldwater Creeks, it is the only surface that can be used for catchment-scale modelling within C-L. Consequently, the start of the model hindcasting period (see Chapter 5) was defined as October 1, 2003.

Table 4.2 Available digital terrain data for the North Fork Toutle River catchment obtained from the USACE Portland District and USGS CVO. Adapted from Simon and Klimetz (2012, p. 36).

Year	Acquisition dates	Collection method	Grid size (m)
2009	September 16-20	Aerial LiDAR	1
2007	October 22-27	Aerial LiDAR	1
2006	October 21	Aerial LiDAR	1
2003	September 19 to October 2	Aerial LiDAR	3
1999	Unknown	Aerial Photography	3
1987	April 27, June 6 & 11	Aerial Photography	3
1980	May 18	7.5-minute USGS Topographic Quad	5

4.2.2 Data preparation

i. Catchment boundary delineation

The boundary of the North Fork Toutle River catchment upstream of the N1 dam was defined using the Watershed Tool in the ArcMap Spatial Analyst Toolbox. The defined catchment area was clipped to remove the drainage basins of Spirit, Castle and Coldwater Lakes. Following delineation of the catchment and the removal of the lakes, the area of the DEM to be included within C-L was approximately 161 km^2 (Figure 4.3). Although lakes can be included within C-L, modelling the routing of water through large water bodies is computationally demanding and requires substantially different parameters from those used for in-channel flow. Furthermore, representing changes in lake level and therefore discharge output is difficult, particularly given that the outlets of all the lakes within the North Fork Toutle River catchment are ungauged. These practical constraints necessitated the removal of lake sub-catchments from the modelled area. Given that lakes are not significant sources of sediment, their removal does not make a considerable difference

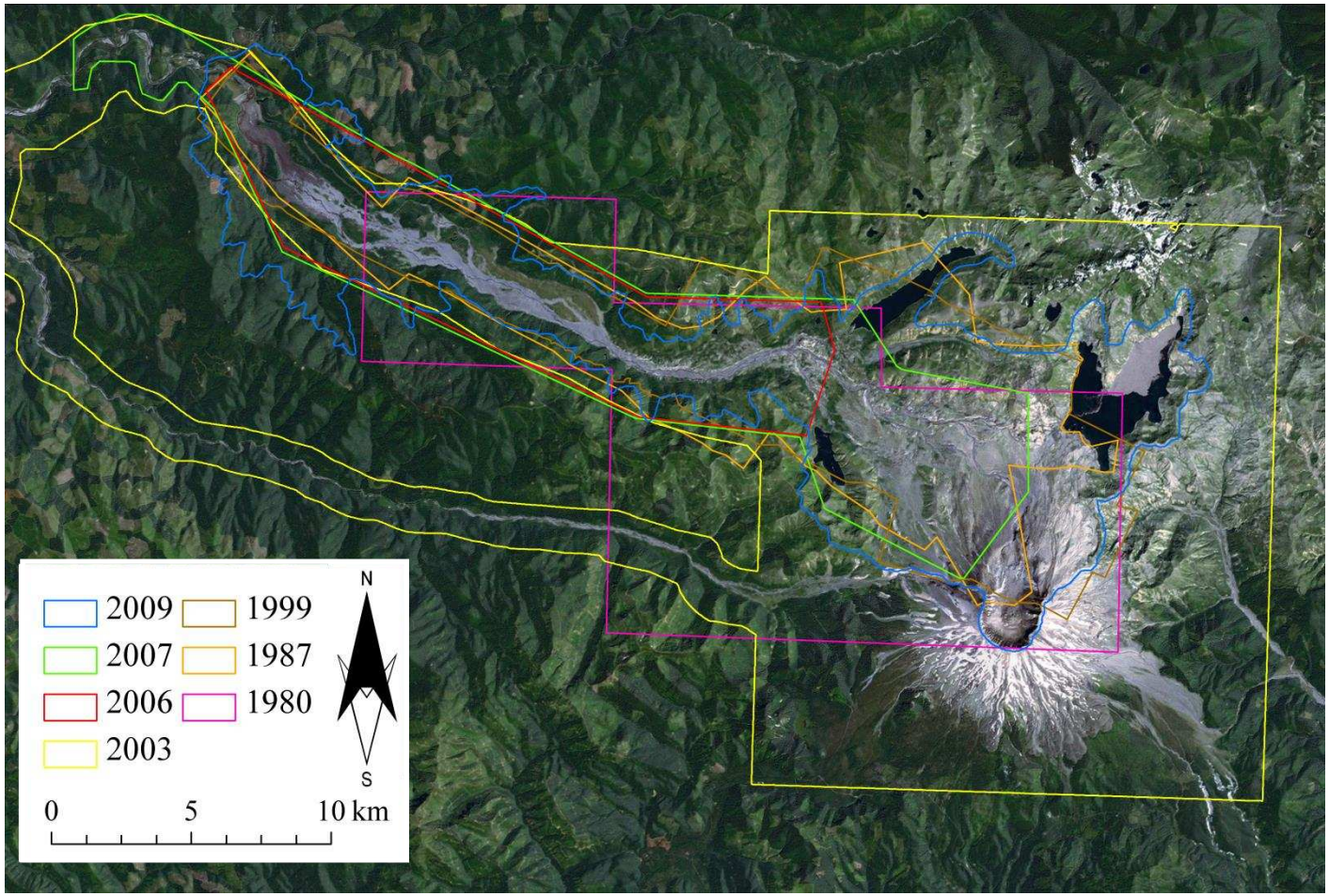

Figure 4.2 Spatial extents of digital terrain data sets collected since 1980. Aerial imagery from DigitalGlobe (Microsoft).

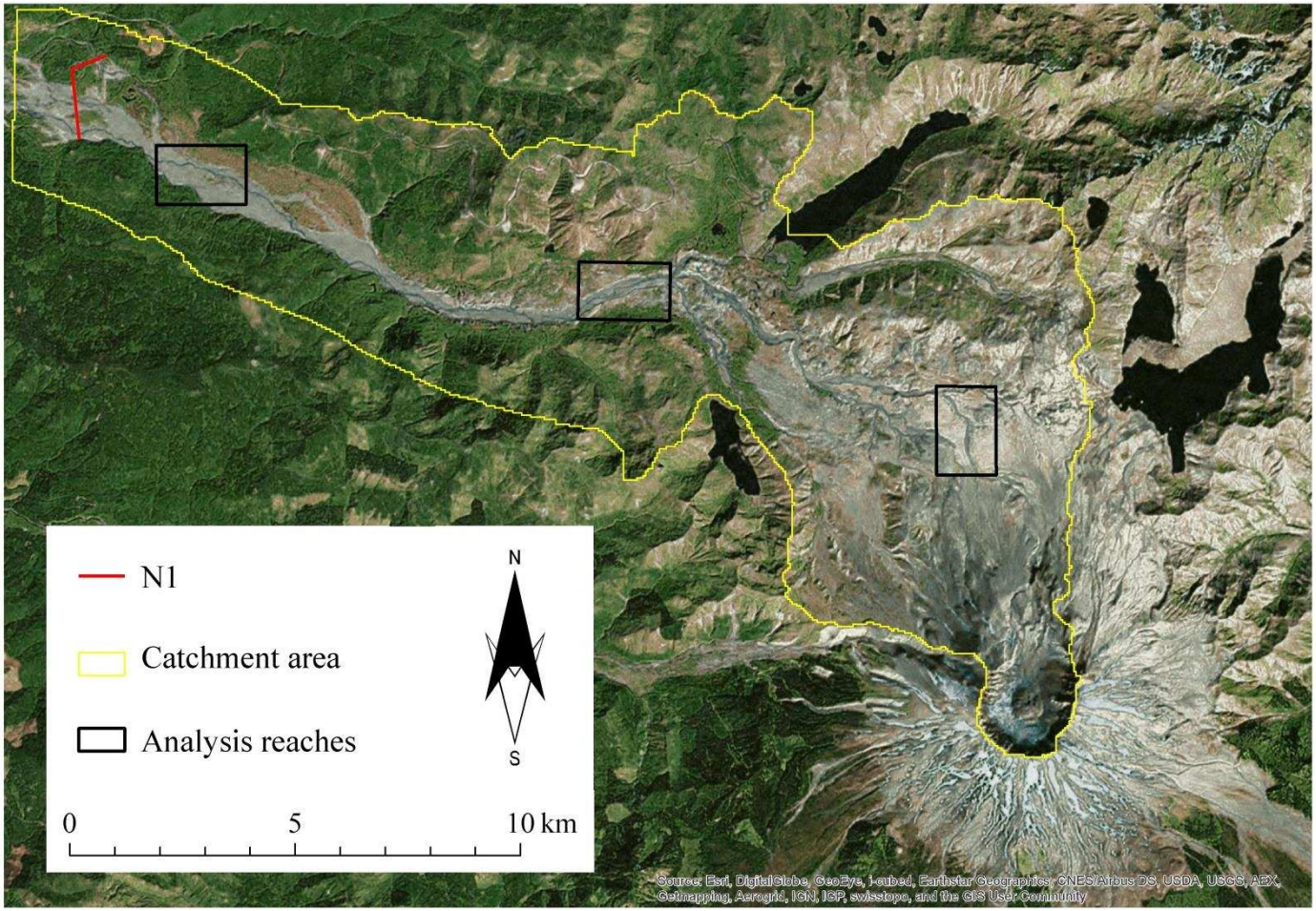

Figure 4.3 Area of the upper North Fork Toutle River catchment included in the C-L model. Reaches used for terrain analysis are also shown. Aerial imagery from DigitalGlobe (Microsoft).

to the model outcomes relevant to this application. Moreover, the modulating influence that the lakes have on the catchment hydrograph is represented by the use of a discharge record rather than a local precipitation record to drive catchment hydrology in the model, as described in Section 4.3.

ii. DEM horizontal resolution

The horizontal resolution of the 2003 raster delivered by the USGS Cascades Volcano Observatory is 3 m (Table 4.2), meaning that the catchment area delineated in Figure 4.3 was composed of almost 18 million individual cells. As C-L run time is proportional to the number of cells, it was necessary to reduce the resolution of the DEM in order to ensure that model run times did not place an unreasonable limit on either the number of simulations that could be carried out for model calibration and forecasting, or the period (in model years) for which future simulations could be conducted. Moreover, running C-L with the original 3 m DEM, which was approximately 175 megabytes in size, would exceed the memory capacity of the computers available for this doctoral research project. C-L operation is particularly memory-intensive as multiple arrays are generated during runtime that hold data calculated by the model, such as elevation, grain size and discharge, and are stored in RAM (random access memory) (Coulthard, 2013).

The DEM was therefore resampled (using the Resample Tool in the ArcMap Data Management Toolbox) to a resolution of 50 m, which reduced the number of cells to 64,308 and file size to approximately 1.2 megabytes. Although it must be noted that this reduction in resolution was essential given the large catchment area, the time periods over which modelling was to be conducted and the computer resources available, the potential implications of using a 50 m DEM rather than a 3 m DEM for terrain representation within C-L should be considered. To this end, the surfaces modelled by the two resolutions were analysed in two ways using the Spatial Analyst Toolbox in ArcMap.

First, hillshades of the catchment were produced using the 3 m and 50 m DEMs (Figure 4.4) to provide a visual comparison of the terrain as represented by the two resolutions. Second, slope maps of the catchment calculated form

the two DEMs are shown in Figure 4.5 in order to illustrate the extent to which topographic features are smoothed by increasing the grid cell size from 3 m to 50 m. The catchment-scale slope maps are supplemented by three additional reach-scale maps (Figures 4.6 to 4.8) that show how slope angles in the vicinity of river channels differ between the two resolutions. These three reaches are located in the upper, middle and lower parts of the catchment, respectively, as shown in Figure 4.3. Additionally, the 3 m and 50 m DEMs were clipped to the extent of these three reaches and used as terrain input for six C-L models which were run in order to demonstrate how in-channel flow is represented by the two resolutions. The outputs from these models are shown in Figures 4.9 to 4.11.

As described in Section 2.3, post-eruption channel response in the upper North Fork Toutle River catchment was dominated by large-scale incision and widening that created a network of canyons typically tens of metres deep and several hundreds of metres wide. Although these canyons are commonly narrower in catchment headwaters than they are farther downstream, widths still generally exceed 50 m in these upstream locations. Photographs of the three reaches used for the detailed slope and channel analyses are presented in Figure 4.12 to illustrate the topography. Lateral erosion of the walls of these canyons and mining of the wide canyon floors by fluvial processes are the primary drivers of elevated sediment yields from the upper North Fork Toutle River catchment (e.g. Major et al., 2000; Major, 2004). It is therefore important that these canyons are represented by the terrain data used in C-L.

The catchment-scale hillshade and slope maps presented in Figures 4.4 and 4.5 show that although some of the finer-scale detail is inevitably lost by reducing the resolution from 3 m to 50 m, the key topographic features remain well-resolved. Specifically, the canyon network is clearly visible at both resolutions indicating that a sufficient level of detail is retained by the 50 m DEM so that canyon walls are adequately represented. The reach-scale slope maps (Figures 4.6 to 4.8) further emphasise the loss of local-scale detail in the more coarse DEM, but again the canyon walls are clearly visible, albeit somewhat smoothed in comparison with the 3 m DEM. For instance, it is evident that the maximum slope angle is generally much lower in the coarser resolution maps,

(a)

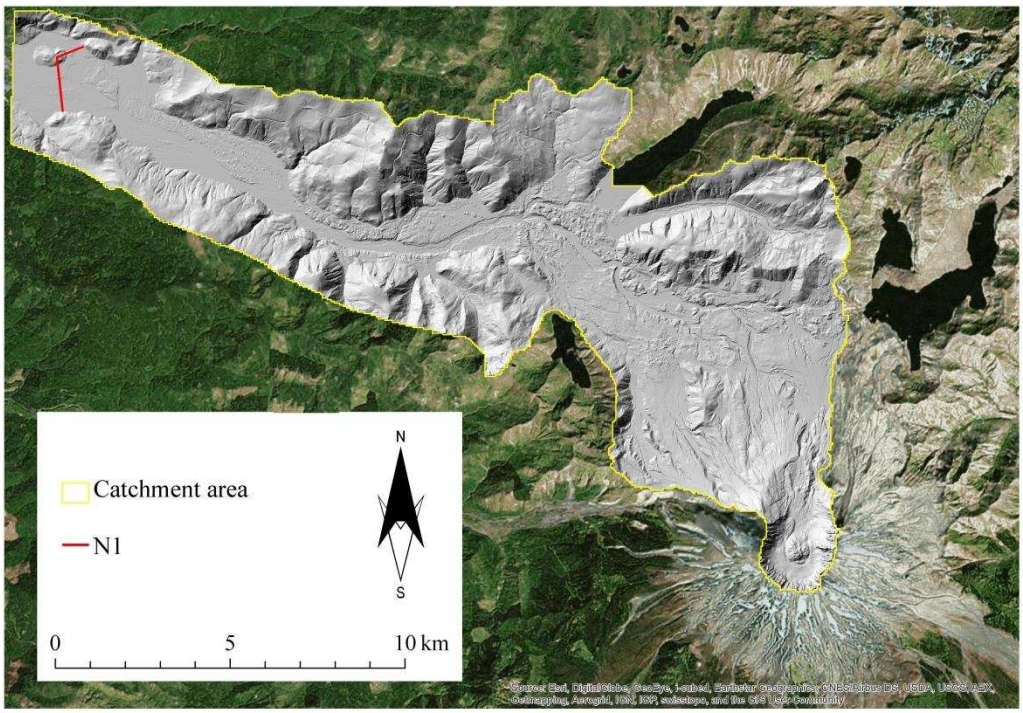

(b)

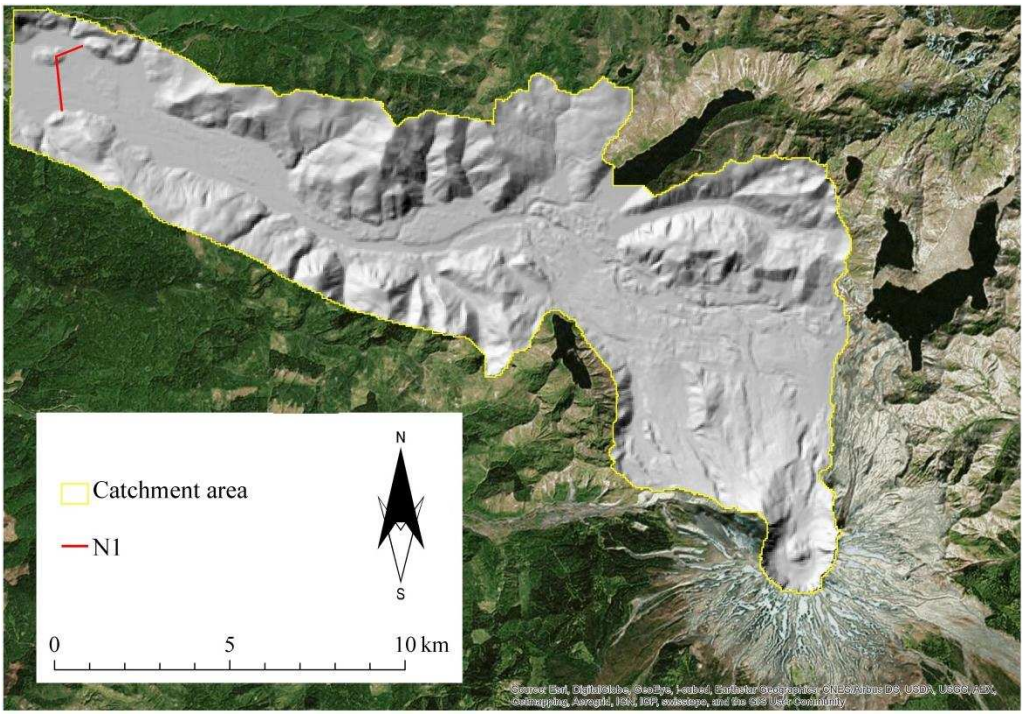

Figure 4.4 Hillshades of the area of the upper North Fork Toutle River included in the C-L model derived from the 3 m (a) and 50 m (b) DEMs.

(a)

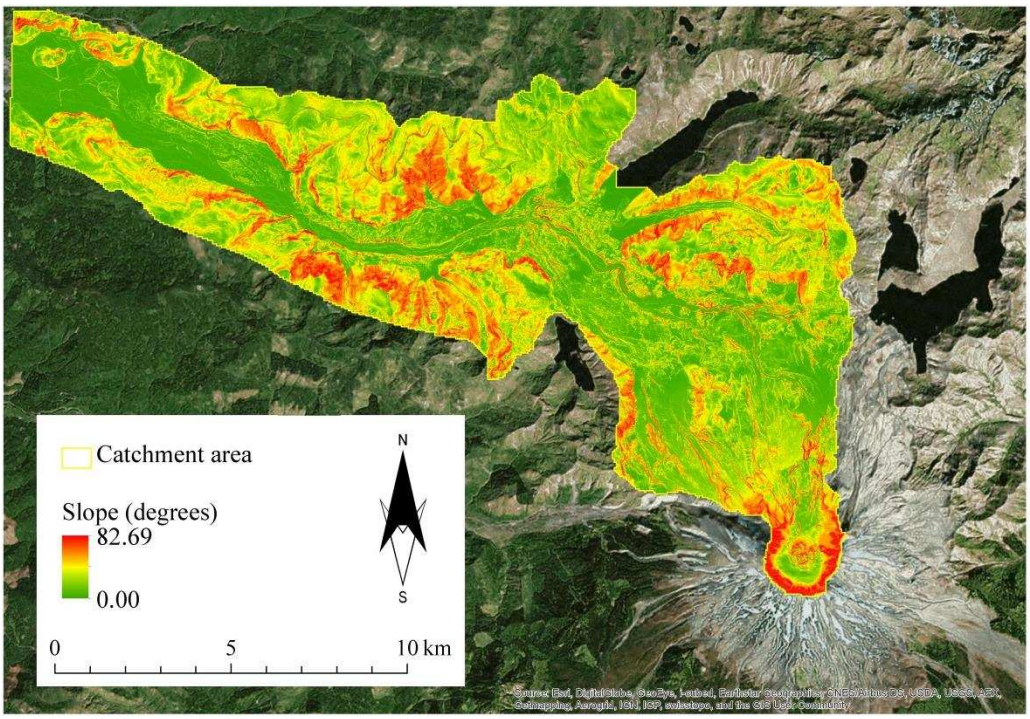

(b)

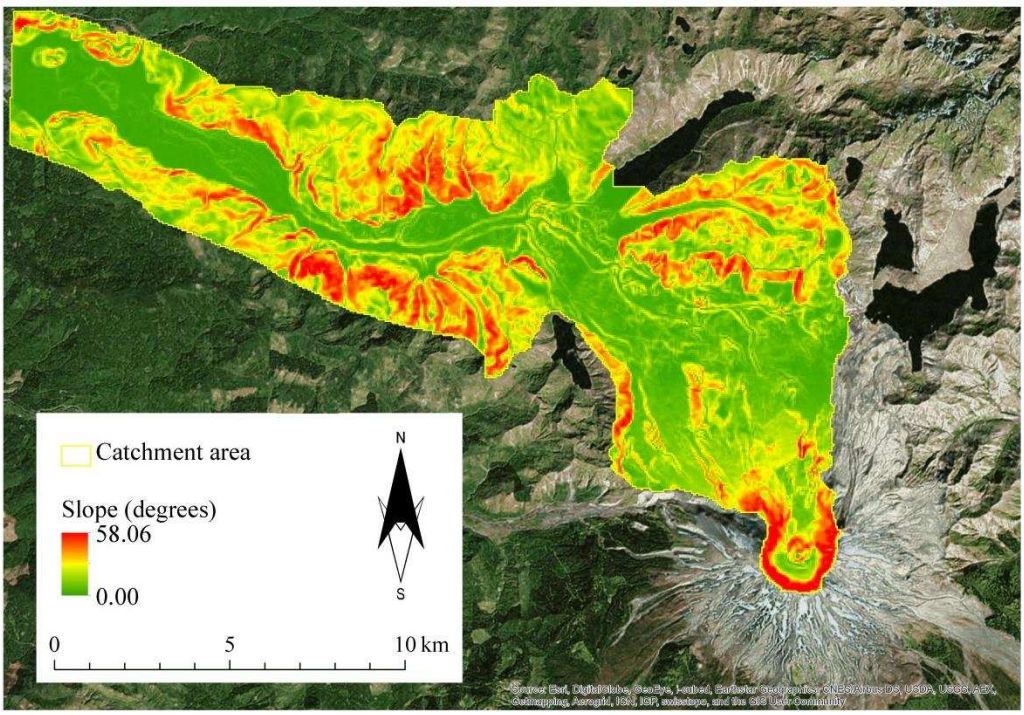

Figure 4.5 Slope maps of the area of the upper North Fork Toutle River included in the C-L model derived from the 3 m (a) and 50 m (b) DEMs.

(a)

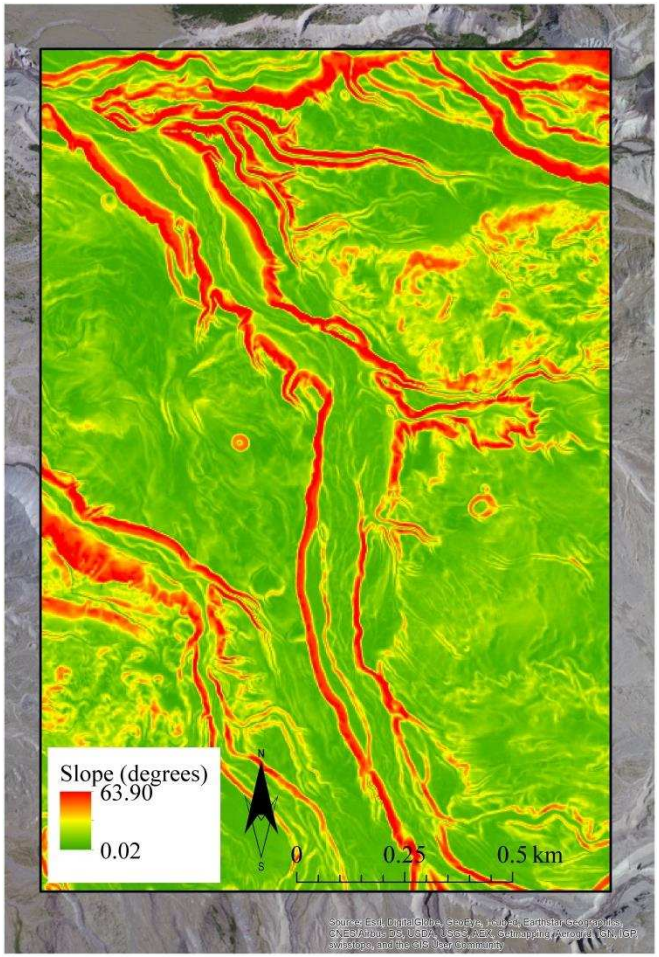

(b)

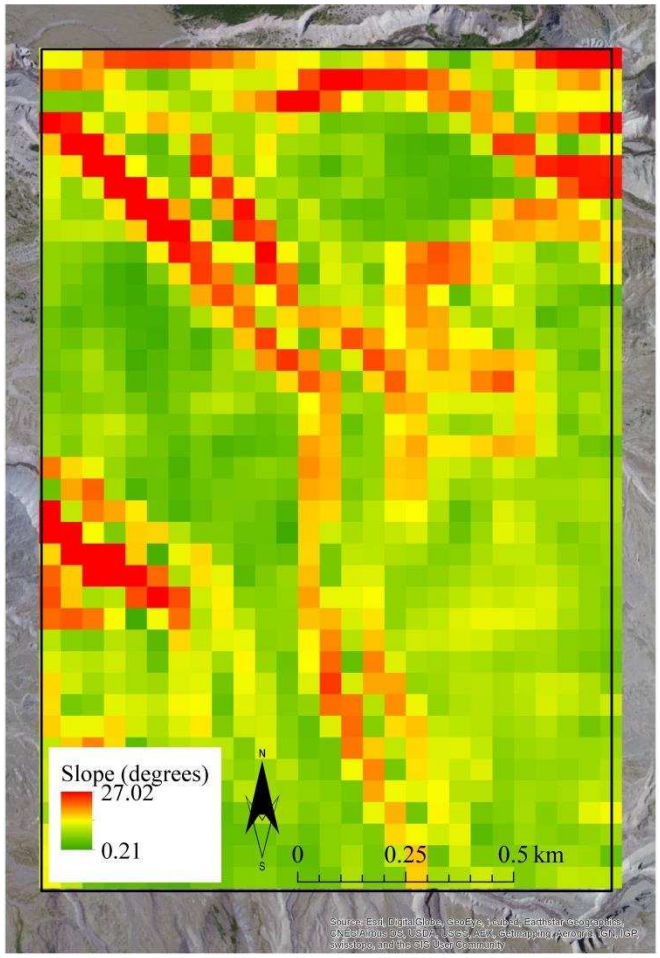

Figure 4.6 Slope maps of the upper analysis reach (see Figure 4.3 for location) derived from the 3 m (a) and 50 m (b) DEMs. Aerial imagery from DigitalGlobe (Microsoft).

(a)

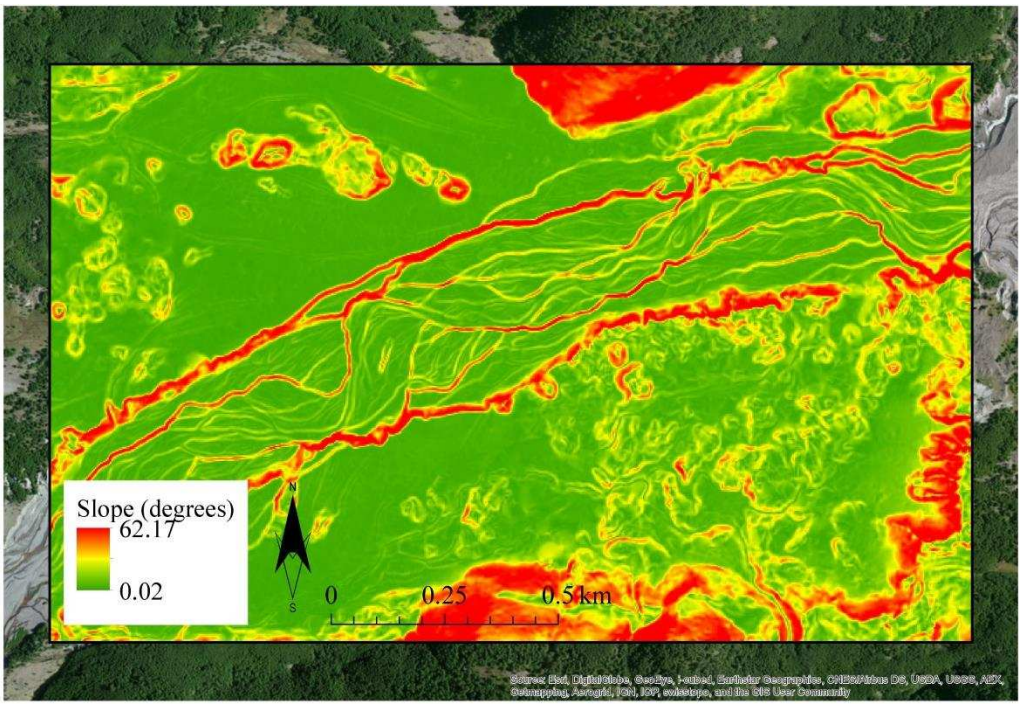

(b)

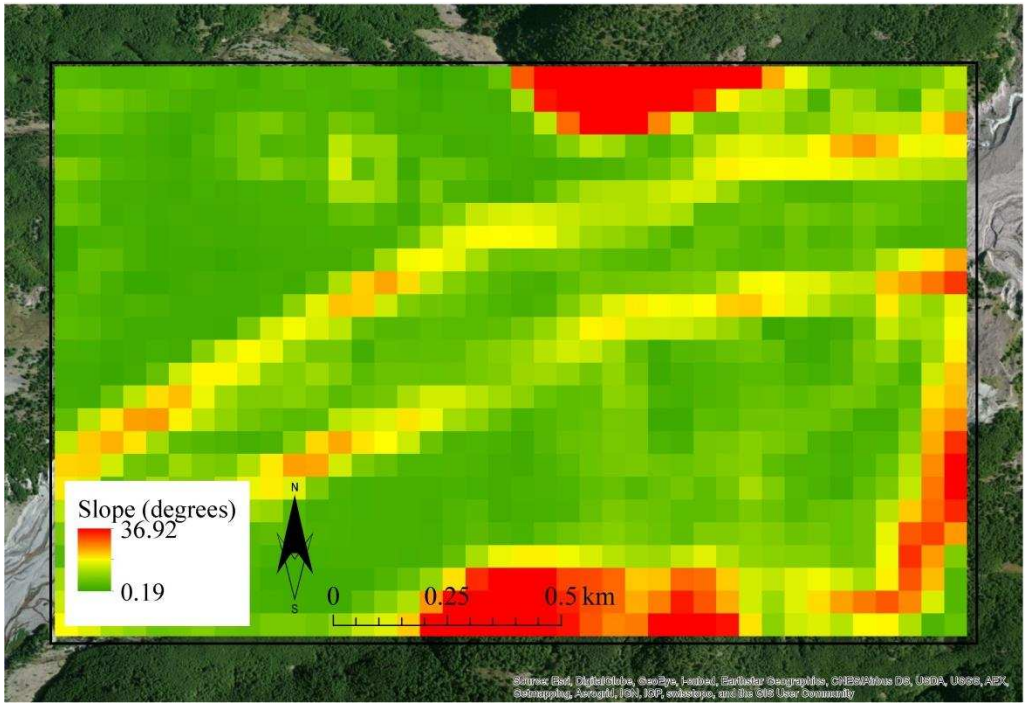

Figure 4.7 Slope maps of the middle analysis reach (see Figure 4.3 for location) derived from the 3 m (a) and 50 m (b) DEMs. Aerial imagery from DigitalGlobe (Microsoft).

(a)

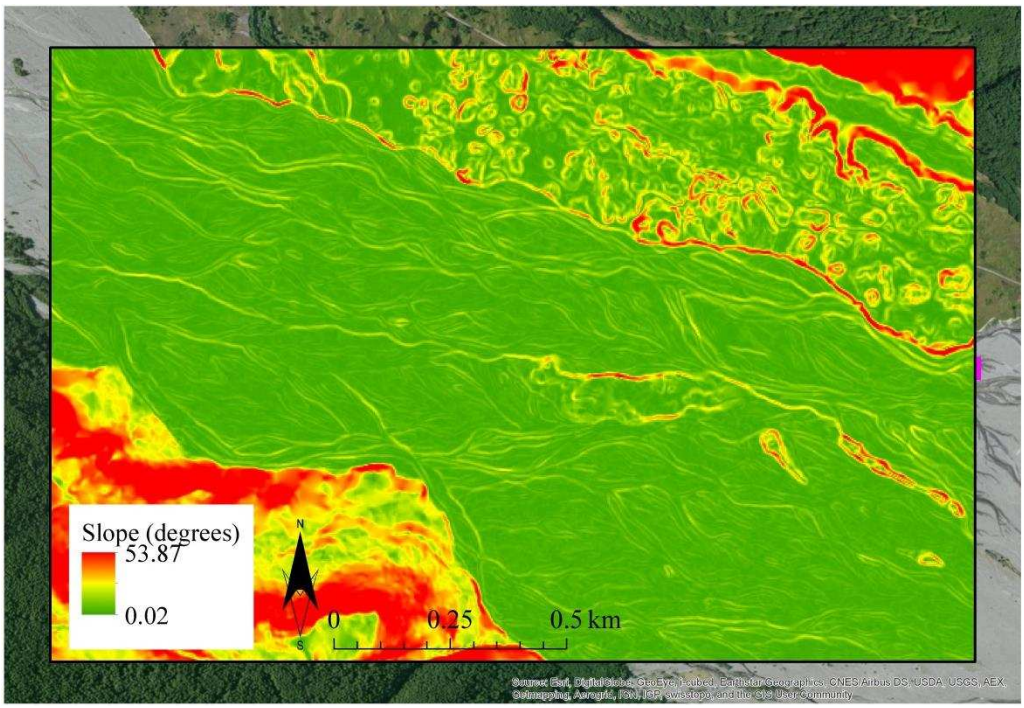

(b)

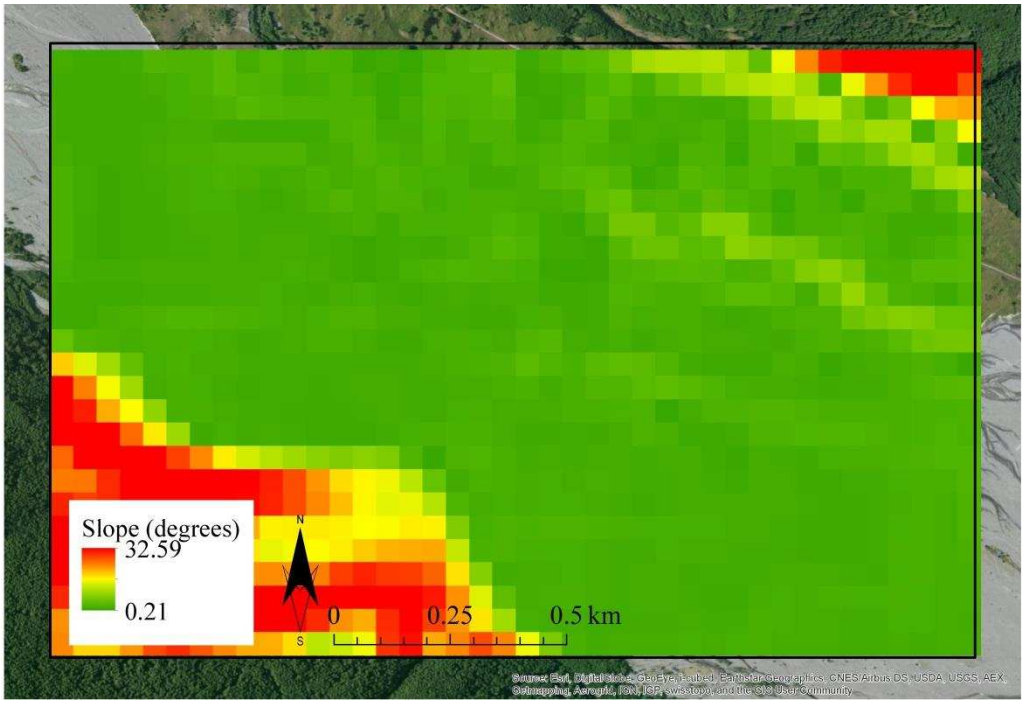

Figure 4.8 Slope maps of the lower analysis reach (see Figure 4.3 for location) derived from the 3 m (a) and 50 m (b) DEMs. Aerial imagery from DigitalGlobe (Microsoft).

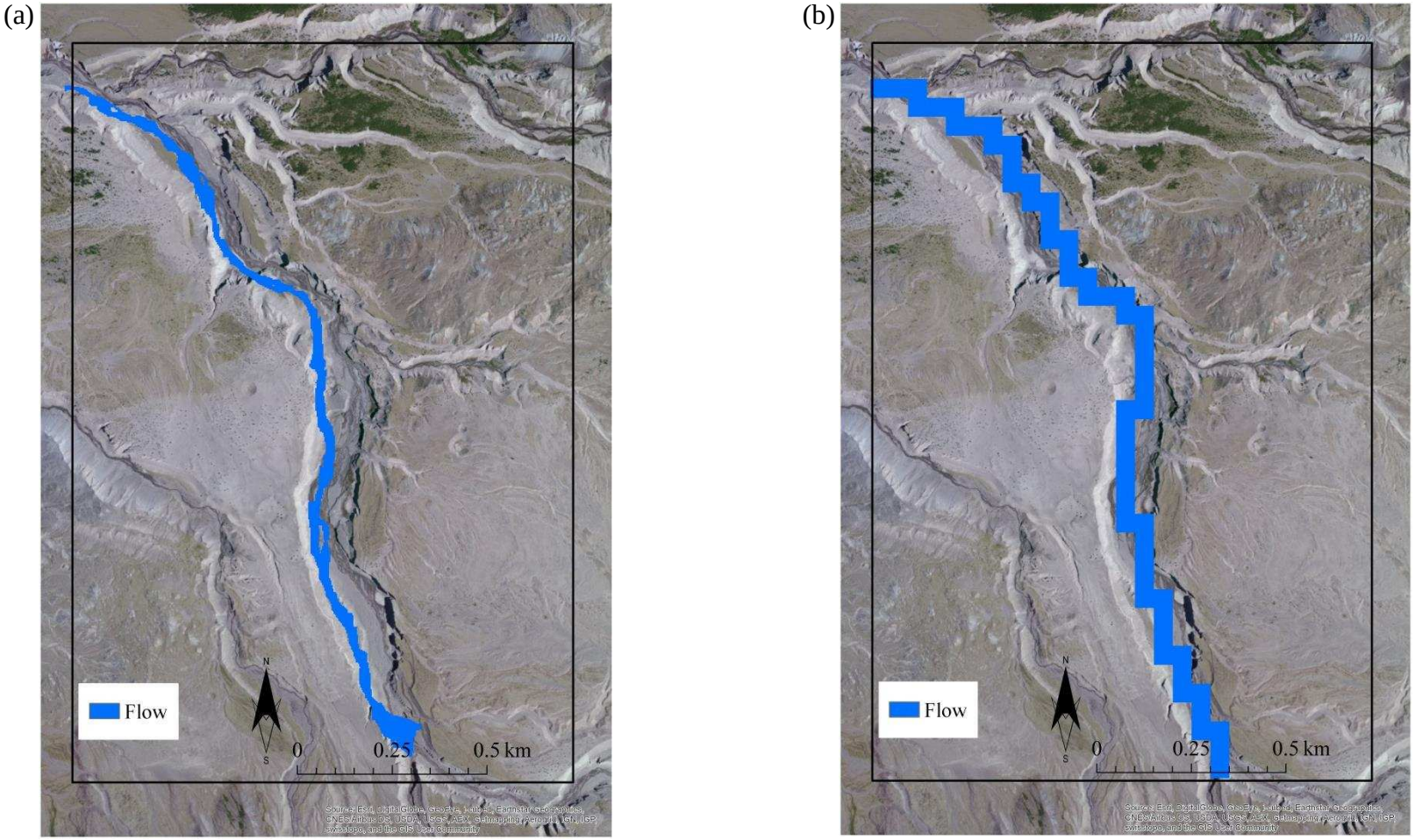

Figure 4.9 In-channel flow in the upper analysis reach (see Figure 4.3 for location) as represented by the 3 m (a) and 50 m (b) DEMs. Aerial imagery from DigitalGlobe (Microsoft).

(a)

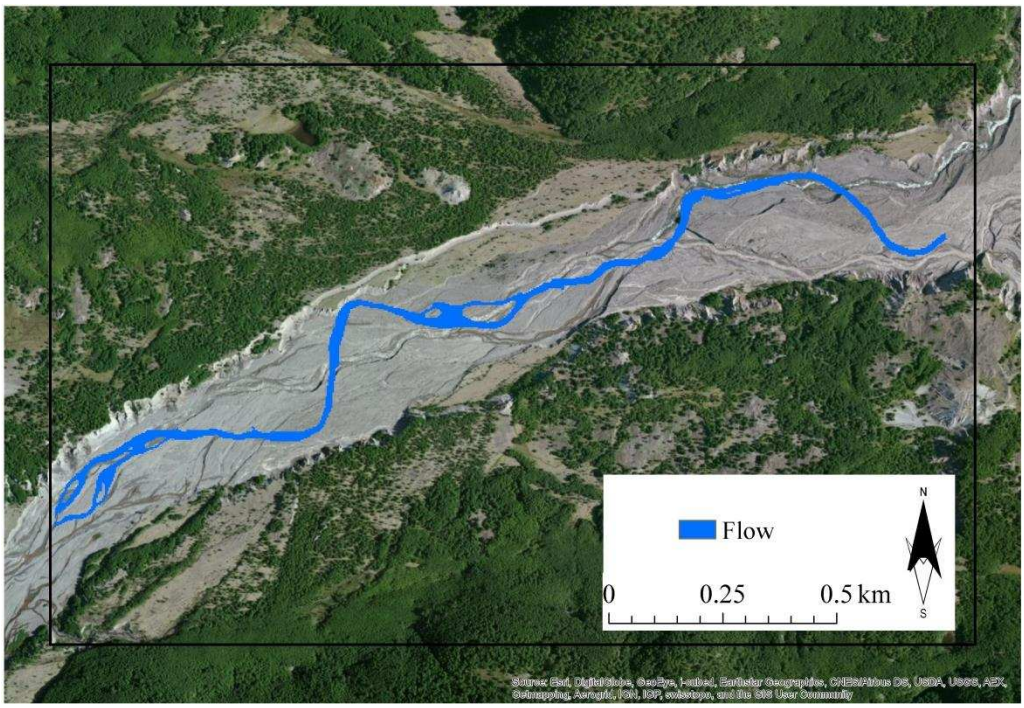

(b)

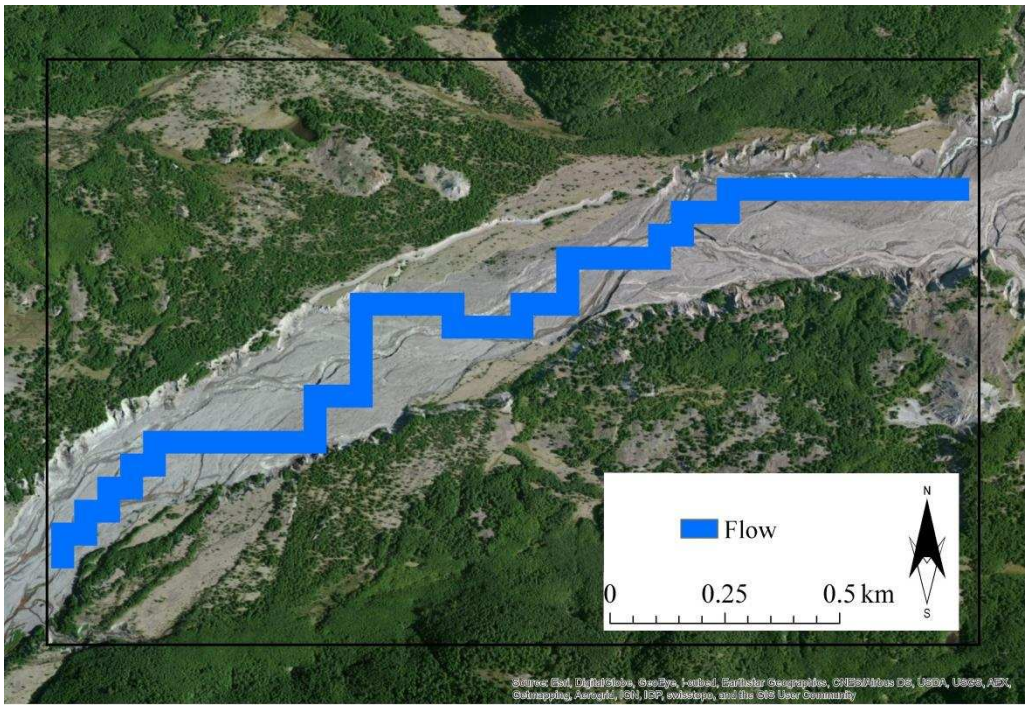

Figure 4.10 In-channel flow in the middle analysis reach (see Figure 4.3 for location) as represented by the 3 m (a) and 50 m (b) DEMs. Aerial imagery from DigitalGlobe (Microsoft).

(a)

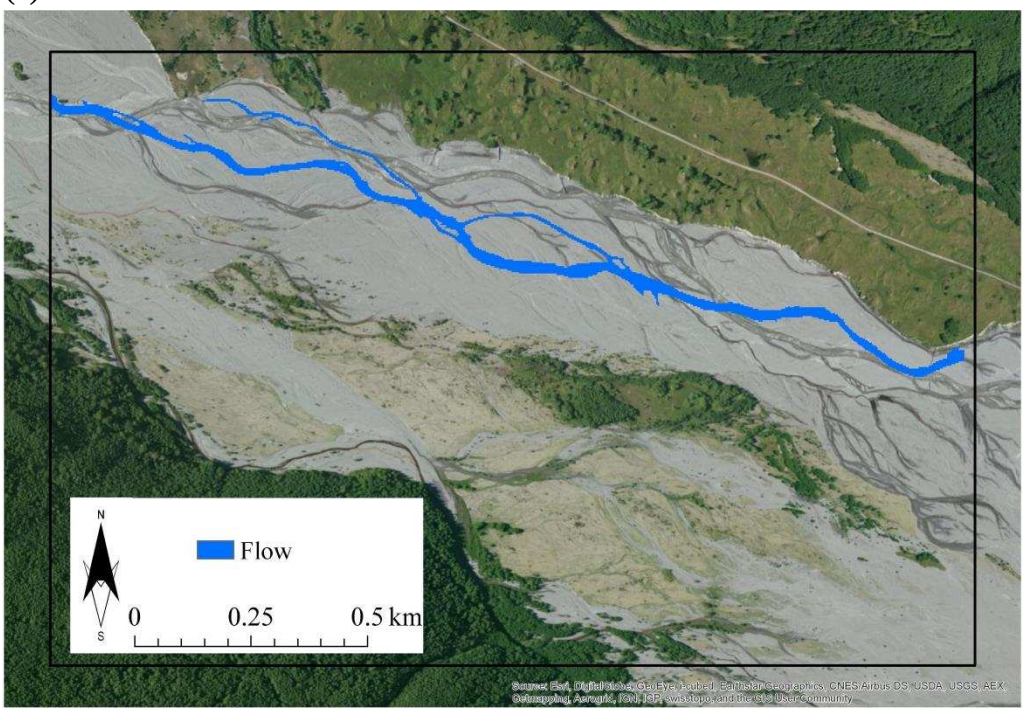

(b)

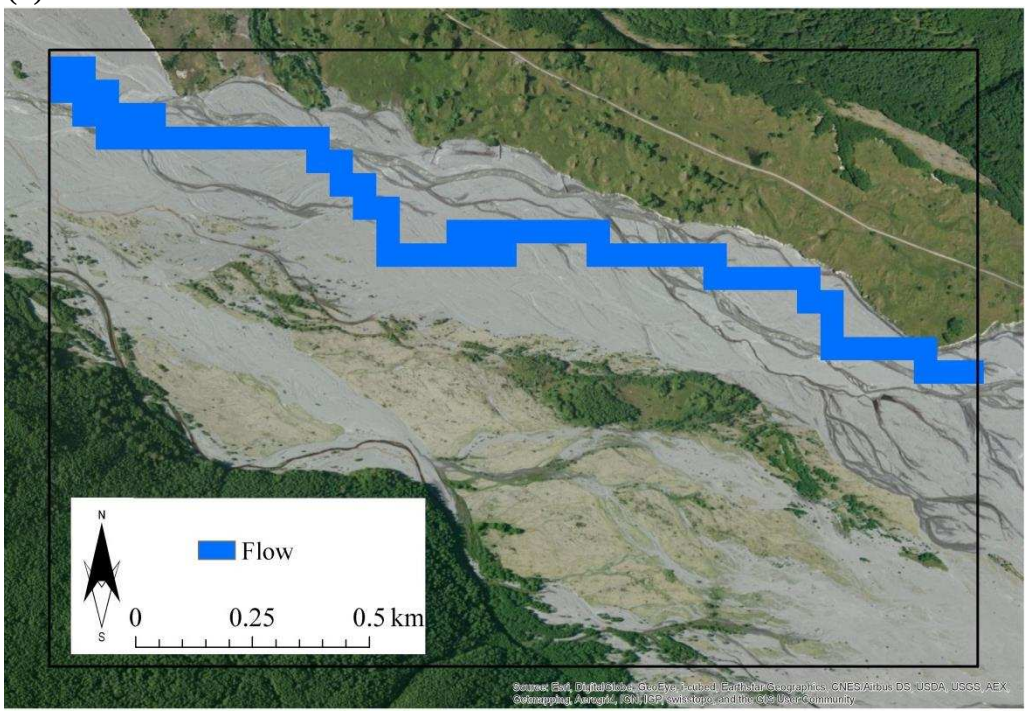

Figure 4.11 In-channel flow in the lower analysis reach (see Figure 4.3 for location) as represented by the 3 m (a) and 50 m (b) DEMs. Aerial imagery from DigitalGlobe (Microsoft).

Figure 4.12 Photographs of the three analysis reaches (see Figure 4.3 for location): (a) upper reach view upstream; (b) middle reach view downstream; (c) lower reach view downstream. All photographs by author (2011).

indicating that the canyon walls are less steep when 50 m rather than 3 m cells are used to represent the terrain. The reduction in slope angle of canyon walls caused by increasing DEM cell size from 3 m to 50 m is likely to have some implications for process-representation within C-L. For instance, it may reduce the frequency with which gravity-driven slope failures are modelled to occur, as this process is explicitly dependent on slope angle. However, such events do not contribute significantly to sediment yield from the upper North Fork Toutle River catchment, as fluvially-driven lateral erosion through basal scour and undercutting is now believed to dominate sediment production.

In this context, it should be noted that the calculation of lateral erosion in C-L is not dependent on the slope angle of bank cells. Rather, C-L's lateral erosion algorithm uses the radius of curvature and shear stress of the cell adjacent to the bank to simulate bank retreat, as described in more detail later in Section 4.4. As such, the smoothing of some canyon wall slopes that results from increasing the grid size is likely to have a negligible impact on the representation of fluvially-driven lateral erosion within C-L.

Figures 4.9 to 4.11 show the nature of the channels as represented by the two resolutions during relatively low flow conditions (approximately 10 $m^3 s^{-1}$) in the three analysis reaches. Inevitably, more complex multi-thread flow patterns are modelled when the 3 m resolution DEM is used than when the 50 m resolution DEM is used. Importantly, however, it is evident that the channels modelled using the lower resolution terrain surface are well-contained within the canyon network and follow largely similar paths to those modelled using the higher resolution surface. As such, it is thought that the channels represented by the 50 m DEM are sufficiently detailed to model the lateral movement of channels within their canyons, and the subsequent erosion of canyon walls and floors by fluvial processes. The additional detail provided by the 3 m DEM is unnecessary for modelling such processes.

Following the analyses described above and presented in Figures 4.4 to 4.11, it is therefore concluded that the essential reduction in DEM resolution is unlikely to have excessively negative implications for the representation of the

dominant processes responsible for long-term channel evolution within, and sediment yield from, the upper North Fork Toutle River catchment.

4.3 THE HYDROLOGICAL MODEL

4.3.1 Operation and data requirements

The following Section outlines the processes and algorithms implemented within C-L for the calculation of water discharge and its subsequent routing between cells. The key parameters discussed in this Section, together with how they can be estimated, are summarised in Table 4.3.

i. The calculation of water discharge

C-L operation begins by calculating the water discharge of each individual cell, Q_{tot}, using either a rainfall or discharge record as the input. In both cases, a temporal resolution of one hour is required. If a rainfall record is being used, the calculation of Q_{tot} is based on an adaptation of TOPMODEL (Beven and Kirkby, 1979), which takes one of two forms depending on the local rainfall rate r (mm h^{-1}) specified in the input file. When $r > 0$, equations 4.1 and 4.2 are used to calculate Q_{tot}:

$$Q_{tot} = \frac{m}{T} \log \left(\frac{(r - j_t) + j_t \exp\left(\frac{rT}{m}\right)}{r} \right) \tag{4.1}$$

$$j_t = \frac{r}{\left(\frac{r - j_{t-1}}{j_{t-1}} \exp\left(\left(\frac{(0 - r)T}{m} \right) + 1 \right) \right)} \tag{4.2}$$

where, m = a user-defined parameter (see Table 4.3); T = time (seconds); j_t = soil moisture store; and j_{t-1} = soil moisture store from the previous iteration.

Table 4.3 Details of parameters used for the calculation of discharge and flow routing.

Parameter	Unit	Operational purpose	Impact and model sensitivity	Recommended or default values	Notes and comments
$Q_{\min}$	$m^3 s^{-1}$	Run time optimisation. The minimum discharge in a cell that is required for depth to be calculated in that cell. Prevents calculation of depth for insignificant flows.	Higher values reduce model run times, but may restrict flow and therefore erosion in peripheral cells if set too high.	One-tenth of grid cell size.	No further guidance given regarding adjustments to this parameter.
$d_{\min}$	m	Run time optimisation. The minimum depth of water in a cell that is required for erosion to be calculated in that cell.	Higher values reduce model run times, but may restrict flow and therefore erosion in peripheral cells if set too high.	0.01	Can be lowered for very fine resolution (<5 m) DEMs, or increased for very coarse resolution (>50 m) DEMs.
Q_{diff}	$m^3 s^{-1}$	Run time optimisation. The difference between the input and expected output discharge that is acceptable to allow the model to shift to the faster steady state mode.	Higher values reduce model run times, but may cause the model to run too fast resulting in smaller magnitude discharge events to be missed.	Can be approximated by the mean annual flow (Q_{MAF}) of the catchment.	Also requires judgement regarding the acceptable difference between the input and output discharge, as well as speed of model operation.
h_{flow} threshold	m	Run time optimisation. The depth through which water can flow between two cells. Prevents calculation of flow over very low gradients.	Higher values reduce model run times, but could unrealistically limit flow when the gradient between cells is low.	0.00001	No further guidance given regarding adjustments to this parameter, although it seemingly could be increased if further run time optimisation was required.

Courant number (α)	-	To calculate model time step and enhance stability.	Higher values increase model time step but are more unstable, and can result in chequerboarding (rapid reversals of flow between adjacent cells).	0.2 – 0.7	Coarser resolution DEMs are generally more stable and can therefore have values towards the upper end of this range.
Froude number (Fr)	-	To enhance model stability. Controls the rate of flow between cells.	Lower values increase stability, but reduce the speed of a flood wave through a reach which may reduce erosion. Higher values can result in chequerboarding.	0.8	Can be adjusted depending on the nature of the catchment being modelled. Lower values, for instance, could be used in the case of very deep, slow flows.
Manning's n	-	Calculation of flow depth.	Higher values result in greater flow depths and may reduce erosion rates.	-	Can be estimated from catchment characteristics, field data or relevant literature.
Slope for edge cells (S_{edge})	-	Calculation of flow out of the model at the downstream boundary.	Higher values can result in scour and upstream-propagating knickpoints; lower values can cause pooling and sediment deposition at the outlet.	Mean bed slope of the channel near the catchment outlet.	Should be calculated directly from the DEM.
m	m	Controls the shape of the modelled hydrograph.	Higher values result in lower flood peaks and slower decline of the recession limb.	0.005 – 0.02	Can be estimated from catchment hydrograph or previous applications.

However, if $r = 0$ (i.e. there is no precipitation for that iteration), equations 4.3 and 4.4 are used:

$$Q_{tot} = \frac{m}{T} \log\left(1 + \left(\frac{j_t T}{m}\right)\right) \tag{4.3}$$

$$j_t = \frac{j_{t-1}}{1 + \left(\frac{j_{t-1} T}{m}\right)} \tag{4.4}$$

In these formulae, m = a parameter used in TOPMODEL to represent the exponential subsurface store (Beven and Kirkby, 1979) and it effectively imitates the effect of vegetation on the movement and storage of water within the soil (Welsh et al., 2009). This parameter is responsible for controlling the rise and fall of the soil moisture deficit (Coulthard, 1999) and it therefore influences the characteristics of the modelled flood hydrograph (Welsh et al., 2009). Specifically, higher values of m increase soil moisture storage, leading to lower flood peaks and a slower rate of decline of the recession limb of the hydrograph, and therefore represent a well-vegetated catchment (Welsh et al., 2009). Conversely, lower values of m represent more sparsely vegetated catchments with flashier hydrological regimes.

The calculated value of Q_{tot} for each cell is then multiplied by the cell's drainage area to determine the discharge that would be present in each cell as a result of upstream contributions. Calculation of depth and subsequent routing of flow using the LISFLOOD-FP hydrodynamic flow code (described below) are subsequently restricted to only those cells in which the calculated discharge value is greater than a user-specified value, termed $Q_{\min}$ (Table 4.3). Depth is not calculated in cells with discharge less than $Q_{\min}$ during any given time step. It must be noted that the purpose of multiplying drainage area by Q_{tot} is simply to identify those cells for which depth will be calculated. The resulting

discharge it is not used in flow routing calculations, and instead each cell has the same discharge added to it during each time step (i.e. Q_{tot}).

Alternatively, Q_{tot} can be derived directly from a hydrograph. In this case, the input to the hydrological model is a time series of instantaneous hourly discharges ($m^3 s^{-1}$) measured at the catchment outlet. During each time step, the discharge at the catchment outlet is first divided by the total number of cells in the model DEM to obtain an average discharge value for each cell. Then, the drainage area of each cell is multiplied by the previously calculated average discharge value to obtain the discharge that would be present in each cell as a result of upstream contributions. Cells with a resulting discharge greater than $Q_{\min}$ are identified and added to a list of catchment input points.

For each of these identified points, Q_{tot} is then calculated by dividing the input discharge value for that time step by the total number of catchment input points (Tom Coulthard, University of Hull, personal communication, 2011). As such, all cells identified as catchment input points during a given time step have an equal volume of discharge added to them during that time step (i.e. Q_{tot}). The volume of water added to each of the input cells is then routed to its neighbouring cells using the LISFLOOD-FP hydrodynamic flow code (described below). Cells with a discharge less than $Q_{\min}$ do not have water added to them during that time step.

The addition of the $Q_{\min}$ parameter in the algorithms described above helps to optimise run times by reducing the need for the model to route water in cells with very little flow. However, restricting flow in marginal areas may have implications for the representation of catchment hydrology and, therefore, the production of sediment in headwater catchments. This could result in the development of unrealistic patterns of erosion throughout the catchment and this potential limitation is addressed in more detail in Chapter 5.

ii. Hydraulic routing using LISFLOOD-FP

The routing of flow between cells within C-L is carried out using the LISFLOOD-FP hydrodynamic flow model developed by Bates et al. (2010)

that was discussed briefly in Chapter 3. Flow is routed to the four Manhattan neighbours of each cell using equation 4.5:

$$q_{t+\Delta t} = \frac{q_t - g h_t \Delta t \frac{\partial (h_t + z)}{\partial x}}{\left(1 + g h_t \Delta t n^2 q_t / {h_t}^{10/3}\right)} \tag{4.5}$$

where, Δt = length of time step (s); t and $t + \Delta t$ denote the present and next time steps, respectively; q = flow per unit width (m^2 s^{-1}); g = gravitational acceleration (m s^{-2}); h = flow depth (m); z = bed elevation (m); n = Manning's n; x = grid cell size (m); and, $\frac{\partial (h_t + z)}{\partial x}$ = water surface slope.

To improve model stability, the model time step at $t + \Delta t$ is estimated using equation 4.6, where α = a coefficient, described in C-L literature as the Courant number (Table 4.3) and defined by the user.

$$\Delta t_{\max} = \alpha \frac{\Delta x}{\sqrt{g h_t}} \tag{4.6}$$

Although model stability is enhanced significantly by inclusion of the Courant number (α), chequerboarding effects can still result if too much flow is allowed between cells in a given time step. This can be controlled within C-L by specifying a maximum Froude number (Fr), which reduces the maximum potential rate of flow between two cells (Table 4.3).

Operation of the hydrologic model within C-L has been optimised to reduce run times in a number of ways. The first of these relates to the LISFLOOD-FP parameter h_{flow} which represents the depth through which water can flow between two cells, and is defined as the difference between the highest free surface elevation in the two cells and the highest bed elevation (Bates et al., 2010). Within C-L, a minimum value of h_{flow} must be exceeded before water will be routed between the two cells, and this value is known as the h_{flow} threshold (Table 4.3). The h_{flow} threshold, which must be specified by the user,

prevents the model from spending time moving water between cells when the gradient is very low.

Furthermore, C-L switches between two different modes of operation depending on the balance between the input discharge, Q_{tot}, and the calculated output discharge. When the difference between these two values is below a certain user-specified threshold (Q_{diff}) (Table 4.3), the flow model is deemed to be running in a steady state and the time step is therefore assumed to be stable. In this case, the time step is determined by the quantity of fluvial erosion, which enables it to be extended up to an hour during periods of low flow, when processes responsible for geomorphological adjustments operate at low rates.

Following the routing of water using the LISFLOOD-FP code, the depth of water within each cell is updated. C-L then uses these updated depths to identify the active cells, which are defined as those within which water depth is greater than a user-specified value, termed d_{min} (Table 4.3). Processes of fluvial erosion and deposition, as described in Section 4.4, are represented only in these active cells, while inactive cells are checked for hillslope processes and mass movements every 1,000 iterations. This scheme optimises model run times by concentrating the majority of the model's operations on those cells in which fluvial processes are likely to dominate, with fewer operations representing longer-timescale, hillslope processes (Coulthard et al., 2002).

Although, as discussed in Chapter 3, adoption of the LISFLOOD-FP code in C-L represented a significant improvement on earlier versions of C-L (as well as other reduced complexity cellular models), LISFLOOD-FP nonetheless remains a simplified and incomplete representation of flow hydraulics. For instance, it neglects the advection term from the St Venant equation (Bates et al., 2010), which has been shown to be important for the accurate representation of flow dynamics (Dottori and Todini, 2011). Moreover, LISFLOOD-FP fails to incorporate secondary or cross-channel flows, which are known to play key roles in the development of channel morphology. The potential impacts that these limitations may have on model outputs are discussed during model evaluation undertaken in Chapter 5, Section 5.6.

4.3.2 Identification of requisite input data and parameter definition

As discussed above, the hydrological model used within C-L requires either a local precipitation record or a record of discharge from the catchment outlet, both with a temporal resolution of one hour, to calculate the total surface water discharge (Q_{tot}). Selection and implementation of an appropriate hydrological input are discussed in this Section.

i. Justification of modelling methodology

For the current application, the option of using a discharge record was preferred to that of using a local precipitation record for two principal reasons. First, it was not the aim of this research to develop a rainfall-runoff model for the catchment, but rather to model and predict long-term catchment sediment yields. In this context, the use of a precipitation record was unnecessary and would have introduced additional uncertainties into the modelling process which would have detracted from the primary aim of the project. Second, it is known that the hydrological regime of the upper North Fork Toutle River catchment is dominated by inputs of water from point sources (including springs and lakes), as well as snow accumulation and melt (see Chapter 2) that are ungauged. Hence, runoff generated directly by rainfall is not the primary source of discharge to the upper North Fork Toutle River, meaning that catchment hydrology cannot be accurately represented using a precipitation record as the sole input to the model.

Given these conditions, use of a discharge record overcame was most appropriate as it ensured that the observed and modelled hydrographs agreed well. Adopting this approach also meant that uncertainties in the representation of catchment hydrology associated with using local precipitation records from a very limited number of rain gauges with long gaps in their records, were avoided. Although this method is successful in reproducing the discharge measured at the catchment outlet, the spatial distribution of the discharge inputs may not be adequately represented. Specifically, the lake and spring sources are not explicitly modelled, but rather the discharge is distributed throughout the catchment as described in Section 4.3.1. This shortcoming may

negatively impact the extent to which the model is able to reproduce spatial patterns of geomorphological change throughout the catchment. These issues are explored in greater detail in Chapter 5.

An additional reason for using a discharge record rather than a precipitation record to drive the model relates to the forecasting of future sediment yields undertaken in Chapter 6. Specifically, predictions of future precipitation patterns in Washington State were not available. However, a comprehensive database of hydrologic data, including stream flow estimates within the Toutle River basin that incorporate climate change information, was available from the Columbia Basin Climate Change Scenarios Project (CBCCSP), which will be discussed in more detail in Chapter 6.

ii. Available discharge data

Flow data are recorded at a number of gauging stations operated by the USGS throughout the Toutle-Cowlitz River system. However, efforts to maintain gauging stations on the debris avalanche have been hampered by highly mobile channel boundaries (Simon and Klimetz, 2012) and, consequently, there are no discharge records upstream of the SRS (Jon Major, USGS Cascades Volcano Observatory, personal communication, 2011). Nonetheless, hourly discharge data have been collected at two locations further downstream: on the North Fork Toutle River below the SRS (USGS gauge 14240525); and on the mainstem Toutle River at Tower Road (USGS gauge 14242580) (Figure 3.1). These stations are located approximately 18 and 54 km downstream of the N1-DRS, respectively, and both have continuous records of river discharge.

The accuracy of the discharge data collected at these sites has not been quantified. However, records at both the Tower Road and SRS gauges are subjectively described as ‘fair’, meaning that the published values are within 10% of the actual flow for 90% of the time (Jim Kolva, USGS Office of Surface Water, personal communication, 2011). A continuous record of hourly instantaneous discharges is available from the gauge at Tower Road since October 1, 1992. However, records at the gauge below the SRS are less complete, and data are not available between October 1, 2002 and September

30, 2006. Both of these data sets can be used in combination to generate estimates of flow at the N1-DRS, and the following sub-section describes how this has been achieved.

4.3.3 Estimating discharge at the N1-DRS

The method employed here for estimating flow at the N1-DRS required, first, completing the flow series at the SRS and, second, transferring the completed SRS flow series upstream to the N1-DRS. The need to infill or extend discharge records is common to many applications within hydrology, and a variety of techniques can be used for estimating missing flow data (Harvey et al., 2010). A frequently employed method is to obtain a relationship between the station at which additional data is required (the target) and a nearby base station (the donor) during periods with coincident data (Hirsch, 1982; Cigizoglu, 2003). The derived relationship can then be applied to flows at the donor station to estimate flow at the target station during periods of missing data. In this case, the target station is the SRS gauge, while the donor station is the gauge on the Toutle River at Tower Road (see Section 4.3.2).

The method used to obtain the necessary relationship between flows gauged at Tower Road and the SRS was simple linear regression which represents the relationship between two variables (in this case the donor and target discharge flow series) by a straight line of best fit (Montgomery et al., 2001). The linear regression model takes the form:

$$y = \beta_0 + \beta_1 x + \varepsilon \tag{4.7}$$

where, y = dependent variable (target discharge, $m^3\ s^{-1}$); x = independent variable (donor discharge, $m^3\ s^{-1}$); β_0 = intercept on the y-axis; β_1 = slope of the line; and ε = error between the observed value of y_i and the fitted value on the straight line $\hat{y}_i$ ($m^3\ s^{-1}$). The regression coefficients β_0 and β_1 were estimated using the least squares approach, which minimises the sum of the

squares of ε (Montgomery et al., 2001) in order to generate optimal estimates of y at each point (Moog et al., 1999).

i. Data preparation

Hourly instantaneous discharge data were obtained from both the Tower Road and SRS gauges for two main periods: October 1, 2001 to September 30, 2002; and October 1, 2006 to September 30, 2009. The second, longer period was used to develop a relationship between the two stations (referred to hereafter as the training data set), while the first, shorter period was used to assess the ability of the derived solution to predict discharge at the SRS (referred to hereafter as the testing data set). Prior to undertaking regression analysis on the training data set, however, several pre-processing steps were required. Given that both the Tower Road and SRS gauge records were characterised by a number of gaps ranging from one hour to several days, it was necessary to first extract coincident pairs of data. This reduced the training data set to 18,566 points and the testing data set to 8,080 points.

The training data were then assessed to determine whether it was necessary to apply a time shift to the flow series to account for the time taken for a flood wave to travel downstream from the SRS to Tower Road. Given that the data necessary to calculate the travel time for a flood wave moving between the two sites (i.e. average flow velocity or channel geometry) were unavailable, this was instead estimated directly by comparing the hydrographs for the two stations. The method involved visually identifying and matching selected, distinctive discharge peaks that were evident in both records, which could be taken to represent the passage of a single flood wave along the channel, and then determining the time difference between each peak being recorded at the upstream and downstream stations. 24 suitable flood peaks were identified from the training data set for this analysis, and these are shown in Figure 4.13. Travel times varied from one to six hours, although a three hour time difference was by far the most common (Figure 4.14). On the basis of this result, the record at the SRS gauge upstream was shifted forwards by three hours to account for the travel time between the two gauging stations.

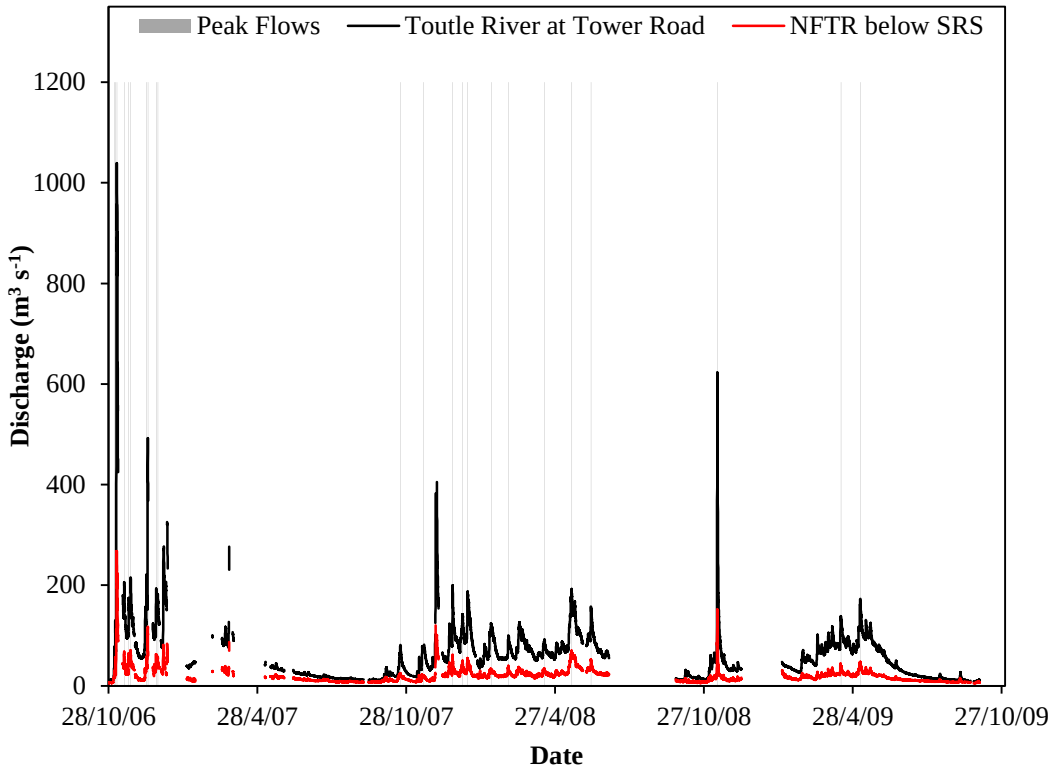

Figure 4.13 Peak flows identified for time lag analysis.

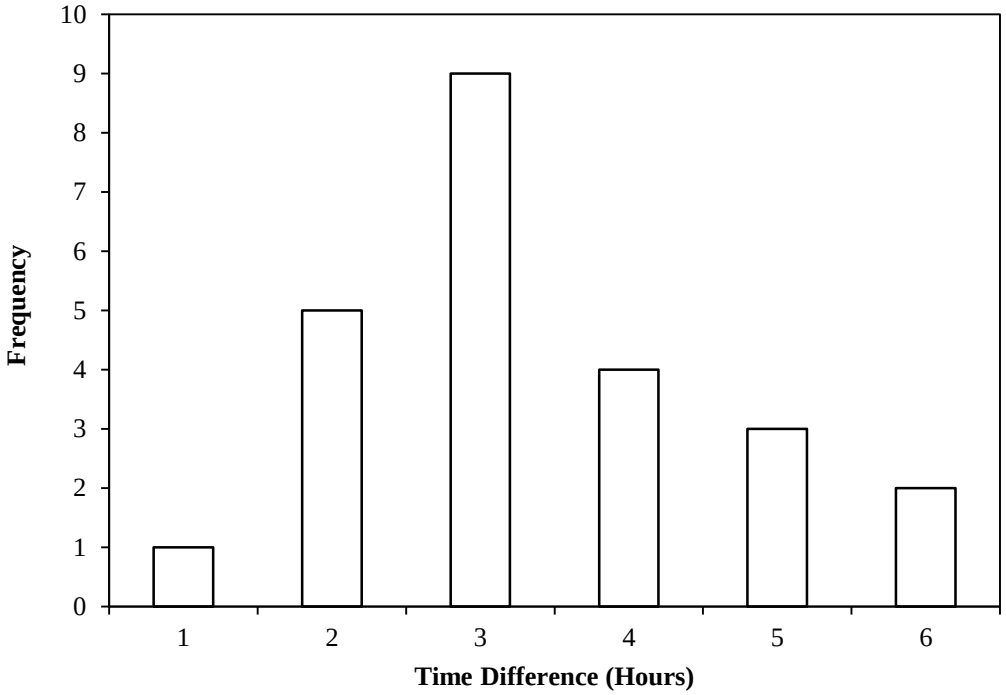

Figure 4.14 Frequency distribution of time differences between peak flows recorded at the SRS and Tower Road gauges.

ii. Results

Figure 4.15 shows the relationship between the SRS and Tower Road discharge records for the training data set, and includes the linear regression equation derived to describe this relationship. The derived equation was applied to the testing data set, with agreement between model predictions and observations assessed using the Nash Sutcliffe Model Efficiency (NSE), which is a widely used statistic for assessing goodness of fit in hydrological models (McCuen et al., 2006; Dawson et al., 2012). NSE is calculated using equation 4.8:

$$NSE = 1 - \frac{\sum_{i=1}^{n}(O_i - P_i)^2}{\sum_{i=1}^{n}(O_i - \bar{O})^2} \tag{4.8}$$

where, P = the modelled (or predicted) value; O = the observed value; $\bar{O}$ = mean of the observed values; and i = 1 to n data points. A scatter plot of observed versus predicted discharges for the testing data set is presented in Figure 4.16, together with the calculated NSE score, while the observed and modelled hydrographs are also plotted in Figure 4.17.

It is apparent from Figure 4.16 and Figure 4.17 that the simple linear regression model provides a good approximation of observed discharge at the SRS during water year 2002 (WY[1]). Peak discharge events, which are arguably of most importance in determining channel evolution, are generally well represented. The model, however, appears to underestimate discharges during periods of lower flow (Figure 4.17). The poorer correlation at low flows may be caused by the attenuation of flood peaks as they travel downstream. Nonetheless, the NSE score of 0.938 indicates that the overall agreement between modelled and observed values is good. Therefore, the linear regression equation presented in Figure 4.15 was used to produce a complete hydrograph from October 1, 2003 to September 30, 2009 (the model hindcast period). Of the 52,608 hours during this period, observed data were available for 18,720 hours (approximately 36% of the time). The completed time series is presented in Figure 4.18.

[1] A water year extends from October 1 of the previous year to September 30.

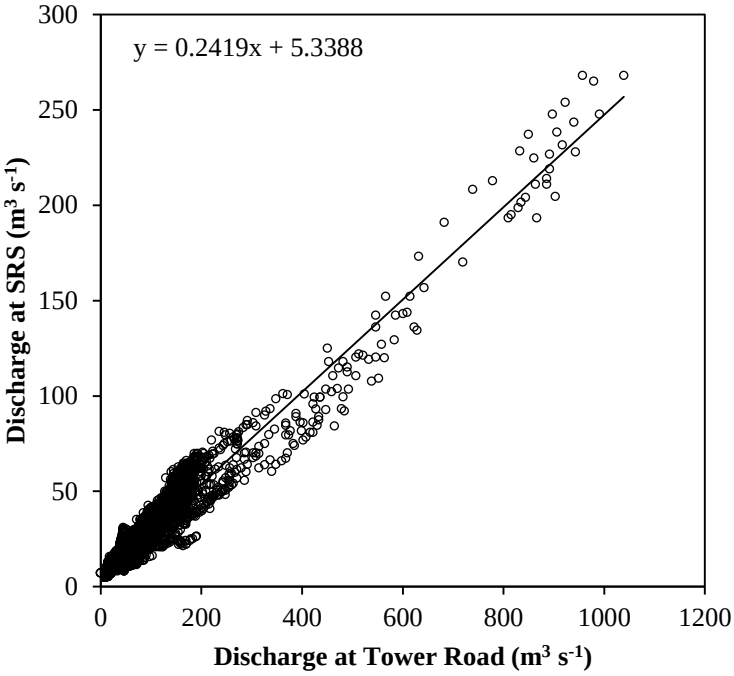

Figure 4.15 Relationship between (adjusted) discharge recorded at the Tower Road and SRS gauging stations between October 1, 2006 and September 30, 2009.

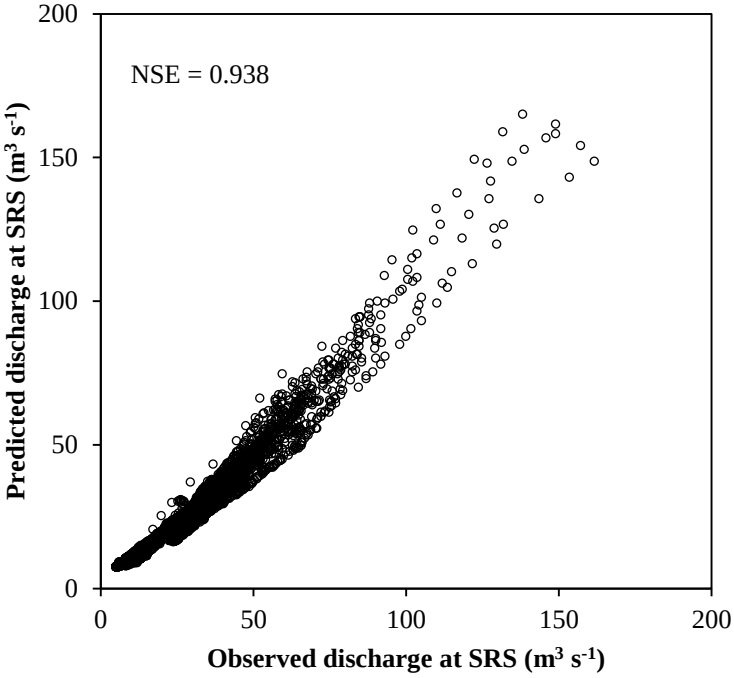

Figure 4.16 The relationship between observed discharge and discharge predicted by the linear regression model at the SRS gauging station for WY 2002 (October 1, 2001 to September 30, 2002).

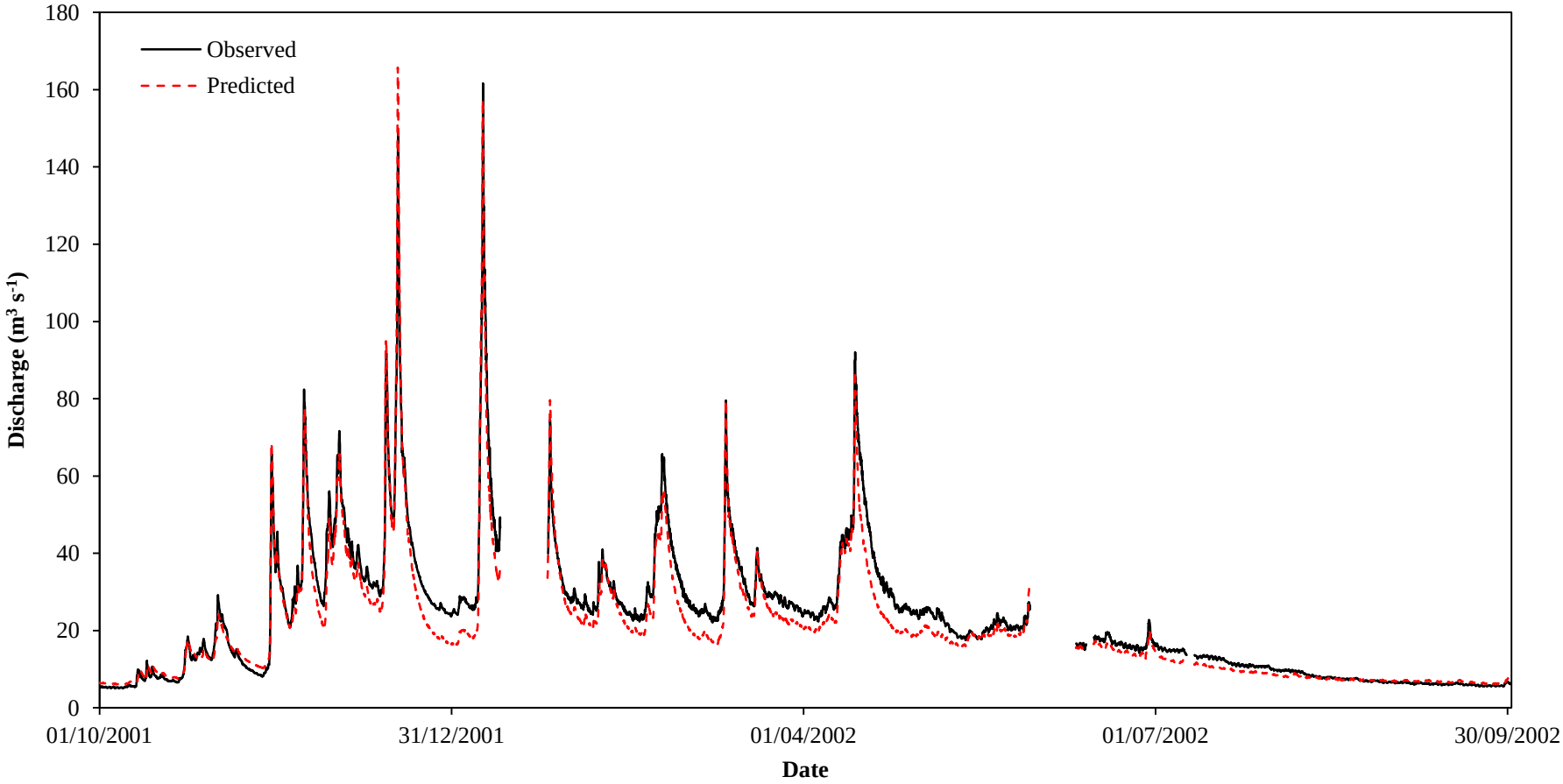

Figure 4.17 Observed and predicted hydrographs at the SRS for WY 2002 (October 1, 2001 to September 30, 2002).

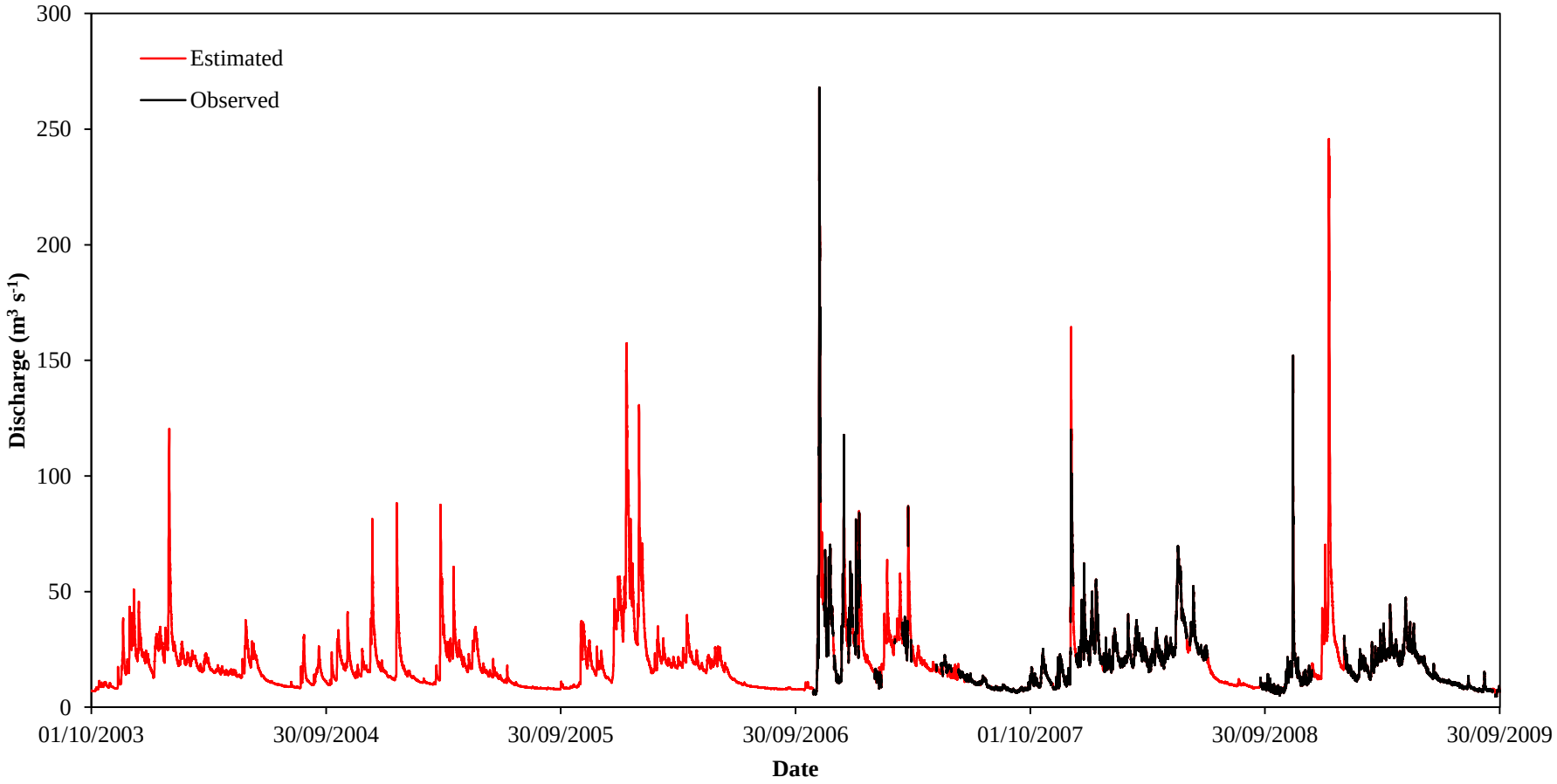

Figure 4.18 Completed hydrograph at the SRS gauge for the period October 1, 2003 to September 30, 2009 to be used for model testing and calibration undertaken in the Chapter 5.

iii. Transferring the SRS flow series to the N1-DRS

Discharge records were transferred from the SRS gauge to the N1-DRS site using the method previously employed by WEST (2002) and USACE (1985). This method involves applying drainage area (DA) and normal annual precipitation (NAP) adjustments to the discharge values measured at the SRS, according to equation 4.9:

$$Q_{\mathrm{N1}} = \left(\frac{DA_{\mathrm{N1}} NAP_{\mathrm{N1}}}{DA_{\mathrm{SRS}} NAP_{\mathrm{SRS}}}\right) Q_{\mathrm{SRS}} \tag{4.9}$$

where, Q = discharge ($m^3\ s^{-1}$); DA = drainage area (km^2); NAP = normal annual precipitation (mm). In this case, DA_{SRS} = 453.25; DA_{N1} = 277.13; NAP_{SRS} = 2057.40; and, NAP_{N1} = 2514.60 WEST (2002). When these values are substituted into equation 4.9 this yields, $Q_{\mathrm{N1}} = 0.75\ Q_{\mathrm{SRS}}$. Although this is a very simple technique, it is often the only reasonable method that can be used when measurements of flow at the ungauged site are unavailable (Hirsch, 1979), as is the case for the N1-DRS site.

It is evident that equation 4.9 assumes a linear relationship exists between annual runoff and catchment area. Although the veracity of this assumption has not been explicitly tested, its relevance has been demonstrated by the ability of a linear regression model to describe the relationship between hourly discharge at the SRS and Tower Road gauging stations (Figure 4.15 and Figure 4.16, above). Moreover, Leopold (1994) suggests a linear relationship exists between mean annual discharge and drainage area for Western Cascade Range streams. However, sufficient data from the region, particularly relating to NAP, are not available to examine equation 4.9 in more detail.

Following the development of input hydrological data described above, values of other parameters required to run C-L's hydrological model (Table 4.3) were then selected. The selection of these values is documented and explained in Table 4.4.

Table 4.4 Selected values for parameters required to run the hydrological model within C-L.

Parameter	**Units**	**Selected value**	**Justification**	**Notes and comments**
$Q_{\min}$	$m^3 s^{-1}$	0.5	One-tenth of grid cell size.	The suitability of this parameter is further tested in Chapter 5.
$d_{\min}$	m	0.01	This is the default value. Suggested conditions for when this parameter should be adjusted are not met.	The defined value is physically realistic as flow depths of <0.01 m are unlikely to cause significant erosion.
Q_{diff}	$m^3 s^{-1}$	10	Estimated on the basis of the Q_{MAF} (15.47 $m^3 s^{-1}$) of the flow series at the N1 dam.	Set slightly below Q_{MAF} to minimise the discrepancies between input and output discharge. Values less than 10 $m^3 s^{-1}$ would compromise run times.
h_{flow} threshold	m	0.00001	This is the default value.	Sufficient information is not available on which to justify adjustments to this parameter.
Courant number (α)	-	0.7	The resolution of the DEM used here (50 m) allows values towards the upper end of the recommended range to be used. A higher value will also reduce run time.	Potential chequerboarding instabilities resulting from the specification of this parameter will be evident during model calibration undertaken in Chapter 5.
Fr	-	0.8	Sub-critical Fr specified because: – Interactions between channel hydraulics and bed	Given that Fr can be justified physically, adjustments to this parameter will be avoided.

			configuration prevent super-critical Fr from persisting for more than short distances or periods of time (Grant, 1997). – Cross-sectional averaging of channel characteristics is likely to indicate sub-critical Fr (Tinkler, 1997).	
Manning's n	-	0.04	Taken from Chow (1959) for channel type 2a: mountain streams with little in-channel vegetation, steep banks and predominantly gravel and cobble beds.	Given that n can be justified physically, adjustments to this parameter will be avoided.
Slope for edge cells (S_{edge})	-	0.01	Calculated gradient of DEM near the catchment outlet.	Given that S_{edge} can be justified physically, adjustments to this parameter will be avoided.
m	m	Undefined	The use of discharge rather than precipitation to drive the hydrological model negates the need to specify a value for m.	-

4.4 ALLUVIAL DYNAMICS

This Section outlines the processes and algorithms implemented within C-L to calculate the spatial distributions and time rates of fluvial erosion, sediment transport and deposition. The key parameters discussed in this Section, together with how their values may be estimated, are summarised in Table 4.5.

4.4.1 Operation and data requirements

i. Sediment transport

Once flow rates have been calculated for each cell using the methods described in Section 4.3.1, water depths are updated and processes of fluvial erosion are simulated. C-L represents the fluvial erosion, transport and deposition of heterogeneous sediment using nine user-defined grain size fractions that are embedded within a three-dimensional active layer system (Coulthard and Van De Wiel, 2007; Van De Wiel et al., 2007; Hancock et al., 2010). A key data requirement for modelling sediment transport using C-L is, therefore, a grain size distribution that adequately represents the characteristics of the sediment throughout the catchment. Given that this grain size distribution is initially applied to all the cells in the modelled basin, the data should be representative of hillslope and valley floor areas, rather than in-channel deposits (Coulthard, 1999). Coarsening of the channel boundary material is accounted for by processes of selective sediment entrainment and transport that are represented in the model.

The active layer system used to represent alluvial processes consists of a single active layer, multiple buried layers (strata) and a bedrock layer (Figure 4.19) (Van De Wiel et al., 2007). These layers contain quantities of sediment for each of the nine size fractions (Hancock et al., 2010), allowing the model to account for the presence of layers of relatively coarse or fine sediment deposited during past sediment transport events as a limited

Table 4.5 Parameters used in modelling the spatial and temporal distributions of fluvial erosion, sediment transport and deposition in C-L.

Parameter	**Units**	**Operational purpose**	**Impact and model sensitivity**	**Recommended/ default values**	**Notes and comments**
Sediment transport formula	-	Calculation of the volume of material eroded from a cell during a single iteration.	Estimates of sediment transport rates are known to vary significantly between formulae.	-	Wilcock and Crowe (2003) or Einstein (1950). Testing and calibration necessary.
v_{f}	m s^{-1}	Fall velocity for calculation of suspended sediment deposition.	Low values increase suspended sediment deposition.	-	Can be estimated using the Stokes' law.
$\Delta Z_{\max}$	m	Restricts model time step to enhance stability. The maximum elevation change allowed per cell per iteration.	Higher values reduce model run times but can cause instability if excessive volumes of material are allowed to move between cells.	0.02	Lower values (c. 0.01) may be required for fine resolution DEMs (c. 10 m).
L_h	m	Defines the thickness of each stratum within the active layer system.	Could influence sediment transport rates if set very low through detachment-limitation.	0.1 – 0.2	Must be at least four times $\Delta Z_{\max}$.
N_{smooth}	-	Specifies the number of passes made by the edge smoothing filter which is used to calculate the local radius of curvature (R_{ca}) and thus lateral erosion (ζ).	Low values may result in irregular lateral development, while high values can produce over-smoothed channels.	10 – 50	Low values for high sinuosity meandering or braided channels; higher values for gently meandering or straighter channels.

Λ	-	A scaling factor used to calculate lateral erosion (ζ).	Higher values increase lateral erosion, i.e. the volume of material eroded from the outer bank of a meander bend.	0.0001 – 0.01	This parameter requires calibration. Higher values are more appropriate for channels that are highly laterally mobile.
$\Delta\nabla_{\max}$	-	Calculates a cross-channel gradient from R_{ca} values which is used to control the lateral distribution of eroded sediment from the outer bank to the inner bank (point bar) of a meander bend.	Lower values ensure distribution across the width of the channel, but may increase model run time. Higher values can result in the deposition of sediment in the middle of the channel, rather than on a point bar.	0.0001	Lower values are recommended in the case of wide channels (>10 cells) to ensure full lateral distribution.
N_{shift}	-	Determines the number of cells that the cross-channel gradient is shifted downstream in order to simulate downstream migration of meander bends.	May result in unrealistic patterns of meander bend development if set incorrectly.	One-tenth of N_{smooth}	This value must be an integer. No further guidance given regarding adjustments to this parameter.
λ	-	Controls in-channel lateral movement of sediment. Prevents positive feedback that can result in the development of deep, single-thread channels.	Higher values result is shallow, wide channels. Lower values result in deep, narrow channels.	10 – 20	This parameter requires calibration. No further guidance given regarding adjustments to this parameter.

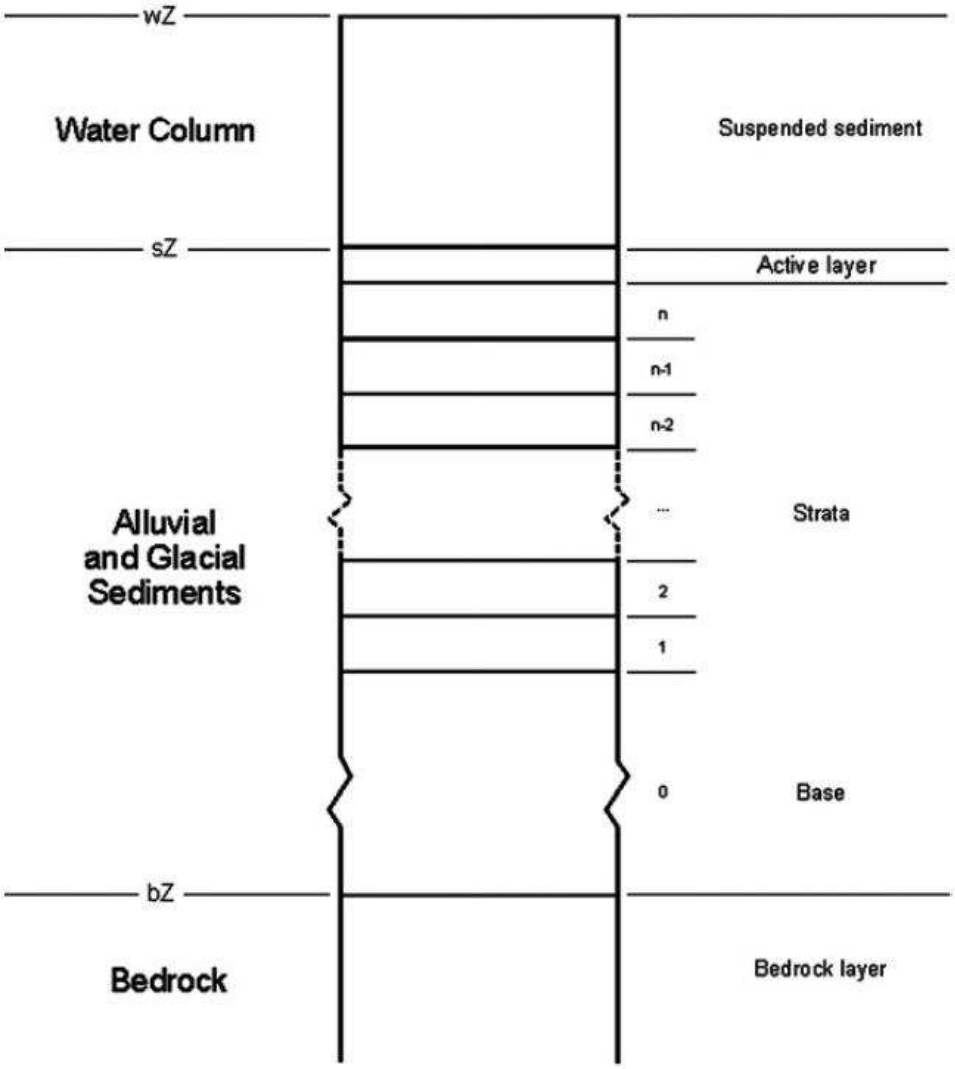

Figure 4.19 Active layer system implemented within C-L. Taken from Van De Wiel et al. (2007, p. 287).

number of stratigraphic units (Coulthard and Van De Wiel, 2007). This method allows for the emergence of key phenomena associated with heterogeneous sediment mixtures including, most significantly, development of an armour layer on the bed surface in gravel-bed channels as a result of hiding effects, selective entrainment, and downstream and vertical winnowing (Coulthard and Van De Wiel, 2007).

The thickness of the strata below the active layer is defined by the user and termed L_h (Table 4.5). The thickness of the active layer, which is the topmost layer in the system, varies between 25% and 150% of L_h. If the thickness of the active layer becomes less than 0.25 L_h, then the upper stratum is incorporated into the active layer, with a subsequent increase in the thickness of the active layer. Conversely, if the thickness of the active layer exceeds 1.5 L_h, the active layer is divided so that its thickness is reduced (Van De Wiel et al., 2007).

The volume of sediment eroded from a cell and transported to its downstream neighbours during a single iteration may be calculated by C-L based on either the Einstein (1950) or the Wilcock and Crowe (2003) transport equations (Coulthard et al., 2012). Calculation of sediment transport for each size fraction D_i using the Einstein (1950) formula involves first determining the balance between the forces acting to move and restrain a particle:

$$\psi = \frac{(\rho_s - \rho)D_i}{\rho dS} \tag{4.10}$$

In equation 4.10, the term ρdS is equivalent to τ/g, where, τ = shear stress (N m^{-2}). A dimensionless bedload transport rate ϕ can then be estimated from ψ using the relationship established by Einstein (1950):

$$\phi = 40(1/\psi)^3 \tag{4.11}$$

The value of ϕ is then inserted into equation 4.12 to find q_i, the rate of sediment transport ($m^3 s^{-1}$):

$$\phi = q_i \sqrt{\frac{\rho}{(\rho_s - \rho) g {D_i}^3}} \tag{4.12}$$

If the Wilcock and Crowe (2003) formula is selected, sediment transport rates for each sediment fraction (q_i) are found using:

$$q_i = \frac{F_i U_*^3 W_i^*}{\big((\rho_s - \rho) - 1\big) g} \tag{4.13}$$

where, F_i = fractional volume of the i-th sediment in the active layer, U_* = shear velocity ($U_* = [\tau/\rho]^{0.5}$) and W_i^* = function that relates the fractional transport rate to the total transport rate (Van De Wiel et al., 2007). To find W_i^*, it is first necessary to calculate τ_{rm}, which is the reference or critical shear stress for the mean size of the bed sediment. τ_{rm} is approximated by a function that relates the Shields parameter for the mean bed material size (τ_{rm}^*) to the percentage of sand on the bed surface (F_s):

$$\tau_{\mathrm{rm}}^* = 0.021 + 0.015 \ \exp[-20F_s] \tag{4.14}$$

The dimensionless τ_{rm}^* can then be converted to a dimensioned shear stress ($N m^{-2}$) using: $\tau_{\mathrm{rm}} = \tau_{\mathrm{rm}}^* \rho g D_{s50}$ and equation 4.15 may be rearranged to yield values for τ_{ri}, the reference or critical shear stress for the i-th size fraction:

$$\frac{\tau_{ri}}{\tau_{rm}} = \left(\frac{D_i}{D_{s50}}\right)^b \tag{4.15}$$

where, b = an exponent with the form of the equation overleaf:

$$b = \frac{0.67}{1 + \exp\left(1.5 - \frac{D_i}{D_{sm}}\right)} \tag{4.16}$$

with, D_{sm} = mean grain size of bed surface (mm).

W_i^* can then be calculated using:

$$W_i^* = \begin{cases} 0.002\phi^{0.75} & \text{for } \phi < 1.35 \\ 14\left(1 - \frac{0.894}{\phi^{0.5}}\right)^{4.5} & \text{for } \phi \geq 1.35 \end{cases} \tag{4.17}$$

where, $\phi = \tau/\tau_{\mathrm{ri}}$. W_i^* is then substituted into equation 4.13 to obtain the sediment transport rate, q_i (m^3s^{-1}).

Calculation of bed shear stress (τ) is essential to the application of both the Einstein (1950) and Wilcock and Crowe (2003) formulae available in C-L. The value of τ is determined from flow velocity using:

$$\tau = \rho C_{\mathrm{d}} u^2 \tag{4.18}$$

where, ρ = density of water (kg m^{-3}); u = flow velocity (m s^{-1}) and C_{d} = a drag coefficient determined using equation 4.19:

$$C_{\mathrm{d}} = g n^2 h^{0.33} \tag{4.19}$$

Where, n = Manning's n. Selection of either equation 4.12 or 4.13 yields a sediment transport rate for each grain size fraction, which must be converted into a volume for the time step and then summed for the entire size distribution. The volumetric conversion is achieved by multiplying the transport rate by the duration of the time step:

$$V_i = q_i \mathrm{d}t \tag{4.20}$$

where, i = grain size fraction; V = volume (m^3); q = transport rate ($m^3 s^{-1}$); and $\mathrm{d}t$ = time step (s) (Van De Wiel et al., 2007). However, C-L employs a variable time-step and $\mathrm{d}t$ is controlled by a user-defined variable that specifies the maximum change in elevation that is allowed during an iteration, $\Delta Z_{\max}$ (Table 4.5). This parameter is incorporated into equation 4.21 below, where $q_{\max}$ = maximum transport rate calculated for a given iteration, and Dx = grid cell size (m):

$$\mathrm{d}t = \frac{\Delta Z_{\max} Dx^2}{q_{\max}} \tag{4.21}$$

This operation ensures that the time step decreases to less than a second during periods of intense geomorphic activity, but expands to an hour during periods of stability (Van De Wiel et al., 2007).

Eroded material is transported as either bedload or suspended load (although only the finest size fraction can be specified as being carried in suspension), and distributed to neighbouring cells according to flow velocity (Van De Wiel et al., 2007). At the end of each iteration, all of the material transported as bedload is deposited in the receiving cells ($V_{i,\mathrm{dep}} = V_i$), where it is available to be re-entrained during the next and following iterations. In contrast, deposition of suspended sediment is calculated on the basis of the sediment fall velocity, v_f (m s^{-1}) (Table 4.5) which is specified by the user, and the suspended sediment concentration, κ (Van De Wiel et al., 2007), using:

$$V_{\mathrm{dep}} = \kappa \, v_\mathrm{f} \, Dx^2 \, \mathrm{d}t \tag{4.22}$$

In addition to the capacity-limitation placed on the rate of sediment transport by the selected sediment transport formula, the rate may also be limited by the availability of a given sediment fraction in the active layer. Specifically, the

transported volume of each size fraction (V_i) must be less than or equal to the volume present in the active layer ($V_{AL,i}$) (Van De Wiel et al., 2007).

Although both the Einstein (1950) and Wilcock and Crowe (2003) formulations are mixed-size transport models that are applicable (at least theoretically) to both sand and gravel-bed channels, they were developed using empirical data from radically different channels and bed types. For example, the Einstein (1950) equation was derived with reference to channels with predominantly sand-beds that included grains ranging in size between 0.785 and 28.65 mm (Gomez and Church, 1989). The Wilcock and Crowe (2003) formula, however, was developed from flume experiments using five different sand-gravel mixtures, with grain sizes ranging between 0.5 and 64 mm (Wilcock and Crowe, 2003). These two formulae are likely to perform with varying levels of success under different conditions, although no sediment transport formula has been found to consistently predict transport rates to an acceptable level of accuracy unless calibrated using measured sediment transport data (Gomez and Church, 1989).

Given the difficulty associated with predicting sediment transport rates in general, application of either the Einstein (1950), Wilcock and Crowe (2003), or indeed any of the other sediment transport equations currently available, inevitably introduces a degree of uncertainty into the operation of C-L. As discussed later in the thesis, this uncertainty can be reduced, though not of course eliminated, by calibrating the sediment fluxes modelled using C-L against observed fluxes, when the model is optimised through hindcasting.

ii. Lateral erosion

Lateral erosion (for example, undercutting of the channel banks at the outside of river bends) that results in the development of meandering and braided channel patterns is incorporated into C-L (Coulthard and Van De Wiel, 2006). The lateral erosion algorithm proceeds by determining the local radius of bend curvature (R_{ca}) on a cell-by-cell basis (Coulthard and Van De Wiel, 2006). This is achieved by making a number of passes over the grid in order first to

identify edge cells (or cells representing the channel banks), and then to determine whether these edge cells are on the inside or outside of a meander bend (Coulthard and Van De Wiel, 2006) by counting the number of wet and dry cells around the edge cells (Coulthard et al., 2007). However, this calculation can result in cells on the outside bank being wrongly identified as inside bank cells, and vice versa (Van De Wiel et al., 2007). Consequently, a smoothing filter is repeatedly passed over the edge cells, averaging the curvature between adjacent cells and ensuring that each cell is correctly defined (Figure 4.20). The accuracy of calculated R_{ca} values depends, therefore, on the number of passes that the edge smoothing filter makes, and this is controlled by a user-defined parameter (termed here, N_{smooth}; Table 4.5).

Once the radius of curvature has been determined, lateral erosion (ζ) is calculated using:

$$\zeta = \frac{1}{R_{\mathrm{ca}}} \Lambda \tau T \tag{4.23}$$

where, Λ = lateral erosion rate (user-defined; Table 4.5); τ = shear stress of the cell adjacent to the bank (N m^{-2}); and T = time (seconds). The material eroded from the bank cell is then deposited in the cell adjacent to the bank and redistributed laterally across the channel to simulate deposition along the inside bank of the meander bend and the subsequent development of point bars. Redistribution is achieved through the use of a cross-stream, bed gradient calculated from the previously derived values of R_{ca} (Van De Wiel et al., 2007). As this algorithm assigns negative R_{ca} values to cells on the inside bank and positive R_{ca} values to cells on the outside bank, the cross-stream gradient can be determined by interpolating the R_{ca} values across the channel (Van De Wiel et al., 2007). A lateral sediment flux, Ψ_n, can then be calculated from this cross-stream gradient:

$$\Psi_n = a\left(R_{ca,n} - R_{ca,n-1}\right)h_n \tag{4.24}$$

where, n and $n-1$ respectively denote the donor cell and the receiving cell; a = a coefficient; and h = flow depth (Van De Wiel et al., 2007). The values are interpolated, or smoothed, across the channel through use of an averaging filter, which progressively makes the gradient smoother with each pass that it makes. The smoothness of the cross-channel gradient therefore depends on the number of smoothing iterations, which is in turn controlled by a user-defined parameter ($\Delta\nabla_{\max}$; Table 4.5) that specifies the maximum difference that can be allowed in the R_{ca} values of in-channel cells between consecutive smoothing iterations. Specifying a low value of this parameter results in greater cross-channel smoothing, while higher values may result in the deposition of sediment in the middle of the channel, rather than at the inner bank.

Although the radius of curvature method used to simulate lateral erosion in C-L has been shown to produce qualitatively realistic retreat of the outer banks of meander bends, there is no physical basis for assuming that cross-channel gradient of curvature governs lateral distribution of eroded sediment (Coulthard and Van De Wiel, 2006). Furthermore, deposition of sediment onto point bars at the insides of meander bends is not an emergent property of the model, but rather has to be coded explicitly. This is due to the fact that secondary circulation at a bend, which would result in preferential deposition on point bars as a result of in-channel hydraulics and sediment fluxes, is not represented by the flow model (Coulthard and Van De Wiel, 2006; Van De Wiel et al., 2007). Moreover, the algorithm fails to simulate cut-off of tortuous meander bends, which can lead to development of over-sinuous channel patterns in the C-L model (Coulthard and Van De Wiel, 2006).

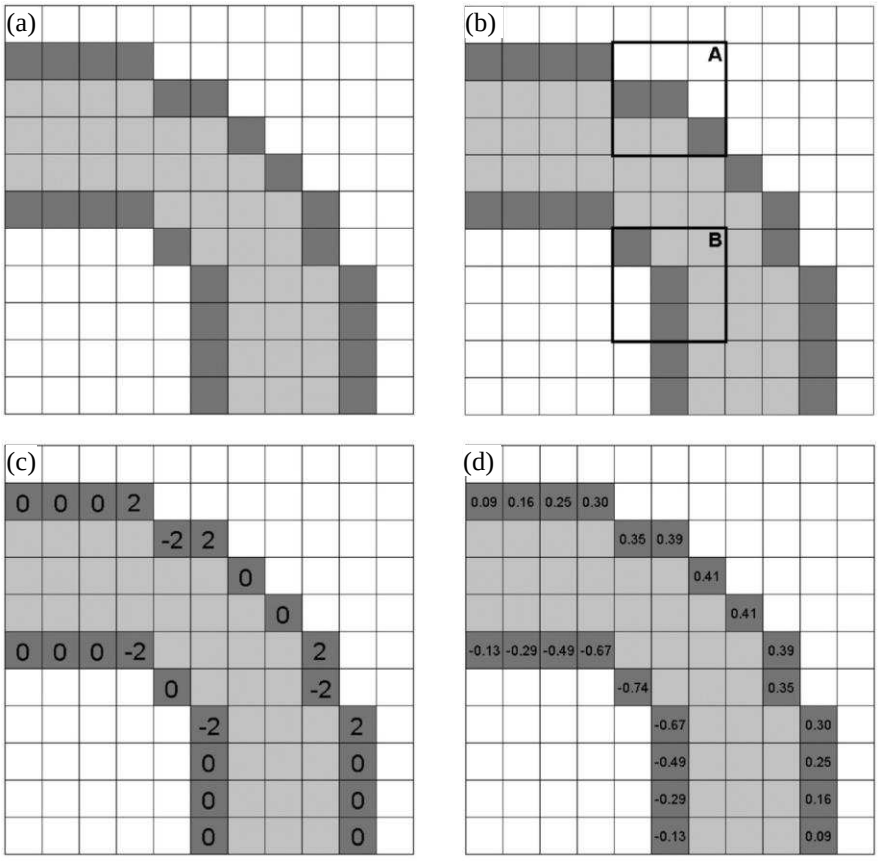

Figure 4.20 Calculation of curvature coefficient used in lateral erosion algorithm: (a) determination of edge cells (dark); (b) counting number of dry and wet cells in a 3 x 3 filter; (c) difference between dry and wet cells assigned to centre of filter; (d) repeated smoothing interpolates values of edge cells. Taken from Van De Wiel et al. (2007, p. 289).

Finally, the downstream migration of meander bends, which occurs in nature due to concentration of erosion downstream of the bend apex, on the downstream limb of the outer bank (Knighton, 1998), is modelled in a very simplified manner. Specifically, C-L shifts the previously calculated cross-channel gradient downstream by a number of cells specified by a user-defined parameter, N_{shift} (Table 4.5). This acts to move the maximum gradient of cross-channel sediment flux downstream and, thus, shifts the focus of lateral erosion to downstream cells. This simplified representation of channel planform development is a key limitation of the way lateral erosion is represented in C-L and this may have significant implications for the ability of the model to replicate geomorphological changes driven by channel planform evolution, at least at the local-scale.

C-L also moves sediment laterally within the channel independently of meander sinuosity effects represented using the lateral erosion algorithm described above which refers only to local bank retreat due to meander bend growth. The in-channel lateral erosion rate is controlled by a user-defined parameter (λ) (Table 4.5) designed to prevent positive feedback mechanisms that can otherwise result in the development of excessively deep, single-thread channels. Within the formulation, material from an adjacent in-channel (donor) cell is added to any (recipient) cell that has experienced erosion during a given iteration, in order to distribute bed erosion more evenly across the channel. The volume of material moved from the donor cell is dependent on the value of λ, the volume of material previously removed from the recipient cell and the difference in elevation between the donor and recipient cells. This formulation can be summarised as:

$$\Delta Z_{n-1} = \frac{E_{n-1}\,\lambda(Z_n - Z_{n-1})}{Dx} \tag{4.25}$$

where, n and $n-1$ respectively denote the donor cell and the receiving cell; Z = cell elevation; ΔZ = change in cell elevation (m); E = volume of material eroded (m^3); λ = user-defined in-channel lateral erosion rate; and Dx = grid cell size (m).

Physically, this parameter can be considered to represent the effects of cohesion between the sediments making up the channel boundary materials (Coulthard, 2013). High values of this parameter are analogous to noncohesive sediments in which in-channel lateral transport and sediment redistribution occurs readily, resulting in channels that are shallow and wide. Lower values represent cohesive boundary materials that allow limited re-distribution of eroded sediments through lateral transport and which, therefore, tend to be associated with channels that are narrow and deep.

4.4.2 Identification of requisite input data and parameter definition

The key requirement for the calculation of erosion and deposition using C-L is a data set from which the representative size distribution of sediment within the catchment can be derived. As discussed in Section 4.4.1, such a data set should have two fundamental characteristics:

1. it should relate to material that has not been reworked by fluvial processes; and,
2. it should be characteristic of material found throughout the catchment rather than being representative of a small number of point locations.

The debris avalanche deposited during the 1980 eruption of Mount St Helens (Chapter 2) represents the dominant sedimentary unit in the upper North Fork Toutle River basin. Although the debris avalanche was blanketed by deposits associated with the lateral blast, these were generally no more than 1 m thick (Hoblitt et al., 1981; Moore and Sisson, 1981). Pyroclastic flow deposits were also deposited in the catchment following the May 18 eruption, but these were also thinly distributed (generally less than several metres), small in volume (less than 5% of the volume of the debris avalanche) and highly localised (confined mainly to the upper slopes of Mount St Helens and the pumice plain) (Rowley et al., 1981).

The blast and pyroclastic flow deposits are, therefore, superficial and do not represent significant sources of sediment within the upper North Fork Toutle River catchment. Moreover, channel incision, which was the dominant initial adjustment process (Simon, 1999; Zheng et al., 2014), lowered stream bed elevation in the order of tens of metres (Meyer and Martinson, 1989). Processes of lateral adjustment through bank collapse, which is the primary contemporary mechanism of sediment entrainment in the catchment (Major et al., 2000), are therefore operating within the debris avalanche material. Consequently, it was necessary to characterise the gradation of the debris avalanche deposit in order to represent the dominant sediment source within the upper North Fork Toutle River catchment.

However, characterising the grain size distribution of the avalanche deposit is difficult as it extends over a substantial area and is widely graded, with particles ranging from clay-sized to blocks several thousand cubic metres in volume (Voight et al., 1981). The extensive field sampling that would be required to accurately represent the size distribution of the avalanche deposit simply was not feasible given the resources available to support this thesis. Instead, existing data sets that could be used to derive a general gradation curve were assembled, as summarised in Table 4.6. Evidently, the majority of sediment size data relates to material that has already been mobilised by fluvial processes and they are therefore not representative of the full range of grain sizes present within the debris avalanche.

The only identified data sets that related specifically to original debris avalanche material were those reported by USACE (1984) and Voight et al. (1981). The Voight et al. (1981) data were, however, limited to only 19 samples of 15 kg, and the authors also conceded that larger size fractions were inadequately represented by their sampling. This shortcoming is evidenced by the fact that the maximum sampled particle size is less than 80 mm. In contrast, the USACE (1984) data consist of 3,070 samples, including bed, bank and terrace deposits for the debris avalanche, the North and South Fork Toutle Rivers, and the Toutle River mainstem, as well as the Cowlitz and Columbia Rivers. Coarse material is better represented in this data set, although no particles greater than 512 mm were sampled.

The Voight et al. (1981) data are therefore limited, predominantly in terms of the number of samples available, and are unlikely to be representative of the composition of the debris avalanche as a whole. Consequently, the USACE (1984) data were selected for use as the primary basis for representing the initial sediment size distribution in model hindcasting and forecasting (Chapters 5 and 6, respectively).

Within the project database, samples were collated and summarised according to river, river mile and the type of deposit from which the sample was taken. This organisation facilitated the extraction of gradation data for 471 samples

pertaining solely to the original debris avalanche deposit and excluding coarser, reworked alluvium or lag deposits. These samples were collected between Spirit Lake (river mile 36.5) and the N1-DRS (North Fork Toutle River, mile 20). A summary gradation curve based on compilation of all the samples, together with the mean +/- one standard deviation, is presented in Figure 4.21 (a). The mean gradation curve was subdivided into nine grain size fractions for implementation within C-L, as shown in Figure 4.21 (b). Although the derived grain size distribution is initially applied to all cells within the catchment, the processes of fluvial erosion, transport and deposition included within the model modify this distribution through time. Indeed, redistribution of sediment grain size is one of the key purposes of the 'spin up' period, which is described in more detail in Section 4.7.

Although a lack of metadata is a significant shortcoming of the database presented within the Sedimentation Study (USACE, 1984), it was the most appropriate source of information regarding the size distribution of the debris avalanche that could be identified. Moreover, the data extracted satisfy the two criteria outlined above. Significantly, they relate to un-reworked material and therefore include the full range of grain sizes that are available for erosion within the catchment. The size of the extracted data set (471 samples) and its wide spatial extent also ensures that it is representative of the sediment size distribution throughout the catchment. Data from USACE (1984) were also used by the Biedenharn Group (2010) to characterise the composition of the debris avalanche material.

Table 4.7 summarises the values defined for each of the additional parameters that require specification (Table 4.5), together with an explanation of how these parameters have been estimated.

Table 4.6 Sources of sediment size distribution data in the North Fork Toutle River catchment.

Source	Type of sediment sampled	Location of samples taken	Collection period
Simon and Klimetz (2012)	Active channel bed and bank material	North Fork Toutle River above the SRS	2009 – 2010
Biedenharn Group (2010)	Suspended sediment	North Fork Toutle River below the SRS	2001 – 2009
Biedenharn Group (2010)	Active channel bed material	SRS sediment plain	2007
Dinehart et al. (1981); Dinehart (1986; 1992; 1998)	Active channel bed material Suspended load	North Fork Toutle at Kid Valley below the SRS	1980 – 1990
Paola and Seal (1995)	Active channel bed material	SRS sediment plain below N1-DRS	1990
Simon (1999)	Active channel bed material and subpavement	North Fork Toutle River above the SRS	1991 – 1992
USACE (1984)	Debris avalanche	North Fork Toutle River between N1-DRS and Spirit Lake	1980 – 1984
USACE (1988)	Active channel bed material Suspended load	North Fork Toutle River between mouth and Spirit Lake	1980 – 1988
USACE (1989, 1990, 1991, 1992)	Active channel bed material	SRS sediment plain below N1-DRS	1989 – 1992
Voight et al. (1981)	Debris avalanche	North Fork Toutle River and tributaries upstream of N1-DRS	1981
WEST (2002)	Active channel bed material	North Fork Toutle River and tributaries upstream of N1-DRS	2000

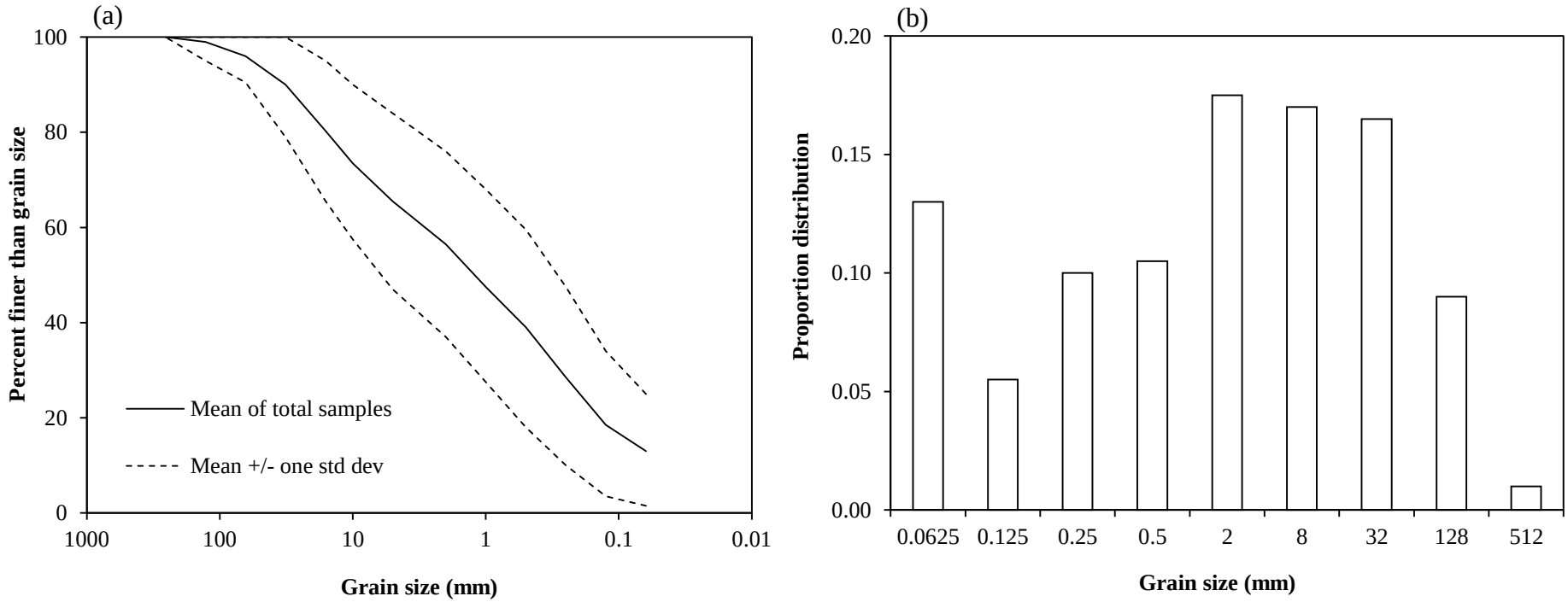

Figure 4.21 Sediment data derived from the USACE (1984) Toutle and Cowlitz Rivers Sedimentation Study: (a) cumulative frequency curve and (b) nine grain size fractions defined for use within C-L.

Table 4.7 Selected values for each of the parameters required for calculation of fluvial erosion within the C-L model.

Parameter	**Units**	**Selected value**	**Justification**	**Notes and comments**
Sediment transport formula	-	Undefined	Both the Einstein (1950) and Wilcock and Crowe (2003) formulations are mixed-size transport models that and could be applicable to the study catchment.	Testing and specification of this parameter is undertaken in Chapter 5.
v_{f}	m s^{-1}	0.0032	Calculated using Stokes' law: $v_{\mathrm{f}} = \frac{g(\rho_p - \rho_f)d^2{}_p}{18\mu}$, where g = gravitational acceleration (m s^{-2}); ρ_p = density of particle (kg m^{-3}); ρ_f = density of fluid (kg $^{-3}$); d_p = particle diameter (m); and μ = absolute viscosity of fluid (N m^{-2}).	Calculated for the finest size fraction (0.0625 mm). No data were available for particle density, and so a value of 2,650 kg m^{-3} for sand was used. Given that v_{f} can be justified physically, adjustments to this parameter will be avoided.
$\Delta Z_{\max}$	m	0.02	This is the default value. Suggested conditions for when this parameter should be adjusted are not met.	-
L_h	m	0.1	This value is within the 'normal' range and is greater than four times $\Delta Z_{\max}$.	Sufficient information is not available on which to justify adjustments to this parameter.
N_{smooth}	-	30 and 40	This parameter could not be defined conclusively, but could be estimated on the basis of channel sinuosity, calculated by digitising high resolution aerial photography.	The two values are implemented in a suite of model runs described in Chapter 5.

			Average sinuosity (ratio of channel length to valley length) was 1.12 indicating that channels in the catchment are gently meandering rather than tortuous. Values towards the upper end of the recommended range (which is 10 – 50) were therefore considered to be most appropriate for this application. Two values were selected given uncertainties surrounding the exact definition.	
Λ	-	Undefined	This parameter could not be estimated with any confidence on the basis of empirical data. The fact that the recommended values range over two orders of magnitude necessitates additional work in order to constrain this range.	Testing and specification of this parameter is undertaken in Chapter 5.
$\Delta\nabla_{max}$	-	0.0001	This is the default value. Suggested conditions for when this parameter should be adjusted are not met.	-
N_{shift}	-	3 and 4	One-tenth of the two values used for N_{smooth} respectively.	The two values are implemented in a suite of model runs described in Chapter 5.
λ	-	10, 15 and 20	This parameter could not be defined conclusively or estimated on the basis of empirical data. However, the range of recommended values could be represented using the three values specified here.	The three values are implemented in a suite of model runs described in Chapter 5.

4.5 SLOPE PROCESSES

4.5.1 Model operation

Mass movements are represented in the C-L model as instantaneous slope failures that move material from an upslope cell to the adjacent, downslope cell when the slope between the two cells exceeds a user-defined, critical threshold (Coulthard et al., 2002) (Table 4.8). As failure scarps often propagate upslope, the model employs an iterative procedure to check for failures of adjacent cells until the slope becomes stable (Coulthard et al., 2000). As with all model parameters, the slope instability threshold is applied uniformly through both space and time, and although recent work has investigated varying the failure threshold according to soil saturation (Coulthard, 2013), this functionality is not yet available. Inclusion of mass movements within C-L enables material derived from both local failures, such as streambank collapse, and large scale events, such as landslides, to be fed into the fluvial system (Hancock et al., 2011).

Soil creep (m) is also modelled within C-L using equation 4.26:

$$Creep = \frac{SC_{\mathrm{rate}}T}{Dx} \tag{4.26}$$

where, S = slope; C_{rate} = user-specified rate of soil creep (m yr^{-1}) (Table 4.8); and T = time (years). This equation represents diffusion-like processes whereby sediment flux is linearly proportional to surface slope (Carson and Kirkby, 1972). Additionally, C-L represents soil erosion by surface wash using an adaptation of the Universal Soil Loss Equation (USLE) (Wischmeier and Smith, 1978). The USLE developed for estimating sheet and rill erosion is defined by:

$$A = RKLSCP \tag{4.27}$$

where, A = calculated soil loss; R = rainfall-runoff erosivity factor; L = slope length factor; S = slope steepness factor; C = land cover management factor; and P = supporting practices factor (Renard et al., 1991). Within C-L, this equation is simplified and takes the form:

$$A = \frac{SE_{\mathrm{r}}LT}{Dx} \tag{4.28}$$

where, E_{r} = a user-defined soil erosion rate (m yr^{-1}) (Table 4.8); and slope length, L, is estimated as the square root of the upstream drainage area for a given cell. The inclusion of the E_{r} parameter allows the rate of soil erosion by surface wash to be calibrated for the particular catchment being modelled, as the rate is likely to vary between different soil types and land management practices, for instance. The three parameters that require definition by the user are summarised in Table 4.8.

4.5.2 Parameter definition

To define the slope failure threshold, slope angles were calculated from the original (3 m horizontal resolution), 2003 LiDAR DEM (Section 4.2) using the Slope Tool in the ArcMap Spatial Analyst Toolbox. This Tool calculates the maximum rate of change in elevation between each cell and its neighbour (ESRI, 2013) and produces a raster with a slope value for each cell. The output raster indicated that the angle of alluvial terraces was often greater than 40^{o}, but rarely greater than 60^{o} (Figure 4.22). Hence, the slope failure threshold was set to 60^{o} as this appears to represent the maximum stable slope within the upper NFTR catchment. Although individual slopes may locally exceed this angle, a value of 60^{o} was selected as being the most appropriate at the catchment-scale.

Processes of soil creep and erosion by surface runoff were not included in the C-L model applied in this research for four reasons. First, the data necessary to define the parameters required to apply the relevant algorithms do not exist and

Table 4.8 Parameters required to model slope processes in C-L.

Parameter	**Units**	**Operational purpose**	**Impact and model sensitivity**	**Recommended/ default values**	**Notes and comments**
Slope failure threshold	Degrees	Defines the maximum stable slope. Landslides occur when the angle between two adjacent cells exceeds this value.	Higher values may result in overly steep slopes; lower values may increase slope failure frequency excessively.	-	Can be estimated from relevant data, DEM analysis or field reconnaissance.
C_{rate}	m yr^{-1}	Used to calculate diffusion-like processes of soil creep	Results in erosion of steeper slopes and the rounding of sharp terrain features.	0.0025	-
E_{r}	m yr^{-1}	Used to calculate soil erosion by surface wash processes.	Unknown	-	This parameter remains under development and has not been tested or calibrated.

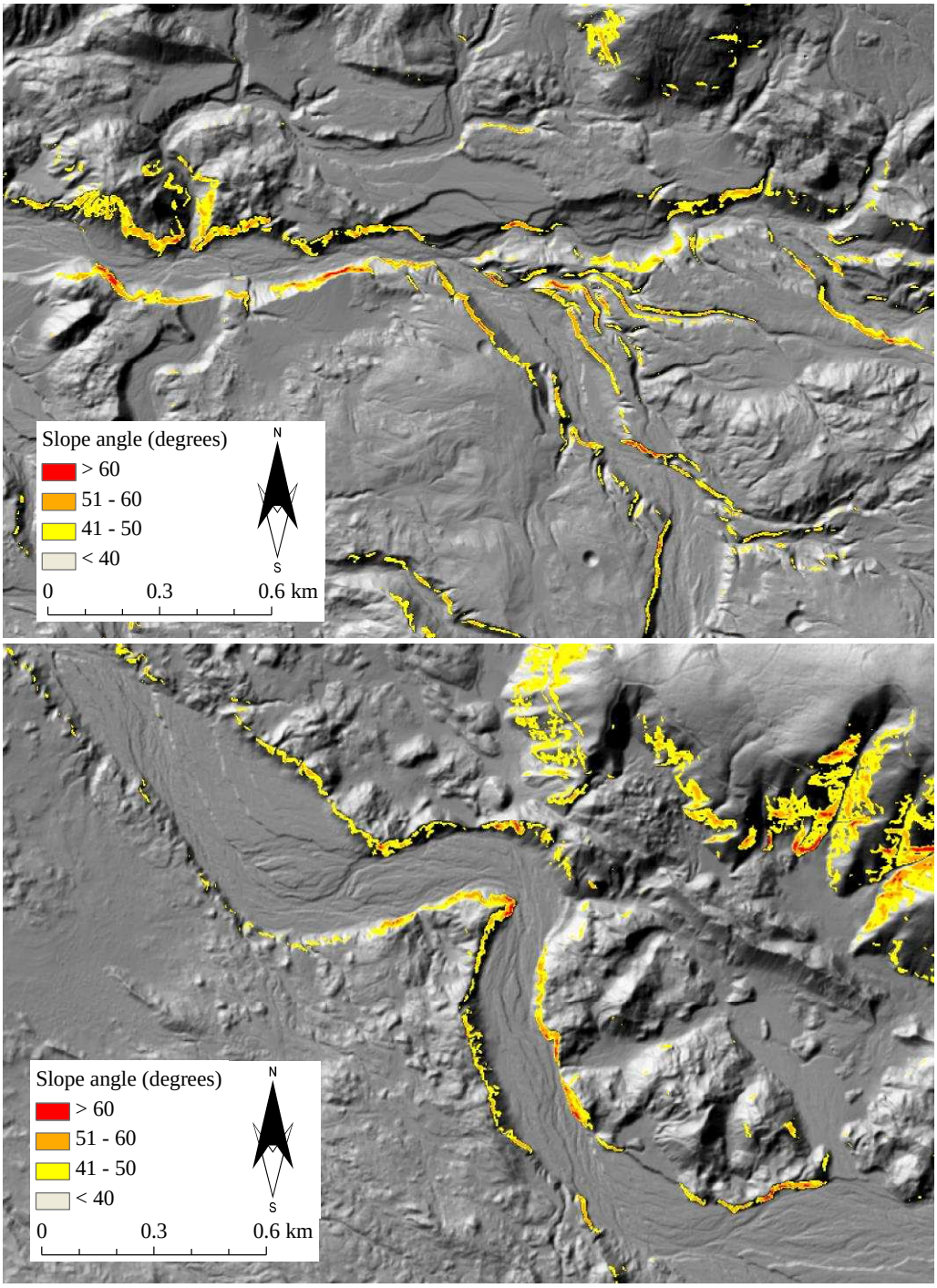

Figure 4.22 Slope angles mapped onto the DEM in two areas of the upper North Fork Toutle River catchment, demonstrating the prevalence of terrace slopes with angles between 40 and 60°.

the extent of sampling that would be necessary to derive them through primary data collection was not possible given the resources available to support the doctoral research project. Second, these processes operate over long timescales and are not particularly effective over the timescale relevant to the current modelling application. Specifically, it is unlikely that the influence of soil creep and slope wash on landscape evolution would be discerned at the sub-decadal timescale used in the hindcasting calibration run, rendering meaningless their inclusion in the sensitivity analysis. Further, the timescale of forecasting is, as described in Chapter 6, also decadal and, therefore, probably too short for processes of soil creep and surface erosion to substantially influence the catchment-scale sediment yield.

Third, relative to fluvial processes operating in the basin, surface erosion is not a significant source of sediment (Jon Major, USGS Cascades Volcano Observatory, personal communication, 2012). As discussed in Section 2.4, short-term rainfall intensity is low and periods of rain generally occur continuously over a period of time rather than falling as short, heavy downpours (Meyer and Martinson, 1989; Uhrich, 1990). As such, surface erosion from high-intensity rainfall events is not a significant process at the annual scale. It is also unlikely that possible increases in rainfall due to climate change will increase the contribution of surface erosion as surfaces not impacted by fluvial processes (interfluves) will continue to revegetate. As discussed in Section 4.6, however, revegetation is unlikely to reduce the future rate of fluvially-driven erosion. Finally, the parameters C_{rate} and E_{r} are still under development and have not yet been extensively tested (Coulthard, 2013).

4.6 VEGETATION

4.6.1 Model operation

The influence of in-channel and riparian vegetation on processes of fluvial erosion can be modelled within C-L using a simplified vegetation growth model, the parameters of which are summarised in Table 4.9. The model

Table 4.9 Parameters used to model the influence of vegetation on fluvial erosion in C-L.

Parameter	**Units**	**Operational purpose**	**Impact and model sensitivity**	**Recommended/ default values**	**Notes and comments**
T_{veg}	Years	Specifies the time taken for the vegetation layer to reach full maturity; controls the gradient of the relationship between maturity and time.	Higher values will negate the influence of this parameter over short timescales.	-	Can be estimated based on known rates of vegetation growth.
τ_{crveg}	N m^{-2}	The value of bed shear stress above which vegetation will be removed (i.e. maturity re-set to zero).	Lower values relate to vegetation that is less resistant.	-	Can be estimated based on known strength of vegetation.
Proportion of erosion that can occur when vegetation is fully grown.	-	Determines how vegetation maturity influences processes of fluvial erosion.	Values of 1 mean that vegetation has no impact on erosion, even at full maturity; values of 0 mean that no fluvial erosion will occur when the vegetation layer is fully mature.	0 – 1	Can be estimated based on known strength of vegetation.

operates by allowing a vegetation layer to develop above the active layer. The development of this layer acts to limit the volume of material that can be removed from a cell and so allows the model to represent increases in the erosion resistance of bed and bank materials that result from the growth of vegetation. The resistivity of the vegetation layer increases gradually through time, at a rate defined by the user, to simulate the progressive growth of vegetation. Specifically, the user selects the length of time (in years) required for the vegetation layer to reach full maturity (T_{veg}) (Table 4.9), at which point it exerts its strongest influence on fluvial erosion processes.

Additionally, the user can adjust the influence that the vegetation has when it is fully 'grown' (maturity = 1) by specifying the percentage of material that has been calculated to be removed from a cell (by the erosion model) that will actually be entrained and moved to downstream cells. The model will then calculate a value for vegetation maturity between 0 (no vegetation) to 1 (full maturity) for each time step by linear interpolation, and multiply this by the value of vegetation resistance at full maturity to calculate resistivity due to erosion at a given time step. However, the model recognises that vegetation can be destroyed during extreme flood events, and accounts for this by defining a critical shear stress for vegetation removal by fluvial erosion (τ_{crveg}) (Table 4.9). If this value is exceeded in a cell, vegetation maturity in that cell will be re-set to zero.

4.6.2 Parameter definition

In applying C-L to the upper catchment of the North Fork Toutle River, the relevant parameters were set to negate the influence of vegetation in limiting fluvial erosion (T_{veg} = 100; τ_{crveg} = 0.001; Proportion of erosion that can occur when vegetation is fully grown = 1). The reasoning that led to this decision is set out below. The current extent and successional stages of vegetation vary widely across the catchment. While elevated terrace surfaces are covered with herbaceous vegetation, and thickets of willow and alder grow along groundwater seeps and stable, spring-fed channels, vegetation remains sparse

on floodplains and is practically absent from the banks of streams making up the main drainage network owing to the high mobility of boundary sediments and their unstable and rapidly shifting nature (Major et al., 2009). Lateral channel change on the debris avalanche deposit has therefore persisted at a pace that has suppressed establishment of extensive riparian vegetation (Swanson and Major, 2005).

This implies that vegetation has not in the past and is not currently acting to limit fluvial erosion by stabilising the channel margins. On the contrary, fluvial erosion and frequent reworking of the floodplains is evidently limiting the spread of vegetation. Vegetation effects may become more important in future, but only once conditions for its establishment and succession in floodplains and along actively migrating channels become more favourable. As stated by Swanson and Major (2005), however, biotic stabilisation along the banks of unstable river reaches on the debris avalanche deposit appears to be years in the future.

The largely negligible influence of vegetation recovery on the rate of channel adjustment in severely disturbed fluvial systems has also been observed in a number of previous studies. For instance, Gran and Montgomery (2005) found that ecological recovery following the 1991 eruption of Mount Pinatubo, Philippines, was prohibited by high sediment transport rates and persistent channel instability. In their study, Gran and Montgomery (2005) also noted that high terraces with sheer cliffs tens of metres high (which represent the dominant sediment source at Mount St Helens) are essentially immune to any stabilising effects of vegetation as they are well above the rooting depth of most plants.

Similarly, Simon and Hupp (1987) showed that high rates of channel widening along hundreds of kilometres of streams recovering from channelisation in West Tennessee, USA, preclude substantial vegetation establishment. All species were found to have positive associations for low widening rates, suggesting a pervasive influence of widening characteristics in patterns of species distribution (Simon and Hupp, 1987). Moreover, Hupp (1992) observed

that establishment of woody vegetation along recovering West Tennessee streams coincided with the site of initial geomorphic restabilisation. As such, Hupp (1992) concluded that some minimum amount of bank stability must be attained, geomorphically, before successful vegetation establishment occurs. The findings of these studies support the contention that revegetation is unlikely to play a major role in controlling channel evolution and sediment yields in the upper North Fork Toutle River catchment, which are predominantly driven by high rates of lateral erosion.

Moreover, the effect of riparian and bank vegetation in reducing sediment yields could not be assessed during model testing, as this was based on hindcasting during a period when there was no significant vegetation in and around the main channels of the drainage network. Due to lack of the data necessary to calibrate the required parameters it was, therefore, necessary to conclude that evolution of the fluvial system to date has been unhindered by the stabilising effects of in-channel or riparian vegetation and there is no reason to assume that this will change in the next few decades.

4.7 ADDITIONAL MODEL CONFIGURATION

4.7.1 Specifying the depth of erodible sediment

The depth and distribution of unconsolidated sediment that is characterised by the nine grain size fractions specified in Section 4.4.2 and available for erosion can be incorporated into C-L through the use of a second elevation model. This additional DEM represents the bedrock surface beneath the surficial deposits, which is non-erodible over the timescales relevant to this study and which therefore acts to limit the potential depth of channel incision. In order to determine whether it was necessary or appropriate to include a bedrock layer for the current application, a 1:100,000 scale geological map of the North Fork Toutle River catchment was obtained from Washington State Department of Natural Resources (WADNR, 2011) and used to identify areas where bedrock

outcrops are likely to act as local controls on bed elevation and gradient and so play a significant role in limiting fluvial erosion.

The map in Figure 4.23 displays the major geologic units present in the North Fork Toutle River valley. Where unconsolidated units associated with the 1980 eruption were identified, specifically debris avalanche, pyroclastic flow and lahar deposits, bedrock elevation was set to zero, meaning that vertical incision was not limited in these areas. Available data on local variations in the thickness of the debris avalanche and associated deposits were insufficient to construct a detailed DEM for the bedrock surface. Also, no significant bedrock outcrops or bed controls were identified during extensive ground and aerial surveys of the entire drainage network performed during summer fieldwork in 2011 and 2012. Consequently, it was concluded that there was no basis upon which to model bed rock outcrops as limiting fluvial erosion in areas where unconsolidated units associated with the 1980 eruption have been identified. This finding is consistent with published explanations of how channel incision in the North Fork Toutle River has been limited not by geology but by converging trends of decreasing bed shear stress and increasing bed material size (Simon and Thorne, 1996; Zheng et al., 2014).

In areas where Tertiary bedrock units are present, principally on the valley valley sides, Coldwater Ridge and Johnston Ridge, bedrock was specified to exist at a depth of 2 m below the surface. Again, this is a generalisation that had to be made in the absence of sufficient data to map the thickness of surficial deposits in detail, but it is based on knowledge of the catchment derived from the literature and field reconnaissance performed as part of this study, in 2011 and 2012. As discussed in Chapter 2, these areas did not experience deposition of significant quantities of sediment during the eruption of 1980, and it is known that sediment yield from hillslopes declined to background levels within 5 years of that event (Major et al., 2000).

Moreover, given that the grain size distribution obtained from USACE (1984) relates to the debris avalanche deposit, it is not an adequate representation of the sediment present on these hillslope areas. Additionally, bedrock exposures

are evident on many of the steeper slopes of Johnston and Coldwater Ridge (Figure 4.24), while other areas identified as being either Tertiary bedrock or Quaternary glacial till have already fully revegetated (Figure 4.25). Specifying a shallow bedrock depth is, therefore, reasonable in order to preclude the possibility of unrealistic rates of erosion being modelled in these areas. A 2 m bedrock depth was, however, specified to allow channels to develop during the initial model evolution period, which is described in the following sub-section.

4.7.2 Evolving model initial conditions

Prior to undertaking the hindcasting simulations, it was necessary to define the initial conditions for grain size and topography, a process which is difficult to achieve with any accuracy through manual techniques. This is commonly referred to in the literature as the model 'spin up' period (e.g. Coulthard, 1999; Coulthard et al., 2002; Hancock et al., 2010). During 'spin up', the model is run for a period of time sufficient to allow the initial conditions to evolve to the point that excessive variability in rates of erosion and deposition operating within the model settle towards a degree that is more representative of that exhibited by the prototype fluvial system. For example, 'spin up' enables the model to smooth out unrealistically steep gradients between cells that have been introduced during DEM production and resampling.

Additionally, as the grain size distribution developed in Section 4.4.2 is initially applied homogeneously throughout the catchment, the 'spin up' period provides the opportunity for cells within the channels to coarsen through selective entrainment, and for armour layers to develop in those reaches where the initial size distribution is conducive to armouring. Flushing of fines from the in-channel cells and smoothing of topographic features during model 'spin up' generally results in a period of very high sediment output which is not representative of catchment behaviour and should therefore be excluded from model analyses (Coulthard, 1999; Coulthard et al., 2002; Hancock et al., 2010).

The duration of the ‘spin up’ period required to enable initial conditions to settle, as described above, varies between model applications, and determining the appropriate length is somewhat subjective. In this study, the hydrograph for the 2004 water year (October 1, 2003 to September 30, 2004) was repeated six times to facilitate inter-annual comparisons of modelled catchment sediment discharge in an attempt to identify the point at which the initial model adjustment phase was complete.

It was anticipated that this initial adjustment phase would be marked by elevated sediment yields and substantial reductions in sediment production year-on-year, while the subsequent equilibrium phase would be characterised by reduced sediment yields and much subdued inter-annual variability. The transition between the two phases should then be marked by a break of slope in plots of annual sediment yield, which would correspond to the necessary duration of the ‘spin up’ period. Annual sediment yields are plotted in Figure 4.26 for each of the ten, initial model testing runs, the details of which are described fully in the next Chapter. These plots were used to assess whether the type of transition described above can be identified and applied to define the run duration required for the model ‘spin up’ period.

Test Run 1 shows a sharp decline in sediment yield from year one to year two, followed by stabilisation in sediment production with only small inter-annual variability between years two and six. The transition between years one and two may, therefore, represent the expected break of slope described above. In contrast, annual sediment yield generally increases during the first years of Test Runs 2 and 3, with maximum erosion evident during years three and four, respectively. Although this initial adjustment is somewhat counterintuitive, sediment production is again seen to stabilise as expected. In the remainder of the plots (Test Runs 4 to 10), however, sediment yields are elevated during the first three years, with the maximum annual sediment yield observed either in year one or two. Sediment yields subsequently plateau at a relatively low value for the final three years of the simulation. These later plots, therefore, correspond more closely to the expected pattern of model adjustment described above.

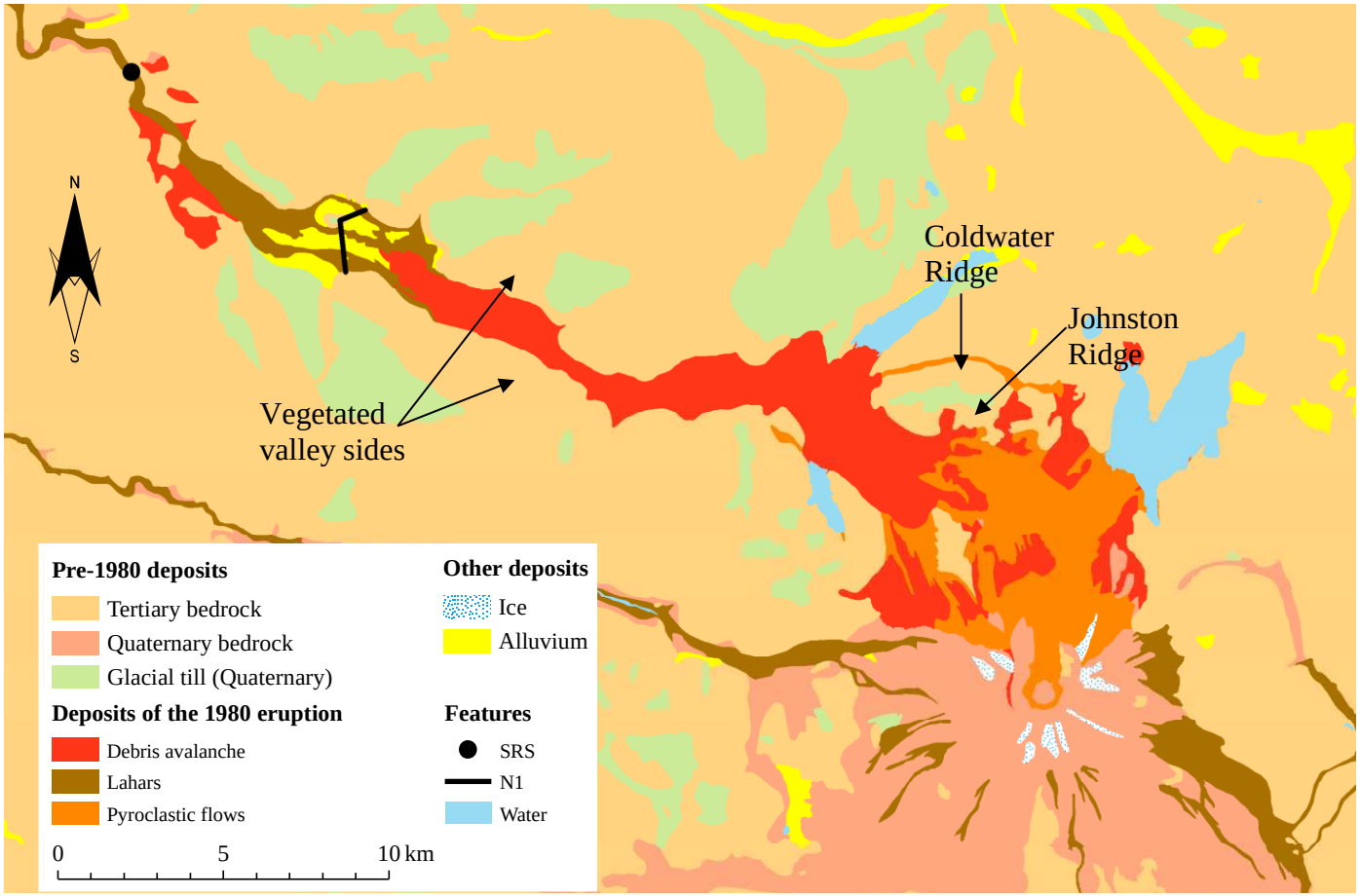

Figure 4.23 Major geologic units in the upper North Fork Toutle River catchment. USGS 1:100,000 scale Geologic Quad sheets downloaded from Washington State Department of Natural Resources (WADNR, 2011).

Figure 4.24 Bedrock outcrops on the southern side of Johnston Ridge. Photograph by author (2011).

Figure 4.25 Vegetated valley sides and unvegetated floodplain along the main channel of the North Fork Toutle River near N1-DRS. Photograph by author (2011) looking upstream in an easterly direction.

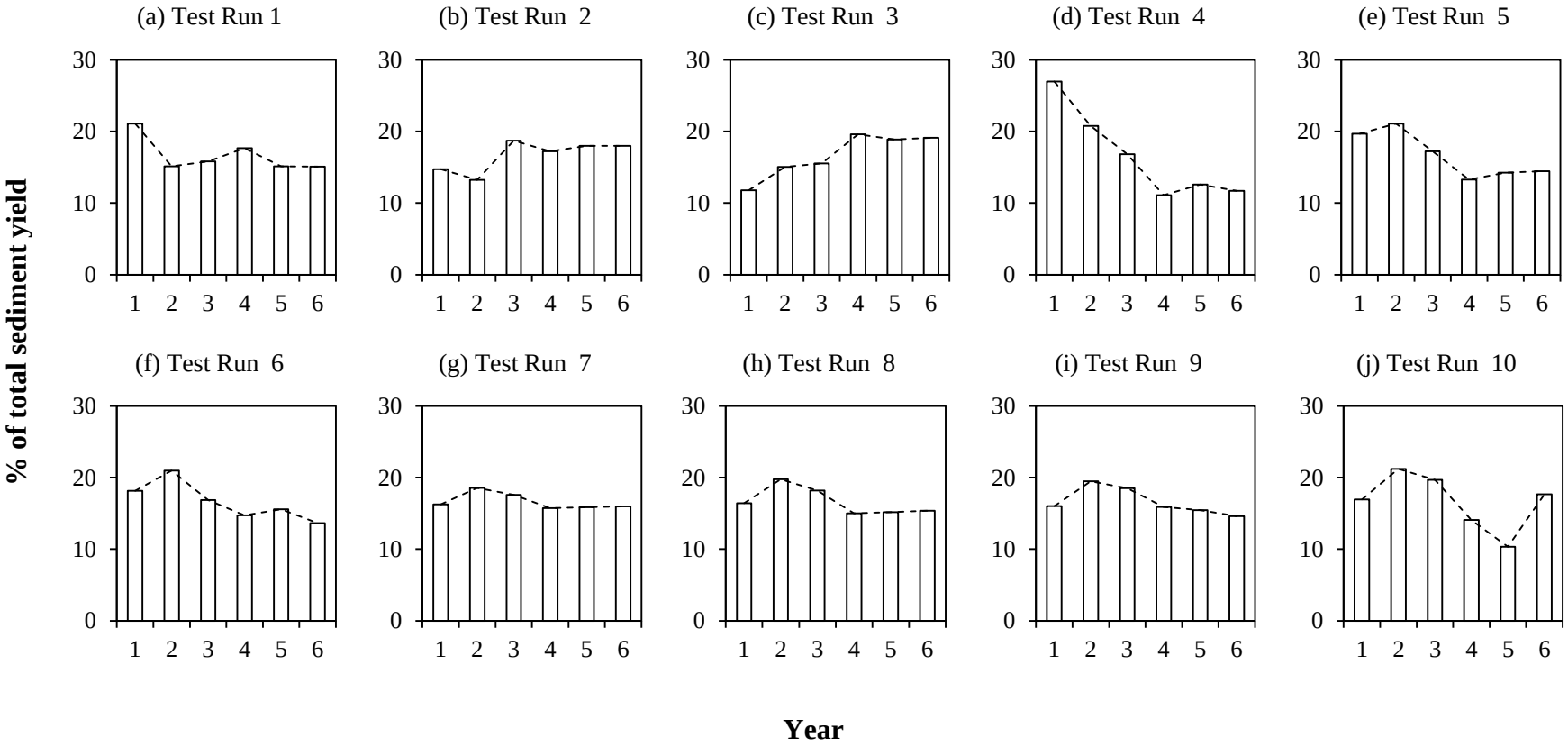

Figure 4.26 Modelled annual sediment yields produced in runs designed to identify the optimum model 'spin up' duration, using the hydrograph from water year 2004 repeated six times.

Although there is clearly some variation between the models in terms of the trends of sediment production, the results of these analyses are useful in defining the appropriate duration for the 'spin up' period. With the exception of Test Run 1, the first three years are characterised by substantial inter-annual variability, with sediment yields showing either strongly increasing or decreasing trends. These trends imply that rapid elevation adjustments are on-going within the model, and that sediment yields are not solely discharge-dependent during this time. The elevated sediment yields and the occurrence of peak sediment yield during the first three years in the majority of simulations (with the exception of Test Runs 2 and 3) also indicate that this amount of time is required to flush fine sediment from the catchment and to coarsen in-channel cells.

The reduced inter-annual variability observed for the majority of models after three years suggests that the initial adjustment processes are complete by this point, and that the model has reached a good operating condition. The secondary peak during year six for Run 10 may indicate that a longer 'spin up' period could be used for that particular set up. However, extending the duration of the 'spin up' to six years would considerably increase overall run times and, therefore reduce the number of scenarios that could be assessed as part of the model evaluation. Consequently, a period of three years was selected as the optimum duration for model 'spin up' in the current study and this was applied in all the model runs described in the next Chapter.

CHAPTER 5 HINDCASTING: SIMULATING RECENT GEOMORPHOLOGICAL EVOLUTION IN THE UPPER NORTH FORK TOUTLE RIVER CATCHMENT

5.1 INTRODUCTION

5.1.1 Model validation, evaluation, calibration and selection

Common to all modelling applications that aim to generate long-term forecasts of a particular phenomenon is the need to assess the extent to which the model is likely to be representative of reality in new spaces and/or times (Lane and Richards, 2001). This process has conventionally been associated with the term validation, which has been taken to mean a demonstration that the model accurately reflects the underlying natural processes and therefore provides a valid basis for decision-making (Oreskes and Belitz, 2001). However, the ability of modellers to assert that a model is valid in this sense – that it is an accurate representation of physical reality – has been extensively questioned. Lane and Richards (2001), for instance, argue that validation is philosophically impossible as no amount of empirical testing can guarantee that the model will perform adequately outside the observed range of conditions or events. Moreover, Oreskes et al. (1994) suggest that validation is precluded by the fact that natural systems are open and that it is not possible to demonstrate the truth of any proposition within such open systems.

Validation therefore implies a legitimacy that cannot be justified, and as such the misleading use of this term should be avoided (Oreskes and Belitz, 2001). Instead, the terms evaluation (Oreskes, 1998) or assessment (Lane and Richards, 2001) have been advocated as preferable ways of describing the process of model testing. Oreskes (1998) argues that evaluation implies a test in which both positive and negative results are possible, and that such tests should lead to modification and even rejection of the model if necessary. Model evaluation also allows for an open discussion of uncertainties, while the language of validation obscures uncertainty (Oreskes, 1998). Similarly, Lane

and Richards (2001) argue for the adoption of model assessment rather than validation to refer to a more wide-ranging and holistic array of testing procedures that recognise the contributions from model uncertainties and data limitations. In such procedures, the model is explicitly represented as an evolving tool whose current status is transitory and, as such, model assessment is part of an ongoing process of development (Lane and Richards, 2001).

The present study therefore does not attempt to validate C-L, but rather to evaluate and assess its performance in the sense of Oreskes (1998) and Lane and Richards (2001). Central to the approach adopted here is the comparison of modelled outputs with observed data, as understanding deviation between observations and predictions is an important part of the scientific research process (Lane and Richards, 2001). Furthermore, when the purpose of a model is to make quantitative forecasts, as is the case for the current study, the most appropriate way to test the model is to compare model predictions with measurements (Murray, 2007). As stated by Beven (2001), predictive power in the sense of consistency with observables is always required by users of model predictions. Such a comparison can also highlight the diagnostic characteristics of evolving fluvial systems and lead to an improved understanding of natural river behaviour (Thomas et al., 2007). In this sense, the evaluation of models in the context of empirical data can have significant heuristic value and can be used to guide further observation and investigation (Oreskes, 2003).

Model evaluation is often undertaken in parallel with model calibration. As outlined in Chapter 4, C-L, like the majority of numerical models, contains some parameters (independent variables) which are incompletely known and are not directly measureable (Janssen and Heuberger, 1995). Even for the most physically-based hydrological models, the measurement or estimation of parameter values is problematic, not least because the scales at which parameters can be measured tend to be very different from the scale at which the model requires effective values (Beven, 1996). Conversely, the distribution of the dependent variables in Earth sciences is often much better known (Oreskes et al., 1994). Therefore, model calibration – the manipulation of adjustable parameters in order to ensure optimal agreement between modelled

and observed data – is a necessary and critical phase in the modelling process (Oreskes et al., 1994; Martin and Church, 2004).

Calibration generally involves performing multiple model runs in which values for selected parameters are adjusted within a feasible range, with model outcomes being compared with observations. Commonly, the aim of this process is to maximise an appropriate objective function (Beven, 2002) or, similarly, to minimise misfit measures (functions of the error between predictions and measurements) (Janssen and Heuberger, 1995). Quantitative testing through the calculation of such numerical metrics to characterise model performance is essential, as it provides a single common point for comparison between models and can, if necessary, facilitate automation of the calibration process (Bennett et al., 2013). Ultimately, the processes of model evaluation and calibration should instil confidence that the model will fulfil its purpose, and that a better model could not have been selected given the available resources (Bennett et al., 2013).

Conventionally, the focus of model evaluation and calibration has been to facilitate the selection of a single, optimal model configuration that can be used for forecasting (Beven and Freer, 2001). However, it is now widely recognised that the concept of the optimum parameter set is flawed (Beven, 1993) because the use of a different calibration period or different goodness-of-fit statistics would result in a different ranking of parameter sets in fitting the observations (Beven, 1996). Consequently, it is argued that a degree of model equifinality in reproducing the observations with model predictions is inevitable, as many different parameter sets within a chosen model structure may be acceptable in reproducing the observed behaviour of that system (Beven, 1996; Beven and Freer, 2001).

Equifinality is therefore a fundamental issue in modelling (Oreskes and Belitz, 2001), particularly where highly parameterised models requiring calibration are fitted to limited data (Beven and Binley, 1992; Beven, 1996). The concept of equifinality also implies uncertainty in the use of models for prediction (Beven, 2001), and therefore the selection of a single optimal model should be rejected

in favour of multiple models that can be used to give a range of predictions (Beven and Freer, 2001; Beven, 2006). However, it is often the case that the degree of uncertainty in results of models with large numbers of parameters is not communicated (Ewen and Parkin, 1996).

In this context, Beven and Binley (1992) developed the Generalised Likelihood Uncertainty Estimation (GLUE) procedure for calibration and uncertainty estimation of physically-based distributed hydrological models. GLUE is based on the realisation that all model structures must be in error to some extent, and that all observations and measurements on which model calibration is based must also be subject to error. As such, it cannot be assumed that any one set of parameter values will represent a true parameter set, and it is therefore only possible to make an assessment of a particular parameter set being an acceptable simulator of the system (Beven and Binley, 1992). The GLUE procedure is therefore based upon making a large number of runs of a given model with different sets of parameter values (chosen randomly from specified parameter distributions). Each set of parameter values is then assigned a likelihood of being a simulator of the system on the basis of comparisons between predicted and observed variables (Beven and Binley, 1992). All simulations with a likelihood measure significantly greater than zero are retained for consideration and used to generate uncertainty bounds on the model outputs (Beven and Binley, 1992; Bathurst et al., 2004).

However, the GLUE procedure is computationally intensive as several thousand parameter sets are typically generated during the process (Beven and Binley, 1992; Bathurst et al., 2004). An alternative approach was therefore proposed by Ewen and Parkin (1996) that can be used to generate output uncertainty bounds from a much smaller number of simulations (Bathurst et al., 2004). In this method, the final bounds of the parameter values, which are used to generate the output uncertainty bounds, are not set on the basis of extensive calibration, and instead expert judgement, literature reviews or field measurements are used (Ewen and Parkin, 1996; Bathurst et al., 2004). Simulations are then carried out by applying the maximum and minimum values of each parameter in turn, keeping the others at a baseline value

(Bathurst et al., 2004). Simulation outputs are then superimposed on each other and the uncertainty bounds are represented by the maximum and minimum values of the model predictions for each measured value (Ewen and Parkin, 1996; Bathurst et al., 2004). In this way, the bounds on the model parameters translate into bounds on the model output (Bathurst et al., 2004), and the fitness of the model is judged by the width of the bounds and the degree to which the measured values lie within the bounds (Ewen and Parkin, 1996).

Importantly, the modeller is not allowed sight of output data (i.e. data pertaining to features of the modelled system for which predictions are required) for the test catchment when setting the parameter bounds. As such, this procedure is referred to as 'blind' testing, and the resulting simulations do not represent a calibrated or optimised best-fit model based on a comparison of measured and simulated output responses (Ewen and Parkin, 1996; Bathurst et al., 2004). The rationale for this approach is that there should be as much similarity as possible between how a model is run when being tested and when being used in practice (i.e. for prediction), and that output data are not available when predicting future conditions, so calibration is not possible (Ewen and Parkin, 1996).

Although neither the GLUE nor 'blind' testing procedures described above are explicitly adopted in this thesis, many of the key features and principles are incorporated into the evaluation and calibration methodology outlined in the following Sections. Importantly, output uncertainty will be explicitly recognised by determining bounds for the magnitude of the predicted catchment features, and attempts to identify a single, optimum parameter set will be avoided.

5.1.2 The evaluation and calibration of the CAESAR-Lisflood landscape evolution model

Documented attempts to evaluate and calibrate C-L in the context of empirical data are uncommon within the published literature. This may be due in large part to the experimental and exploratory nature of many of the previous

applications of the model. For instance, Coulthard and Van De Wiel (2007) and Van De Wiel and Coulthard (2010) used experimental catchments to investigate emergent properties of river basin evolution, including non-linearity and self organised criticality. These studies therefore did not attempt to replicate the behaviour of a specific river catchment. As a result, comparison with empirical data was not only impossible but irrelevant. When real catchments have been used, the aim of the research was often exploratory and centred on broad attempts to understand the effects of hypothetical changes in climate and land use on catchment morphology and sediment discharge (e.g. Coulthard et al., 2000; Coulthard et al., 2002). Such studies therefore focused on identifying the relative impact of changing model parameters (such as flood frequency, magnitude and vegetation cover) rather than on the realism of model outputs.

Where attempts to match C-L model outputs to observations have been made in the past, these have often been qualitative in nature and restricted by a lack of available data. Although some aspects of model performance, including flow depths and inundation areas, can be compared with empirical data, the simulation of geomorphological change is more difficult to assess (Coulthard et al., 2007). The main reason for this is the paucity of detailed topographic data over the timescale of many modelling applications (Van De Wiel et al., 2011). In an attempt to overcome these problems, Coulthard and Macklin (2001) and Coulthard et al. (2005) used a histogram of ^{14}C-dated alluvial units to represent the timing of geomorphologically significant changes in river activity over the last 9,000 years. The simulated and observed records were found to "correspond well" (Coulthard et al., 2005, p. 238), and this correspondence was taken to indicate that the model was "functioning correctly" (Coulthard and Macklin, 2001, p. 350). However, such a comparison provides little information beyond that which could be deduced intuitively: that both modelled sediment yield and observed geomorphological activity (inferred from the frequency of alluvial units) are dependent on precipitation, as peaks in both records were seen to occur during wetter periods.

Similar, qualitative comparisons between C-L model outputs and reconstructed environmental variables have been made in the course of several other studies. Hancock and Coulthard (2012, p. 668), for instance, found that modelled decadal-scale soil erosion rates were "comparable" to measured values quantified using ^{137}Cs analysis. Additionally, Welsh et al. (2009) visually compared modelled catchment sediment discharges (AD 1825 to 2005) with rates of sedimentation derived from the analysis of lake sediment records. Again, an "overall match" between modelled outputs and lake sediment proxies was reported (Welsh et al., 2009, p. 795).

Although qualitative agreements between simulated and observed records were found in each of these examples, the methodologies employed represent only basic assessments of model performance. Simply matching the temporal patterns of modelled outputs with proxies of past geomorphological change gives no indication that the magnitude or mechanisms of sediment delivery simulated by the model correspond to those that actually occurred. As noted by Coulthard et al. (2005), nearly a decade ago, further field evidence is required to more completely assess some of the simulated responses that C-L produces.

In the context of the limitations of past studies that have attempted to fully evaluate the performance of C-L, model evaluation undertaken as part of the current study and presented in this Chapter therefore serves two important purposes:

1. it will address a general need for a more rigorous test of C-L model performance in the context of observed data; and,
2. it will assess the extent to which C-L is an appropriate tool for long-term forecasting of sediment yield from the upper North Fork Toutle River catchment.

It is intended, therefore, that the model evaluation described in the following Sections will contribute to the ongoing development of C-L, not only in terms of the veracity of the model itself but also in terms of the methods that can be used to test the performance of the model. Given that no standard procedure for

evaluating and calibrating C-L exists, a novel approach was required; one that could meet the specific aims of the project in the context of available empirical data. The development of this approach is described throughout this Chapter.

5.2 MODEL EVALUATION CRITERIA

To assess whether C-L is able to reproduce the processes of geomorphological change in the upper North Fork Toutle River, three broad aspects of model performance should ideally be tested:

1. catchment water discharge;
2. volume of sediment yield, in terms of:
    i. timing, and
    ii. spatial distribution; and,
3. mechanisms of sediment yield, in terms of the channel processes responsible.

Given that catchment hydrology is the primary driver of sediment erosion, it is essential that C-L is able to reproduce the observed hydrograph during the model hindcast period. However, the use of a discharge record to drive C-L's hydrological model, as described in Chapter 4, has ensured that the observed and modelled hydrographs will agree well. As such, further testing of this aspect of model performance is irrelevant.

The volume of sediment output from the catchment is an important evaluation criterion as this is the key dependent variable that this study aims to forecast. Additionally, the timing of sediment delivery could also be evaluated to provide an indication of the relationship between modelled sediment transport and water discharge. The mechanisms responsible for generating modelled sediment yields are also a vital aspect of model performance, however, as they indicate whether the processes simulated by the model are reasonable approximations of those observed in reality. Not only will such tests determine the confidence with which predictions can be made, but they will also provide valuable information regarding the operation of C-L. The available empirical

data that could be used to test these various components of model performance are listed in Table 5.1. The following Sections outline the selection of appropriate evaluation criteria, and these are summarised in Table 5.2.

5.2.1 Sediment yield

An obvious way of evaluating both the modelled volume and timing of sediment yield would be to compare modelled and observed time series of sediment yields at the catchment outlet. However, as shown in Table 5.1, the nearest such record is that obtained from the Tower Road gauging station on the Toutle River mainstem, approximately 22 km downstream from the outlet of the modelled catchment at the former site of the N1-DRS. The use of this record for calculating the observed volume of sediment yield from the upper North Fork Toutle River catchment is therefore hampered by deposition behind the SRS, and is further complicated by sediment inputs from bed and bank erosion along the lower North Fork, South Fork, and upper Toutle Rivers and the Green River (Biedenharn Group, 2010). Moreover, the data represent only the suspended fraction of the total load and are also unavailable for the first year of the calibration period (October 1, 2003 to September 29, 2004).

However, the volume of sediment eroded from the catchment can be estimated from analysis of LiDAR-derived DEMs, three of which have been produced since 2003 (Table 5.1). Although the spatial extent of the 2006 and 2007 surfaces is insufficient to facilitate such a calculation, the 2009 DEM provides full coverage of the catchment area and it can therefore be used to estimate total sediment yield between October 2003 and October 2009. Sediment yield was calculated by subtracting the 2009 DEM from the 2003 DEM, and volumes are presented in Table 5.3. Modelled sediment yields can be calculated in the same way to facilitate direct comparison. This calculation was restricted to areas where unconsolidated units associated with the 1980 eruption were identified, as other areas were defined as bedrock (see Section 4.7.1) and would therefore not contribute significantly to catchment sediment yield. This area is mapped in Figure 5.1. Sediment yield between 2003 and 2009 can also be obtained at a sub-catchment-scale in order to obtain

information regarding the spatial distribution of erosion. It is important to test C-L in terms of the coarse-scale sediment budget of the catchment as this will indicate whether the model is adequately representing zones of sediment production, transport and deposition. Sub-catchment volumetric changes therefore represent the second evaluation criterion.

The delineation of sub-catchments used for this analysis, shown in Figure 5.1, was based on the five tributaries that contribute flow to the mainstem of the upper North Fork Toutle River. These are: Loowit Creek; Carbonate Springs; Truman Channel; Castle Creek; and Coldwater Creek. The mainstem of the upper North Fork Toutle River itself was sub-divided into three reaches (uNFTR A, B and C) that represent different geomorphological conditions. Reach A is a headwater sub-catchment on the flank of Mount St Helens with high stream gradients, while Reaches B and C are located below the confluence of the upper North Fork Toutle River with Castle and Coldwater Creeks and both have much lower gradients. Reach B, however, is constrained in a relatively narrow valley, while Reach C has a much wider floodplain and is less constrained laterally. Volumes of erosion for each of these eight sub-catchments between 2003 and 2009, calculated by differencing the respective DEMs with a 3 m horizontal resolution, are presented in Table 5.3.

The observed sediment yields listed in Table 5.3 were derived from the higher resolution (i.e. 3 m) 2003 and 2009 DEMs despite the fact that C-L will be run using a DEM with a 50 m horizontal resolution (as described in Section 4.2). This was done so that model outputs could be compared with the most accurate representation of catchment elevation change available. If models such as C-L are to be used to address real-world problems, they should be able to replicate accurate observations of reality rather than downgraded versions of these observations. Nonetheless, it was necessary to compare sediment yields derived from the 3 m resolution DEMs with those derived from 50 m resolution DEMs. The yields derived from the more coarse DEMs are also listed in Table 5.3 and indicate that there is not a significant difference between the yields derived from the two resolutions, with a maximum absolute percentage difference of 67% for the eight sub-catchments. Significantly, the

percentage difference between the total catchment sediment yields derived from the two resolutions was only 0.01%.

It should be noted that for the purposes of this study, the catchment sediment yield is assumed to be represented by the loss in net elevation distributed across the catchment (or sub-catchments) and over a period of time. In general, though, sediment yield is determined in units of mass, from measurements of sediment transport. As such, comparison of the results of this study to wider data sets would require the volumes to be converted to mass using a representative value of bulk density. Although such a conversion could be carried out using the mean bulk density of the debris avalanche deposit reported in Glicken (1996), for instance, this was not deemed necessary for the present study for three reasons. First, the same conversion would be applied to both modelled and observed sediment yield values, so would not impact on the results of model evaluation, calibration and selection reported later in this Chapter. Second, the trends and mechanisms of modelled future sediment yield (Chapter 6) are considered of greater importance than its absolute value in the context of long-term sediment management in the Toutle-Cowlitz River system. Third, previous studies of relevance to the study catchment (WEST, 2000; Biedenharn Group, 2010; Simon and Klimetz, 2012) have reported projections of future sediment yield in units of volume rather than in units of mass.

However, it is also possible that the bulk density of sediment may change as a result of erosion, transport and deposition by fluvial processes. As such, the bulk density of the sediment at the point at which it is initially eroded may be different from the bulk density of the sediment where it is deposited along a river channel. For instance, a given volume of material may occupy a lesser volume when deposited and would therefore register as a lower elevation. In this case, the catchment and sub-catchment sediment yield calculated as net erosion would be overestimated. However, change in bulk density is unlikely to be significant in the upper North Fork Toutle River catchment. The debris avalanche material, which represents the primary source of sediment, is loosely compacted and similar in consistency to the alluvium formed when the eroded

material is redeposited. As such, there is unlikely to be a marked difference in packing patterns or fabrics between source material and fluvial deposits, meaning that bulk densities will also be similar. Glicken (1996), for instance, found that mean bulk density of the debris avalanche deposit was on the order of 1850 kg m^{-3}, with an approximate range from 1440 to 2180 kg m^{-3}. This is similar to typical fluvial deposits, which generally have bulk densities of around 2000 kg m^{-3}.

5.2.2 In-channel fluvial processes

Identification of whether processes of channel adjustment responsible for sediment yield from the upper North Fork Toutle River catchment are accurately reproduced in C-L can be achieved through a local-scale analysis of channel morphology. Specifically, changes in channel characteristics, such as cross-sectional area and thalweg elevation, can be quantified using repeat cross-section surveys at monumented sites. As described in Chapter 3 (sub-section 3.2.3), the USGS established a network of 70 cross-sections throughout the catchment that have been surveyed at varying intervals since 1980. However, the frequency of surveys has decreased significantly in recent years, meaning that this data set is inadequate for evaluating modelled mechanisms of channel evolution and sediment yield post-2003. Cross-sections can, however, be extracted from the 2003 and 2009 LiDAR DEMs to facilitate this analysis, and the USGS network is useful in selecting appropriate locations.

Only ten cross-sections have been surveyed once or more in the decade since 2003 (LO030, LO033, LO040, NF100, NF110, NF120, NF130, NF300, NF320 and NF350), and these sites represent locations that are of continuing interest to the USGS with respect to channel response and morphological evolution. These cross-sections therefore provide a good indication of the important geomorphological hotspots within the catchment and as such represent meaningful areas at which model performance can be tested at a local-scale. All of these cross-sections, with the exception of LO033, NF110 and NF130, were included as they provide a variety of patterns and trends of channel

change, including aggradation, degradation and widening, against which to evaluate C-L outputs.

In addition to the seven selected locations, three additional cross-sections were selected to include a site farther downstream on the North Fork Toutle River mainstem (NF375) and one on each of the two major tributaries of Castle Creek (CA225) and Coldwater Creek (CW245). The locations of the ten cross-sections are illustrated in Figure 5.2, while the profiles extracted from the 2003 and 2009 DEMs are shown in Figure 5.3. Photographs of each cross-section are presented in Figure 5.4. Changes in both cross-sectional area and thalweg elevation were calculated at each location (Table 5.4) as this enabled the relative contributions of vertical and lateral processes to be inferred.

Change in cross-sectional area gives a good indication of net erosion or deposition occurring at a given location; however, it does not indicate whether erosion is the result of incision or widening. This additional information is provided by the change in thalweg elevation. Specifically, a widening channel will experience a change in cross-sectional area in the absence of any significant change in thalweg elevation, whereas an incising channel will experience change in both area and elevation. Therefore, although bank and bed erosion are not measured explicitly, this approach quantifies the key processes of channel change and facilitates meaningful comparisons to be made between model outputs and observations.

Table 5.1 Available empirical data for evaluating geomorphological aspects of C-L model performance.

Data type	Years of available record	Location	Aspect of model performance[†]	Source	Comment
LiDAR DEM	2006	uNFTR and tributaries	V, Msd, Mcp	USACE/USGS	Incomplete spatial coverage.
LiDAR DEM	2007	uNFTR and tributaries	V, Msd, Mcp	USACE/USGS	Incomplete spatial coverage.
LiDAR DEM	2009	uNFTR and tributaries	V, Msd, Mcp	USACE/USGS	Complete spatial coverage.
Repeat cross-section surveys	2004-2007	uNFTR and tributaries	Mcp	USACE/USGS	Incomplete temporal and spatial coverage.
Daily suspended sediment record	2004 - 2012	Toutle River at Tower Road	V, T	USGS (Water Data Reports)	Incomplete temporal coverage, suspended sediment only, collected downstream of the SRS.

[†] V = volume; Msd = mechanism (spatial distribution); Mcp = mechanism (channel processes); T = timing.

Table 5.2 Criteria used to evaluate model performance in the context of available empirical data.

Evaluation criterion	**Observed data**	**Number of observations per model**	**Units of measurement**	**Aspects of model performance evaluated**
Total catchment sediment yield	2003 and 2009 LiDAR surfaces	1	m^3	Volume and spatial distribution of sediment yield
Sub-catchment sediment yield		8	m^3	
Change in cross-sectional area		10	m^2	Mechanisms of sediment yield
Change in thalweg elevation		10	m	

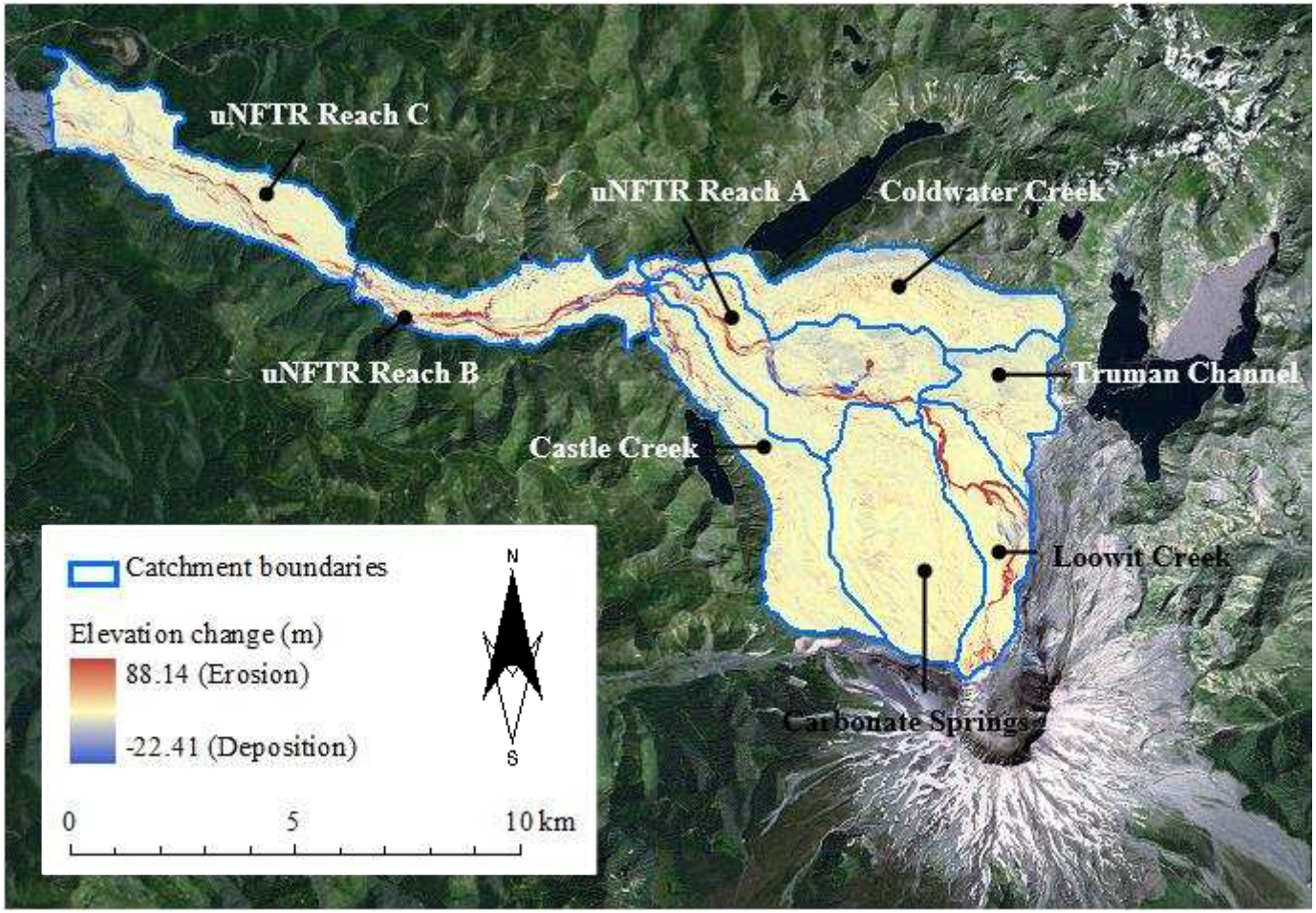

Figure 5.1. Differencing of 2003 and 2009 LiDAR DEMs showing catchment and sub-catchment delineations. Sediment yields calculated for each sub-catchment are listed in Table 5.3. Aerial imagery from DigitalGlobe (Microsoft).

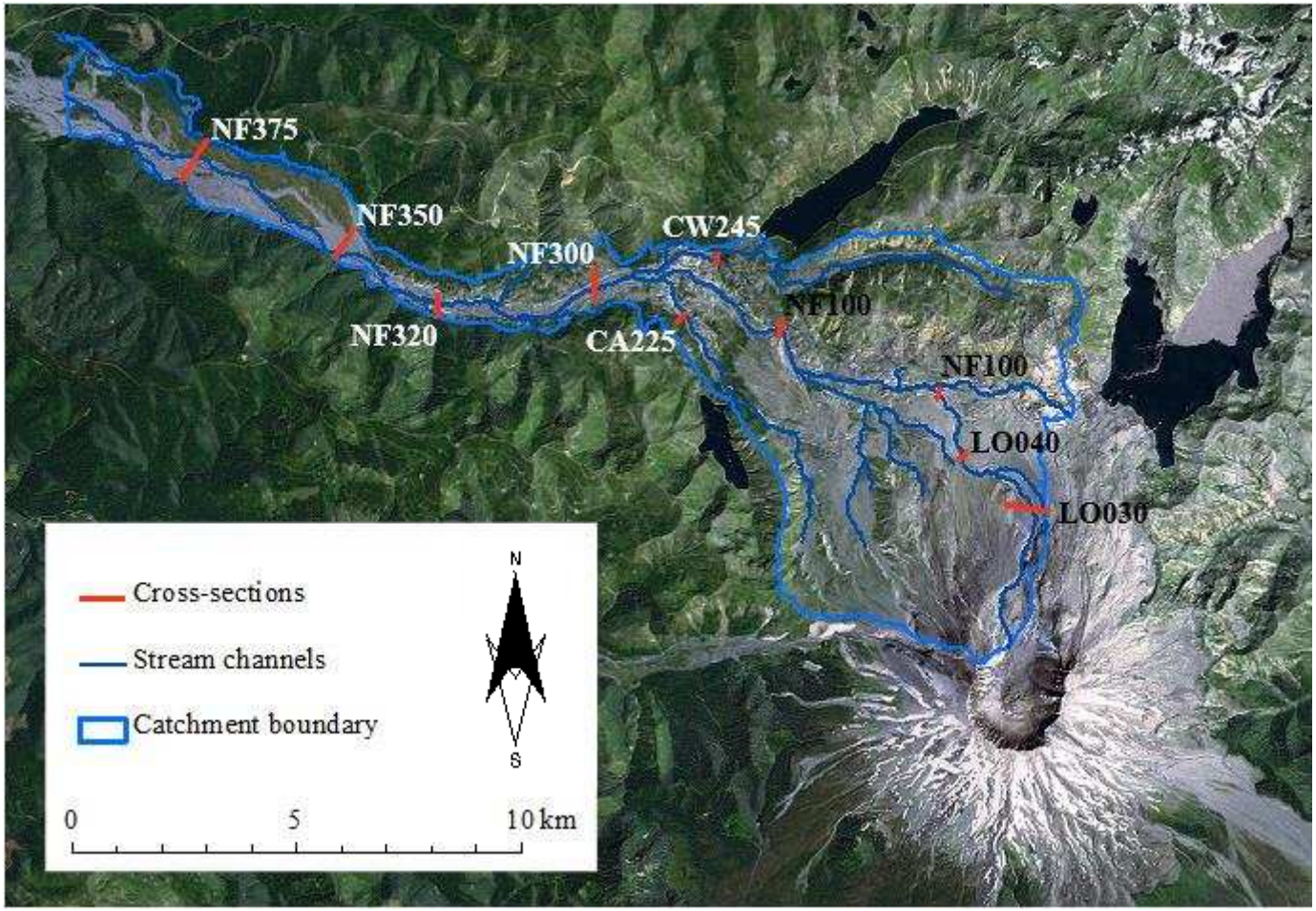

Figure 5.2 Locations of the ten cross-sections selected for use in model evaluation. Changes in cross-sectional area and thalweg elevation at each location are listed in Table 5.4. Aerial imagery from DigitalGlobe (Microsoft).

Table 5.3 Sediment yields derived from LiDAR analysis for the eight sub-catchments shown in Figure 5.1.

Sub-catchment	Sediment yield (million m^3) derived from 3m DEMs	Sediment yield (million m^3) derived from 50m DEMs	Absolute percentage difference (%)
Loowit Creek	8.04	6.67	18.68
Carbonate	3.13	5.00	46.00
Truman Channel	0.14	0.11	22.22
Castle Creek	1.84	0.92	66.64
Coldwater Creek	1.17	0.82	35.29
uNFTR Reach A	2.24	2.26	0.86
uNFTR Reach B	3.53	3.80	7.38
uNFTR Reach C	0.66	1.03	43.73
Total	20.75	20.60	0.01

Table 5.4 Changes in cross-sectional area and thalweg elevation derived from LiDAR analysis for the ten locations shown in Figure 5.2.

Cross - section	Change in area (m^2)	Change in elevation (m)
LO030	23.56	-0.62
LO040	1253.74	9.43
NF100	422.59	5.71
NF120	178.31	0.20
NF300	1105.14	-0.33
NF320	53.63	0.19
NF350	78.88	-0.45
NF375	108.77	0.20
CA225	254.05	1.10
CW245	395.15	2.03

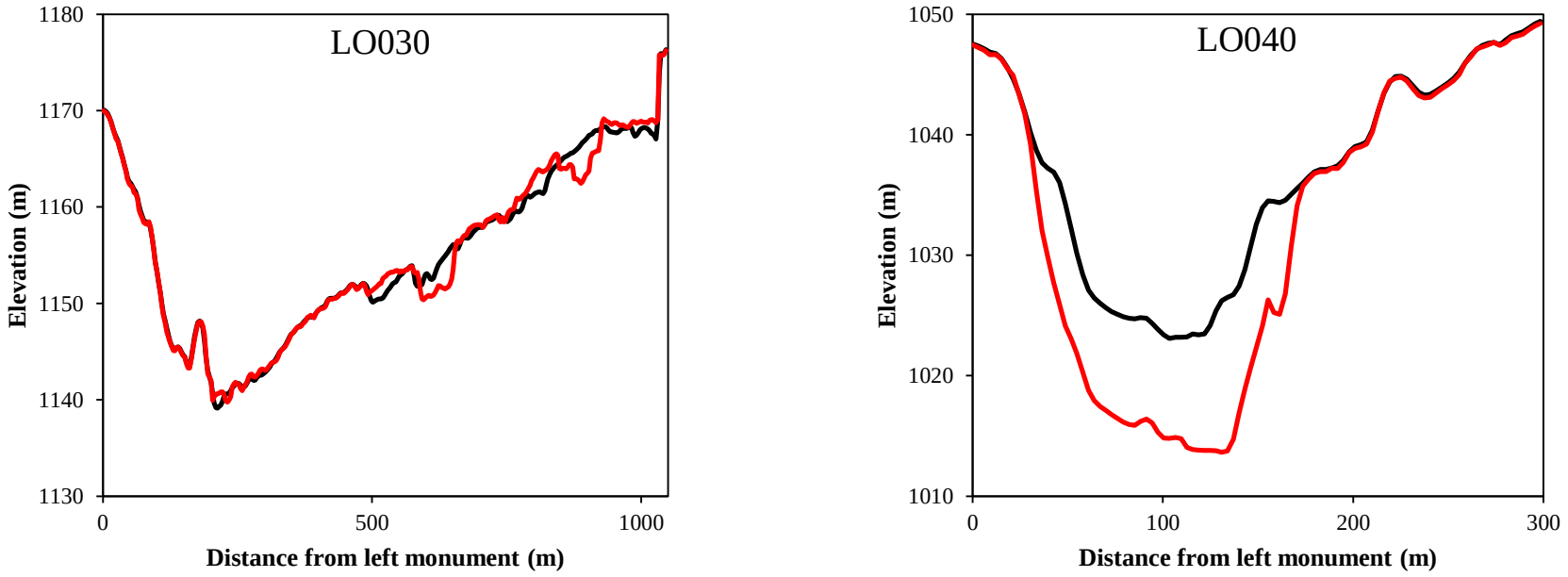

Figure 5.3 Cross-sections extracted from the 2003 (black) and 2009 (red) LiDAR-derived DEMs at the ten locations shown in Figure 5.2.

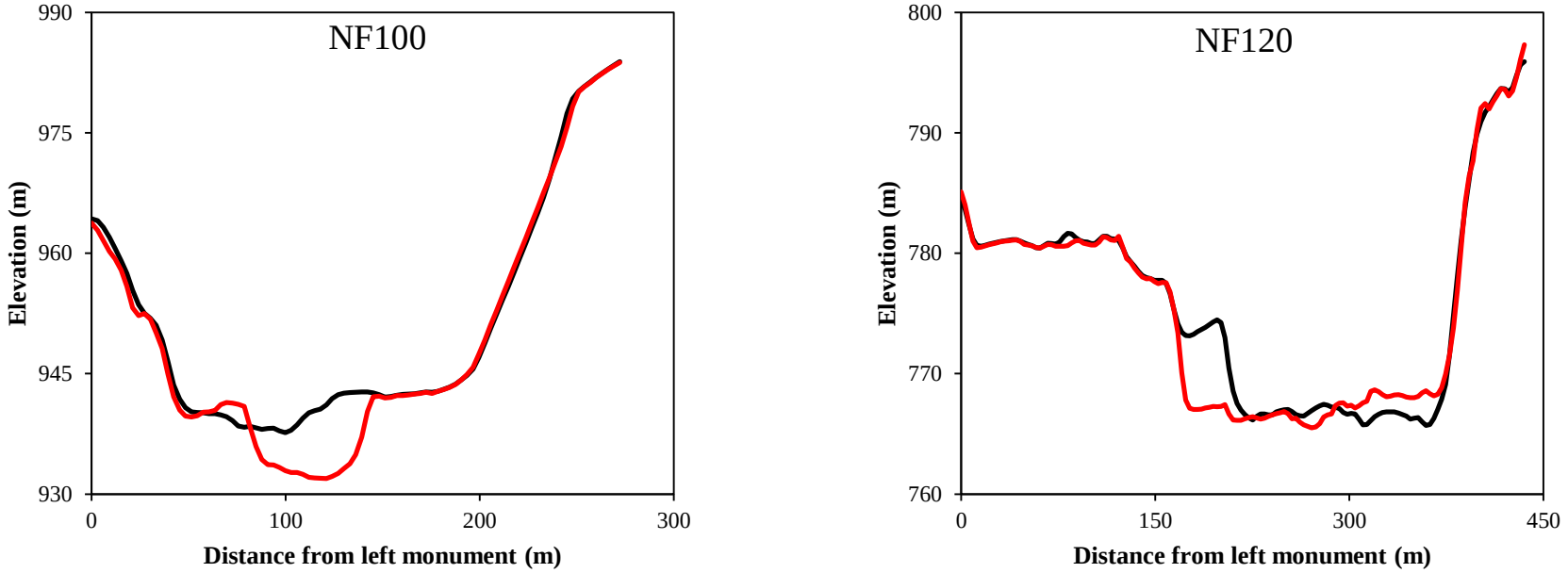

Figure 5.3 (cont.) Cross-sections extracted from the 2003 (black) and 2009 (red) LiDAR-derived DEMs at the ten locations shown in Figure 5.2.

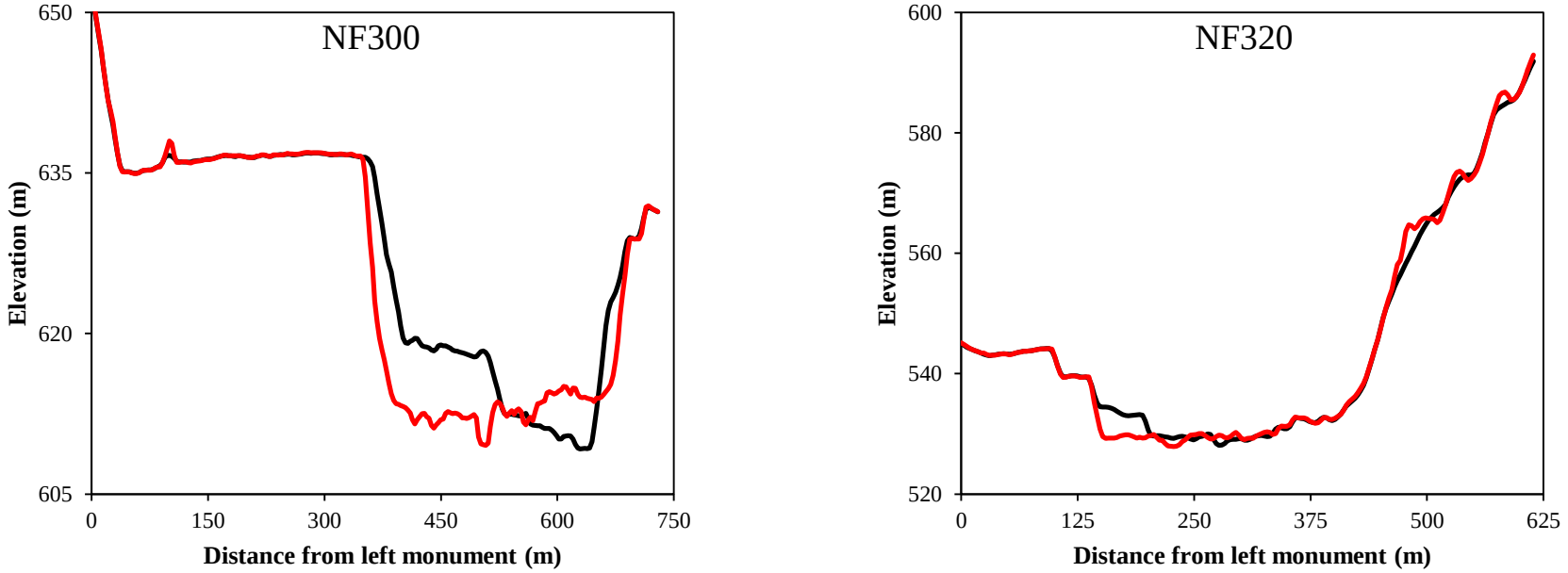

Figure 5.3 (cont.) Cross-sections extracted from the 2003 (black) and 2009 (red) LiDAR-derived DEMs at the ten locations shown in Figure 5.2.

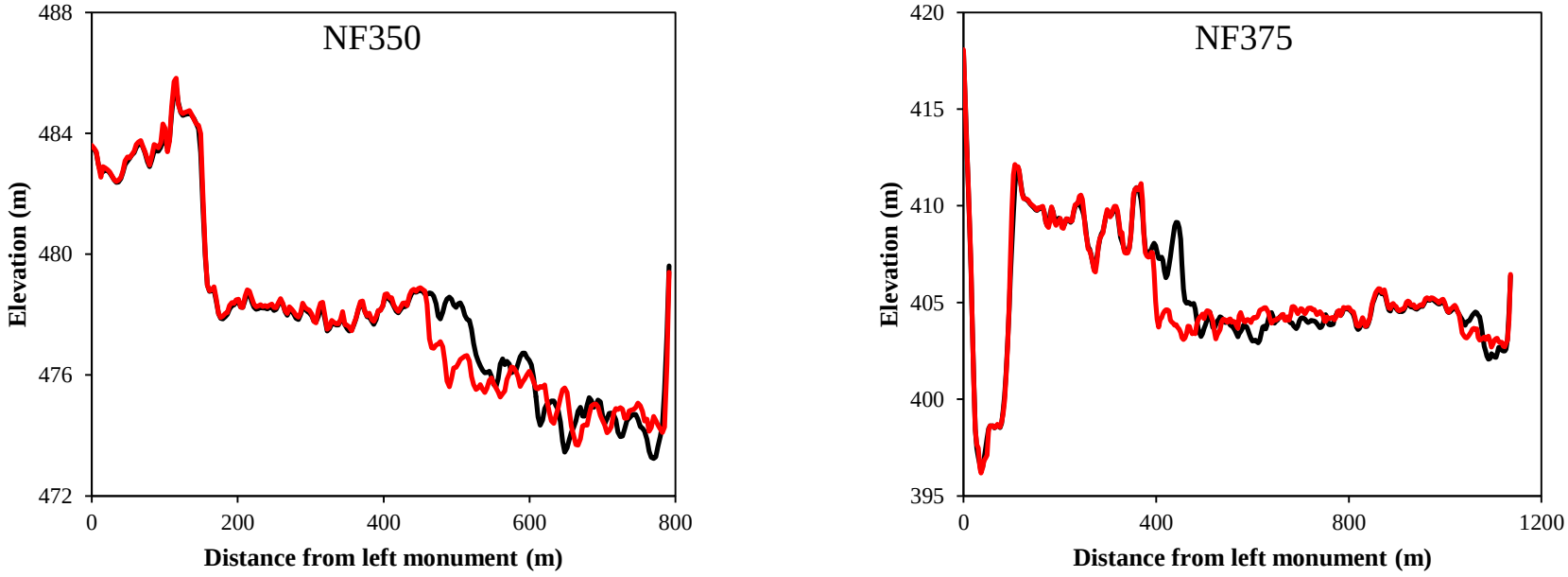

Figure 5.3 (cont.) Cross-sections extracted from the 2003 (black) and 2009 (red) LiDAR-derived DEMs at the ten locations shown in Figure 5.2.

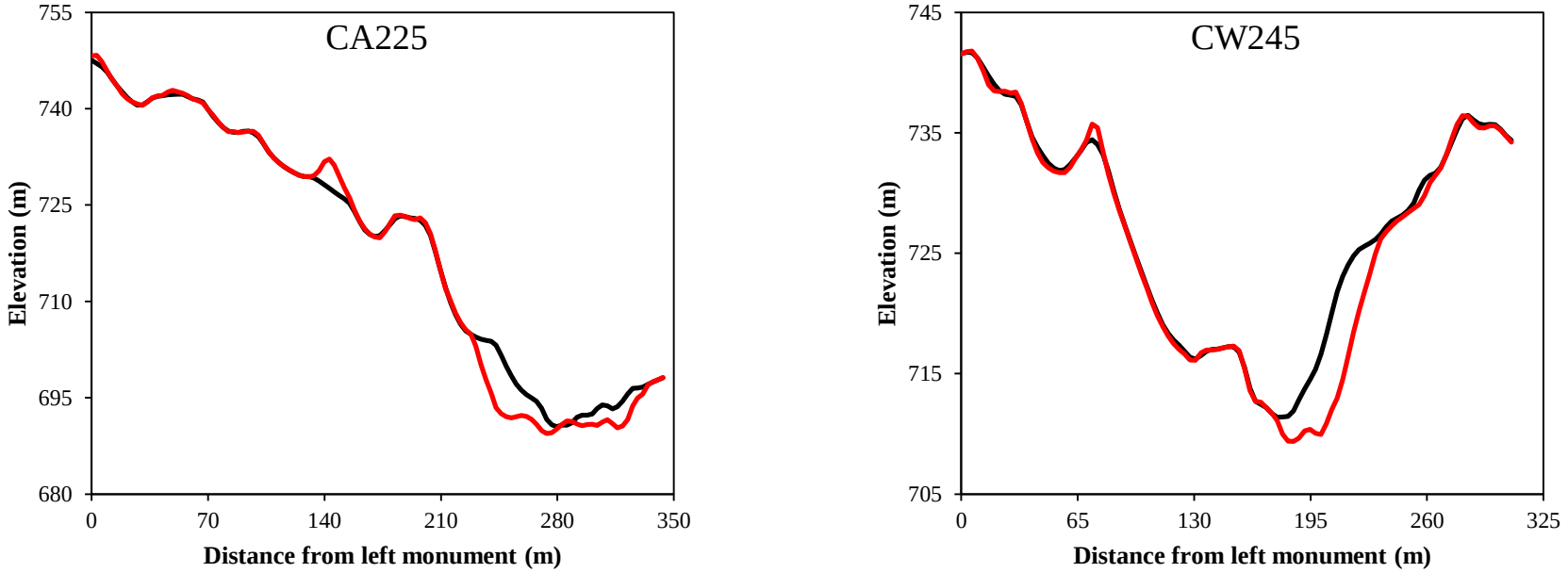

Figure 5.3 (cont.) Cross-sections extracted from the 2003 (black) and 2009 (red) LiDAR-derived DEMs at the ten locations shown in Figure 5.2.

(a)

(b)

Figure 5.4 Photographs of cross-sections at the ten locations shown in Figure 5.2. All photographs by author unless otherwise stated. (a) LO030. Photograph by Adam Mosbrucker (2009); (b) LO040. Both looking upstream.

(c)

(d)

Figure 5.4 (cont.) Photographs of cross-sections at the ten locations shown in Figure 5.2. (c) NF100; (d) NF120. Both looking downstream.

(e)

(f)

Figure 5.4 (cont.) Photographs of cross-sections at the ten locations shown in Figure 5.2. (e) NF300 looking cross-channel. Photograph by Adam Mosbrucker (2006); (f) NF320 looking downstream.

(g)

(h)

Figure 5.4 (cont.) Photographs of cross-sections at the ten locations shown in Figure 5.2. (g) NF350 looking upstream; (h) NF375 looking cross-channel.

(i)

(j)

Figure 5.4 (cont.) Photographs of cross-sections at the ten locations shown in Figure 5.2. (i) CA225; (j) CW245. Both looking upstream.

5.3 INITIAL MODEL TESTING AND PARAMETER REFINEMENT

As illustrated in Chapter 4, several of the parameters needed to calculate fluvial erosion and transport could not be specified on the basis of empirical data, a priori knowledge or pre-existing, recommended values. Specifically, these relate to the sediment transport law and the lateral erosion parameter (Λ). These parameters were therefore tested and calibrated, with the results reported in Sections 5.3.1 and 5.3.2, respectively. Furthermore, as discussed in Chapter 4, the spatial variation of rainfall, particularly driven by orographic effects, as well as lake and spring-fed discharge inputs are not explicitly represented in the model and this may have an impact on the modelled spatial distribution of sediment yield within the catchment. Consequently, it was necessary to perform an initial test of erosion volumes for the eight sub-catchments in order to determine whether modifications to the model were required in this respect. These tests are described in Section 5.3.3. A total of 10 models were run as part of this initial testing phase, the basic configurations of which are summarised in Table 5.5. The results of catchment and sub-catchment erosion volume analyses, which formed the basis of the analysis during this phase, are presented in Table 5.6.

5.3.1 The sediment transport law

The sensitivity of model outputs to the choice of sediment transport equation was assessed during Test Runs 1 and 2, which used the Einstein (1950) and Wilcock and Crowe (2003) formulae, respectively. The results of these two runs (Table 5.6) indicated that modelled erosion volumes are highly dependent on the selected sediment transport law, with the Einstein (1950) formula (Run 1) producing approximately 3.4 times more sediment than the Wilcock and Crowe (2003) equation (Run 2) during the six-year testing period (41.58 and 12.29 million m^3, respectively). It is evident that while Run 1 overestimates the observed erosion volume (20.75 million m^3) by approximately 100%, Run 2 underestimates by around 40%. Although the error associated with both models is large, the results of Runs 1 and 2 suggested that the Wilcock and Crowe

equation performed better than that of Einstein. In addition to significantly overestimating erosion volume, the Einstein (1950) equation also increased the simulation time in Run 2 by 20%. Thus, use of this formula would limit the number of runs that could be undertaken in comparison to using the Wilcock and Crowe (2003) equation. In summary, the results of Runs 1 and 2 indicated that the Wilcock and Crowe (2003) formula should be used for the remainder of the study.

5.3.2 Mechanisms of sediment yield

The key parameter responsible for controlling the mechanisms of sediment production is the lateral erosion parameter, Λ. This is particularly important in the upper North Fork Toutle River catchment where bank erosion rather than hillslope erosion represents the dominant source of sediment (Meyer and Martinson, 1989; Simon and Thorne, 1996; Major et al., 2000). As discussed in Chapter 4, although it is possible to estimate an approximate value for this parameter based on recommended values, its exact specification will vary between applications. To determine whether the value of 1.0×10^{-4} used in Runs 1 and 2 (Table 5.5) was appropriate, a visual comparison was made between the modelled pattern of channel development and that indicated by LiDAR surface differencing.

Figure 5.5 shows the modelled pattern of erosion and deposition for Test Run 2, and this was compared with the observed pattern shown in Figure 5.1. Although the value of 1.0×10^{-4} used in Test Run 2 is at the lower end of the suggested range, it is apparent that this is still too high for the current application. Specifically, it is evident that channels on the main stem of the North Fork Toutle River show a tendency to meander and widen (Figure 5.5) significantly more than is suggested in Figure 5.1. The modelled channel in uNFTR Reach C also appears to shift across the floodplain more than has been observed. Comparison of modelled cross-section plots with those extracted from the LiDAR surfaces also reveals considerable differences in the patterns of channel development.

Table 5.5 Model configurations used for the ten Test Runs.

Test Run number	Test parameters					Constant parameters		
	Transport formula	A	Q_{min}	Q_{max}	X_{max}	λ	N_{smooth}	N_{shift}
1	Einstein	1.0×10^{-4}	0.5	-	-	15	30	3
2	W&C	1.0×10^{-4}	0.5	-	-	15	30	3
3	W&C	1.0×10^{-5}	0.5	-	-	15	30	3
4	W&C	1.0×10^{-6}	0.5	-	-	15	30	3
5	W&C	5.0×10^{-6}	0.5	-	-	15	30	3
6	W&C	5.0×10^{-6}	0.1	-	-	15	30	3
7	W&C	5.0×10^{-6}	0.1	0.5	-	15	30	3
8	W&C	5.0×10^{-6}	0.1	1	-	15	30	3
9	W&C	5.0×10^{-6}	0.1	2	-	15	30	3
10	W&C	5.0×10^{-6}	0.1	0.5	323	15	30	3

Table 5.6 Sub-catchment and total sediment yield for the ten Test Runs.

	Sediment yield (million m^3)										
Sub-catchment	**Observed**	**Run 1**	**Run 2**	**Run 3**	**Run 4**	**Run 5**	**Run 6**	**Run 7**	**Run 8**	**Run 9**	**Run 10**
Loowit Creek	8.04	-	-	0.19	0.09	0.11	0.30	0.80	0.64	0.49	1.75
Carbonate Springs	3.13	-	-	0.20	0.24	0.22	0.82	1.17	1.06	0.84	1.88
Truman Channel	0.14	-	-	0.01	0.01	0.00	0.07	0.20	0.13	0.11	0.33
Castle Creek	1.84	-	-	0.82	0.21	0.31	0.49	0.75	0.71	0.65	1.23
Coldwater Creek	1.17	-	-	0.67	0.45	0.48	0.69	0.78	0.63	0.55	1.19
uNFTR Reach A	2.24	-	-	2.12	0.73	1.04	1.88	2.61	2.64	2.46	3.26
uNFTR Reach B	3.53	-	-	3.19	1.36	2.23	2.55	2.79	2.89	2.73	3.65
uNFTR Reach C	0.66	-	-	3.55	1.42	3.27	2.85	2.37	2.84	2.99	1.90
Total	20.75	41.58	12.29	10.75	4.51	7.67	9.66	11.47	11.55	10.82	15.19

At NF120 and NF375, for instance, excessive widening and bank erosion are evident, together with considerable aggradation and an increase in the elevation of the channel thalweg (Figure 5.6). The inconsistencies between these plots and those shown in Figure 5.3 indicate that the value of the lateral erosion parameter should be adjusted downwards in order to improve process representation within the model. To ascertain a more appropriate value of Λ, that would produce more realistic rates of bank erosion and meander development, Λ was reduced by one and two orders of magnitude in Runs 3 and 4, respectively (Table 5.5).

The modelled patterns of channel development were again compared qualitatively with the observed pattern using maps produced from DEM differencing as well as cross-section profiles. The influence of reducing the value of Λ is evident from these analyses. Figure 5.7 and Figure 5.9 reveal the modelled channels of Test Runs 3 and 4 have reduced tendencies to migrate laterally compared with Test Run 2 (Figure 5.5). This effect is clearly stronger for Test Run 4 (Figure 5.9), which has the lowest value of Λ (1.0×10^{-6}). Significantly, it is evident from Test Run 4 that the channel in uNFTR Reach C downstream of the valley constriction has not avulsed during the six-year model period and has remained as a single thread meandering channel. This is in contrast to Test Runs 2 and 3, which both show clear evidence of significant lateral channel shifting across the valley floor in this sub-catchment.

Cross-sections for Test Runs 3 and 4 are presented in Figure 5.8 and Figure 5.10, respectively, and highlight the impacts of lowering the value of Λ on the nature of channel development and the rate of bank erosion. NF120 and NF375 are again used as examples and the modelled cross-sections appear to provide a more satisfactory fit to those extracted from the LiDAR surfaces in comparison to Test Run 2. A general widening trend is still apparent at NF120 for Test Run 3 (Figure 5.8), whereas incision and a lowering of the channel thalweg can be seen at NF120 for Test Run 4 (Figure 5.10). Similarly, at NF375, Test Run 3 appears to over-estimate lateral movement while insufficient channel migration is evident in Test Run 4.

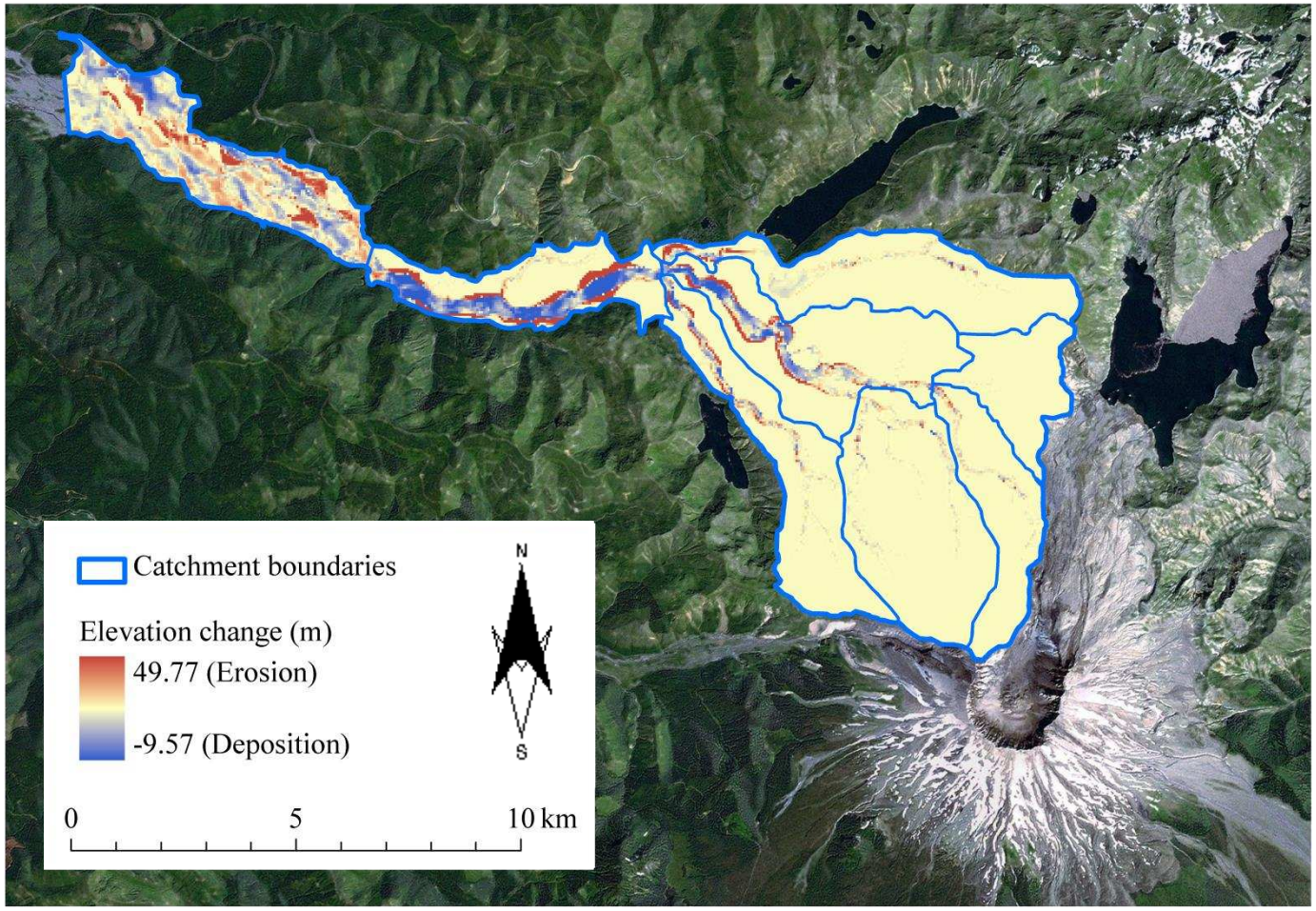

Figure 5.5 Pattern of erosion and deposition produced by Test Run 2. Aerial imagery from DigitalGlobe (Microsoft).

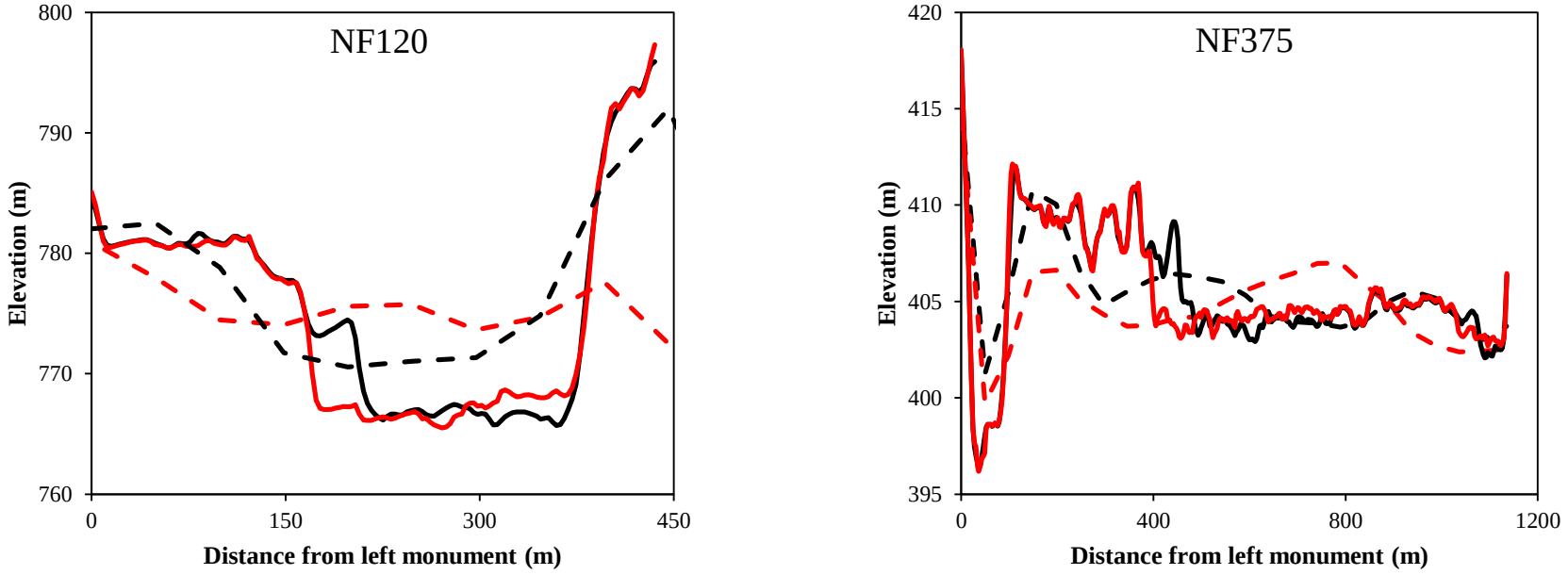

Figure 5.6 Cross-sections at NF120 and NF375 for Testing Run 2. Solid lines are the LiDAR-derived profiles while dashed lines are the modelled profiles. Black lines represent the initial and red lines the final, topography.

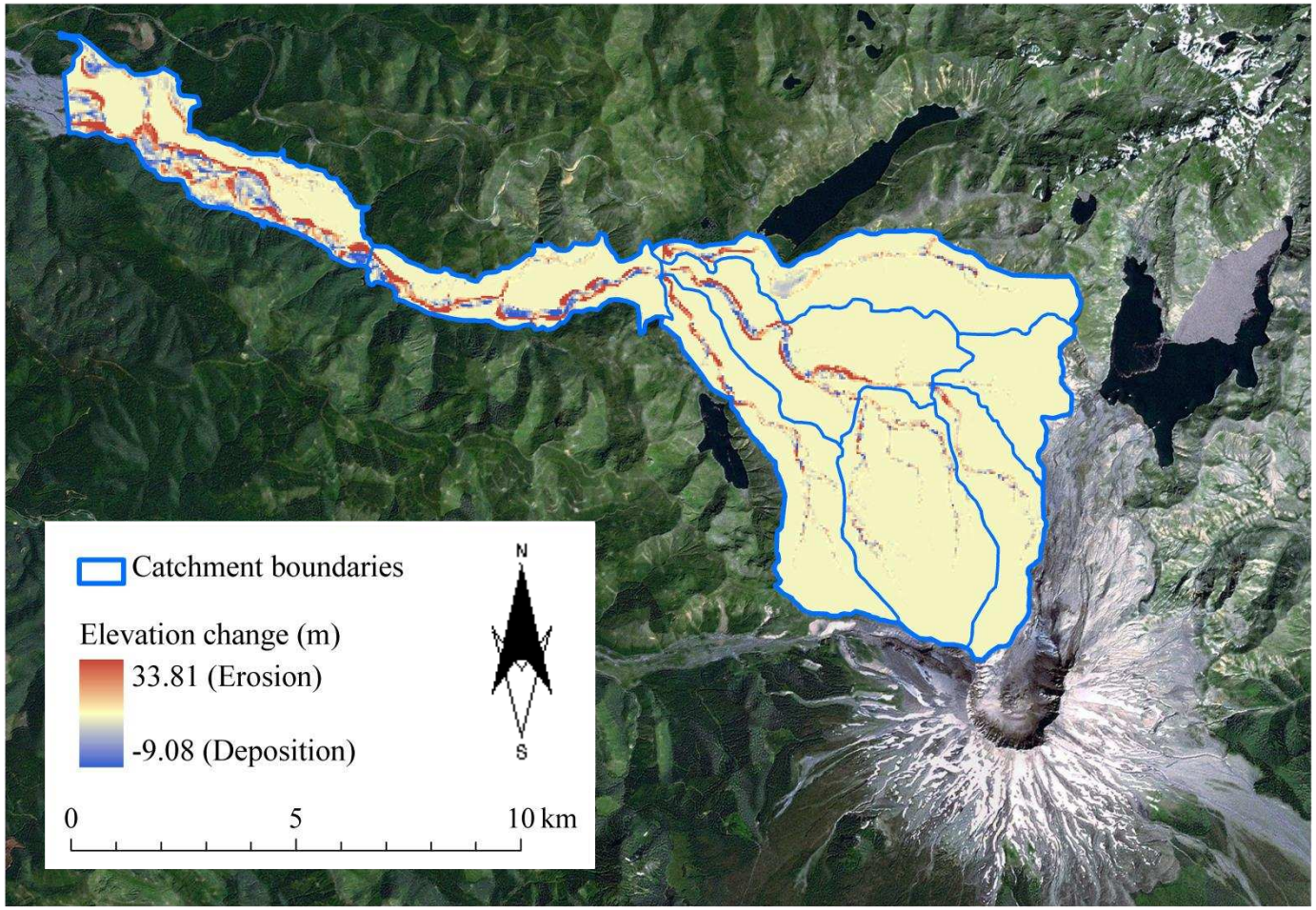

Figure 5.7 Pattern of erosion and deposition produced by Test Run 3. Aerial imagery from DigitalGlobe (Microsoft).

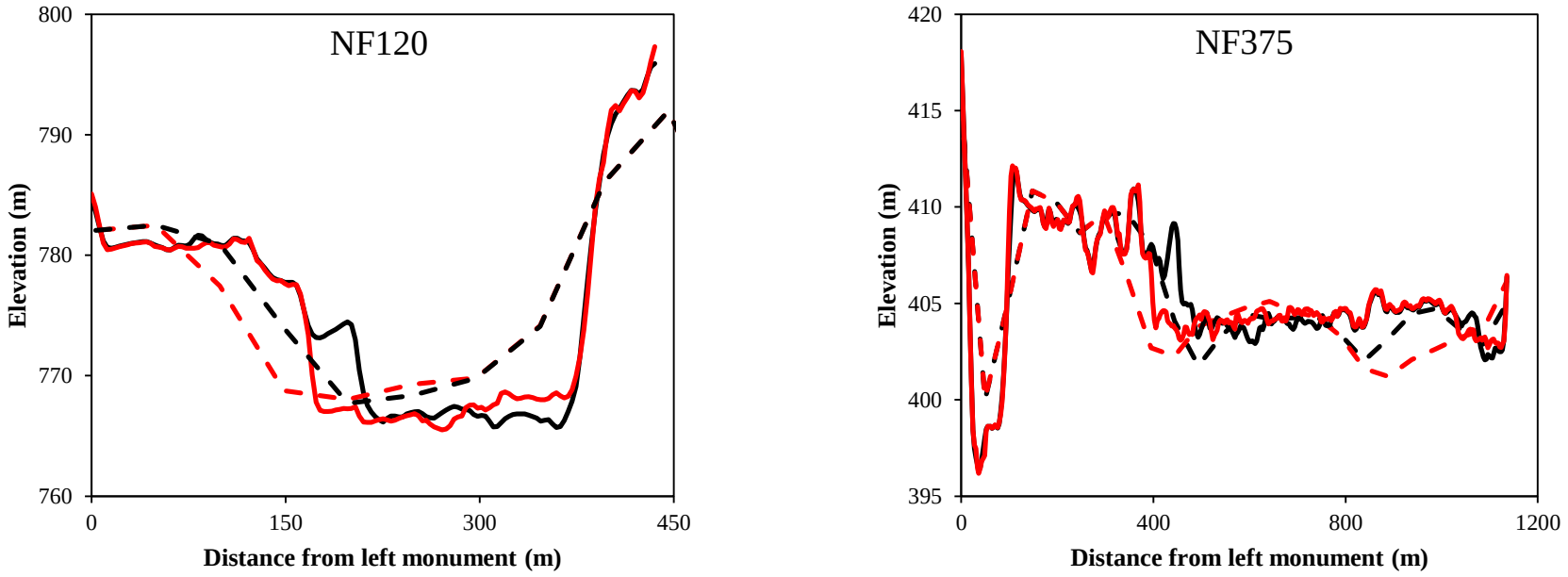

Figure 5.8 Cross-sections at NF120 and NF375 for Test Run 3. Solid lines are the LiDAR-derived profiles while dashed lines are the modelled profiles. Black lines represent the initial and red lines the final, topography.

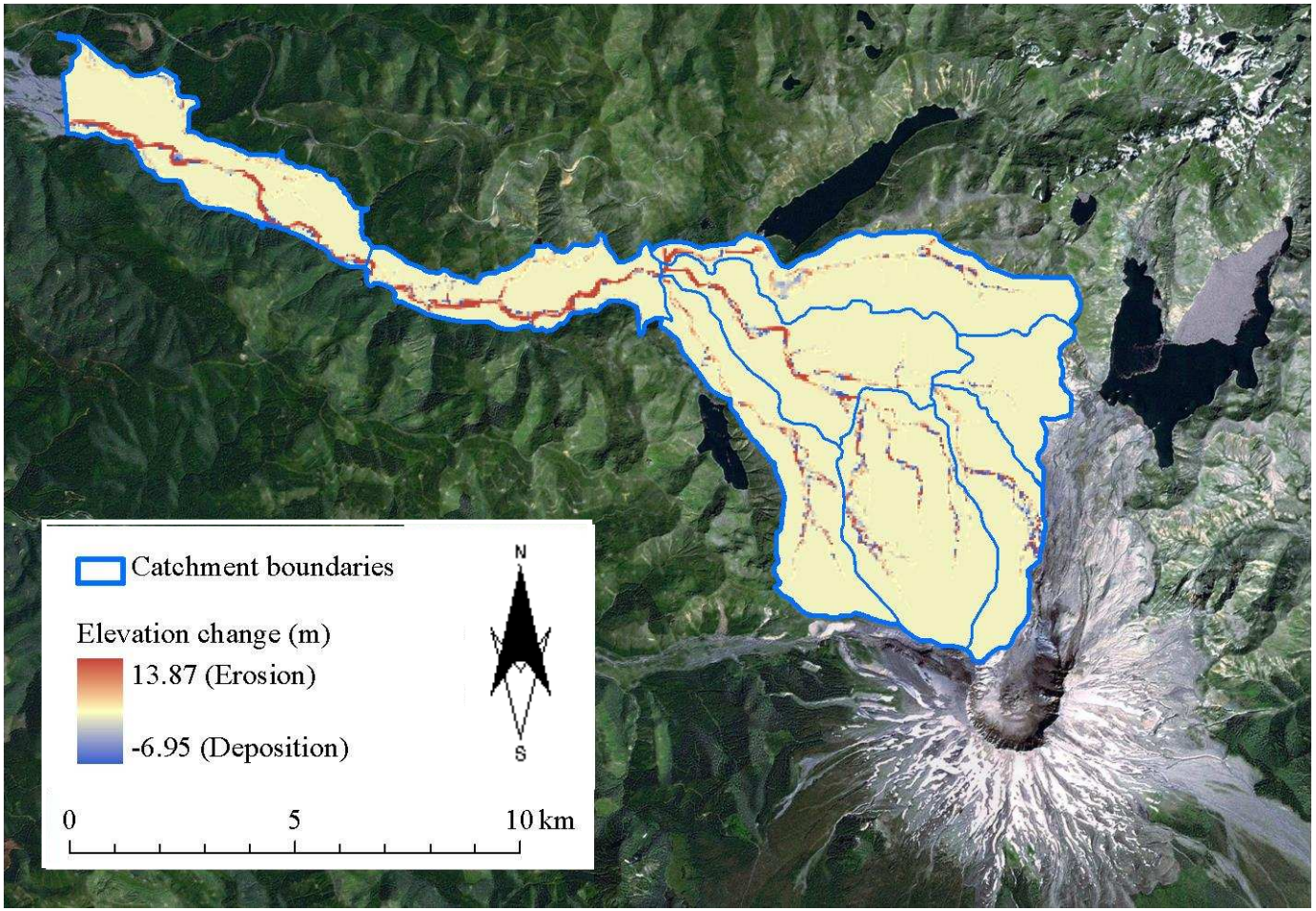

Figure 5.9 Pattern of erosion and deposition produced by Test Run 4. Aerial imagery from DigitalGlobe (Microsoft).

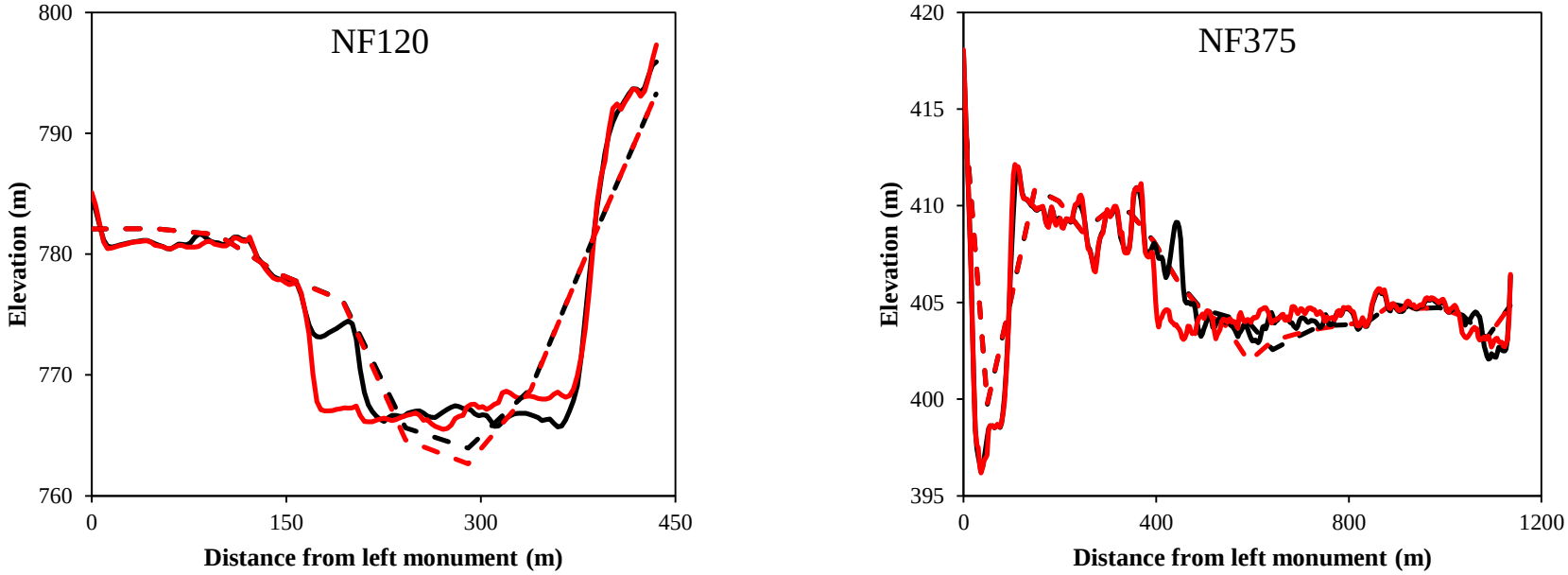

Figure 5.10 Cross-section profiles at NF120 and NF375 for Test Run 4. Solid lines are the LiDAR-derived profiles while dashed lines are the modelled profiles. Black lines represent the initial and red lines the final, topography.

This analysis suggests that the values of Λ used during Test Runs 3 and 4 (1.0 x 10^{-5} and 1.0 x 10^{-6}, respectively) are more appropriate for the current application than that used during Test Run 2 (Λ = 1.0 x 10^{-4}). It is also apparent, however, that model outputs are extremely sensitive to this parameter and significant differences in the representation of channel processes are evident between Test Runs 3 and 4. Moreover, total sediment output differs by 6.24 million m^3 (Table 5.6) between the two runs, further emphasising the sensitivity of overall model results to the selected value of Λ. It is clear from these findings that more rigorous testing of this parameter is essential to identify the most suitable value. It is also evident that the values used in Test Runs 3 and 4 are potentially at the extreme ends of a range of possible values, with lateral erosion still slightly greater than observed when Λ = 1.0 x 10^{-5}, whereas excessive channel incision is evident when Λ = 1.0 x 10^{-6}. Consequently, it was decided that values of Λ between 2.0 x 10^{-6} and 8.0 x 10^{-6}, with increments of 1.0 x 10^{-6}, should be tested as part of the extensive model calibration, as reported in Section 0.

5.3.3 The spatial distribution of sediment yield

Once a feasible range for Λ (2.0 x 10^{-6} to 8.0 x 10^{-6}) was identified, evaluation of modelled erosion volumes was undertaken at the sub-catchment scale to assess spatial patterns of sediment yield. Sub-catchment volumetric change calculations were conducted for Test Runs 3 and 4, as well as an additional model run in which Λ = 5.0 x 10^{-6} (Test Run 5), representing a value approximately in the middle of the range of Λ previously specified. The results of all three simulations indicated that there were significant discrepancies between modelled sediment outputs for a number of the sub-catchments, particularly Loowit Creek, Carbonate Springs and uNFTR Reach C (Figure 5.11).

Specifically, it is evident that all model set-ups overestimated erosion in the most downstream reach (uNFTR Reach C), yet significantly underestimated erosion in the headwater sub-catchments of Loowit Creek and Carbonate

Springs. Lack of channel development in the headwaters is also evident in Figure 5.5, Figure 5.7 and Figure 5.9. Although there were variations between the different model set-ups, this spatial pattern of error was consistent across the range of Λ values, suggesting that its cause might be an incorrect value specified for a different parameter. The most likely explanation for the apparent discrepancies between the modelled and observed spatial pattern of erosion evident in Figure 5.11 is the way in which the hydrological input was distributed throughout the catchment within C-L.

Specifically, as discussed in Chapter 4, C-L does not account for the spatial distribution of inputs to the drainage system from precipitation, snow melt, springs or lakes. Orographic effects, for instance, mean that inputs from precipitation are likely to be much greater in the headwaters than lower down in the catchment. Additionally, inputs from snow melt at higher altitudes will increase runoff in headwater streams, while lake and spring sources, which represent important hydrological features within the upper North Fork Toutle River catchment, are also not included. This problem is exacerbated by the fact that the model only inputs water to cells in which the discharge is greater than the user-defined threshold $Q_{\min}$ (in this case 0.5 m^3 s^{-1}; see Chapter 4), meaning that cells farther downstream are preferentially selected as water input points as they have a greater drainage area and therefore a higher calculated discharge. As a result, the upstream extents of reaches affected by processes of fluvial erosion during a given flood are limited by the threshold discharge, and it may be that in this regard a value of 0.5 m^3 s^{-1} for $Q_{\min}$ is too high and overly restricts erosion in headwater channels.

It is therefore thought that the method by which C-L represents hydrological inputs is unrepresentative of the field situation in the upper North Fork Toutle River. As such, it was necessary to modify this aspect of the model's operation in order to better match the inputs of water to those expected in this catchment. Improving the representation of catchment hydrology should also have the added benefit of improving the spatial distribution of channel scour and deposition. The first step in this process was to test whether lowering the $Q_{\min}$ parameter could result in more of the incoming water entering the drainage

network via headwater cells, thus representing the greater hydrological inputs expected at higher altitudes. This could also have the effect of increasing erosion in upstream reaches while reducing sediment transport capacities and so promoting deposition farther downstream in the fluvial system. $Q_{\min}$ was therefore reduced to 0.1 $m^3 s^{-1}$ for Test Run 6 and sub-catchment erosion volumes were re-analysed. Lowering $Q_{\min}$ increases the number of cells in which C-L has to calculate erosion and, therefore, increases model run times. In the current application, it was found that reducing $Q_{\min}$ below 0.1 $m^3 s^{-1}$ would be impractical due to the excessive increased run times that would result.

The results of Test Run 6 (Figure 5.12) indicate that the reduction of $Q_{\min}$ to 0.1 $m^3 s^{-1}$ increased the volume of erosion in the Loowit Creek and Carbonate Springs sub-catchments by about 170% and 270%, respectively, relative to Test Run 5. Despite these increases, the modelled volume eroded from Loowit Creek remained less than 4% of that observed, while that from Carbonate Springs was just over a quarter of the LiDAR-derived value. Test Run 6 was also associated with a reduction of about 13% in the volume of erosion from uNFTR Reach C relative to Test Run 5, although the modelled value of 2.85 million m^3 is still four times greater than that observed. In summary, although reducing the value of $Q_{\min}$ to 0.1 $m^3 s^{-1}$ had some benefits in terms of redistributing erosion within the catchment, the spatial pattern of error still remained. It is therefore apparent that this measure was unsuccessful in improving the representation of catchment hydrology in the upper North Fork Toutle River and additional modifications are required.

The first modification was to introduce an additional parameter, $Q_{\max}$, which is similar to $Q_{\min}$ but instead sets an upper threshold value of discharge for C-L to calculate a flow depth within a cell. Effectively, the addition of $Q_{\max}$ acts to designate a range of cells to which water will be added rather than just a lower limit as was the case when $Q_{\min}$ was the only factor controlling the distribution of the water input. In theory, this should prevent the addition of water to cells lower in the catchment, which would generally have calculated discharge values greater than $Q_{\max}$, and so increase the rate of water added to cells in the

catchment headwaters. This should mean that the spatial distribution of rainfall runoff would be more representative of the field situation. To test the influence of the additional, $Q_{\max}$ parameter on redistributing erosion within the catchment, three models were run (Test Runs 7, 8 and 9) with $Q_{\max}$ set at 0.5, 1 and 2 $m^3 s^{-1}$, respectively (Table 5.5). In all three cases, $Q_{\min}$ was held at the lower value of 0.1 $m^3 s^{-1}$, and it remained at this level for all further simulations.

Visual inspection of Figure 5.13 indicates that the addition of the $Q_{\max}$ parameter in Test Runs 7, 8 and 9 results in greater erosion in headwater sub-catchments relative to Run 6. Specifically, as evident in Table 5.6, sediment yield from Loowit Creek increased by around 170%, 113% and 53% in Test Runs 7, 8 and 9, respectively. Furthermore, respective increases of about 43%, 30% and 2% for the three runs were observed within the Carbonate Springs sub-catchment. Reductions of 18% and 0.35% in the volume of erosion were also evident in uNFTR Reach C for Test Runs 7 and 8, although for Test Run 9 an increase of 5% was observed in this sub-catchment.

These results indicate that, as expected, the value selected for $Q_{\max}$ has a profound impact on the redistribution of sediment and adjustment of this parameter has great potential to improve the fit of the model outputs. On this basis, more detailed assessment of the impact of different values of $Q_{\max}$ was carried out as part of the extensive model calibration reported in Section 0. The finding that lower values of $Q_{\max}$ result in improved model performance led to values of 0.2, 0.3 and 0.4 $m^3 s^{-1}$ being selected during these later calibration runs. Although introducing the $Q_{\max}$ parameter was clearly beneficial, modelled volumes of erosion in uNFTR Reach C remained significantly greater than LiDAR-derived values, while those upstream in Loowit Creek were still much lower than expected (Table 5.6). It was therefore evident that the addition of the $Q_{\max}$ parameter alone did not provide sufficient improvements in the representation of catchment hydrology in the upper North Fork Toutle River by C-L. It was recognised that rectifying this problem was essential to improve representation of the catchment-scale sediment budget.

A second modification was therefore made to directly limit the spatial extent of the cells to which water from the hydrological model was added, in order to further shift inputs of water to the headwater catchments and therefore better represent upstream hydrological inputs. Given that the orientation of the catchment below the confluence of the North Fork Toutle River with Castle and Coldwater Creeks is predominantly east-west, it was possible to specify an x-coordinate that could act to limit the downstream extent of the hydrological input, referred to as $X_{\max}$. The boundary between uNFTR Reaches B and C was specified to represent this downstream limit (Figure 5.1), as it ensured that water was added to all the main tributaries contributing flow to the main channel, while preventing the addition of significant quantities of water directly to the river in the lower part of the debris avalanche.

Test Run 10 was undertaken with this downstream limit in place and a $Q_{\max}$ value of 0.5 $m^3 s^{-1}$ in order to facilitate direct comparison with Test Run 7 (shown in Figure 5.14). The volume of sediment eroded from uNFTR Reach C in Test Run 10 was reduced by about 20% compared with that in Test Run 7 (Table 5.6). Although the modelled volume of 1.90 million m^3 is nearly three times the LiDAR-derived volume, this represents a substantial improvement over earlier test runs. Furthermore, erosion volume increased by 120% and 70% in the Loowit Creek and Carbonate Springs sub-catchments, respectively (Table 5.6). These increases suggest that addition of the $X_{\max}$ parameter better represents the hydrology of the upper North Fork Toutle River by simulating increased water inputs to headwater streams which result from orographic effects and snow accumulation and melt, as well as lake and spring inputs.

A consequence of the modifications to C-L's hydrological model has been an improvement in the representation of the catchment-scale sediment budget. Although it may be argued that the modifications described above simply involved adjusting the input (the spatial distribution of water discharge) to better match the output (the spatial distribution of erosion and deposition), the modifications were physically-based as precipitation inputs are known to be greater at higher altitudes in the headwaters of mountainous catchments. Moreover, it should be noted that the water availability is not itself being

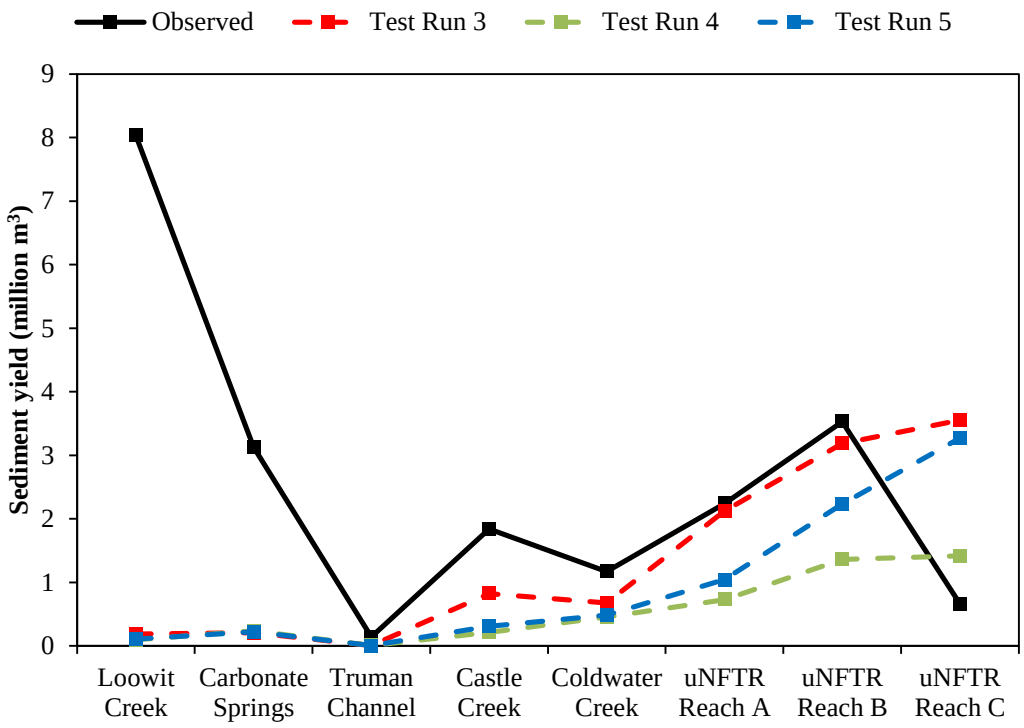

Figure 5.11 Sediment yields for selected sub-catchments in Test Runs 3, 4 and 5 compared with LiDAR-derived values.

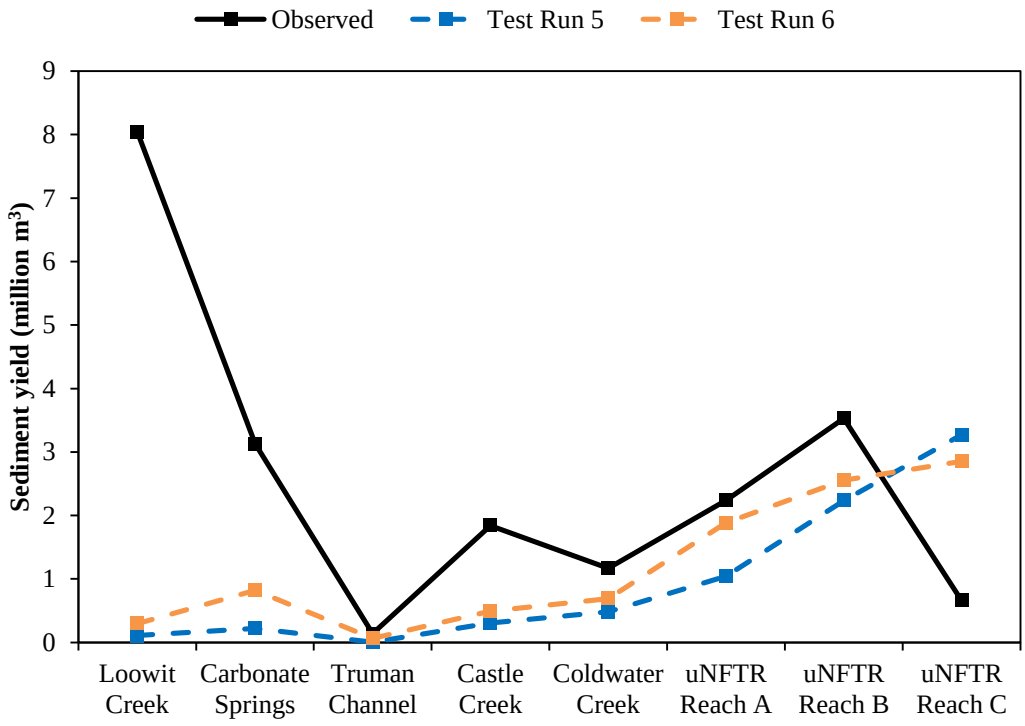

Figure 5.12 Sediment yields for selected sub-catchments in Test Runs 5 and 6 compared with LiDAR-derived values.

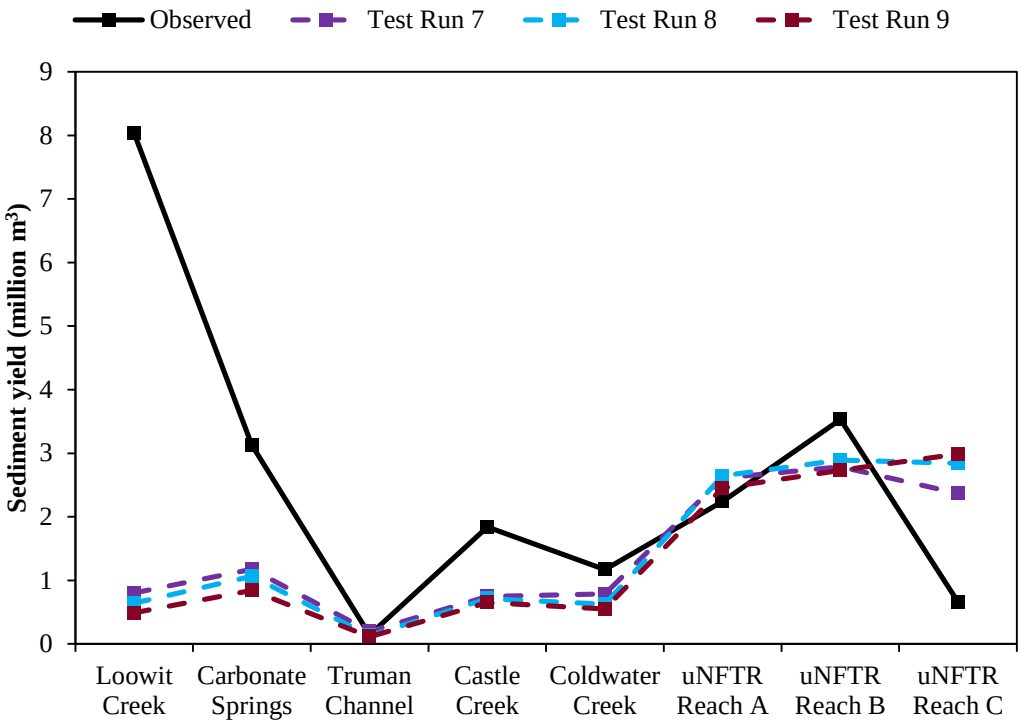

Figure 5.13 Sediment yields for selected sub-catchments in Test Runs 7, 8 and 9 compared with LiDAR-derived values.

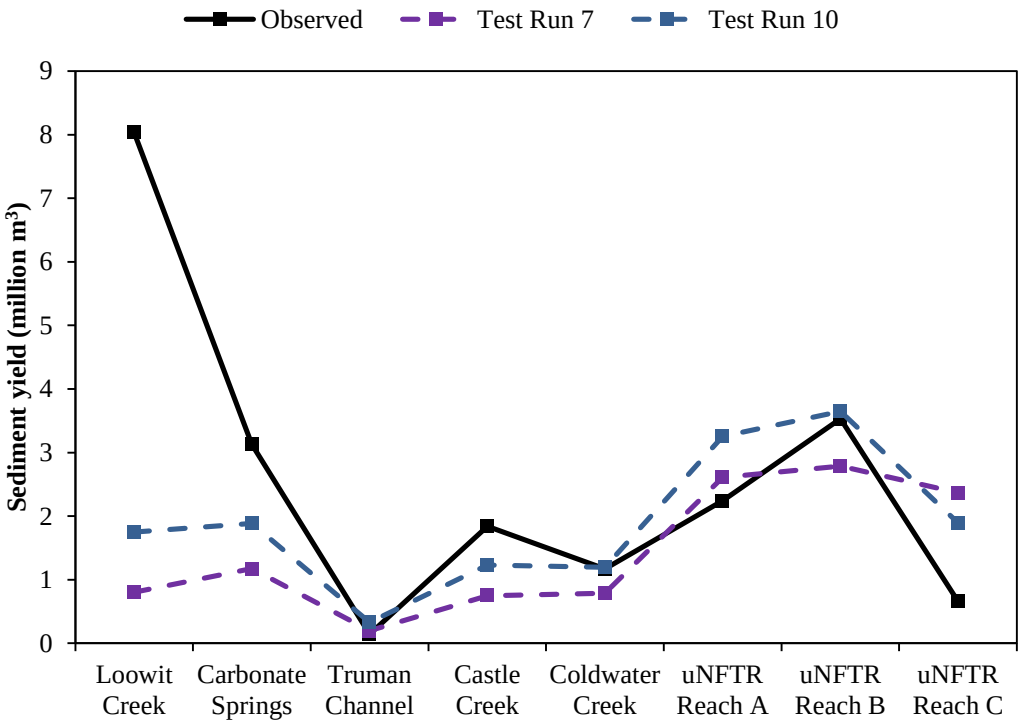

Figure 5.14 Sediment yields for selected sub-catchments in Test Runs 7 and 10 compared with LiDAR-derived values.

modelled in this study, and modifications were purely undertaken in order to obtain a realistic distribution of water availability to drive calculations of sediment erosion, transport and deposition.

5.4 MODEL CALIBRATION

5.4.1 Model configurations

Although the tests reported in the previous Section established the basic configuration for the C-L model, uncertainty remained concerning the most appropriate specifications for Λ, λ, N_{smooth}, N_{shift} and Q_{max} and the impact that varying these parameters in combination might have on model outcomes. The investigations performed to assess these specifications and impacts are the focus of this Section. The range of values for each parameter together with the interval between each value in the range and the subsequent number of values (n) are summarised in Table 5.7. These values produce the 126 parameter combinations explored as part of the final calibration exercise. The aim of this calibration exercise was to identify a sub-set of best-fit model configurations that could then be used to make predictions of future sediment yield from the North Fork Toutle River catchment. The process of model selection based on the calibration and evaluation reported in this Section is described in Section 5.5.

Table 5.7 Ranges and intervals of parameter values used in the 126 model calibration runs.

Parameter	Min.	Max.	Interval	n
Λ	2.0×10^{-6}	8.0×10^{-6}	1.0×10^{-6}	7
λ	10	20	5	3
N_{smooth}	30	40	10	2
N_{shift}	3	4	1	2
Q_{max}	0.2	0.4	0.1	3

5.4.2 Summary of results

Figures 5.15 to 5.17 present the observed values for sub-catchment sediment yield, changes in channel thalweg elevations and changes in cross-sectional area, respectively, together with the maximum, minimum and mean values from the 126 C-L model runs. The maximum and minimum values represent uncertainty bounds on the model outputs in the sense of Ewen and Parkin (1996) and Bathurst et al. (2004), which were discussed in sub-section 5.1.1 above. Figure 5.15 shows that seven out of the eight measured values (88%) of sub-catchment sediment yield are contained within the uncertainty bounds. In both Figure 5.16 and Figure 5.17, it is evident that nine of the ten measured values (90%) of change in channel thalweg elevation and cross-sectional area, respectively, are contained within the uncertainty bounds. These data are also summarised in Tables 5.8 to 5.10.

Figure 5.15 and Table 5.8 indicate that, with the exception of Loowit Creek, the models set ups all produce spatial distributions of erosion that are similar to those derived from LiDAR surface differencing. However, despite the modifications made to the hydrological model described in Section 5.3.3, all model set ups underestimate erosion in Loowit Creek, which is the sub-catchment farthest upstream in the drainage system. Similarly, total catchment sediment yield is consistently underestimated by all models, as shown by the data listed in Table 5.8. Mean modelled total catchment sediment yield is, however, within 20% of the observed value (Table 5.8). However, this general agreement between modelled and observed data at the sub-catchment scale is somewhat less apparent at the scale of individual cross-sections.

Marked discrepancies between modelled and observed channel thalweg elevation changes are evident at the majority of cross-sections. Significantly, incision at LO040, observed to be 9.43 m between 2003 and 2009, was consistently underestimated in all model set-ups, which further emphasises the problems of process-representation in the headwaters that were evident from sub-catchment analyses described earlier. At other cross-sections, however, thalweg elevation change was both under- and overestimated, with very little

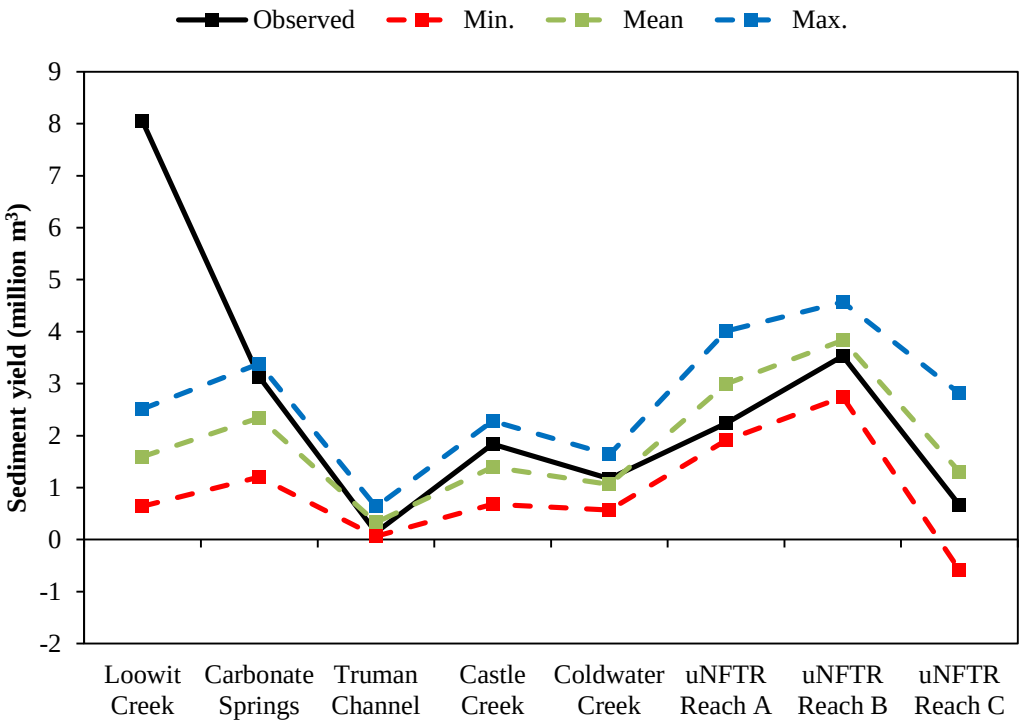

Figure 5.15 Minimum, mean and maximum values of sediment yields from the eight sub-catchments observed and modelled during model calibration.

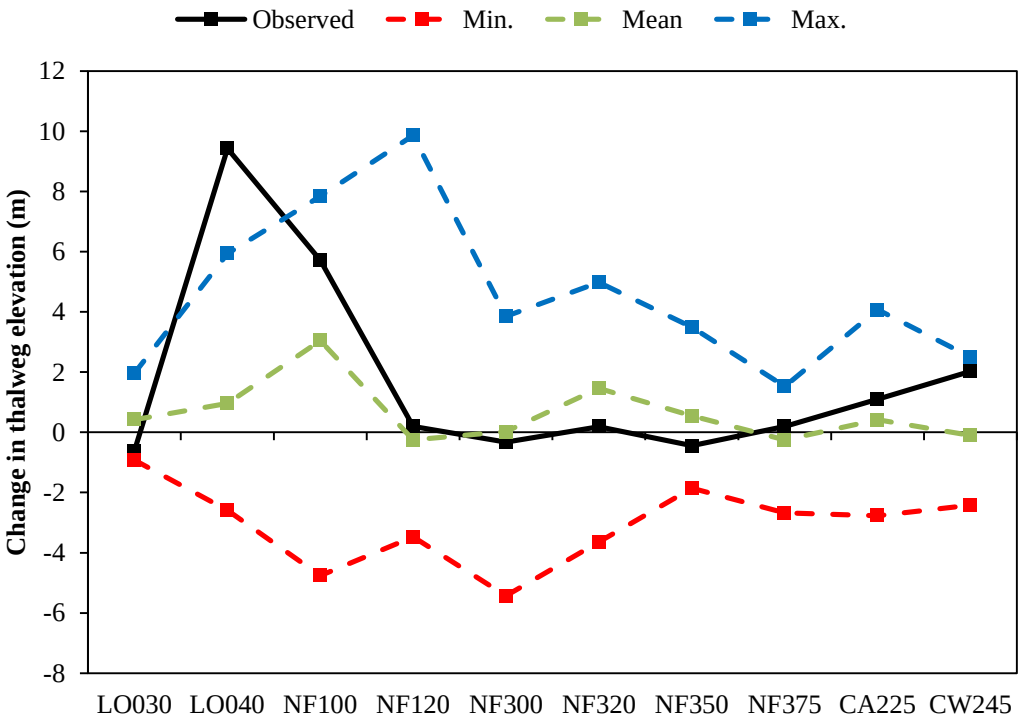

Figure 5.16 Minimum, mean and maximum values of change in thalweg elevation at the ten cross-sections observed and modelled during model calibration.

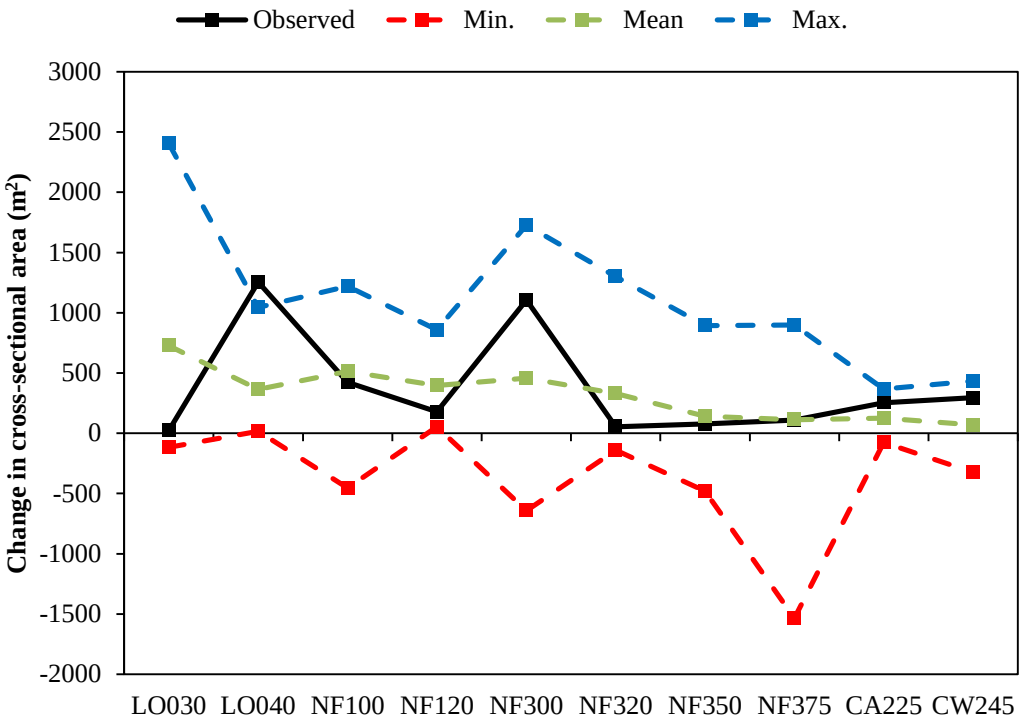

Figure 5.17 Minimum, mean and maximum values of change in area at the ten cross-sections observed and modelled during model calibration.

Table 5.8. Minimum, mean and maximum values of sediment yields from the eight sub-catchments observed and modelled during model calibration.

Sub-Catchment	Observed (million m^3)	Modelled (million m^3)		
		Min.	Max.	Mean
Loowit Creek	8.04	0.65	2.51	1.60
Carbonate Springs	3.13	1.20	3.38	2.34
Truman Channel	0.14	0.07	0.63	0.33
Castle Creek	1.84	0.68	2.28	1.39
Coldwater Creek	1.17	0.57	1.63	1.06
uNFTR Reach A	2.24	1.91	4.01	3.00
uNFTR Reach B	3.53	2.74	4.57	3.84
uNFTR Reach C	0.66	-0.59	2.81	1.30
Total	20.75	10.46	17.48	14.85

Table 5.9 Minimum, mean and maximum values of change in thalweg elevation at the ten cross-sections observed and modelled during model calibration.

Cross-section	Observed (m)	Modelled (m)		
		Min.	Max.	Mean
LO030	-0.62	-0.93	1.96	0.42
LO040	9.43	-2.59	5.94	0.97
NF100	5.71	-4.76	7.85	3.05
NF120	0.20	-3.47	9.86	-0.25
NF300	-0.33	-5.43	3.86	0.02
NF320	0.19	-3.65	4.98	1.46
NF350	-0.45	-1.86	3.49	0.55
NF375	0.20	-2.68	1.53	-0.25
CA225	1.10	-2.77	4.07	0.42
CW245	2.03	-2.42	2.50	-0.11

Table 5.10 Minimum, mean and maximum values of change in area at the ten cross-sections observed and modelled during model calibration.

Cross-section	Observed (m^2)	Modelled (m^2)		
		Min.	Max.	Mean
LO030	23.56	-115.84	2402.40	726.21
LO040	1253.74	17.44	1043.63	364.13
NF100	422.59	-454.68	1221.14	512.00
NF120	178.31	53.31	858.08	395.26
NF300	1105.14	-641.43	1726.10	457.49
NF320	53.63	-140.38	1300.44	328.87
NF350	76.88	-481.54	893.58	142.29
NF375	108.77	-1535.59	897.88	112.94
CA225	254.05	-75.36	367.89	123.98
CW245	295.15	-324.18	432.33	69.49

consistency between model set-ups (Figure 5.16; Table 5.9). The results presented in Figure 5.17 and Table 5.10, which summarise model outputs in terms of changes in cross-sectional area, share many of the same characteristics as those for thalweg elevation changes. Erosion is again consistently underestimated at LO040, while both large negative and positive discrepancies are evident at other cross-sections.

The discrepancies noted at the local-scale (i.e. at cross-sections) may be the result of a number of factors. For instance, as outlined in Chapter 4, the algorithm used to simulate lateral erosion and the in-channel movement of sediment is a simplified representation of the processes that generate meander development in natural river systems. Consequently, it is unlikely that modelled patterns of cross-sectional change will accurately reproduce those

observed in the actual system. Furthermore, uncertainties surrounding initial conditions resulting from errors in the LiDAR surface also reduce the likelihood that modelled outputs will match observations at the local-scale. Given these factors, the actual values of error statistics (calculated in Section 5.5) are difficult to interpret and cannot be used as a basis to accept or reject the applicability of C-L for the purposes of the current study. They do, however, provide important insights regarding the relative performance of individual model configurations that informed parameter selection and model set-up for the predictive runs, as explained in Section 5.5.

5.5 MODEL SELECTION

This Section summarises the methodology used to identify the set of models selected from the 126 configurations described in the previous Section for use in forecasting long-term sediment yields from the upper North Fork Toutle River catchment. This methodology is summarised in Figure 5.18.

5.5.1 Quantifying model performance

The first step required for model selection was to quantify the discrepancies between the observed and modelled values noted in Section 5.4.2 for each of the four evaluation criteria. Discrepancies can be quantified using a number of diverse statistics (Dawson et al., 2012), although not all are appropriate to the current study. This Section therefore discusses the various metrics that might be implemented and defines those that were selected for use.

i. Absolute measures

Legates and McCabe (1999) suggest that it is important to quantify error in terms of the units of the variable and, as such, dimensioned, or absolute, measures of performance are desirable. Commonly used dimensioned measures of average error are Mean Bias Error (MBE; equation 5.1), Mean Absolute Error (MAE; equation 5.2) and Root-Mean-Square Error (RMSE; equation 5.3) (Willmott and Matsuura, 2005).

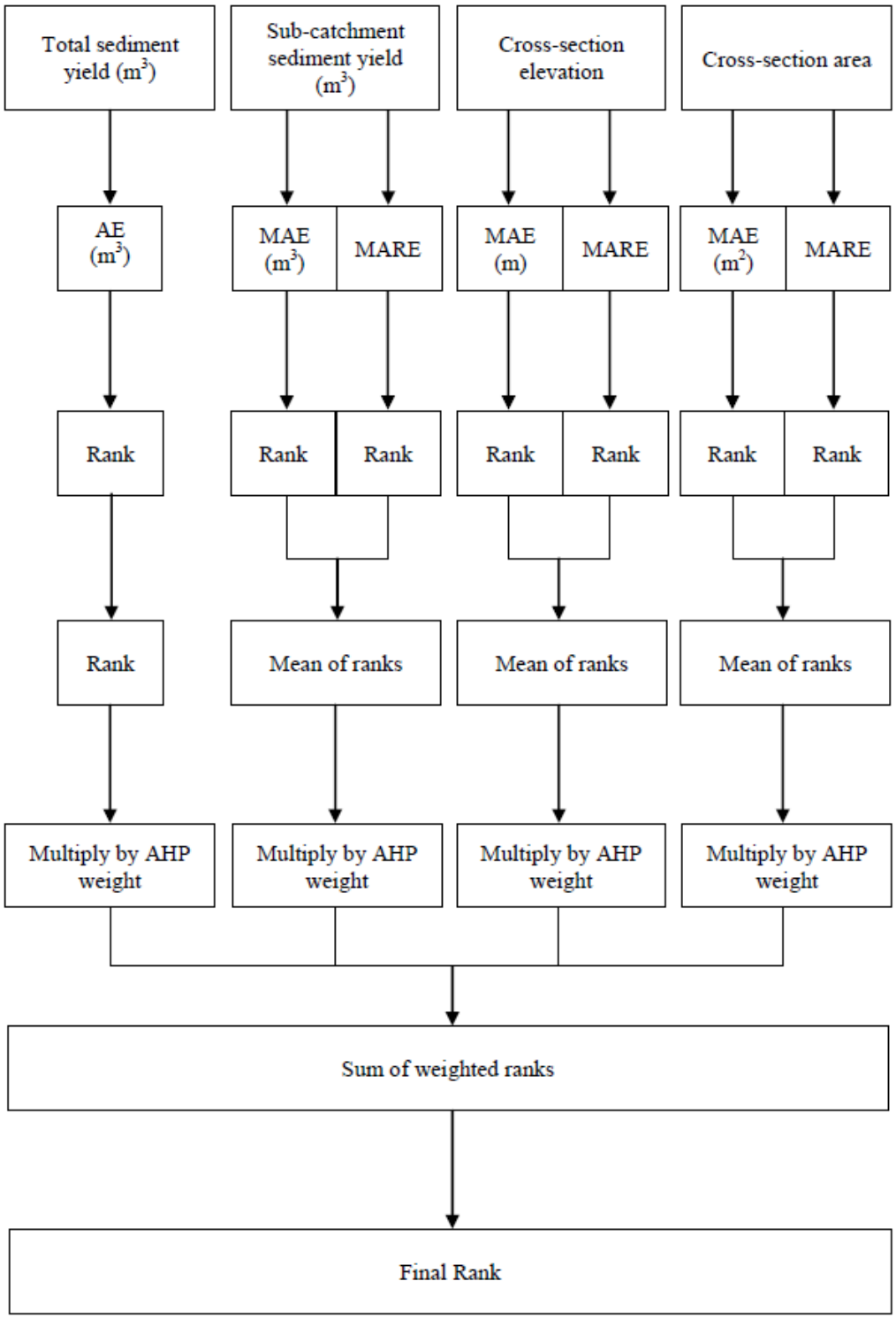

Figure 5.18 Schematic representation of model selection procedure.

$$\mathrm{MBE} = \frac{1}{n}\sum_{i=1}^{n} P_i - O_i \tag{5.1}$$

$$\mathrm{MAE} = \frac{1}{n}\sum_{i=1}^{n} |P_i - O_i| \tag{5.2}$$

$$\mathrm{RMSE} = \frac{1}{n}\sqrt{\sum_{i=1}^{n} (P_i - O_i)^2} \tag{5.3}$$

where, P = the modelled (or predicted) value; O = the observed value; and i = 1 to n data points. MBE is simply the mean of the residuals and is predominantly used to discern whether a model is systematically over- or under-estimating the observed data (Bennett et al., 2013). Although the ideal value of zero for MBE indicates that there is no overall bias in the model predictions, a value close to zero does not necessarily mean a model is performing well because positive and negative errors tend to cancel each other out (Mayer and Butler, 1993; Dawson et al., 2007). MBE is therefore not a good indicator of model performance and was not selected for use in this study.

RMSE and MAE are non-negative metrics in that all errors contribute positively to the score, regardless of their sign. Hence, ambiguities associated with the interpretation of MBE values are irrelevant to RMSE or MAE, and these are more generally preferred. Given that RMSE and MAE are dimensioned metrics, they are both scale-dependent and increase with the magnitude of the observation. The inherent bias of RMSE and MAE towards higher magnitude observations is useful in characterising model performance at the upper end of the data set where absolute errors tend to be larger, and this can be a useful attribute of these metrics (Fischer et al., 2013). The main difference between these metrics is that RMSE is far more sensitive to extreme values than MAE (Willmott, 1982, 1984; Hyndman and Koehler, 2005), because its squaring process gives a disproportionate weight to very large errors (Dawson et al., 2007).

However, Willmott and Matsuura (2005) point out that RMSE is a function of the average error (MAE), the variance associated with the distribution of error magnitudes, and the square root of the number of errors ($n^{0.5}$), and therefore does not describe average error alone. Willmott and Matsuura (2005) argue that as a result there is no clear interpretation of RMSE and that it should be disregarded in favour of MAE. Additionally, Armstrong and Collopy (1992) found RMSE to be extremely unreliable for assessing model accuracy, and they too recommended against its use.

On the basis of the identified limitations associated with RMSE, MAE was selected as the dimensioned measure of error to be used in this study. Although the bias of MAE towards the upper end of the data range is beneficial, it does mean that errors associated with lower magnitude observations will be under-represented. Hence, an additional measure is required in order to assess the accuracy of model predictions for smaller values within the data set. Alternative metrics can generally be classified into two groups: dimensionless coefficients and relative measures (Dawson et al., 2007).

ii. Dimensionless coefficients

Three commonly used dimensionless coefficients of possible relevance to the current study are the coefficient of determination (r^2, referred to hereafter as RSqr; equation 5.4), the Nash-Sutcliffe Model Efficiency (NSE; equation 5.5) and the Index of Agreement (IoAd; equation 5.6) (Legates and McCabe Jr., 1999; Dawson et al., 2007; Bennett et al., 2013).

$$\text{RSqr} = \left[\frac{\sum_{i=1}^{n}(O_i - \bar{O})(P_i - \bar{P})}{\sqrt{\sum_{i=1}^{n}(O_i - \bar{O})^2 \sum_{i=1}^{n}(P_i - \bar{P})^2}}\right]^2 \tag{5.4}$$

$$\text{NSE} = 1 - \frac{\sum_{i=1}^{n}(O_i - P_i)^2}{\sum_{i=1}^{n}(O_i - \bar{O})^2} \tag{5.5}$$

$$\text{IoAd} = 1 - \frac{\sum_{i=1}^{n}(O_i - P_i)^2}{\sum_{i=1}^{n}(|P_i - \bar{O}| + |O_i - \bar{O}|)^2} \quad (5.6)$$

RSqr describes the total variance in the observed data that can be explained by the model (Legates and McCabe Jr., 1999) and comprises the squared ratio of two series to the total dispersion of the observed and modelled series (Dawson et al., 2007). However, the fact that RSqr quantifies only dispersion means that a model that systematically over- or under-estimates the real data will still produce good RSqr values (i.e. values close to 1.0) even if all the predictions are wrong (Krause et al., 2005). Furthermore, given that the differences between the observed and predicted values in NSE and IoAd are calculated as square values, both of these metrics are extremely sensitive to large values and are therefore inappropriate for characterising model performance at lower magnitudes (Legates and McCabe Jr., 1999; Krause et al., 2005; Dawson et al., 2007).

iii. Relative measures

None of the dimensionless coefficients discussed above can be used to supplement MAE in order to assess model outputs over the full range of the observed data for each evaluation criterion. Relative measures, which record the difference between observed and modelled values as the ratio of the calculated error to the observed value (i.e.$(O_i - P_i)/O_i$) (Dawson et al., 2007) are more suitable for these purposes. Relative measures are biased towards smaller values, which generally tend to have much higher relative errors in comparison with larger ones (Bennett et al., 2013), and are therefore good indicators of model performance at the lower end of the data set. Relative measures that could be used here include Relative Absolute Error (RAE; equation 5.7), Mean Relative Error (MRE; equation 5.8), Mean Squared Relative Error (MSRE; equation 5.9) and Mean Absolute Relative Error (MARE; equation 5.10) (Dawson et al., 2007).

$$\mathrm{RAE} = \frac{\sum_{i=1}^{n} |O_i - P_i|}{\sum_{i=1}^{n} |O_i - \bar{O}|} \tag{5.7}$$

$$\mathrm{MRE} = \frac{1}{n} \sum_{i=1}^{n} \left(\frac{O_i - P_i}{O_i} \right) \tag{5.8}$$

$$\mathrm{MSRE} = \frac{1}{n} \sum_{i=1}^{n} \left(\frac{O_i - P_i}{O_i} \right)^2 \tag{5.9}$$

$$\mathrm{MARE} = \frac{1}{n} \sum_{i=1}^{n} \frac{|O_i - P_i|}{O_i} \tag{5.10}$$

RAE expresses the error relative to the variation about the mean of the observed record rather than the observed record itself (Dawson et al., 2007), leading Makridakis (1993) to argue that RAE-based measures have little physical meaning and are difficult for non-expert stakeholders and decision makers to interpret. On the other hand, MRE, MSRE and MARE comprise the mean of the error made relative to the observed record, and are therefore more easily interpreted. However, MRE and MSRE suffer from potential cancelling of positive and negative errors which can over-estimate model performance (Dawson et al., 2007). For these reasons, MARE was selected as the most appropriate relative measure to supplement MAE.

Beneficially, MARE is an easily comprehended metric that can also be expressed in percentage terms (Mean Absolute Percentage Error (MAPE)), which is useful for communicating results to non-expert stakeholders. Furthermore, particularly large values of ARE ($|O_i - P_i|/O_i$) result when the value of O_i is small and therefore good information regarding outliers at the lower end of the data range is provided (Makridakis, 1993). Although the division of the calculated error by O_i means that MARE can be undefined if any observed value is zero (Mayer and Butler, 1993), this is not a problem in the current study as no zero values are present in the observed data for any of the evaluation criteria.

For both the absolute (MAE) and the relative (MARE) measures of model performance, the arithmetic mean was preferred as the measure of central tendency in order to preserve as much information as possible regarding extreme errors. This is preferable to the median, for instance, which is far less sensitive to outliers as it discards high and low values (Armstrong and Collopy, 1992; Dawson et al., 2007) and is therefore less effective at discriminating between predictions, particularly when large errors are present for only a small number of data points. The values of MAE and MARE calculated from the 126 model runs for each of the four evaluation criteria are summarised in Table 5.11.

5.5.2 Integrating evaluation criteria and performance metrics

Following quantification of the discrepancies associated with each model set-up, it was necessary to combine both the two error statistics and the four criteria into a single score that would indicate the performance of each model relative to the other 125. As shown in Figure 5.18, this was achieved by ranking each aspect of a model's performance to standardise the values. For the sub-catchment erosion volume, change in cross-section elevation and change in cross-sectional area, each model was given a rank for both MAE and MARE, together with a rank for the absolute error calculated for the total catchment sediment yield. Calculating relative error for the total catchment erosion volume was unnecessary as the subsequently assigned rank would be the same as that for absolute error, and would therefore effectively result in double-counting of the total catchment erosion volume criterion. As a result, each model received seven separate rankings. In all cases, the model with the lowest error (best performance) was assigned a rank of 1, while the model with the greatest error (worst performance) was assigned a rank of 126.

Table 5.11 Minimum, mean and maximum values of the error statistics (MAE and MARE) calculated for each evaluation criterion.

		Min.	Max.	Mean
Total catchment erosion volume	AE (million m^3)	3.27	10.28	5.89
	ARE	0.16	0.50	0.28
Sub-catchment erosion volume	MAE (million m^3)	0.95	1.73	1.27
	MARE	0.36	0.85	0.58
Cross-section elevation	MAE (m)	1.25	2.93	2.19
	MARE	1.47	6.58	3.19
Cross-section area	MAE (m^2)	208.11	609.16	389.58
	MARE	1.03	13.19	4.49

The mean of the seven separate rankings was then calculated to provide the final score that represented the summary, relative performance of each of the model set-ups. However, although each of the evaluation criteria specified in Section 5.2 describes an important aspect of model performance, they are not necessarily of equal importance in the context of the aims of this research. Therefore, it was desirable to weight the rankings so that the criteria of greatest significance contributed more to the final model score than those of lesser importance.

To ensure that the weightings were defined objectively and transparently, the method of criteria inter-comparison developed as part of the Analytic Hierarchy Process (AHP) (Saaty, 1980) was utilised here, and its background and implementation are summarised in the following Sections.

5.5.3 Weighting criteria using the Analytic Hierarchy Process

i. Background

AHP is a decision-making tool that provides a framework for selecting the best from a set of competing alternatives that are evaluated under conflicting criteria (Saaty, 1986) and is therefore ideally suited to the current study. Central to the AHP methodology is the formulation of simple pair-wise comparison judgements between two elements, or criteria, to define how many times more important or dominant one element is compared with another (Saaty, 1986; Vargas, 1990). The judgements are recorded in a square matrix in which each element is compared with all the others (Saaty, 1994a). Each judgement represents the dominance of an element in the column on the left over an element in the row on the top using the scale of 1 to 9 specified in Table 5.12. If, however, the element on the left is less important than that on the top of the matrix, the reciprocal value is entered (Saaty, 1994a). Therefore, the scale effectively ranges from 1/9 for 'least valued than' to 9 for 'absolutely more important than', while a value of 1 indicates that the elements are of equal importance (Vaidya and Kumar, 2006).

Priorities, or weights, are then derived from the pair-wise comparisons by successively squaring the matrix, summing the judgement values in each row and dividing by the sum of all judgements to normalise the sums (Saaty, 1994a). The iterative process stops when the difference between these sums in two consecutive calculations is less than a small, predetermined value (Saaty, 1987). This approach has been shown to account for inconsistent relationships between elements that may result from judgement errors (Saaty, 1994a, b; Forman and Gass, 2001).

ii. Implementation

Table 5.13 summarises the pair-wise comparisons made between the four evaluation criteria regarding their importance relative to model performance, and the scores subsequently assigned to them using the 1 to 9 scale. Given that

the aim of this research is to model future sediment yields from the North Fork Toutle River, criteria relating to sediment yield were taken to be more important than those relating to cross-sectional changes, with the total catchment sediment yield also preferred over sub-catchment sediment yield.

The lower importance assigned to the cross-sectional parameters is also borne out from the fact that it is not the aim of this research to replicate local-scale geomorphic change, but rather to estimate catchment-scale erosion. Nonetheless, it is important for the reasons outlined earlier that relate to process-simulation that cross-sectional changes are still incorporated into the assessment, albeit with a somewhat lower weighting. Consequently, sediment-related criteria were considered to be only weakly or moderately more important than cross-sectional criteria, rather than strongly or extremely more important.

There was no apparent justification for weighting change in cross-sectional area any differently from change in cross-section elevation, and so they were assigned equal importance. These comparisons were then entered into a pair-wise comparison matrix (Table 5.14) and the weights for each criterion were calculated using a Microsoft Office Excel template (Goepel, 2013) according to the methodology described above.

The resulting weights (Table 5.14) imply that total catchment sediment yield should contribute 45.5% to the final model score and sub-catchment erosion volume 26.3%, while changes in cross-sectional area and thalweg elevation each contribute 14.1%.

5.5.4 Sensitivity analysis and final model selection

Although the AHP methodology facilitated quantification of the appropriate weights, these are, nonetheless, subjective. It is conceivable that a range of values would be obtained if the judgements were made by several different people with different opinions regarding the relative importance of each

Table 5.12 1 to 9 scale used for model inter-comparison as part of the Analytic Hierarchy Process (modified from Saaty (2008, p. 86)).

Intensity of importance	**Definition**	**Explanation**
1	Equal importance	Two criteria contribute equally to the objective
2	Weak or slight	--
3	Moderate importance	Experience and judgment slightly favour one criterion over another
4	Moderate plus	--
5	Strong importance	Experience and judgment strongly favour one criterion over another
6	Strong plus	--
7	Very strong or demonstrated importance	A criterion is favoured very strongly over another; its dominance demonstrated in practice
8	Very, very strong	--
9	Extreme importance	The evidence favouring one criterion over another is of the highest possible order of affirmation
Reciprocals of above	If criterion I has one of the above non-zero numbers assigned to it when compared with criterion j, then j has the reciprocal value when compared with i	A reasonable assumption
1.1-1.9	If the criteria are very close	May be difficult to assign the best value but when compared with other contrasting criteria the size of the small numbers would not be too noticeable, yet they can still indicate relative importance of the activities

Table 5.13 Scores assigned to each of the four evaluation criteria on the basis of pair-wise comparisons.

Criterion A		**Criterion B**		**Justification**
Description	**Score**	**Description**	**Score**	
Total catchment sediment yield	2	Sub-catchment sediment yield	1	Total sediment yield is weakly more important than sub-catchment sediment yield.
Total catchment sediment yield	3	Cross-section elevation	1	Total sediment yield is moderately more important than change in cross-section elevation.
Total catchment sediment yield	3	Cross-section area	1	Total sediment yield is moderately more important than change in cross-section area.
Sub-catchment sediment yield	2	Cross-section elevation	1	Sub-catchment sediment yield is weakly more important than change in cross-section elevation.
Sub-catchment sediment yield	2	Cross-section area	1	Sub-catchment sediment yield is weakly more important than change in cross-section area.
Cross-section elevation	1	Cross-section area	1	Change in cross-section elevation is of equal importance to change in cross-section area.

Table 5.14 Pair-wise comparison matrix and calculated weights for each criterion.

	Total catchment sediment yield	**Sub-catchment sediment yield**	**Cross section elevation**	**Cross section area**	**Weights**
Total catchment sediment yield	1	2	3	3	**0.455**
Sub-catchment sediment yield	0.5	1	2	2	**0.263**
Cross section elevation	0.33	0.5	1	1	**0.141**
Cross section area	0.33	0.5	1	1	**0.141**

criterion. To address this issue, a sensitivity analysis was undertaken with the aim of identifying those models which performed consistently well for a range of different possible weighting combinations. For this analysis, the values assigned to the weights were allowed to vary by ±25% and model scores for 100 potential weighting combinations were calculated as outlined above.

Cumulative frequency distributions were constructed for each model and used to identify those that were ranked in the top ten for more than 95% of the weighting combinations, and in the top five for more than 50% of the weighting combinations. Six models met these requirements and were therefore selected as the sub-set of 'best-fit' models. The characteristics of these models, in terms of the calculated error statistics and rank for each of the criteria, are summarised in Table 5.15, while their parameter specifications are presented in Table 5.16.

Table 5.15 suggests that Run 30 performed best overall, in that it was consistently ranked highest and it could, therefore, be argued that this set-up should be used to generate predictions of long-term future sediment yields from the upper North Fork Toutle River catchment. However, although potential uncertainty introduced by subjective judgements regarding the weights assigned to each criterion was reduced through the sensitivity analysis, it is nonetheless preferable to run multiple models rather than selecting a single configuration, for the reasons discussed in Section 5.1 in the context of equifinality. While it may be useful to use each of the six 'best fit' models for the future simulations, this was prohibited by time constraints and computational resources. Furthermore, analysis of the model configurations indicated that it was unnecessary: several models were very similar in terms of their parameterisation and were therefore likely to produce very similar predictions of future sediment yield. In the event, just two model set-ups were selected as being able to encapsulate the range of possible outcomes, as discussed below.

From Table 5.16 it is evident that the most considerable variation between the model set-ups is in the value of Λ, which ranges from 4.0×10^{-6} to 7.0×10^{-6}.

Table 5.15 Calculated error statistics for the six best-performing model runs for the four evaluation criteria. The rank of each model for a given criterion is shown in parentheses.

Run No.	Total sediment yield	Sub-catchment sediment yield		Cross-section elevation		Cross-section area		Final rank 50th percentile	Final rank 95th percentile
	AE (million m^3)	MAE (million m^3)	MARE	MAE (m)	MARE	MAE (m^2)	MARE		
30	4.17 (20)	1.00 (2)	0.57 (60)	1.63 (4)	2.56 (30)	364.53 (53)	4.04 (68)	1	3
60	4.54 (34)	1.03 (4)	0.36 (1)	1.25 (1)	2.29 (17)	438.79 (95)	7.60 (106)	5	10
63	4.36 (26)	1.11 (19)	0.48 (15)	1.75 (10)	2.51 (27)	392.86 (80)	3.46 (60)	2	5
74	3.58 (5)	1.15 (33)	0.49 (18)	2.43 (93)	2.41 (23)	410.12 (88)	6.83 (99)	5	6
75	3.93 (12)	1.14 (29)	0.57 (59)	2.06 (46)	2.22 (12)	389.59 (76)	4.38 (71)	5	8
111	4.04 (14)	1.16 (35)	0.47 (13)	1.82 (17)	2.11 (9)	500.87 (110)	8.11 (110)	4	4

Table 5.16 Values of key parameters for the six best-performing model runs identified in Table 5.15.

Run No.	**Transport formula**	A	Q_{min}	Q_{max}	λ	N_{smooth}	N_{shift}
30	W&C	6.0×10^{-6}	0.1	0.2	20	40	4
60	W&C	4.0×10^{-6}	0.1	0.3	20	40	4
63	W&C	5.0×10^{-6}	0.1	0.3	20	30	3
74	W&C	7.0×10^{-6}	0.1	0.3	15	30	3
75	W&C	7.0×10^{-6}	0.1	0.3	20	30	3
111	W&C	6.0×10^{-6}	0.1	0.4	20	30	3

This indicates that models appear to perform equally well according to the evaluation criteria when channel lateral erosion rates are either relatively high or relatively low. It is therefore essential that this potential range of Λ is fully incorporated into the future simulations. This implies that Run 60, which is the only one of the six configurations to have a value of 4.0×10^{-6} for Λ must be included, together with either Run 74 or 75, which both have values of 7.0×10^{-6} for Λ. Run 75 was subsequently selected because it has a higher value of λ (20) than Run 74, meaning that lateral erosion is more prominent in this configuration. The contrast between Runs 60 and 75 in terms of the representation of lateral erosion is further enhanced by the fact that in Run 60 the model was set-up with higher values of N_{smooth} and N_{shift} (40 and 4, respectively). As explained in Chapter 4, greater smoothing of the local radius of curvature term (R_{ca}) that results from higher values of N_{smooth} and N_{shift} reduces lateral erosion.

Runs 60 and 75 therefore represent low and high lateral erosion scenarios respectively and span the range of potential model configurations that could be defined as best-fit from Table 5.15. Using these two set ups as the basis for future simulations encapsulates the potential variations associated with predictions of future catchment sediment yields that may result from differences in the specification of C-L parameters. Values of MARE and MAE for the two selected model configurations for the four evaluation criteria during the calibration period are summarised in Table 5.15. Further details regarding specific sub-catchments and cross-sections are discussed in the following Section.

5.6 ASSESSMENT OF SELECTED MODELS

5.6.1 Catchment and sub-catchment sediment yields

Both of the selected models were able to replicate the pattern of sub-catchment sediment yield well during the six-year hindcast period, although Run 60 was slightly better (Figure 5.19; Table 5.17). Specifically, the mean absolute errors

for this metric are 36% and 57% in Runs 60 and 75, respectively (Table 5.15). However, these errors were dominated by relatively large errors in a few sub-catchments - specifically Loowit Creek and Truman Channel. The errors evident in Loowit Creek are common to all model configurations and may indicate either a problem with C-L's hydrological model that was not rectified by the modifications made in Section 5.3.3, or the unusual characteristics of the sub-catchment (including dominant glacial and spring water inputs), as discussed earlier. Variation between the two models is minimal, although volumes of sub-catchment sediment erosion are generally greater from Run 75 than Run 60. Overall, Runs 60 and 75 estimated the total catchment sediment yield to within 22% and 19%, respectively during the six years of the hindcast period (Table 5.17).

5.6.2 Mechanisms of sediment yield

The error statistics calculated for changes in cross-sectional characteristics (thalweg elevation and area) reveal limited agreement between C-L outputs and observations for either of the two selected configurations (Figure 5.20 and Table 5.18; Figure 5.21 and Table 5.19). However, given the issues associated with both quantifying and modelling local-scale changes that were discussed in Section 5.4.2, it was necessary to analyse cross-sectional outputs in a more qualitative manner to assess the performance of the selected C-L models at the local-scale. To this end, visual comparisons were made between the LiDAR-derived profiles at the ten selected cross-sections and those produced by Runs 60 and 75 (Figure 5.22). Dominant patterns of channel development were identified from the observed and modelled profiles (Table 5.20) and used to qualitatively evaluate model goodness-of-fit.

It is evident from Figure 5.22 and Table 5.20 that both model configurations were able to replicate trends of channel development observed at selected cross-sections during the hindcast period. Although the magnitudes of the observed and modelled adjustments are somewhat different, the dominant processes responsible for change at a given location (i.e. aggradation, degradation or widening) are correctly simulated by C-L. For instance, at

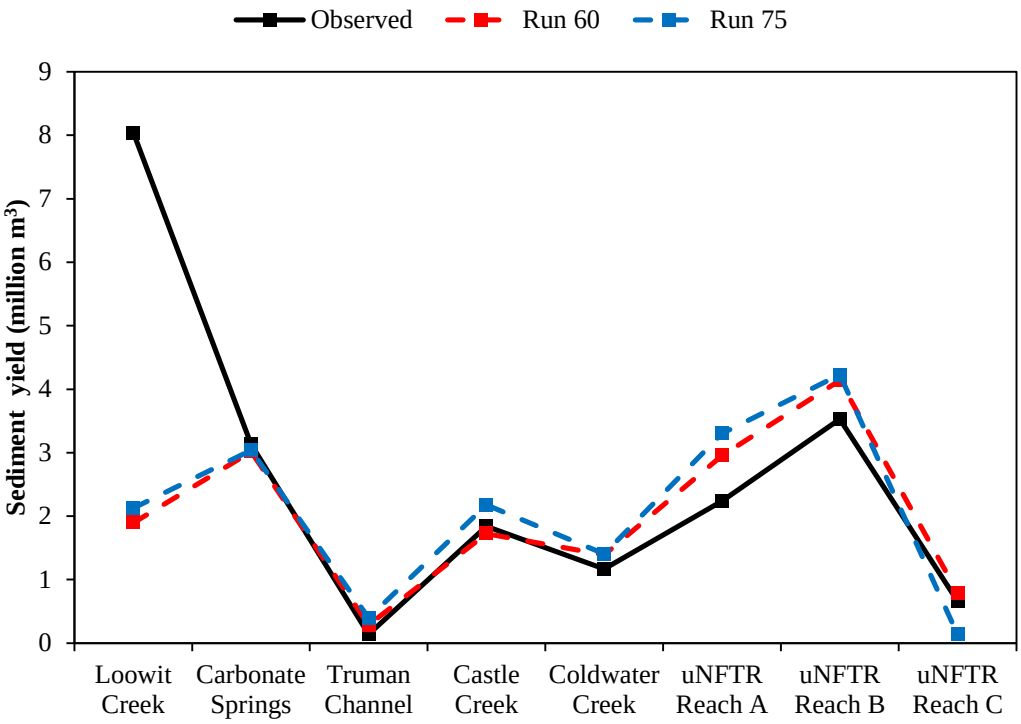

Figure 5.19 Sub-catchment sediment yield for the two selected configurations (Runs 60 and 75) compared with LiDAR-derived values.

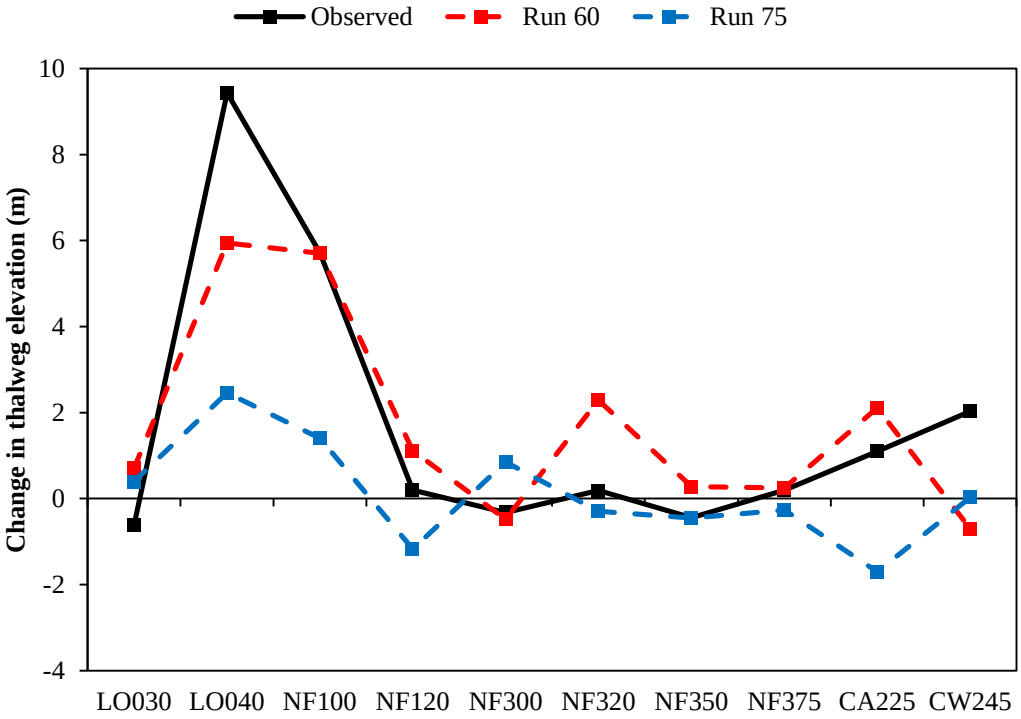

Figure 5.20 Change in channel thalweg elevation for the two selected model configurations (Runs 60 and 75) compared with LiDAR-derived values.

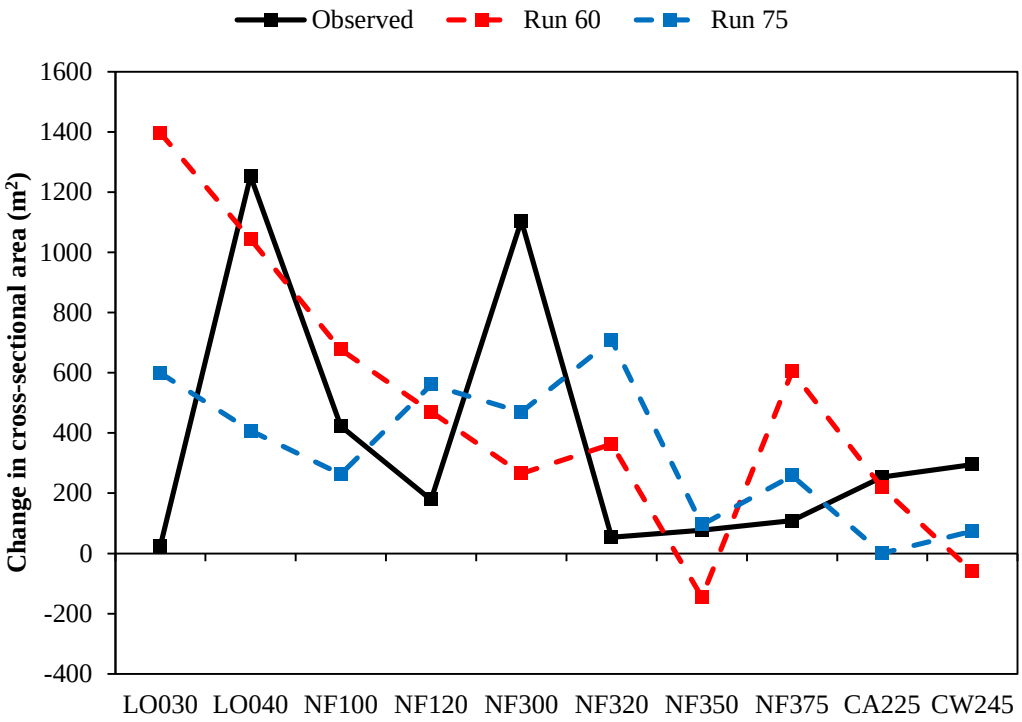

Figure 5.21 Change in cross-sectional area for the two selected model configurations (Runs 60 and 75) compared with LiDAR-derived values.

Table 5.17 Error statistics calculated for sub-catchment sediment yields for the two selected model configurations (Runs 60 and 75).

Sub-Catchment	Observed (million m^3)	Run 60			Run 75		
		Modelled (million m^3)	AE (million m^3)	ARE	Modelled (million m^3)	AE (million m^3)	ARE
Loowit Creek	8.04	1.90	6.14	0.76	2.13	5.91	0.74
Carbonate Springs	3.13	3.02	0.12	0.04	3.04	0.09	0.03
Truman Channel	0.14	0.29	0.15	1.11	0.40	0.26	1.92
Castle Creek	1.84	1.72	0.12	0.06	2.18	0.34	0.18
Coldwater Creek	1.17	1.39	0.22	0.19	1.41	0.24	0.20
uNFTR A	2.24	2.96	0.72	0.32	3.30	1.06	0.47
uNFTR B	3.53	4.14	0.61	0.17	4.23	0.70	0.20
uNFTR C	0.66	0.79	0.13	0.20	0.14	0.53	0.80
Total	20.75	16.20	4.54	0.22	16.82	3.93	0.19

Table 5.18 Change in thalweg elevation error statistics calculated for the two selected model configurations (Runs 60 and 75).

Cross-section	Observed (m)	Run 60			Run 75		
		Modelled (m)	AE (m)	ARE	Modelled (m)	AE (m)	ARE
LO030	-0.62	0.70	1.32	2.12	0.39	1.02	1.63
LO040	9.43	5.94	3.49	0.37	2.46	6.97	0.74
NF100	5.71	5.71	0.01	0.00	1.40	4.31	0.75
NF120	0.20	1.11	0.92	4.66	-1.17	1.37	6.95
NF300	-0.33	-0.48	0.15	0.47	0.85	1.18	3.61
NF320	0.19	2.28	2.10	11.13	-0.30	0.49	2.58
NF350	-0.45	0.28	0.72	1.62	-0.45	0.00	0.01
NF375	0.20	0.25	0.05	0.26	-0.27	0.47	2.35
CA225	1.10	2.11	1.01	0.92	-1.71	2.80	2.55
CW245	2.03	-0.70	2.71	1.34	0.03	2.00	0.99

Table 5.19 Change in cross-sectional area error statistics calculated for the two selected model configurations (Runs 60 and 75).

Cross-section	Observed (m^2)	Run 60			Run 75		
		Modelled (m^2)	AE (m^2)	ARE	Modelled (m^2)	AE (m^2)	ARE
LO030	23.56	1396.93	1373.36	58.29	599.00	575.43	24.42
LO040	1253.74	1043.63	210.11	0.17	407.83	845.92	0.67
NF100	422.59	676.99	254.40	0.60	263.09	159.50	0.38
NF120	178.31	470.43	292.12	1.64	560.44	382.13	2.14
NF300	1105.14	265.59	839.55	0.76	469.07	636.07	0.58
NF320	53.63	362.77	309.14	5.76	708.31	654.68	12.21
NF350	76.88	-145.33	222.21	2.89	95.29	18.41	0.24
NF375	108.77	605.11	496.33	4.56	258.30	149.53	1.37
CA225	254.05	218.64	35.41	0.14	0.99	253.06	1.00
CW245	295.15	-60.10	355.25	1.20	73.95	221.19	0.75

Table 5.20 Dominant processes of channel development between 2003 and 2009 identified from the LiDAR-derived and modelled profiles shown in Figure 5.22. LB = left bank; RB = right bank; agg. = aggradation; deg. = degradation.

Cross-section	Observed	Run 60	Run 75
LO030	Localised channel incision	Localised channel incision	Localised channel incision
LO040	Significant deg.; bank erosion and widening	Significant deg.; bank erosion and widening	Some deg.; bank erosion and widening
NF100	Localised channel incision	Localised channel incision; lateral erosion (LB).	Some deg.
NF120	Lateral erosion (LB). No change in elevation.	Lateral erosion (LB). No change in elevation.	Lateral erosion (LB). No change in elevation.
NF300	Lateral erosion (LB). Localised bed agg.; no net change in elevation.	Lateral erosion (LB). No change in elevation.	Lateral erosion (LB + RB). Localised bed agg.
NF320	Some erosion of LB toe. No change in elevation.	Some erosion of RB toe. Some deg.	Erosion of RB toe and some widening. No change in elevation.
NF350	Localised erosion of terrace edge. Localised deg. and agg.; no net change in elevation.	Significant lateral shifting; localised deg. and agg.; no net change in elevation.	Significant lateral shifting; localised deg. and agg.; no net change in elevation.
NF375	Localised erosion of terrace edge. Localised agg.; no significant change in elevation.	Some erosion of terrace toe. Localised incision.	Erosion of terrace toe. Localised agg. and deg.; no significant change in elevation.
CA225	Lateral erosion (LB + RB). No significant change in elevation.	Lateral erosion (LB + RB). Some deg.	Lateral erosion (RB). Some agg..
CW245	Some incision and lateral erosion (LB).	Some agg..	No significant change.

(a)

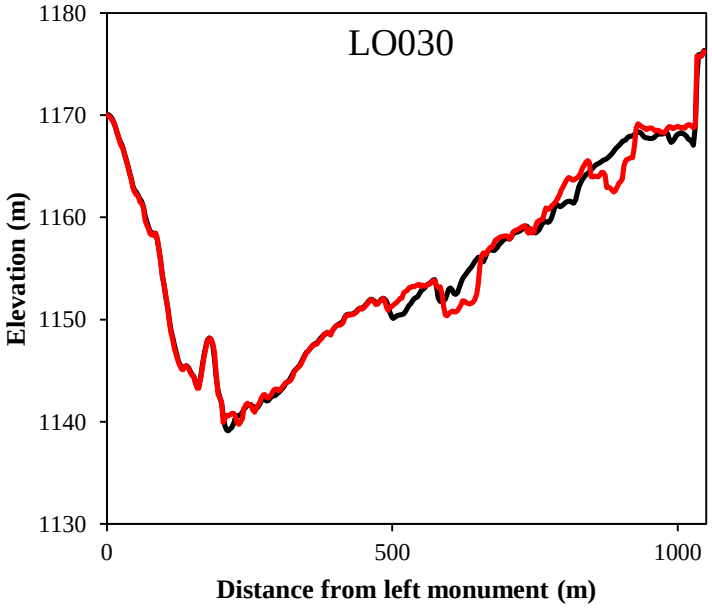

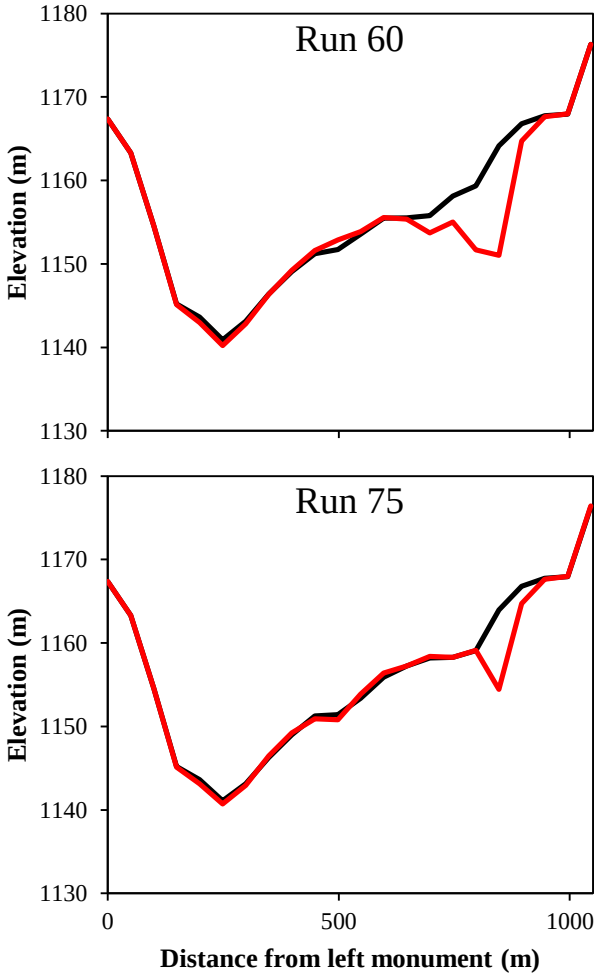

Figure 5.22 Cross-sections extracted from the 2003 and 2009 LiDAR surfaces (above) and modelled cross-sections (right) for the two selected model configurations (Runs 60 and 75) at LO030 (a). Black lines represent the 2003 surface; red lines represent the 2009 surface. LiDAR DEM resolution is 3 m; modelled DEM resolution is 50 m.

(b)

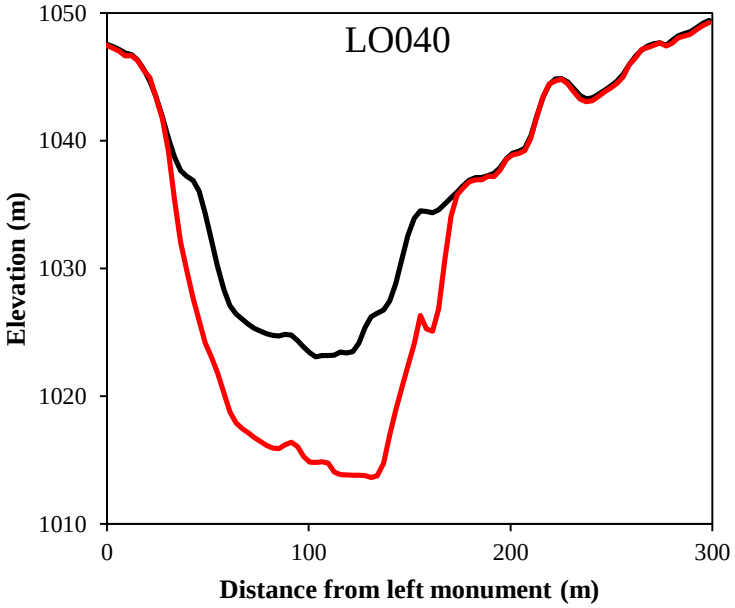

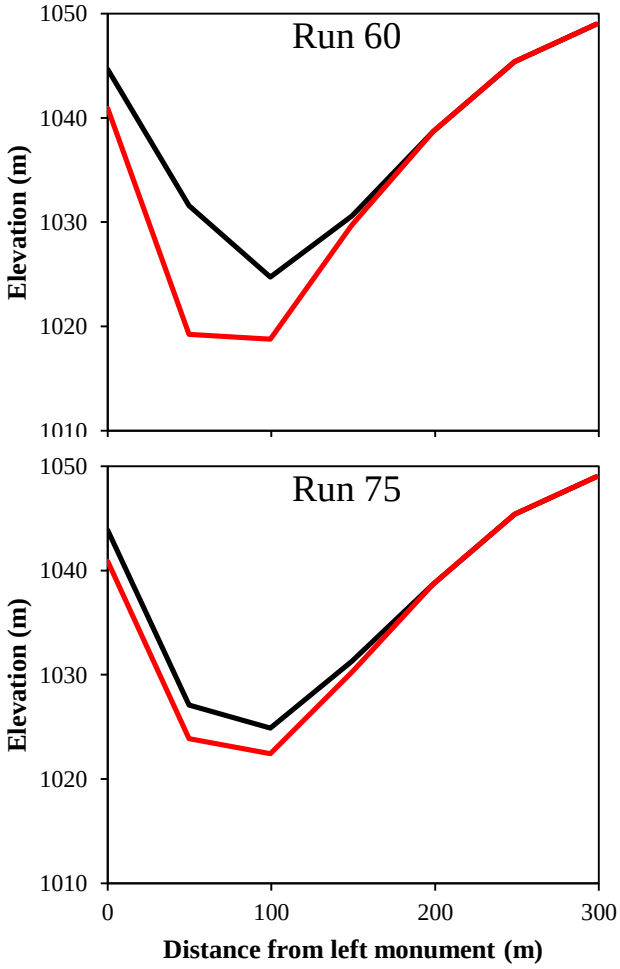

Figure 5.22 Cross-sections extracted from the 2003 and 2009 LiDAR surfaces (above) and modelled cross-sections (right) for the two selected model configurations (Runs 60 and 75) at LO040 (b). Black lines represent the 2003 surface; red lines represent the 2009 surface. LiDAR DEM resolution is 3 m; modelled DEM resolution is 50 m.

(c)

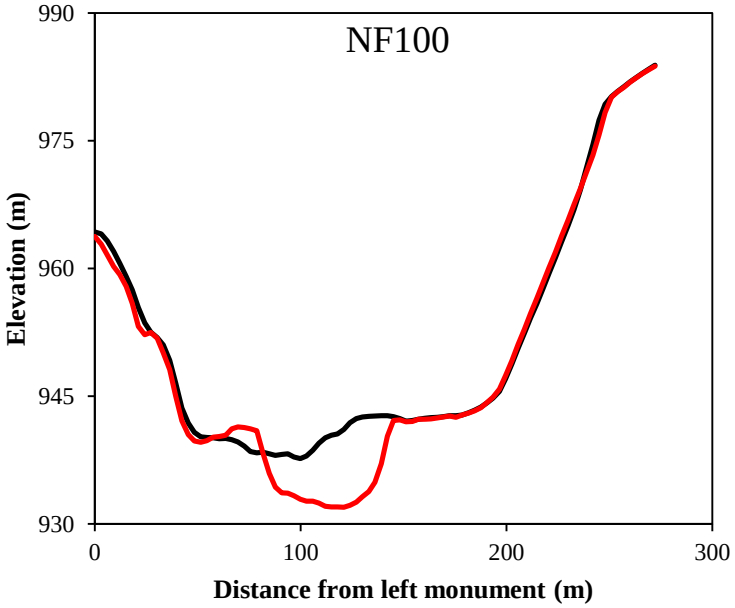

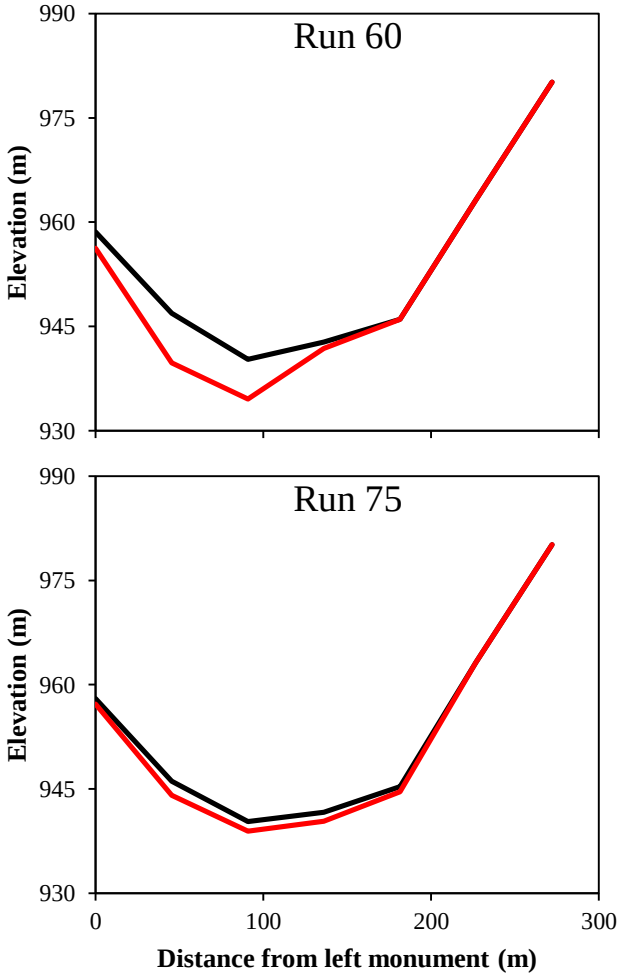

Figure 5.22 Cross-sections extracted from the 2003 and 2009 LiDAR surfaces (above) and modelled cross-sections (right) for the two selected model configurations (Runs 60 and 75) at NF100 (c). Black lines represent the 2003 surface; red lines represent the 2009 surface. LiDAR DEM resolution is 3 m; modelled DEM resolution is 50 m.

(d)

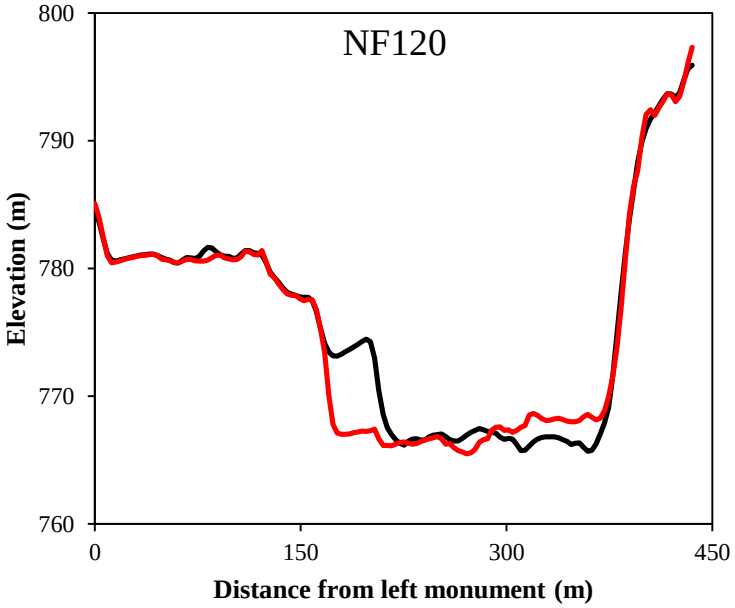

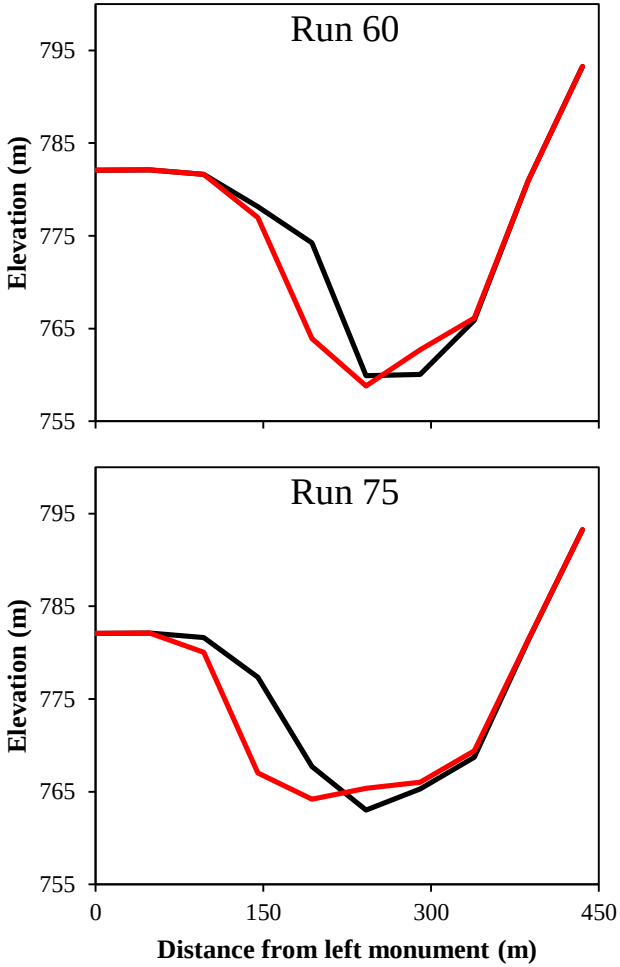

Figure 5.22 Cross-sections extracted from the 2003 and 2009 LiDAR surfaces (above) and modelled cross-sections (right) for the two selected model configurations (Runs 60 and 75) at NF120 (d). Black lines represent the 2003 surface; red lines represent the 2009 surface. LiDAR DEM resolution is 3 m; modelled DEM resolution is 50 m.

(e)

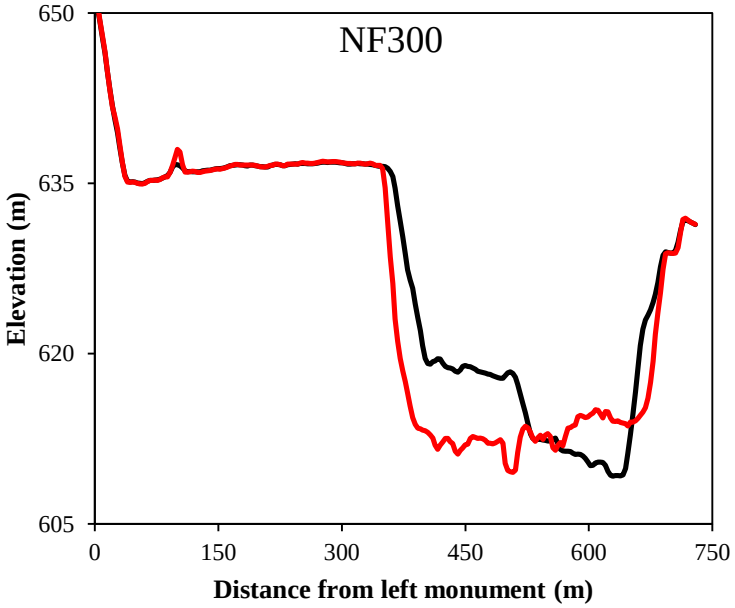

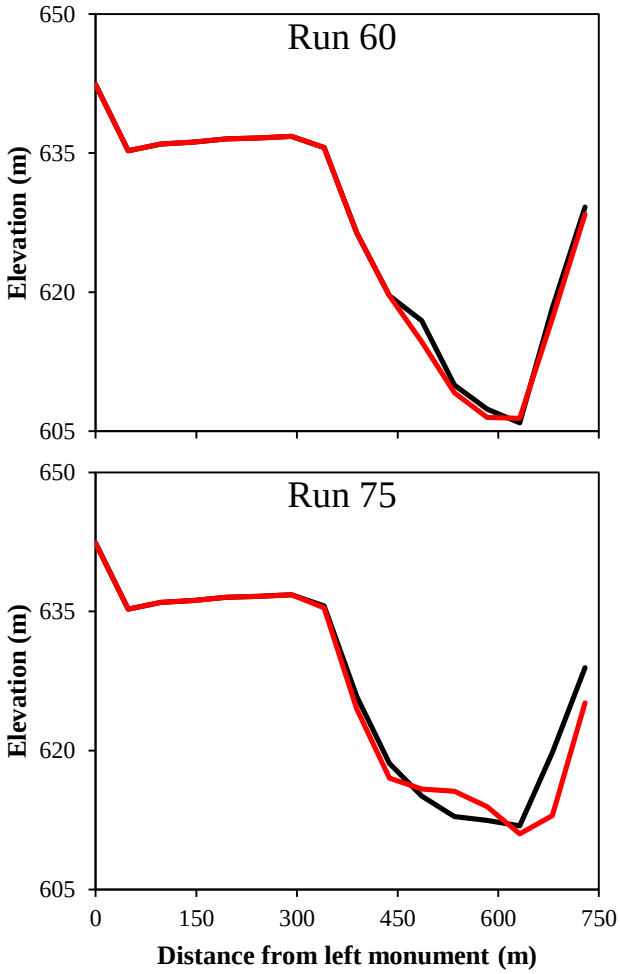

Figure 5.22 Cross-sections extracted from the 2003 and 2009 LiDAR surfaces (above) and modelled cross-sections (right) for the two selected model configurations (Runs 60 and 75) at NF300 (e). Black lines represent the 2003 surface; red lines represent the 2009 surface. LiDAR DEM resolution is 3 m; modelled DEM resolution is 50 m.

(f)

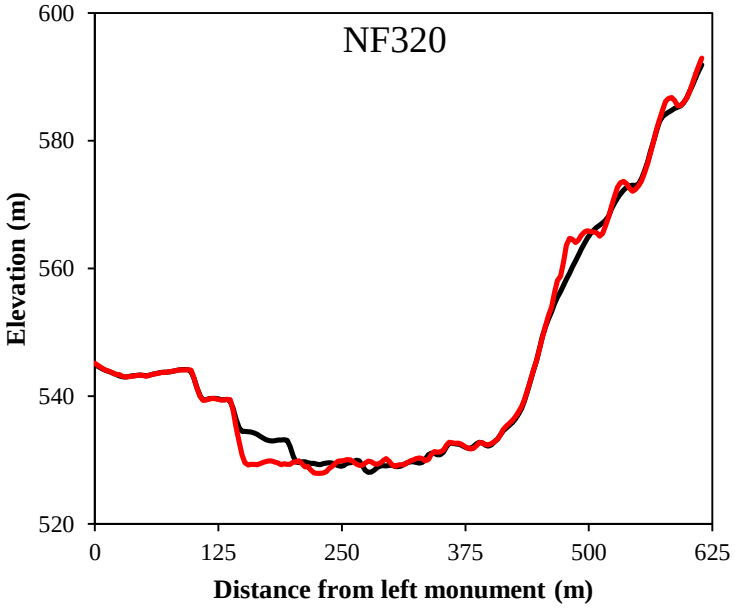

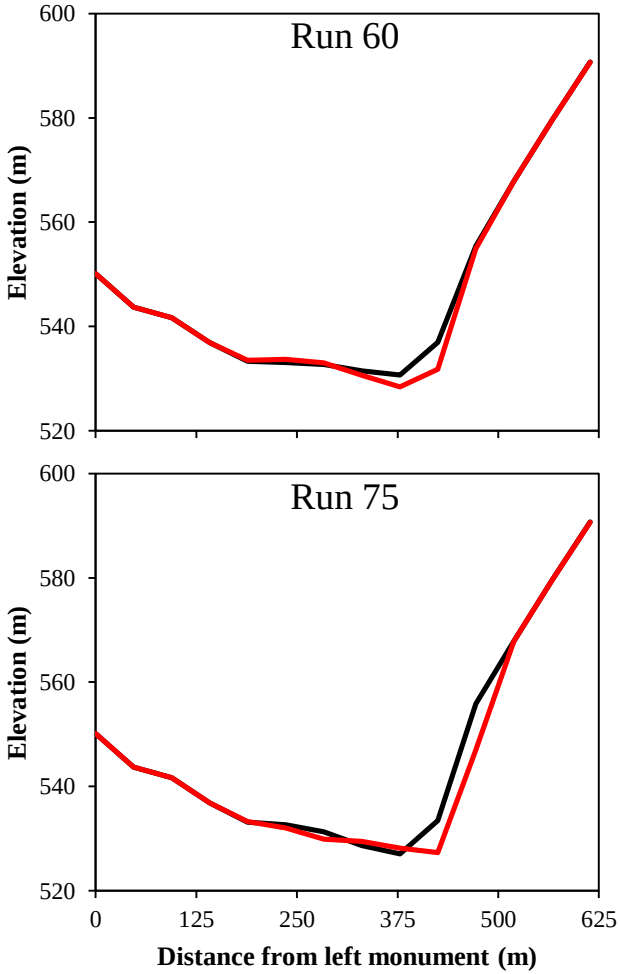

Figure 5.22 Cross-sections extracted from the 2003 and 2009 LiDAR surfaces (above) and modelled cross-sections (right) for the two selected model configurations (Runs 60 and 75) at NF320 (f). Black lines represent the 2003 surface; red lines represent the 2009 surface. LiDAR DEM resolution is 3 m; modelled DEM resolution is 50 m.

(g)

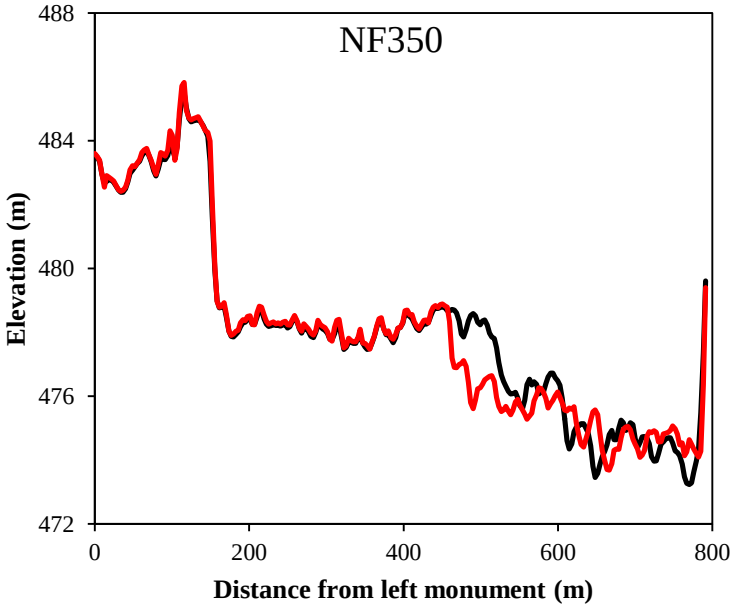

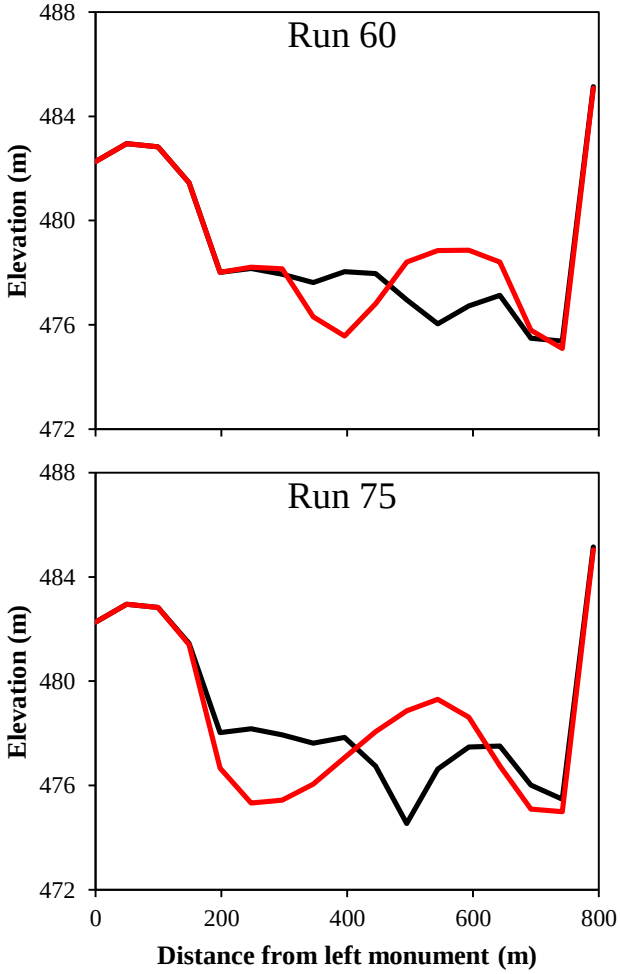

Figure 5.22 Cross-sections extracted from the 2003 and 2009 LiDAR surfaces (above) and modelled cross-sections (right) for the two selected model configurations (Runs 60 and 75) at NF350 (g). Black lines represent the 2003 surface; red lines represent the 2009 surface. LiDAR DEM resolution is 3 m; modelled DEM resolution is 50 m.

(h)

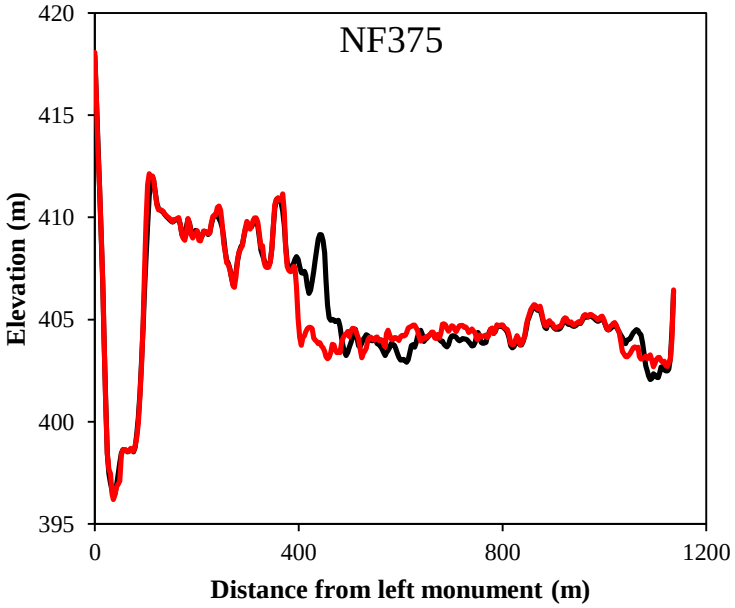

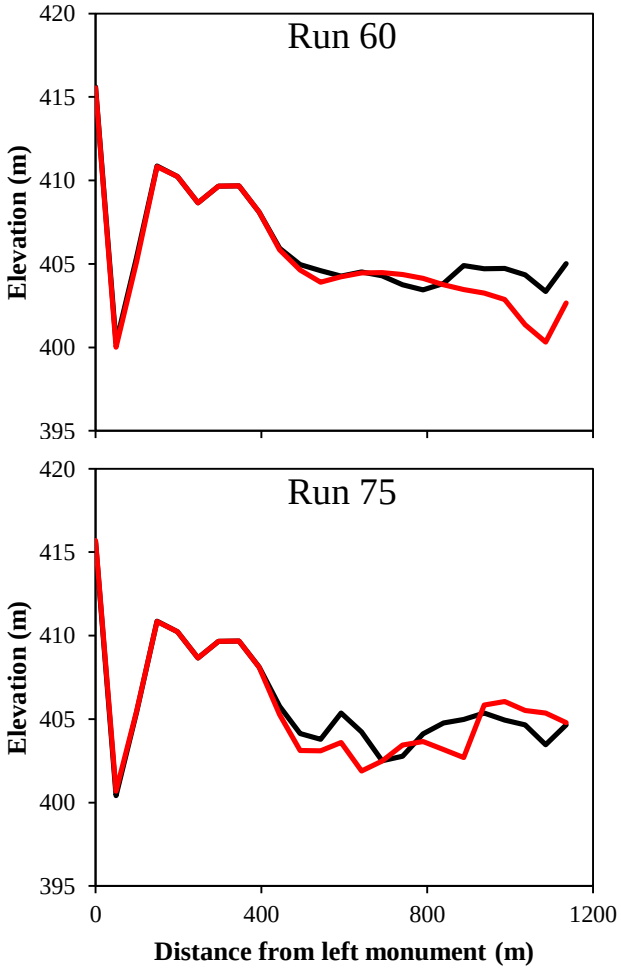

Figure 5.22 Cross-sections extracted from the 2003 and 2009 LiDAR surfaces (above) and modelled cross-sections (right) for the two selected model configurations (Runs 60 and 75) at NF375 (h). Black lines represent the 2003 surface; red lines represent the 2009 surface. LiDAR DEM resolution is 3 m; modelled DEM resolution is 50 m.

(i)

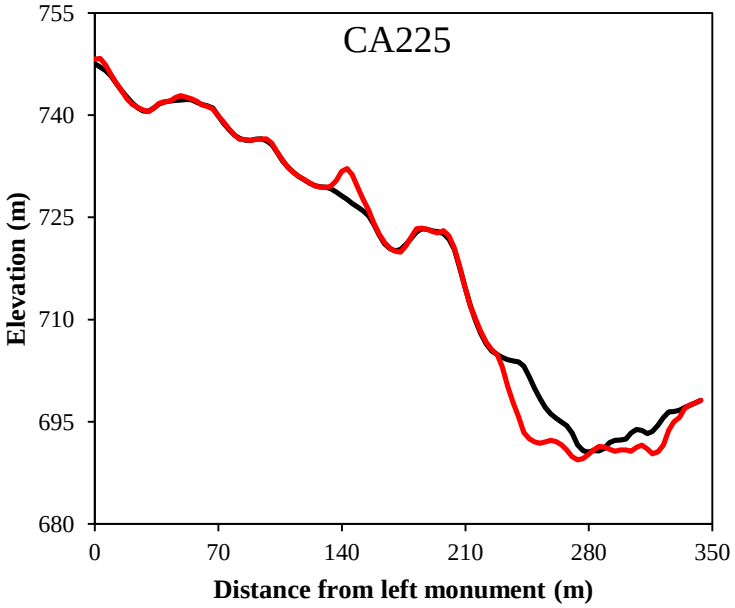

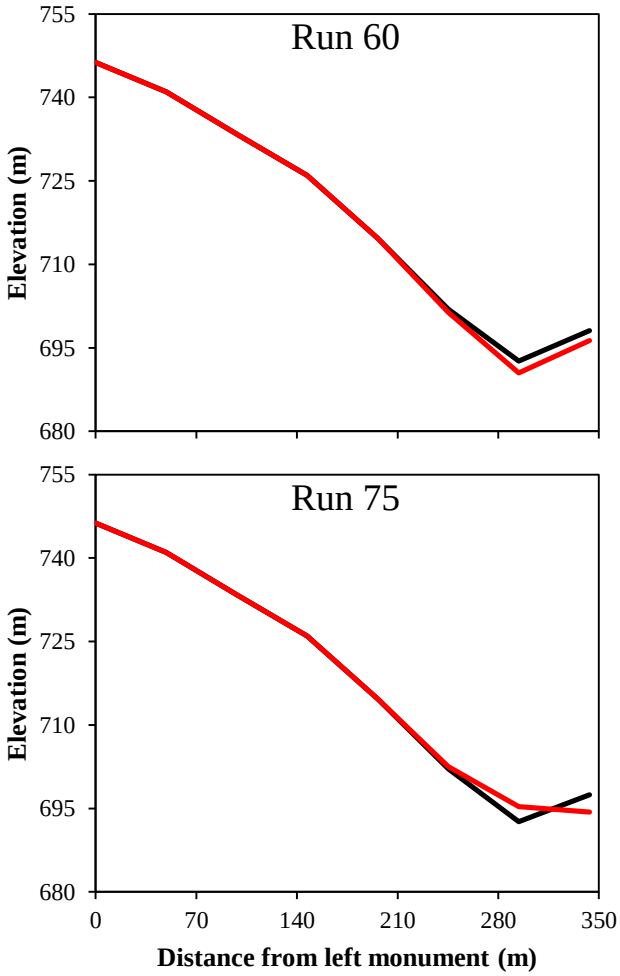

Figure 5.22 Cross-sections extracted from the 2003 and 2009 LiDAR surfaces (above) and modelled cross-sections (right) for the two selected model configurations (Runs 60 and 75) at CA225 (i). Black lines represent the 2003 surface; red lines represent the 2009 surface. LiDAR DEM resolution is 3 m; modelled DEM resolution is 50 m.

(j)

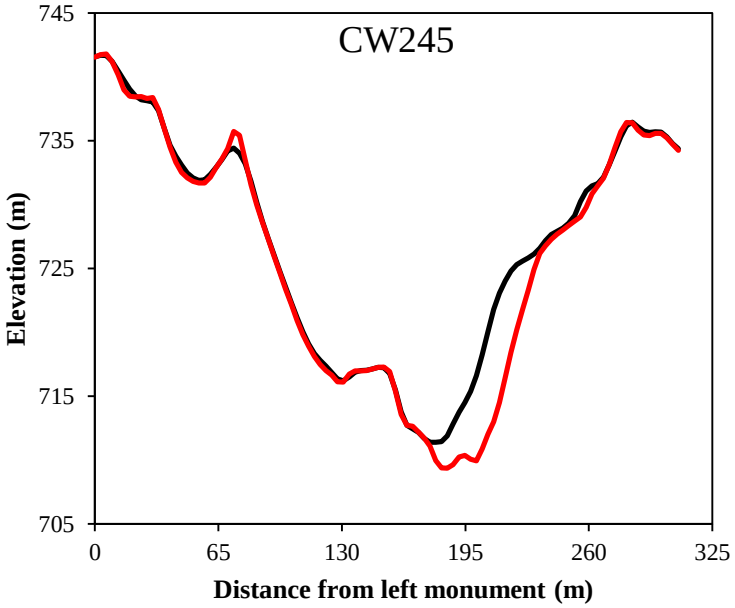

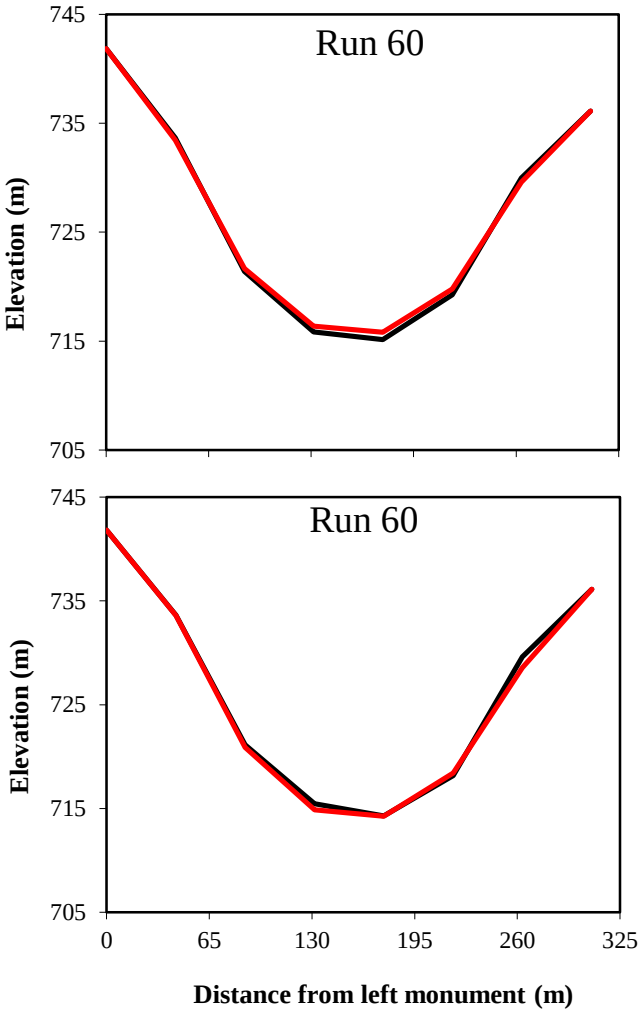

Figure 5.22 Cross-sections extracted from the 2003 and 2009 LiDAR surfaces (above) and modelled cross-sections (right) for the two selected model configurations (Runs 60 and 75) at CW245 (j). Black lines represent the 2003 surface; red lines represent the 2009 surface. LiDAR DEM resolution is 3 m; modelled DEM resolution is 50 m.

LO040 adjustments were dominated by vertical incision. Although underestimated by both model configurations, degradation is clearly the main process simulated by C-L at this location. Similarly, processes associated with meander bend development are evident at NF120, where lateral erosion of the outer bank in the absence of any significant change in channel elevation is the key feature. This pattern is also clearly seen in C-L outputs for both model configurations 60 and 75.

Clearly, however, some of the details of channel adjustments evident from the LiDAR-derived cross-sections are not simulated in model outputs. This is particularly evident at LO030 and NF100, and is the result of reducing the resolution of the DEM from 3 m to 50 m for implementation within C-L. This loss of fidelity is likely to have contributed to the large error statistics reported in Table 5.18 and Table 5.19, but does not mean that C-L is unable to represent the dominant processes of channel change satisfactorily. At both LO030 and NF100, the general trend discernible from LiDAR analysis is degradation (albeit localised), and this trend is replicated in the modelled profiles for both configurations. In other cases, however, for example NF350, modelled channel development does not appear to follow a pattern similar to that observed. The extent of channel lateral migration is clearly overestimated by the model at this location, and this may be a symptom of the simplified nature of the lateral erosion algorithm and limitations of the hydraulic model including its failure to incorporate secondary or cross-channel flows.

At most cross-section locations, the pattern of channel development is broadly similar between the two model configurations, although some differences resulting from variations in parameter specification are evident. Specifically, modelled incision is notably greater for Run 60 (which represents a relatively low lateral erosion scenario) than it is for Run 75 at a number of locations. At cross-sections such as LO040 and NF100, this greater incision is a better representation of the observed processes of channel development (Figure 5.22 (b) and (c)). At NF375 (Figure 5.22 (h)), however, the greater incision modelled by Run 60 produces a worse representation of the observed adjustment in comparison to Run 75 (which represents a relatively high lateral

erosion scenario). These differences, and the associated variations in the extent to which the models agree with observations, highlight the difficulty in specifying single values for particular parameters to represent processes at the catchment-scale. They do, however, justify the need to use both of these model configurations for forecasting, as neither model can be said to simulate all aspects of channel behaviour throughout the catchment.

5.7 SUMMARY

This Chapter began by setting out the need to test the performance of numerical models in the context of observed empirical data, and arguing that such a procedure should be viewed as evaluation or assessment rather than validation. Unlike validation, evaluation implies that both positive and negative results are possible, and that such tests should lead to modification and even rejection of the model if necessary.

The need for calibration of model parameters was also discussed in light of the difficulty associated with defining values for parameters which are not directly measurable and/or are conceptually based. In predictive studies such as the one presented in this thesis, the purpose of model evaluation and calibration is to inform the selection of a model configuration that can be used for forecasting. However, given the inherent problem of model equifinality (i.e. that many different parameter sets may be acceptable in reproducing the observed behaviour of a system) the need to select multiple models rather than a single optimal model configuration was emphasised.

It was also identified at the beginning of this Chapter that documented attempts to evaluate and calibrate reduced complexity models, and in particular C-L, in the context of empirical data are uncommon within the published literature. As such, there was no accepted methodology to be adopted for the purposes of the present study, and development of a novel approach was therefore required. The work presented in this Chapter therefore addresses two important gaps in the current literature. First, C-L model outputs were quantitatively compared with empirical data. Second, a method by which such comparisons and

evaluations can be carried was outlined. Moreover, in the specific context of this thesis, it also provided an assessment of the extent to which C-L is an appropriate tool for long-term forecasting of sediment yield from the upper North Fork Toutle River catchment.

The method involved firstly identifying four physically-meaningful evaluation criteria that could be tested using available data sets. These were: total catchment sediment yield; sub-catchment sediment yield; change in cross-sectional area; and change in thalweg elevation (Section 5.2). This multi-scale approach facilitated both volumes and mechanisms of modelled sediment yield to be compared with observations, which allowed for a comprehensive assessment of model performance to be undertaken. A period of initial testing and parameter refinement was then undertaken in Section 5.3 in order to resolve values for key parameters relating to the sediment transport, lateral erosion and hydrological components of the model.

During this initial testing phase, significant discrepancies were identified between modelled and observed sub-catchment-scale spatial distribution of erosion and deposition (sub-section 5.3.3). These were thought to be the result of deficiencies in how catchment hydrology was modelled in C-L. Specifically, the uniform input of discharge throughout the catchment is a poor representation of the field situation, as inputs are likely to be greater in the headwaters due to orographic effects as well as spring, lake, glacial and snowmelt inputs. Two modifications to the model were subsequently made in collaboration with the model developer to address this issue. These were the addition of a $Q_{\max}$ parameter which prevents water from being added to cells with large catchment areas (i.e. those furthest downstream), and an $X_{\max}$ parameter which directly limits the spatial extent of the cells to which water from the hydrological model is added. Further testing indicated that the fit between modelled and observed spatial patterns of erosion and deposition was better following these modifications, suggesting that they were successful, to an extent, in improving the representation of catchment hydrology in C-L.

The initial testing period identified a feasible range of values for five key parameters (Λ, λ, N_{smooth}, N_{shift} and Q_{max}) with 126 possible combinations from which a sub-set of best-fit models could be selected. The selection procedure began by identifying two independent goodness-of-fit statistics (MARE and MAE) that could be used to quantify the agreement between model outputs and observations for each of the four criteria. The performance criteria and goodness-of-fit statistics for each model were then combined using weights obtained from implementing the Analytic Hierarchy Process (AHP). This gave each model a final score and rank relative to the other 125. Following sensitivity analysis, which involved adjusting the weights assigned to each criterion, a sub-set of six models that provided the best-fit to the observed data was identified.

From this sub-set, two models (Runs 60 and 75) were chosen because their parameters spanned the range of those evident in the sub-set of six. The greatest difference between the six models was in the value of the lateral erosion parameter Λ, and the two selected models therefore represented low and high lateral erosion scenarios, respectively. Specifically, Run 60 has the lowest value of Λ and highest values of N_{smooth} and N_{shift} meaning that rates of lateral erosion are low, while Run 75 has the highest value of Λ and lowest values of N_{smooth} and N_{shift}. The evaluation, calibration and selection procedures undertaken in this Chapter have therefore identified two models that not only provide a good fit to observed data, but also encapsulate the potential variations in future catchment sediment yield that may result from differences in the specification of C-L parameters, and in particular the lateral erosion coefficient. As such, these procedures have instilled confidence that the selected models will fulfil their purpose, and that significantly better models could not have been selected given the available resources. The selected models are implemented in a series of forecasting runs carried out in Chapter 6.

CHAPTER 6 FORECASTING: SCENARIO-BASED PREDICTION OF POSSIBLE FUTURE LONG-TERM SEDIMENT YIELD FROM THE UPPER NORTH FORK TOUTLE RIVER CATCHMENT

6.1 INTRODUCTION

Although development of numerical models in fluvial geomorphology, and in particular that of landscape evolution models, is often motivated by the need to answer practical questions relevant to the needs of society, model applications have focused more on explanation rather than prediction (Murray, 2007). Consequently, examples of landscape evolution models having been used to make quantitative forecasts of geomorphological phenomena, including trends in catchment sediment yield or rates of river channel change, necessary to inform decision-making, are rare. However, the challenges posed by persistent, high sediment yields emanating from the upper North Fork Toutle River (explained in Chapter 2) and the limitations associated with predictions made using other modelling approaches (outlined in Chapter 3), necessitated application of C-L as a forecasting tool in this study.

Lack of examples of landscape evolution models having been applied to predict geomorphological phenomena in the context of societally relevant issues reflects widespread and understandable caution amongst modellers regarding the applicability of their models in this context. This caution stems from the fact that model outcomes are subject to quantitative and qualitative uncertainties, being especially sensitive to gaps in the knowledge concerning initial conditions and historical path dependency in the evolution of the fluvial system (Lancaster and Grant, 2003). Forecasting is further complicated by the complex nonlinear behaviours of disturbed fluvial systems (described in Chapter 3) that may be attributed to the crossing of intrinsic geomorphic thresholds (e.g. Schumm, 1973, 1979) and their operation as complex, dynamical systems (Lane and Richards, 1997). Given these limitations, modellers have been wary of accepting responsibility for making predictions that may be used to inform policy and decision-making.

Moreover, the difficulty in defining antecedent and initial conditions means that making chronological predictions, i.e. not only how a particular system will change but at what rate, is particularly challenging given the lingering influences of prior events (Iverson, 2003). Understandably, researchers prefer to make phenomenological predictions which state more generally that a particular geomorphic phenomenon, such as a slope failure, will occur given specific antecedent and forcing conditions (Iverson, 2003). The forecasting research presented here acknowledges the issues noted above, and while it can neither avoid nor entirely resolve them, the research uses them to contextualise and evaluate predictions made using C-L that are presented later in this Chapter.

A further challenge to the use of reduced complexity landscape evolution models for forecasting is the need to incorporate climate change into hydrological driving data sets. This is particularly important given that global warming impacts the type, quantity, intensity, timing and duration of precipitation, with significant consequences for fluvial systems (Goudie, 2006). A recent study by Arnell and Gosling (2013), for instance, used a climate model to project changes in hydrology across the global domain. The study projected that by 2050 average annual runoff will increase significantly (i.e. greater than the standard deviation in the absence of climate change) across 47% of the land surface and decrease significantly across 36%, with only 17% of the land surface experiencing no significant change. Flood peaks were also projected to increase significantly across more than 50% of the land surface, while drought runoff was projected to decrease across 44%.

Similarly, Döll and Zhang (2010) estimated that climate change will alter seasonal flow regimes significantly (i.e. >10%) on 90% of the global land area, and that the timing of the maximum mean monthly river discharge will be shifted by at least one month (usually earlier) on one-third of the land area. Döll and Zhang (2010) therefore concluded that climate change will have a larger impact on flow regimes than past anthropogenic alterations including dams and water withdrawals.

However, previous applications of CAESAR (the predecessor of C-L) that have attempted to address this issues have often represented climate change very simply, either by increasing or decreasing the magnitude of events in the historical rainfall record (e.g. Coulthard et al., 2000). If predictive studies are to provide more meaningful forecasts, however, representation of the effects of climate change on future precipitation must be more sophisticated. This could be achieved by, for example, downscaling global climate model (GCM) projections for temperature and precipitation changes under different greenhouse gas (GHG) emissions scenarios.

The study by Coulthard et al. (2012) is one example of GCM projections being incorporated into geomorphic model simulations and it clearly demonstrates the benefits of this approach. In that study, CAESAR was used to simulate how the River Swale, Yorkshire, responds to simulated changes in rainfall that result from climatic change. Rainfall scenarios were derived from the UKCP09 weather generator and were based on greenhouse gas (GHG) emission scenarios developed by the Intergovernmental Panel on Climate Change (IPCC) (Nakićenović and Swart, 2000). Model results indicated that increases in mean rainfall could double the annual sediment yield, while the sediment yield associated with the 50-year return period rainfall event may increase fivefold.

Recognising the need to represent the potential impacts of climate change on the hydrology of the upper North Fork Toutle River catchment in a sophisticated manner, this Chapter implements state-of-the-art climate projections specific to the Pacific Northwest region that have been generated using the most up-to-date data made available by the global climate modelling community and, specifically, the Columbia Basin Climate Change Scenarios Project (CBCCSP). This makes the forecasts of sediment yield presented here pertinent to the immediate needs of local planners and flood risk management decision makers.

Within the context provided by the issues outlined above, this Chapter therefore reports how the calibrated C-L models developed in Chapter 5 were

used to make chronological forecasts of landscape evolution in the upper North Fork Toutle River catchment under a range of possible climate change futures. The aim was to estimate the cumulative volumes and temporal trends in the rate of sediment output from the catchment during the remainder of this century, while also seeking to provide causal explanations for these trends in terms of the process-response mechanisms in the fluvial system responsible for them. Given the lack of previous studies that have attempted to make such forecasts, the research presented in this Chapter represents a novel application of a reduced complexity landscape evolution model. Consequently, the findings should be of interest not only to planners, sedimentation engineers and flood risk managers in the Toutle-Cowlitz catchment, but also the geomorphic modelling community more generally.

6.2 THE COLUMBIA BASIN CLIMATE CHANGE SCENARIOS PROJECT (CBCCSP)

The Columbia Basin Climate Change Scenarios Project (CBCCSP) (Hamlet et al., 2010) was an interdisciplinary research venture undertaken by the Climate Impacts Group (CIG) at the University of Washington in collaboration with the Washington State Department of Ecology, Bonneville Power Administration, Northwest Power and Conservation Council, Oregon Water Resources Department, and British Columbia Ministry of the Environment. The primary aim of the project was to develop a comprehensive and up-to-date database of simulated hydrological data in the Columbia River basin that incorporated climate change information from the IPCC Fourth Assessment Report, which could be used to support long-term water resources planning in the basin (Hamlet et al., 2010). The project used raw GCM outputs to develop a suite of datasets, including runoff, precipitation, snow water equivalent (SWE) and temperature for sub-catchments within the Columbia River Basin (Hamlet et al., 2013). The data and outcomes of the CBCCSP are available online at: http://warm.atmos.washington.edu/2860. The following sub-sections and Figure 6.1 summarise the processing sequence undertaken by the CBCCSP.

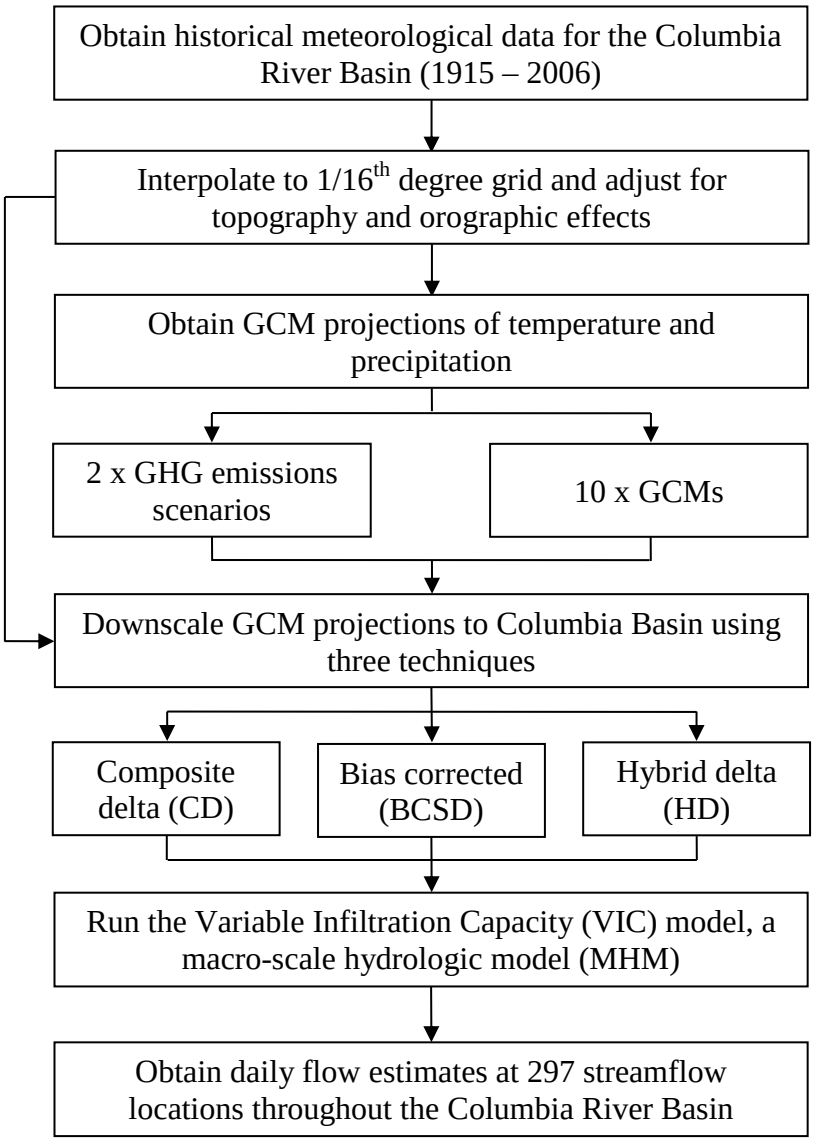

Figure 6.1 Summary of processing sequence used in the CBCCSP.

6.2.1 Historical meteorological data

The method used by the CBCCSP began by compiling available historical meteorological data, including daily total precipitation, and maximum and minimum daily temperature, throughout the Columbia River basin. Data were acquired from the National Climatic Data Centre Cooperative Observer (NCDC COOP) network of meteorological stations, as well as stations operated by Environment Canada (EC). Following a number of quality control steps, the raw meteorological data were interpolated to a $1/16^{th}$ degree latitude/longitude grid (approximately 5 km by 7 km) and adjusted to account for topographic influences, principally orographic effects. The result was a hydrological driving data set with a daily temporal resolution covering the entire Columbia River basin between January 1, 1915 and December 31, 2006 (Hamlet et al., 2010). These meteorological data were used to downscale simulations of monthly temperature and precipitation data produced by global climate model (GCM) simulations, as described below, in sub-section 6.2.3.

6.2.2 Scenarios for future emissions of greenhouse gases

Projections of temperature and precipitation were based on two GHG emissions scenarios developed by the IPCC: A1B and B1, which represent relatively high and low emissions scenarios, respectively (Nakićenović and Swart, 2000). These scenarios, the characteristics of which are summarised in Table 6.1, are commonly chosen for forcing GCMs (Mote and Salathé Jr., 2010). Projected changes in temperature and precipitation averaged over the Pacific Northwest region from an ensemble of 20 GCM simulations for the two emissions scenarios are presented in Figure 6.2. Both scenarios result in mean annual warming by at least 0.1°C per decade during the first part of the 21^{st} century, although considerable divergence is evident after about 2050 as temperatures stabilise in the B1 scenario (Mote and Salathé Jr., 2010). Changes in mean annual precipitation are minimal when averaged over all the models, but individual models predict substantially wetter or drier futures (Mote and Salathé Jr., 2010). Moreover, the majority of models project wetter winters and

drier summers in the Pacific Northwest, although these seasonal differences are more pronounced in the A1B scenario (Mote and Salathé Jr., 2010). These climate changes are translated into hydrologic changes including snow accumulation and melting, streamflow timing and changing evaporation rates through implementation of a macro-scale hydrologic model, which is described in sub-section 6.2.4, below. The impact of these scenarios on the climate and hydrology of the Toutle-Cowlitz River system is discussed in more detail below, in Section 6.3.

Table 6.1 Characteristics of the two GHG emissions scenarios used by the CBCCSP. Information taken from Nakićenović and Swart (2000) and Mote and Salathé Jr. (2010). PNW = Pacific Northwest.

A1B	B1
• Rapid and successful economic development • Rapid introduction of new and more efficient technologies • Reduction in regional differences in average per capita income • Balance across energy sources (fossil and non-fossil) • Increased GHG emissions • Rising PNW temperatures through to the end of the 21st century	• High level of environmental and social consciousness • Globally coherent approach to more sustainable development • Improved resource efficiency, dematerialisation and reduction in pollution • Low greenhouse gas emissions • Stabilising PNW temperatures by the end of the 21st century

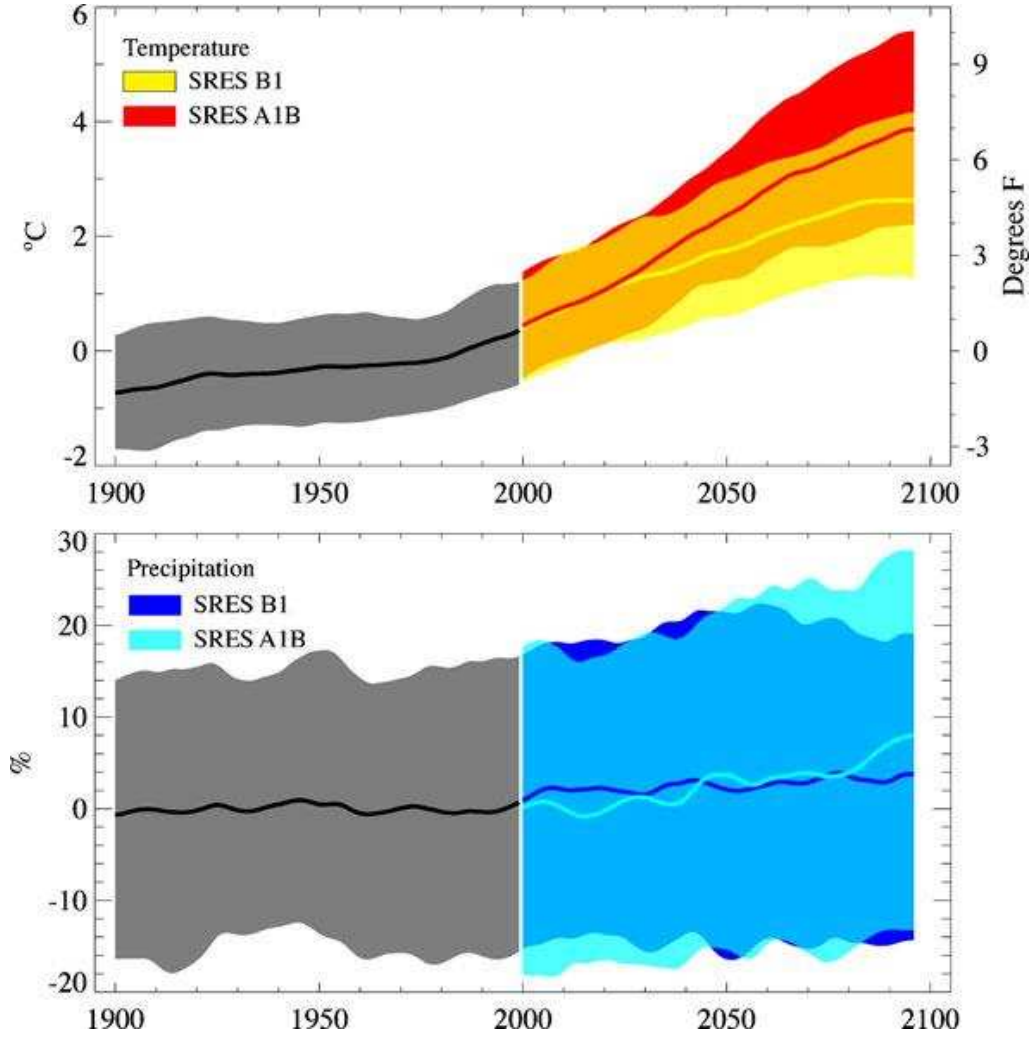

Figure 6.2 Projections of temperature (top) and precipitation (bottom) for the 20th and 21st century model simulations for the Pacific Northwest, relative to the 1971 – 1999 mean. Both A1B and B1 scenarios are shown. The upper and lower bounds of the shaded area are the 5th and 95th percentile of the annual values for the 20 simulations. The heavy smooth curve for each scenario is a weighted average. Taken from Mote and Salathé Jr. (2010, p. 40).

6.2.3 Global climate models and downscaling procedures

Projections from 10 GCMs whose 20th century simulations had the smallest error in temperature and precipitation and were able to simulate the most realistic annual cycles of temperature and precipitation were selected for use by the CBCCSP (Hamlet et al., 2010). Mote and Salathé Jr. (2010) found that the selected models were able to reproduce key features of Pacific Northwest climate during the 20th century, including the sharp contrast between wet winters and dry summers, warming of about 0.8°C, and the mean atmospheric circulation over the North Pacific. These successes were thought to provide confidence in the changes in future climate projected by these models (Mote and Salathé Jr., 2010).

However, the explicit validation of either historical or future results of GCMs is problematic, and as such the quantitative error statistics of the projections presented by the CBCCSP should properly be considered unknown (Tohver et al., 2014). Nonetheless, Tohver et al. (2014) also state that the projections are plausible and physically realistic simulations of potential changes in hydrology resulting from the combined effects of projected warmer temperatures, seasonal precipitation changes, and shifts in the dominant winter storm track. Moreover, the ensemble of 10 GCMs used by the CBCCSP provides an estimate of the uncertainties in temperature and precipitation associated with the different projections (Hamlet et al., 2010; Tohver et al., 2014).

The GCMs used by the CBCCSP are summarised in Table 6.2. Data obtained from these 10 GCMs run using the two GHG emissions scenarios were then downscaled to produce the information required to drive a macro-scale hydrologic model. In general, the resolution of GCM outputs is too coarse to be meaningful for hydrologic studies (Elsner et al., 2010) meaning that downscaling processes are necessary in order to relate information or data at coarse spatial and temporal scales to desired products at finer-scales (Hamlet et al., 2010). The process of downscaling is based on perturbations to the observed, historical, meteorological record (see sub-section 6.2.1, above), and the CBCCSP implemented three alternative techniques: the composite delta

(CD) method; the bias correction and statistical downscaling (BCSD) method; and the hybrid delta (HD) method.

Not all of the three downscaling procedures are necessarily appropriate for implementation within C-L, and the relevant advantages and limitations of each approach are discussed in more detail in sub-section 6.3.1. To summarise the different techniques, the CD technique simply involves applying average (composite) monthly changes in temperature and precipitation from a GCM simulation to the observed historical temperature and precipitation records (Hamlet et al., 2010; Tabor and Williams, 2010). The changes are calculated between the observed record and three future 30-year windows centred on the 2020s (2010 – 2039), 2040s (2030 – 2059) and 2080s (2070 – 2099) (Hamlet et al., 2010). The BCSD approach, however, uses transfer functions derived from cumulative frequency distributions (CFD) of the historic observations and GCM simulations to ensure that the statistical characteristics of the observed record are maintained (Salathé Jr. et al., 2007). Finally, the HD technique is a combination of the CD and BCSD techniques and involves first calculating the difference between the historical observations and the GCM projections for the same three 30-year windows used in the CD technique before transforming the CFD of the observations based on the GCM simulations.

In total, 76 possible realisations of future meteorological variables for the Columbia River basin were developed, as detailed in Table 6.3. These include two GHG emissions scenarios (A1B and B1), 10 GCMs, three downscaling techniques (CD, BCSD and HD) and, for the CD and HD downscaling techniques, three future time periods (2020s, 2040s and 2080s). The BCSD method does not consider the three different time periods because it uses the transient time series behaviour of the monthly GCM simulations for the entire simulation period. The CD and HD methods, on the other hand, adjust the historical record on the basis of meteorological variables from the GCM simulations averaged over the future 30-year windows (Hamlet et al., 2010). Runs for one of the ten GCMs (UKMO-HadGEM1; Table 6.2) were not archived for the B1 emissions scenario, resulting in 9 GCM realisations in this case (Hamlet et al., 2013). For the BCSD runs, which require a greater capacity

to capture the key elements of the climate variability in the region, only the projections based on the seven highest ranked GCMs were selected for each emissions scenario (Hamlet et al., 2013) as indicated in Table 6.3.

6.2.4 Implementing a macro-scale hydrologic model

The CBCCSP coupled the downscaled climate scenarios discussed above to a physically-based, macro-scale hydrologic model (MHM) (the Variable Infiltration Capacity (VIC) model: Liang et al. (1994)) to translate GCM-simulated changes in meteorological variables to changes in the hydrological regime of sub-catchments in the Columbia River basin (Hamlet et al., 2010). The VIC model explicitly represents the effects of vegetation, topography and soils on the fluxes of water and energy at the land surface-atmosphere interface (Payne et al., 2004; Wood et al., 2004; Costa-Cabral et al., 2013). Pertinent processes represented within the model include snow accumulation and melt, soil moisture dynamics, evapotranspiration and the generation and routing of surface runoff and baseflow through a grid-based network to simulate streamflow at selected points within the basin (Christensen et al., 2004). The VIC model is distinguished from other MHMs by its representation of sub-grid-scale spatial variability of both soil infiltration capacity and precipitation (Nijssen et al., 2001), and has been shown to accurately reproduce historical changes in streamflow when driven with historical meteorology (Pierce et al., 2013).

The VIC has conventionally been implemented at $1/8^{th}$ degree resolution or coarser (Elsner et al., 2010). However, in order to more accurately represent topographic features and the sensitivity of smaller basins to changes in climate forcing, the CBCCSP implemented the model at $1/16^{th}$ degree resolution (Hamlet et al., 2010). The model was used to produce daily flow estimates throughout the Columbia Basin, at 297 streamflow locations selected following consultation with the primary funding agencies of the CBCCSP and key water management agencies in the region (Hamlet et al., 2010). Of the 297 selected streamflow locations, one was located in the Toutle-Cowlitz River system at the USGS Tower Road gauge (Figure 3.1). VIC hydrological variables,

Table 6.2 Details of the 10 GCMs selected for use by the CBCCSP (Randall et al., 2007).

Global Climate Model (GCM)	Sponsor(s)
UKMO-HadCM3	Hadley Centre for Climate Prediction and Research; and Met Office, UK
UKMO-HadGEM	
CNRM-CM3	Météo-France; and Centre National de Recherches Météorologiques, France
CCSM3	National Centre for Atmospheric Research, USA
PCM	
ECHAM5	Max Planck Institute for Meteorology, Germany
ECHO-G	Meteorological Institute of the University of Bonn, Germany, and Meteorological Institute of the Korea Meteorological Administration (KMA) and Model and Data Group, Korea
CGCM3.1(T47)	Canadian Centre for Climate Modelling and Analysis, Canada
MIROC3.2	Center for Climate System Research (University of Tokyo), National Institute for Environmental Studies; and Frontier Research Center for Global Change (JAMSTEC), Japan
IPSL-CM4	Institut Pierre Simon Laplace, France

Table 6.3 Matrix of climate change projections used in the CBCCSP. UKMO-HadGEM1simulations were not archived for the B1 emissions scenario. Taken from Hamlet et al. (2013, p. 401).

Downscaling approach			Number of projections	
Method	GCM projections included	Time period	A1B emissions scenario	B1 emissions scenario
Composite delta	Composite of 10 for A1B and 9 for B1	2020s	1	1
		2040s	1	1
		2080s	1	1
BCSD	UKMO-HadCM3 CNRM-CM3 CCSM3 ECHAM5 ECHO-G CGCM3.1(T47) PCM	1950 – 2099	7	7
Hybrid delta	UKMO-HadCM3 CNRM-CM3 CCSM3 ECHAM5 ECHO-G CGCM3.1(T47) PCM MIROC3.2 IPSL-CM4 UKMO-HadGEM1	2020s	10	9
		2040s	10	9
		2080s	10	9

specifically daily streamflow, archived at Tower Road for each of the 76 climate change projections (Table 6.3) and one historical run were, therefore, available for use in future long-term C-L simulations of the upper North Fork Toutle River catchment.

6.3 IMPLEMENTION OF CLIMATE CHANGE PROJECTIONS FOR FORECASTING USING CAESAR-LISFLOOD

It was not necessary to implement all of the 77 streamflow simulations available at the Tower Road gauge for forecasting using C-L, and indeed a number of the simulations available were inappropriate. For instance, as mentioned above in sub-section 6.2.3, the three downscaling procedures are each associated with certain advantages and disadvantages which limit, to varying extents, their applicability to the present study. This is discussed in more detail below, in sub-section 6.3.1. Moreover, a number of the GCM simulations are likely to forecast similar future hydrological regimes within the Toutle River catchment and so it was unnecessary to use all of them. However, given the uncertainties surrounding climate predictions, it is preferable to consider a number of scenarios when assessing the impact of future climatic change (Salathé Jr., 2005). Consequently, a sub-set of climate change projections was selected that could encapsulate the range of all available scenarios so that the uncertainty associated with these forecasts could be represented to as great an extent as possible. This selection procedure is outlined below, in sub-section 6.3.2.

6.3.1 Selected downscaling procedure

The CD technique produces a time sequence of simulated future meteorological variables which matches the historic record, thereby maintaining the temporal structure of the data (Hamlet et al., 2010). However, this method fails to reflect changes in the configurations of the future distributions of temperature and precipitation, meaning that information is lost regarding possible alterations to spatial or temporal patterns, such as the inter-

arrival time, duration or spatial extent of droughts and floods (Goderniaux et al., 2009; Hamlet et al., 2010). A significant limitation of the CD approach is, therefore, its failure to capture the variability or time series behaviour of GCM-simulated temperature and precipitation (Hamlet et al., 2010). Given that changing rainfall variability, rather than just magnitude, is likely to have a significant bearing on fluvial processes and therefore landscape evolution in the catchment, the CD technique was deemed inappropriate for this study.

The BCSD method, conversely, extracts more information regarding the time series behaviour and large-scale spatial variability in the GCM simulations. As a result, projected time series of meteorological variables downscaled using this approach may have substantially different inter-annual and inter-decadal variability in comparison with the observed record, making them useful for analysing changes in inter-arrival times and the duration of climatic extremes (Hamlet et al., 2010). However, daily time step data are generated by a non-physical disaggregation of monthly-mean climate model output, which means that the correspondence between downscaled and historic daily observations is not conserved (Maurer and Hidalgo, 2008). This can produce highly unrealistic behaviours in the daily time series, particularly for precipitation, in terms of rainstorm depth and the exaggeration of extreme events, which are likely to significantly influence hydrological extremes, such as flood peaks (Maurer and Hidalgo, 2008). As such, BCSD results are not recommended for sub-monthly analysis at small spatial scales (Hamlet et al., 2010), and were therefore deemed unsuitable for use in this study.

The HD method was developed by the CBCCSP to avoid the limitations of the CD and BCSD techniques set out above and to support prediction of daily hydrologic extremes (Hamlet et al., 2013). Specifically, the probability distribution of the GCM data is reproduced explicitly in future scenarios, but (in contrast to the BCSD method) the approach maintains realistic values by closely aligning the time series and spatial behaviour of the future values with the gridded (historical) observations. Consequently, this approach preserves the temporal structure of the observed daily data, while allowing for the effects of changing probability distributions of temperature and precipitation on climatic

extremes to be represented (Hamlet et al., 2010). As such, changes in the mean, variance, skewness or other statistical features of the GCM data are reproduced explicitly in the future scenarios (Hamlet et al., 2010).

HD streamflows therefore give a more realistic portrayal of extreme events, which are important mechanisms in the process of landscape evolution in fluvial systems (Ingrid Tohver, University of Washington, personal communication, 2012). For these reasons, data produced using the HD downscaling procedure is suitable for water resources applications at daily timescales and over a range of spatial scales. The HD method is therefore recommended by the CBCCSP (Hamlet et al., 2010), and streamflow simulations based on meteorological variables downscaled from GCM outputs using this approach were selected for the current study.

It must be noted, however, that although the probability distributions of future monthly temperature and precipitation statistics respond directly to changes projected by the GCM in the HD method, the future daily time series behaviour is derived from the historical record obtained from 1915 to 2006 (Tohver et al., 2014). As such, a winter storm or summer dry spell in the future will have the same timing and duration as its occurrence in the historical record, but the intensity of an individual event will be scaled by signals in the monthly GCM simulations (Hamlet et al., 2010; Tohver et al., 2014). Despite the reliance of the HD method on the historical daily time series, the projections developed using this method are able to simulate important changes in climate characteristics, such as shifts in the dominant winter storm track (Salathé Jr., 2006) and increased seasonal variability in precipitation (Mote and Salathé Jr., 2010).

Additionally, a key assumption made by the HD method is that bias in the GCM is constant and extends to future simulations as well as 20th century simulations (Hamlet et al., 2010). However, Salathé Jr. (2004) showed this to be a reasonable assumption by using split sample tests of 20th century climate records to demonstrate that the bias correction process performs equally well when trained on Pacific Decadal Oscillation warm phase epochs and validated

on cool phase epochs, as when trained on cool phase epochs and validated on warm phase epochs (Hamlet et al., 2010; Tohver et al., 2014). Therefore, although the downscaling method was not explicitly evaluated by the CBCCSP, it has been shown by Salathé Jr. (2004) to be a robust method of deriving regional temperature and precipitation information from GCM outputs.

Finally, it should be noted that the HD technique provides a static 91-year time series representing one of three 30-year future time horizons (2020s, 2040s and 2080s), rather than a transient representation of the climate (Hamlet et al., 2010). This is in contrast to the BCSD approach, for instance, which provides a transient realisation that explicitly reproduces the monthly time series behaviour of the GCM simulations of temperature and precipitation (Hamlet et al., 2010). However, as noted above, the non-physical disaggregation of monthly-mean climate model output to daily time step data in the BCSD method means that daily precipitation statistics are unreliable and often unrealistic. As such, the HD method allows for better representation of statistical parameters such as return periods of hydrologic extremes (Hamlet et al., 2010) that are important to modelling fluvial system evolution.

6.3.2 Selected global climate model projections

Three GCM projections were selected from the suite of 10 models used by the CBCCSP: CGCM3.1(T47), ECHO-G, and CNRM-CM3 (Table 6.2). As demonstrated later in this sub-section, these projections were chosen because they represent contrasting futures for the runoff and hydrological characteristics of the Toutle River catchment, as simulated using the 10-model ensemble employed by the CBCCSP. Their selection therefore captures most of the variation in the 10-model ensemble implemented by the CBCCSP. Table 6.4 summarises the key characteristics of the three selected models in terms of their projections of the future hydrological regime of the Toutle River catchment, and the factors driving these changes.

Table 6.4 Key characteristics of the three selected climate models.

Climate model	Relative wetness of scenario	Magnitude and direction of change in runoff relative to historic simulations			Driving factors
		Annual	Cool season	Warm season	
CGCM3.1(T47)	High	Large increase	Large to moderate increase	Moderate decrease	Large increase in annual precipitation; moderate to large increases in both cool and warm season precipitation; moderate decrease in SWE.
CNRM-CM3	Medium	Moderate increase	Moderate increase	Small decrease	Moderate to large increase in annual and cool season precipitation; moderate decrease in warm season precipitation; small decrease in SWE.
ECHO-G	Low	Large decrease	Large decrease to small increase	Moderate to large decrease	Large decrease in annual and cool season precipitation; moderate to large decrease in warm season precipitation; moderate decrease in SWE.

Large = at or near the maximum of the 10-model ensemble implemented by the CBCCSP; moderate = at or near the mean of the 10-model ensemble; and small = at or near the minimum of the 10-model ensemble.

Figures 6.3 to 6.8 and Tables 6.5 to 6.10 summarise the pertinent hydrological variables simulated by the selected models, relative to the 10-model ensemble range and historic observations. These variables include monthly precipitation (Figure 6.3; Table 6.5), temperature (Figure 6.4: Table 6.6), snow water equivalent (Figure 6.5; Table 6.7) and total catchment runoff (Figure 6.6; Table 6.8).

In the context of future catchment runoff, CGCM3.1(T47), CNRM-CM3 and ECHO-G represent high, medium and low scenarios, respectively. While CGCM3.1(T47) and CNRM-CM3 project increases in annual runoff relative to historic observations, ECHO-G projects a decrease. CGCM3.1(T47) forecasts a greater increase in annual precipitation and a more substantial reduction in snowpack water storage (snow water equivalent or SWE) in comparison with CNRM-CM3, and it projects a larger increase in annual runoff. For CGCM3.1(T47) and CNRM-CM3, these trends are amplified from the 2020s to the 2040s and, subsequently, to the 2080s. In the case of ECHO-G, however, annual reductions in runoff are of a similar magnitude for all three future time periods. However, there is an increase in seasonality from the 2020s to the 2080s for this model such that runoff is projected to decrease in both the cool and warm seasons for the 2020s, but by the 2080s there is a projected increase in cool season runoff and a substantial decrease in warm season precipitation.

Differences between the simulated hydrological regimes are further clarified in Figure 6.7 and Table 6.9, and Figure 6.8 and Table 6.10, which describe changes in the magnitude of peak and low flows, respectively. The magnitudes of peak flows with recurrence intervals of 20-, 50- and 100-years are projected to increase by all three GCMs, with the exception of ECHO-G for the B1 emissions scenario in the 2020s and 2040s. The greatest increase in peak flow magnitude is forecast by CGCM3.1(T47), while changes projected by CNRM-CM3 are intermediate between CGCM3.1(T47) and ECHO-G. Similarly, the magnitudes of low-flows (seven-day consecutive lowest flow with a return period of 10-years, or $7Q_{10}$) are projected to decrease by all three GCMs (with the exception of CGCM3.1(T47) for the B1 emissions scenario in the 2020s), indicating increased low-flow risk in the majority of simulations. The $7Q_{10}$

flow is projected to decrease to the greatest extent by ECHO-G and to the least extent by CGCM3.1(T47), whereas CNRM-CM3 again projects a reduction that is intermediate between the two.

The three time periods (2020s, 2040s and 2080s) represent three future 30-year windows (2010 – 2039, 2030 – 2059 and 2070 – 2099, respectively) from which GCM outputs were aggregated for downscaling using the HD technique (see sub-section 6.2.3, above). For each selected GCM, all three future time periods were implemented here with the following justification. Generally, the magnitude of changes in meteorological and hydrological variables relative to historic simulations increases for each subsequent future window: i.e. the 2020s represent the smallest projected changes for a given GCM, while the 2080s represent the greatest. Therefore, each subsequent future window represents a more extreme realisation of projected changes for a given GCM. It follows that using all three future windows helps to encapsulate more fully the range of climate projections developed by the CBCCSP. In total 18 separate flow simulations were extracted from the CBCCSP database and implemented within C-L. These include three GCMs, two GHG emissions scenarios and three future time periods.

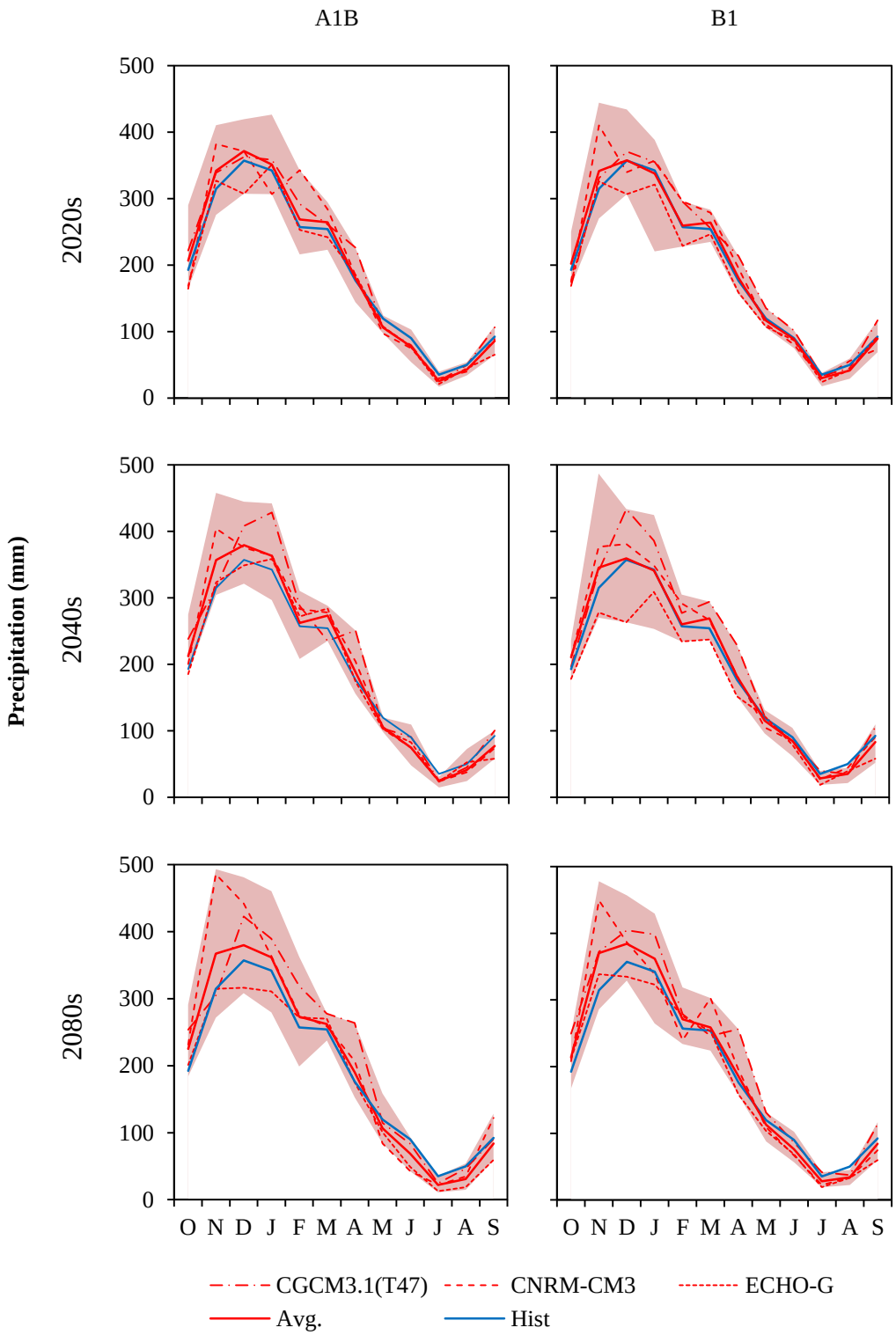

Figure 6.3 Forecasted monthly average total precipitation over the Toutle River basin above Tower Road expressed as an average. The upper and lower bounds of the red shaded area are the maximum and minimum of the monthly values for the ten GCM simulations used in the CBCCSP. The blue line represents the historical average.

Table 6.5 Projected change (%) in precipitation over the Toutle River basin for climate change scenarios relative to historic observations (WYs 1917 – 2006). Cool season defined as October to March, while the warm season is April to September (Vano et al., 2010).

		2020s		2040s		2080s	
		A1B	B1	A1B	B1	A1B	B1
Change in annual precipitation (%)	CNRM-CM3	+ 3.68	+ 5.32	+ 6.15	+ 5.60	+ 12.67	+ 6.37
	ECHO-G	- 5.79	- 7.22	- 0.80	- 13.77	- 7.88	- 4.49
	CGCM3.1 (T47)	+ 6.42	+ 6.16	+ 10.83	+ 11.44	+ 13.56	+ 14.70
	Maximum	+ 8.65	+ 6.68	+ 12.26	+ 11.44	+ 18.85	+ 14.70
	Minimum	- 5.79	- 7.22	- 6.24	- 13.77	- 7.88	- 4.49
	Mean	+ 1.76	+ 1.17	+ 3.31	+ 1.38	+ 3.98	+ 4.39
Change in cool season precipitation (%)	CNRM-CM3	+ 7.78	+ 8.12	+ 10.90	+ 9.16	+ 19.83	+ 12.05
	ECHO-G	- 3.99	- 6.62	+ 3.11	- 12.71	- 1.90	+ 1.10
	CGCM3.1 (T47)	+ 6.83	+ 3.42	+ 11.40	+ 12.23	+ 14.53	+ 13.52
	Maximum	+ 14.12	+ 10.71	+ 18.81	+ 12.23	+ 27.58	+ 21.09
	Minimum	- 3.99	- 6.62	- 0.88	- 12.71	- 1.90	+ 0.57
	Mean	+ 5.05	+ 2.56	+ 7.54	+ 3.92	+ 8.86	+ 8.30
Change in warm season precipitation (%)	CNRM-CM3	- 8.81	- 3.24	- 8.32	- 5.25	- 9.15	- 10.95
	ECHO-G	- 11.27	- 9.05	- 12.73	- 17.01	- 26.12	- 21.54
	CGCM3.1 (T47)	+ 5.16	+ 14.52	+ 9.09	+ 9.01	+ 10.61	+ 18.28
	Maximum	+ 5.16	+ 14.52	+ 9.09	+ 9.01	+ 10.61	+ 18.28
	Minimum	- 18.75	- 14.84	- 26.43	- 23.83	- 28.95	- 21.54
	Mean	- 8.27	- 3.07	- 9.57	- 6.37	- 10.89	- 7.50

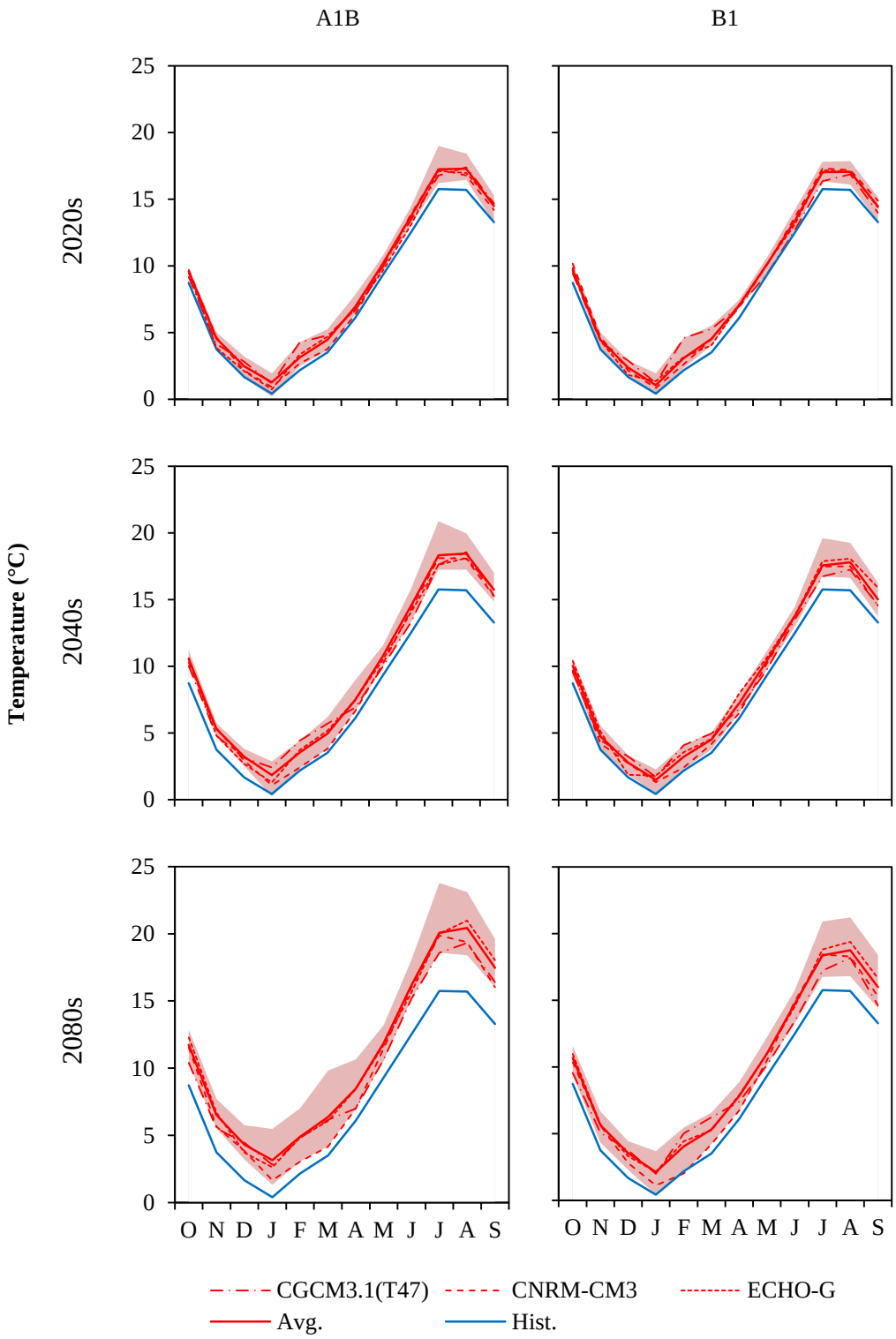

Figure 6.4 Forecasted monthly average temperatures of the Toutle River basin above Tower Road. The upper and lower bounds of the red shaded area are the maximum and minimum of the monthly values for the ten GCM simulations used in the CBCCSP. The blue line represents the historical average.

Table 6.6 Projected change in temperature (°C) of the Toutle River basin for climate change scenarios relative to historic observations (WYs 1917 – 2006). Cool season defined as October to March, while the warm season is April to September (Vano et al., 2010).

		2020s		2040s		2080s	
		A1B	B1	A1B	B1	A1B	B1
Change in annual temperature (°C)	CNRM-CM3	+ 0.78	+ 1.01	+ 1.29	+ 0.97	+ 2.24	+ 1.45
	ECHO-G	+ 0.80	+ 0.89	+ 1.57	+ 1.56	+ 3.19	+ 2.27
	CGCM3.1 (T47)	+ 1.03	+ 0.92	+ 1.61	+ 1.15	+ 2.37	+ 1.64
	Maximum	+ 1.28	+ 1.18	+ 2.62	+ 1.81	+ 4.97	+ 3.10
	Minimum	+ 0.62	+ 0.70	+ 1.23	+ 0.74	+ 2.24	+ 0.95
	Mean	+ 1.04	+ 0.95	+ 1.82	+ 1.31	+ 3.22	+ 2.09
Change in cool season temperature (°C)	CNRM-CM3	+ 0.60	+ 0.79	+ 0.94	+ 0.72	+ 1.63	+ 0.98
	ECHO-G	+ 0.68	+ 0.73	+ 1.34	+ 1.18	+ 2.68	+ 1.93
	CGCM3.1 (T47)	+ 1.02	+ 1.25	+ 1.71	+ 1.30	+ 2.33	+ 1.90
	Maximum	+ 1.17	+ 1.25	+ 2.19	+ 1.72	+ 4.74	+ 2.99
	Minimum	+ 0.60	+ 0.50	+ 0.94	+ 0.61	+ 1.63	+ 0.81
	Mean	+ 0.88	+ 0.82	+ 1.53	+ 1.09	+ 2.79	+ 1.85
Change in warm season temperature (°C)	CNRM-CM3	+ 0.97	+ 1.23	+ 1.64	+ 1.22	+ 2.85	+ 1.92
	ECHO-G	+ 0.92	+ 1.05	+ 1.80	+ 1.94	+ 3.70	+ 2.60
	CGCM3.1 (T47)	+ 1.04	+ 0.59	+ 1.50	+ 1.00	+ 2.42	+ 1.39
	Maximum	+ 1.79	+ 1.45	+ 3.06	+ 2.40	+ 5.20	+ 3.74
	Minimum	+ 0.51	+ 0.55	+ 1.43	+ 0.87	+ 2.42	+ 1.09
	Mean	+ 1.20	+ 1.08	+ 2.10	+ 1.53	+ 3.64	+ 2.33

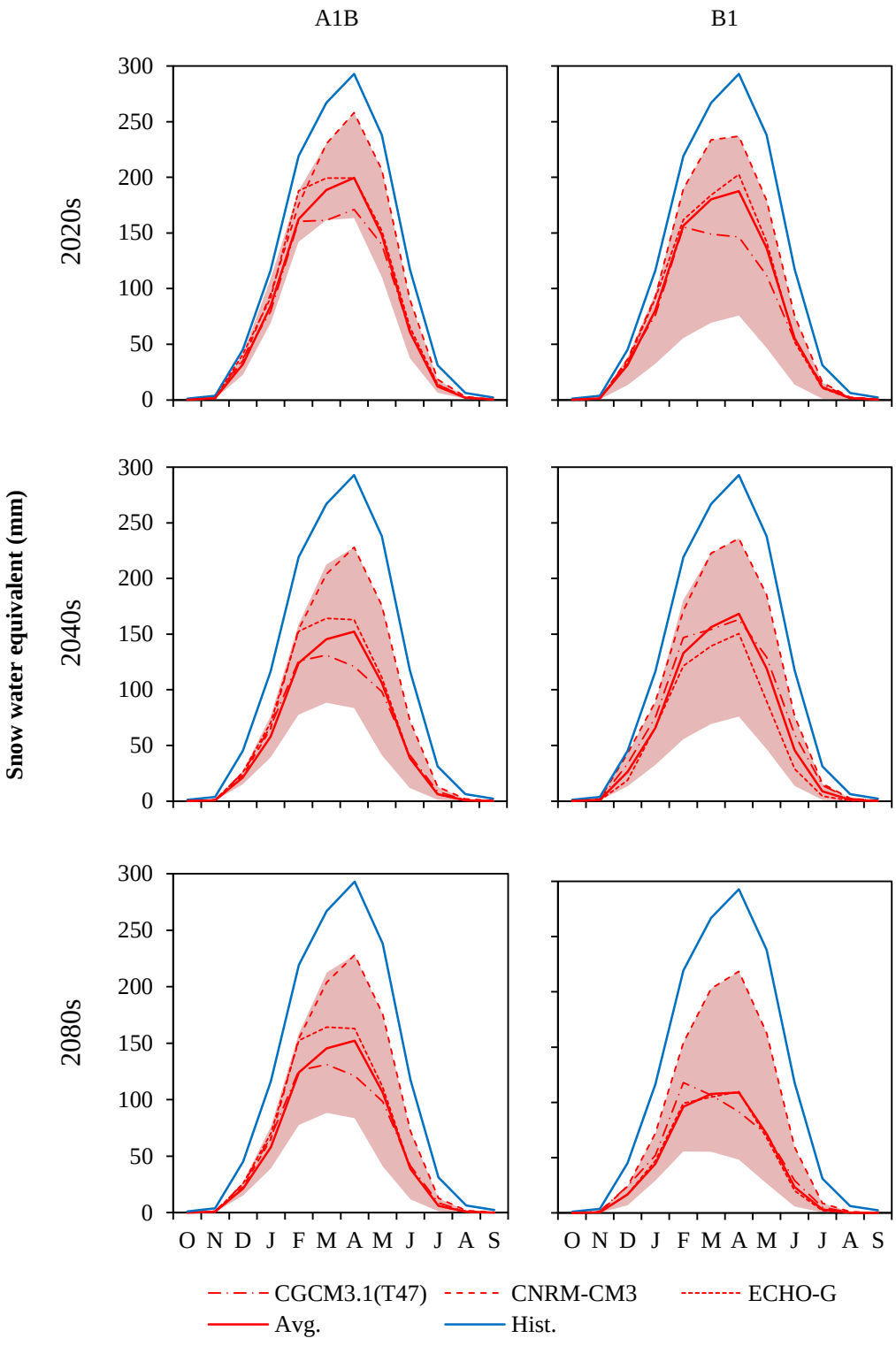

Figure 6.5 Forecasted first day of the month total snow water equivalent (SWE) expressed as a depth averaged over the Toutle River basin above Tower Road.

The upper and lower bounds of the red shaded area are the maximum and minimum of the monthly values for the ten GCM simulations used in the CBCCSP. The blue line represents the historical average.

Table 6.7 Projected change (%) in April 1 SWE over the Toutle River basin for climate change scenarios relative to historic observations (WYs 1917 – 2006).

		2020s		2040s		2080s	
		A1B	B1	A1B	B1	A1B	B1
Change in April 1 SWE (%)	CNRM-CM3	- 13.77	- 12.52	- 23.61	- 16.54	- 39.44	- 23.94
	ECHO-G	- 25.33	- 31.05	- 38.47	- 47.83	- 73.76	- 60.71
	CGCM3.1 (T47)	- 39.52	- 44.16	- 50.92	- 42.17	- 67.96	- 60.05
	Maximum	- 13.77	- 12.52	- 20.38	- 16.54	- 39.44	- 23.94
	Minimum	- 39.52	- 74.04	- 66.90	- 74.04	- 96.58	- 79.27
	Mean	- 29.32	- 32.45	- 45.55	- 41.42	- 71.75	- 59.70

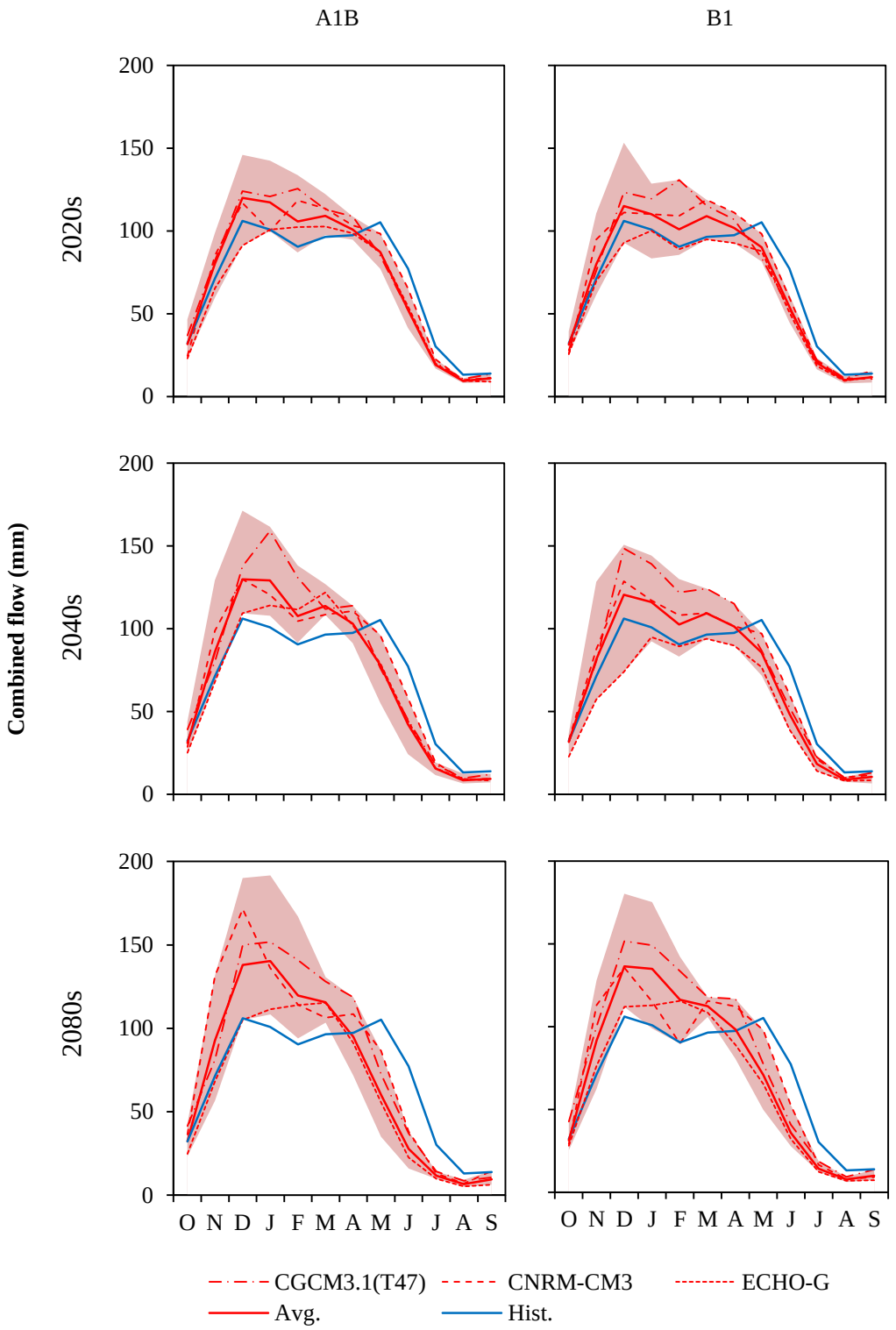

Figure 6.6 Forecasted combined monthly total runoff and baseflow from the Toutle River basin above Tower Road expressed as an average depth. The upper and lower bounds of the red shaded area are the maximum and minimum of the monthly values for the ten GCM simulations used in the CBCCSP. The blue line represents the historical average.

Table 6.8 Projected change (%) in runoff from the Toutle River basin above Tower Road for climate change scenarios relative to historic observations (WYs 1917 – 2006).

		2020s		2040s		2080s	
		A1B	B1	A1B	B1	A1B	B1
Change in annual runoff (%)	CNRM-CM3	+ 4.22	+ 5.66	+ 6.98	+ 6.11	+ 15.51	+ 7.21
	ECHO-G	- 8.43	- 10.88	- 3.10	- 19.94	- 12.57	- 8.17
	CGCM3.1 (T47)	+ 7.03	+ 6.08	+ 11.83	+ 13.27	+ 14.52	+ 16.45
	Maximum	+ 10.31	+ 7.26	+ 13.41	+ 13.27	+ 20.66	+ 16.45
	Minimum	- 8.43	- 10.88	- 10.69	- 19.94	- 12.57	- 8.17
	Mean	+ 1.15	+ 0.03	+ 2.33	+ 0.02	+ 1.80	+ 3.04
Change in cool season runoff (%)	CNRM-CM3	+ 12.37	+ 14.58	+ 18.77	+ 17.38	+ 39.99	+ 20.29
	ECHO-G	- 2.38	- 4.94	+ 10.57	- 13.15	+ 8.34	+ 11.28
	CGCM3.1 (T47)	+ 21.18	+ 19.26	+ 32.50	+ 29.86	+ 39.49	+ 39.80
	Maximum	+ 27.21	+ 23.21	+ 43.57	+ 29.86	+ 63.55	+ 52.00
	Minimum	- 2.38	- 4.94	+ 7.24	- 13.15	+ 6.84	+ 9.50
	Mean	+ 13.43	+ 9.91	+ 20.14	+ 12.94	+ 28.47	+ 25.29
Change in warm season runoff (%)	CNRM-CM3	- 7.80	- 7.51	- 10.40	- 10.53	- 20.60	- 12.08
	ECHO-G	- 17.37	- 19.64	- 23.27	- 29.97	- 43.41	- 36.86
	CGCM3.1 (T47)	- 13.84	- 13.37	- 18.66	- 11.19	- 22.30	- 17.98
	Maximum	- 7.80	- 7.51	- 10.40	- 10.53	- 20.60	- 12.08
	Minimum	- 25.99	- 22.08	- 41.92	- 29.97	- 56.80	- 44.42
	Mean	- 16.98	- 14.54	- 23.94	- 19.02	- 37.54	- 29.77

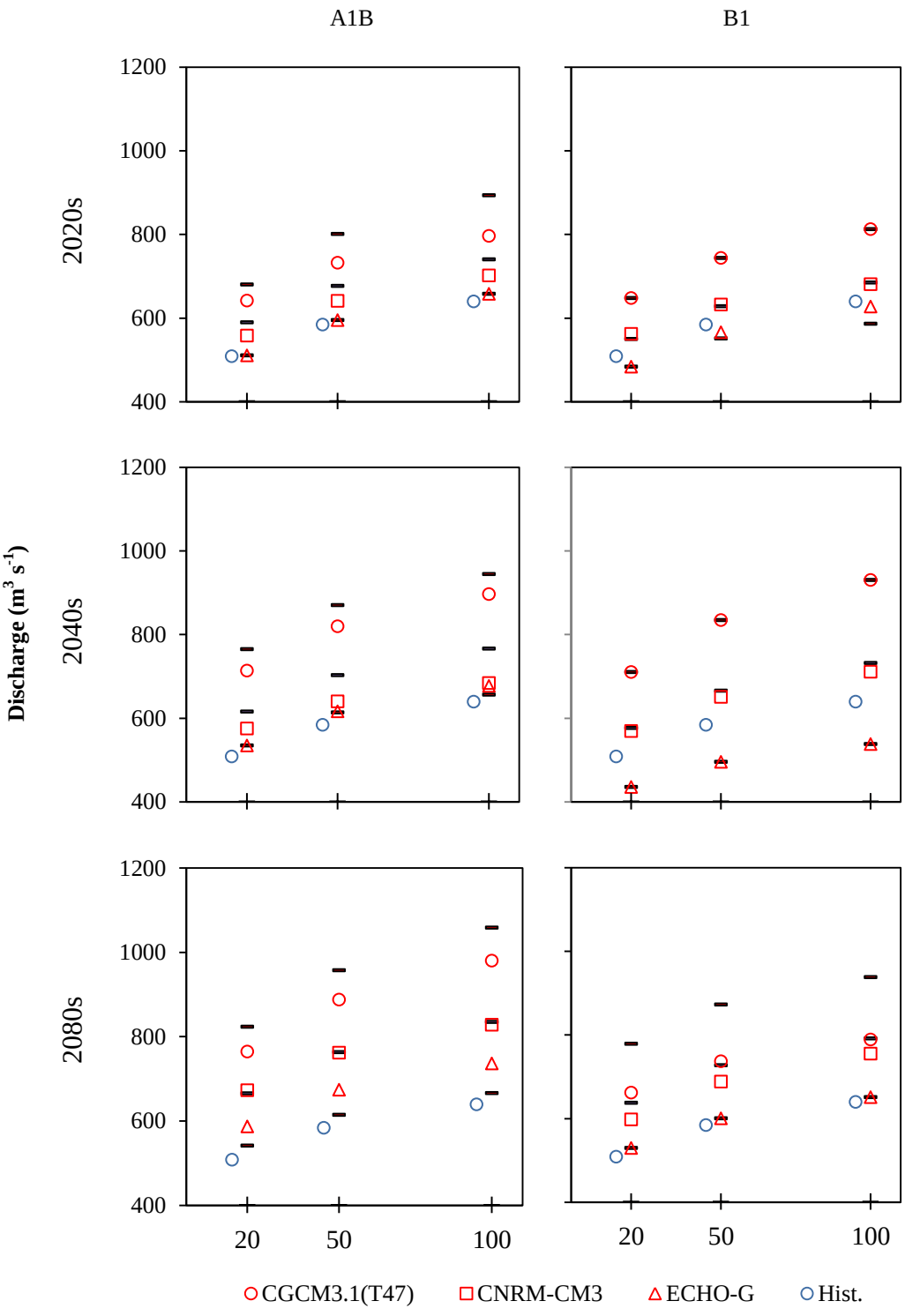

Figure 6.7 Forecasted daily flood statistics for the 20-, 50- and 100-year return period floods in the Toutle River at Tower Road. The black lines represent the maximum, minimum and mean of the ten GCM simulations used in the CBCCSP. The blue circle represents the historical average.

Table 6.9 Projected change (%) in the magnitude of floods with 20-, 50- and 100-year return period floods in the Toutle River at Tower Road for climate change scenarios relative to historic observations (WYs 1917 – 2006).

		2020s		2040s		2080s	
		A1B	B1	A1B	B1	A1B	B1
Change in 20-year flood magnitude (%)	CNRM-CM3	+ 9.72	+ 10.53	+ 13.19	+ 11.94	+ 32.38	+ 17.60
	ECHO-G	+ 0.45	- 4.94	+ 5.13	- 14.34	+ 15.55	+ 4.07
	CGCM3.1 (T47)	+ 26.18	+ 27.39	+ 40.32	+ 39.70	+ 50.48	+ 30.14
	Maximum	+ 33.78	+ 27.39	+ 50.54	+ 39.70	+ 61.97	+ 53.18
	Minimum	+ 0.45	- 4.94	+ 5.13	- 14.34	+ 6.52	+ 4.07
	Mean	+ 15.90	+ 8.09	+ 21.06	+ 13.46	+ 30.91	+ 25.42
Change in 50-year flood magnitude (%)	CNRM-CM3	+ 9.68	+ 8.16	+ 9.60	+ 11.44	+ 30.52	+ 17.76
	ECHO-G	+ 1.80	- 3.19	+ 5.51	- 15.15	+ 15.47	+ 2.79
	CGCM3.1 (T47)	+ 25.33	+ 27.22	+ 40.28	+ 42.83	+ 52.07	+ 26.15
	Maximum	+ 37.12	+ 27.22	+ 48.96	+ 42.83	+ 63.93	+ 49.35
	Minimum	+ 1.80	- 5.64	+ 5.06	- 15.15	+ 5.21	+ 2.79
	Mean	+ 15.82	+ 7.47	+ 20.35	+ 13.98	+ 30.66	+ 24.47
Change in 100-year flood magnitude (%)	CNRM-CM3	+ 9.81	+ 6.45	+ 7.00	+ 11.27	+ 29.57	+ 18.16
	ECHO-G	+ 2.92	- 1.81	+ 5.95	- 15.80	+ 15.29	+ 1.85
	CGCM3.1 (T47)	+ 24.61	+ 27.08	+ 40.28	+ 45.54	+ 53.45	+ 23.37
	Maximum	+ 39.73	+ 27.08	+ 47.84	+ 45.54	+ 65.69	+ 46.71
	Minimum	+ 2.92	- 8.35	+ 2.67	- 15.80	+ 4.23	+ 1.85
	Mean	+ 15.81	+ 7.14	+ 19.90	+ 14.56	+ 30.62	+ 23.87

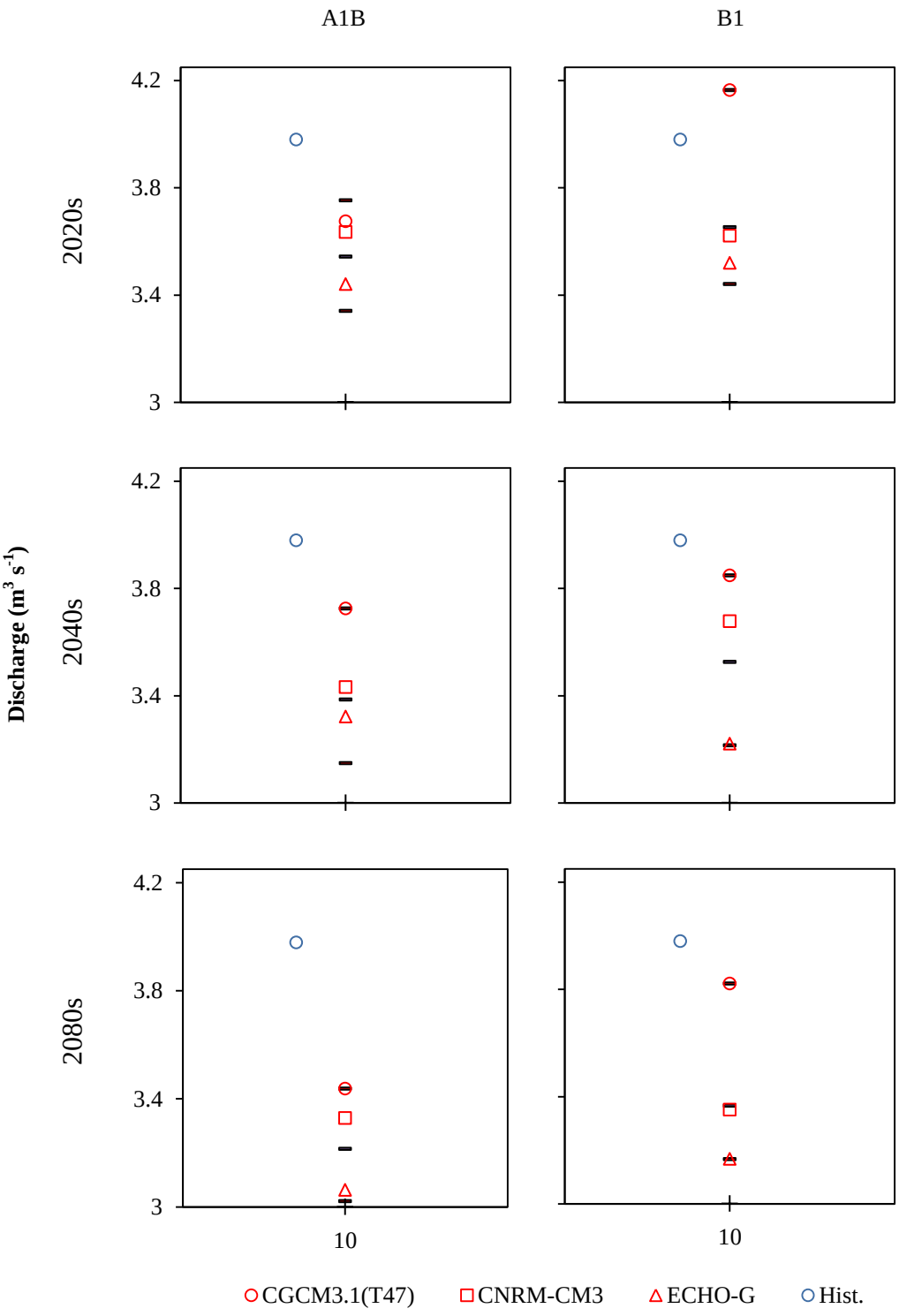

Figure 6.8 Simulated $7Q_{10}$ low flow statistics for the Toutle River at Tower Road. The black lines represent the maximum, minimum and mean of the ten GCM simulations used in the CBCCSP. The blue circle represents the historical average.

Table 6.10 Projected change (%) in the magnitude of the $7Q_{10}$ flood at Tower Road in the Toutle River basin for climate change scenarios relative to historic observations (WYs 1917 – 2006).

		2020s		2040s		2080s	
		A1B	B1	A1B	B1	A1B	B1
Change in $7Q_{10}$ (%)	CNRM-CM3	- 8.66	- 9.02	- 13.75	- 7.58	- 16.34	- 15.78
	ECHO-G	- 13.56	- 11.54	- 16.52	- 19.06	- 23.03	- 20.41
	CGCM3.1 (T47)	- 7.65	+ 4.65	- 6.40	- 3.28	- 13.61	- 3.97
	Maximum	- 5.71	+ 4.65	- 6.40	- 3.28	- 13.61	- 3.97
	Minimum	- 16.07	- 13.55	- 20.89	- 19.21	- 24.09	- 20.42
	Mean	- 10.98	- 8.21	- 14.91	- 11.41	- 19.22	- 15.43

6.3.3 Transferring flow projections from Tower Road to the N1-DRS site

To implement the forecast flow series developed by the CBCCSP and predict long-term future sediment yields from the upper North Fork Toutle River basin, it was first necessary to transfer the data from the Tower Road gauge on the Toutle River to the N1-DRS, which marks the downstream extent of the modelled catchment. This was achieved using a methodology similar to that described in Chapter 4, whereby a relationship was first developed between discharge records at the Tower Road and SRS gauging stations.

Given that the CBCCSP outputs mean daily data, observed mean daily data were first obtained from the Tower Road and SRS gauges between October 1, 1989 and September 20, 2012. Similar pre-processing steps to those described in Chapter 4 were performed, including identification of coincident pairs and removal of gaps in the time series. It was unnecessary, however, to apply a time shift to the data (as in sub-section 4.3.3) given its temporal resolution. The data were split into training and testing sets, with the training data consisting of the first 4,000 coincident pairs (October 1, 1989 to September 13, 2002) and the test set the final 2,176 pairs.

As in Chapter 4, a relationship between the two gauges was obtained using linear regression on the training data set (Figure 6.9). A scatter plot of observed mean daily discharge against mean daily discharge predicted by the linear regression equation for the testing data is presented in Figure 6.10. For reasons similar to those discussed in Chapter 4, NSE was again used to quantify the goodness-of-fit for the testing data. The obtained value of 0.99 indicates that the linear regression equation is able to provide very good estimations of observed discharges at the SRS between September 14, 2002 and September 20, 2012. Moreover, the mean absolute error is only 3.61 m^3 s^{-1}, while the mean absolute relative error is just 0.17, or approximately 17%. It is therefore apparent that, despite the one outlier which may be the result of gauge error during a high flow event, the derived equation is an effective means of estimating mean daily flow at the SRS based on gauged flow at Tower Road.

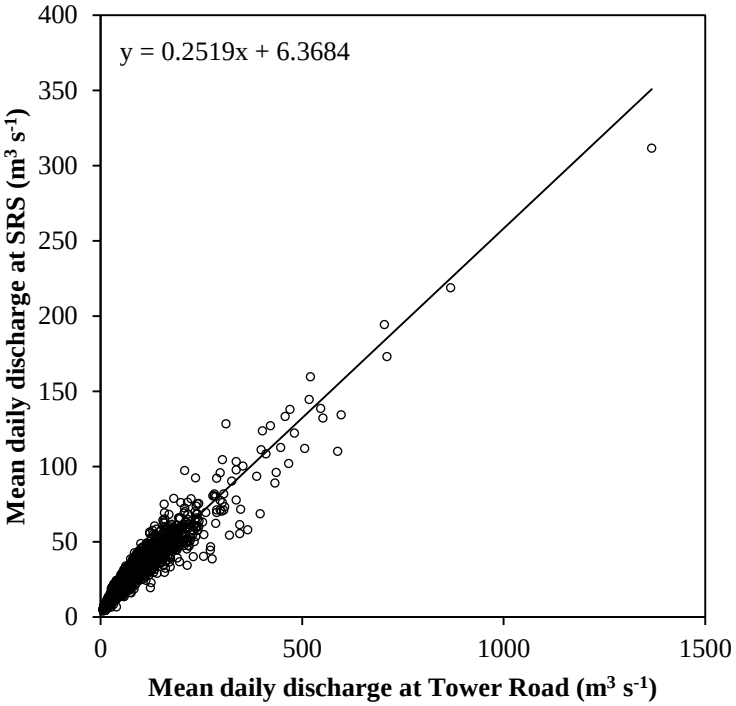

Figure 6.9 Relationship between mean daily discharge recorded at the Tower Road and SRS gauging stations between October 1, 1989 and September 13, 2002.

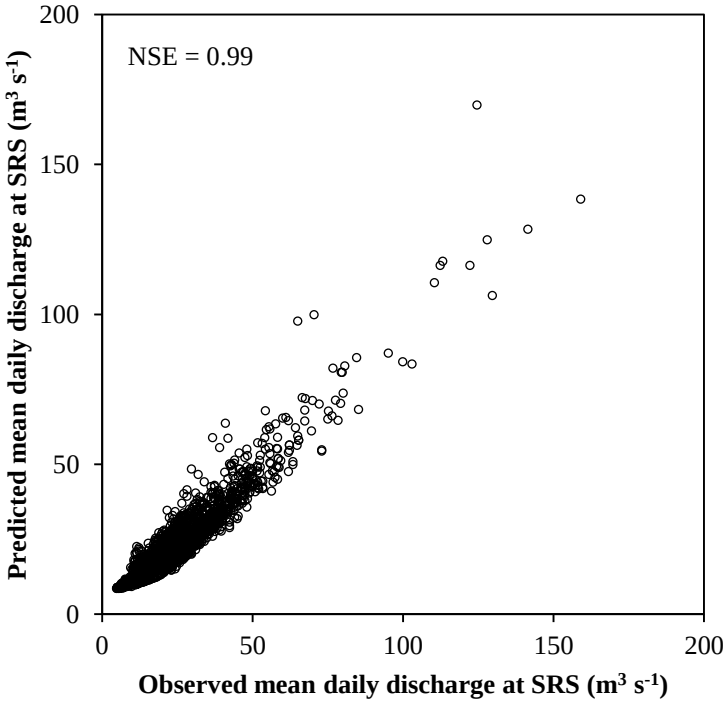

Figure 6.10 The relationship between observed mean daily discharge and discharge predicted by the linear regression model at the SRS gauging station between September 14, 2002 and September 20, 2012.

The linear regression equation was then applied to the CBCCSP flow projections to develop estimates of future flows at the SRS for each of the scenarios. These estimates were subsequently transferred to the N1-DRS by applying the equation $Q_{\mathrm{N1}} = 0.75\ Q_{\mathrm{SRS}}$, which was developed in Chapter 4 on the basis of the drainage area and normal annual precipitation ratios between the two sites. To obtain the hourly time step data required for implementation within C-L, the daily data were interpolated linearly using a freely downloadable Excel add-on (XlXtrFun: www.xlxtrfun.com). This add-on simply fits a straight line between two adjacent points and uses this line to calculate the value of the dependent variable at any given value of the independent variable.

6.3.4 Characteristics of the projected flows

Figure 6.11 shows the per cent departure from mean discharge for the 18 flow simulations between 2009 and 2100. All projections show a similar pattern of relative change through time, which is to be expected as they are all derived from the same historical (1915 to 2006) meteorological driving data (Section 6.2) It is apparent from Figure 6.11 that for about the first 30 years the flow series are characterised by below average discharge conditions, while discharge is generally greater than average during the middle 30 years. The final third of the flow projections contain years that are both above and below average. These hydrological variations, which are likely to be related to the Pacific Decadal Oscillation (PDO) (Mantua et al., 1997; Major, 2004) discussed in Chapter 2, may be significant in determining volumes and trends of sediment output from the upper North Fork Toutle River catchment, and this will be analysed and interpreted in more detail in the following Sections.

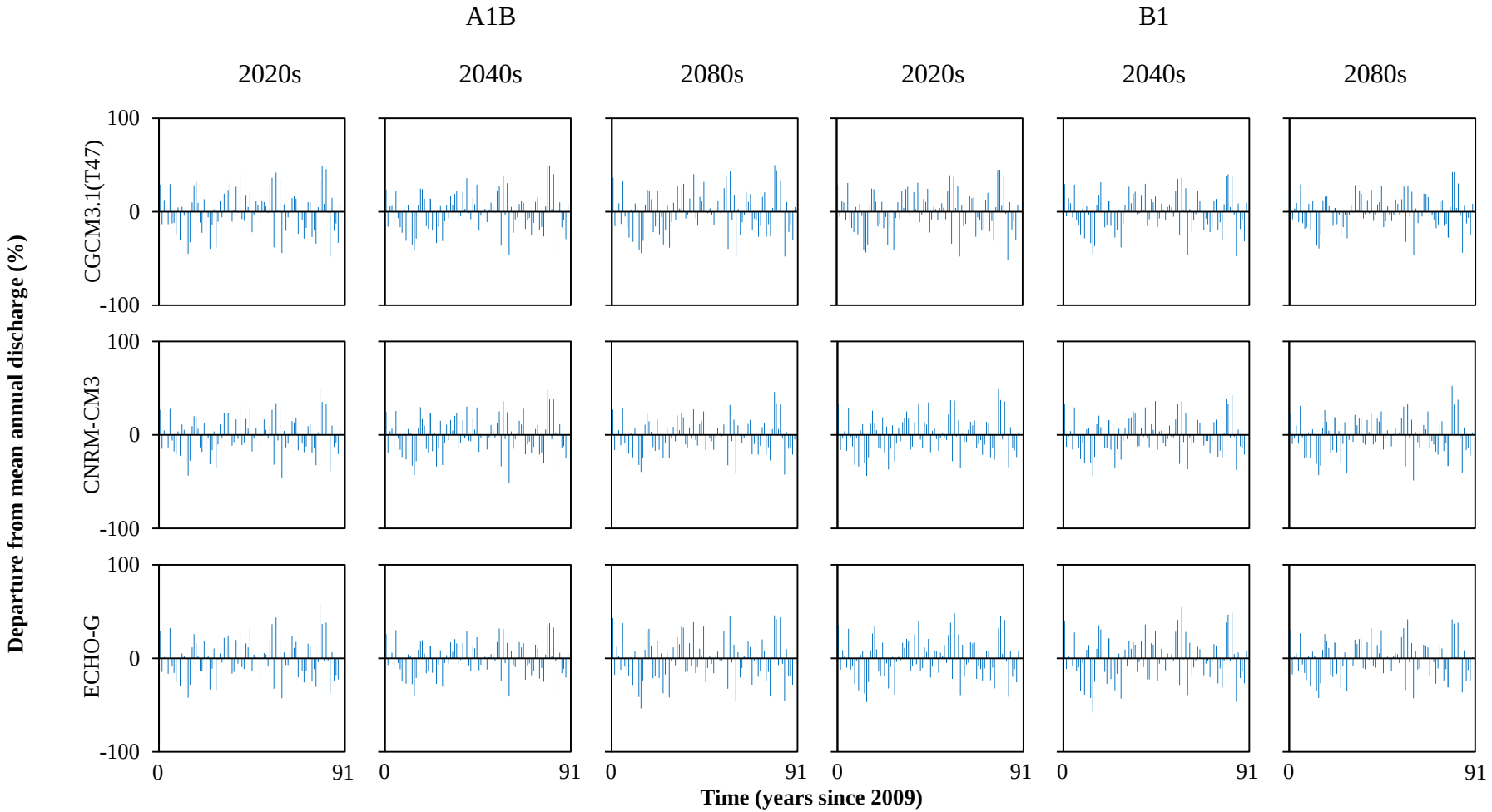

Figure 6.11 Per cent departures from mean annual discharge at the N1-DRS on the North Fork Toutle River for the 18, 91-year streamflow projections used in C-L forecasting runs.

6.4 CUMULATIVE VOLUMES, SPATIAL PATTERNS AND IN-CHANNEL SOURCES OF PREDICTED LONG-TERM SEDIMENT YIELD FROM THE UPPER NORTH FORK TOUTLE RIVER CATCHMENT

The final topography produced by the two selected model configurations from the calibration runs (Chapter 5) was used as the initial surface for the forecast simulations. These forecasts were, therefore, made over a 91-year period extending from 2009 to 2100. Table 6.11 summarises the matrix of 36 model simulations, which include the two selected model configurations, three GCM simulations, two GHG emissions scenarios and three future time periods.

6.4.1 Cumulative sediment yields

Figure 6.12 presents the results of the 36 future simulations in terms of the predicted cumulative catchment sediment yields at six-month intervals, together with estimates over the same period based on the three previous studies introduced in Chapter 3 (WEST, 2002; Biedenharn Group, 2010; Simon and Klimetz, 2012). The data are summarised in Table 6.12 and Figure 6.13. It must be noted that neither the WEST nor Biedenharn Group reports provided estimates of sediment yield beyond the year 2035. However, for comparison with the predictions based on C-L modelling, their estimates were extrapolated by solving the equations presented in these reports for the years 2036 to 2100. This was done purely to contextualise the C-L forecasts developed here. It was not the remit of either the WEST or Biedenharn Group's studies to predict volumes of erosion or sediment yields beyond 2035.

It is evident from Figure 6.12 and Table 6.12 that C-L forecasts of cumulative catchment sediment yields in 2100 fall between those based on the relationships reported by the Biedenharn Group (2010) and Simon and Klimetz (2012). Cumulative yields are, however, similar to those based on WEST (2002). Specifically, the mean of the 36 C-L model forecasts is approximately 175% greater than that predicted by Simon and Klimetz (2012), 36% less than that based on extrapolating the trend up to 2035 reported by the Biedenharn

Table 6.11 Matrix of model runs used to develop estimates of long-term sediment yield from the upper North Fork Toutle River. Model run numbers are shown in the body of the Table.

		A1B			B1		
		2020s	2040s	2080s	2020s	2040s	2080s
Model 60	CGCM3.1(T47)	1	2	3	4	5	6
	CNRM-CM3	7	8	9	10	11	12
	ECHO-G	13	14	15	16	17	18
Model 75	CGCM3.1(T47)	19	20	21	22	23	24
	CNRM-CM3	25	26	27	28	29	30
	ECHO-G	31	32	33	34	35	36

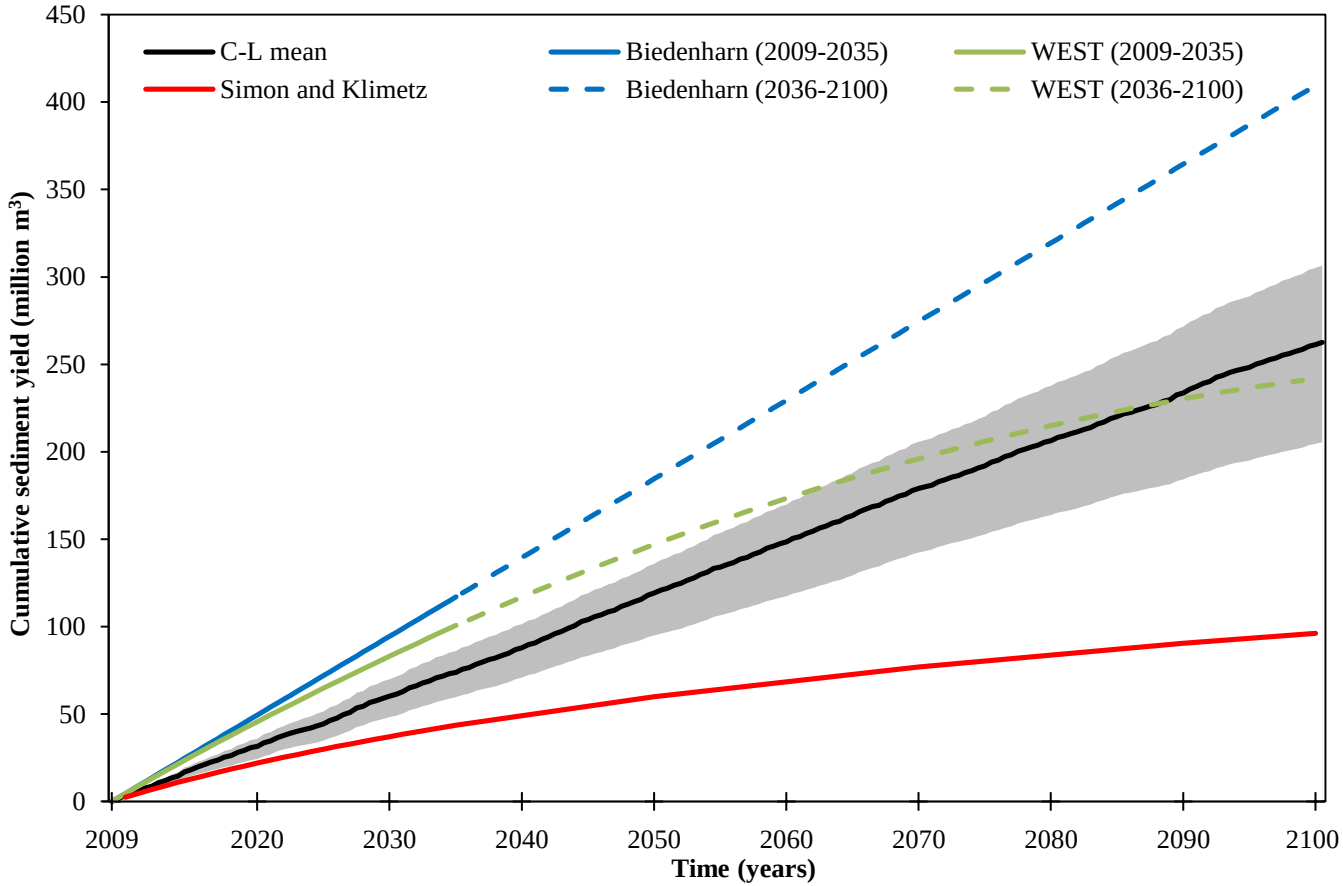

Figure 6.12 Projections of cumulative catchment sediment yield from the upper NFTR catchment from 2009 to 2100. The upper and lower bounds of the shaded area are the maximum and minimum of the six-month values for the 36 C-L model runs. Dashed lines for WEST and Biedenharn Group studies 2036 – 2100 are extrapolated based on trends up to 2035, which was the cut-off date for their predictions.

Table 6.12 Cumulative sediment yields from the upper North Fork Toutle River catchment at specified intervals between 2009 and 2100.

Year	Cumulative sediment yield (million m^3)					
	Simon and Klimetz (2012)	Biedenharn Group (2010)	WEST (2002)	C-L		
				Max.	Min.	Mean
2020	22.00	49.51	45.72	35.91	24.35	31.53
2040	48.50	139.51	116.94	101.47	70.89	87.87
2060	68.45	229.51	173.37	169.83	117.38	148.59
2080	83.80	319.51	215.00	237.74	163.84	206.46
2100	96.27	411.76	240.85	306.54	205.45	262.51

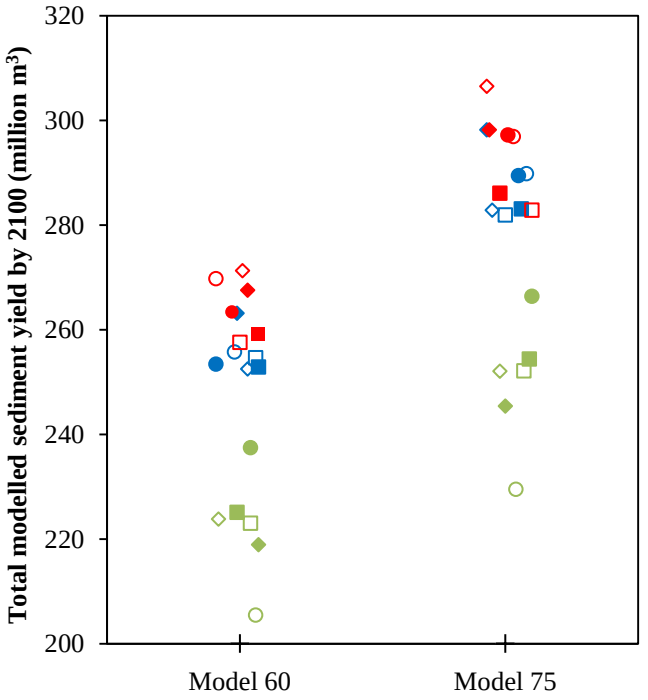

Figure 6.13 Total modelled sediment yield by 2100. Red = CGCM3.1(T47); blue = CNRM-CM3; green = ECHO-G. Solid markers = A1B scenario; Open markers = B1. Squares = 2020s; circles = 2040s; diamonds = 2080s.

Table 6.13 Range of predicted cumulative sediment yields (in million m^3) from the upper North Fork Toutle River catchment in 2100 for the 36 C-L model configurations.

		A1B			B1		
		2020s	2040s	2080s	2020s	2040s	2080s
Model 60	CGCM3.1(T47)	259.17	263.37	267.54	257.59	269.75	271.30
	CNRM-CM3	252.85	253.43	263.15	254.68	255.77	252.51
	ECHO-G	225.08	237.44	218.91	223.03	205.45	223.83
Model 75	CGCM3.1(T47)	286.07	297.22	298.18	282.86	296.91	306.54
	CNRM-CM3	283.10	289.44	298.21	281.93	289.80	282.84
	ECHO-G	254.41	266.40	245.43	252.17	229.49	252.11

Group (2010), but only 8% greater than that based on extrapolation of the trend predicted up to 2035 by WEST (2002). Given that C-L configurations and future hydrologic scenarios were selected to encapsulate the range of likely possible future sediment yields, the projected range of sediment yields forecast by C-L is surprisingly well constrained, in that the difference between the maximum and minimum C-L predictions approximates +/- 50 million m^3, which equates to +/- 20% of the mean predicted value.

Inter-model variability in the total volumes of erosion (Figure 6.13; Table 6.13) follows logically from the differences between the selected climate scenarios and C-L set-ups. The most significant distinction can be made between C-L model configurations. Specifically, the highest and lowest predicted sediment yield volumes over the 91-year period are associated with Model 75 and Model 60, respectively. The fact that Model 75 predicted the highest sediment yield is unsurprising given that this set-up represents a comparatively high lateral migration scenario and that it simulated higher rates of sediment yield during the model hindcast runs compared with Model 60 (see Chapter 5).

It is also evident that predicted sediment yields reflect the characteristics of the climate model simulations from which the flow series were derived. For example, the highest cumulative sediment yields in 2100 are associated with the CGCM3.1(T47) climate model, which projects the greatest increases in runoff relative to the historical simulations (Table 6.4). Conversely, C-L models driven by discharge data projected by the ECHO-G GCM predict the lowest cumulative sediment yield in 2100, which is consistent with decreased annual runoff projected to occur by this model (Table 6.4). CNRM-CM3-driven C-L models forecast, in general, sediment yields that are intermediate between CGCM3.1(T47) and ECHO-G. For models driven by CGCM3.1(T47) and CNRM-CM3 projections of runoff, high sediment yields are predicted for simulations based on the 2080s-adjusted climate, which is the period that features the greatest increases in annual runoff. In the case of ECHO-G-driven models, predicted sediment yields are highest for simulations based on the 2020s-adjusted climate, due to less pronounced reductions in annual runoff projected for this period.

6.4.2 Spatial patterns of future sediment yield

In order to determine the predicted sources and sinks of sediment within the upper North Fork Toutle River catchment, sediment yield was calculated for each of the eight sub-catchments delineated in Chapter 5 (see Figure 5.1). The maximum, minimum and mean values for the 36-model ensemble are shown in Figure 6.14.

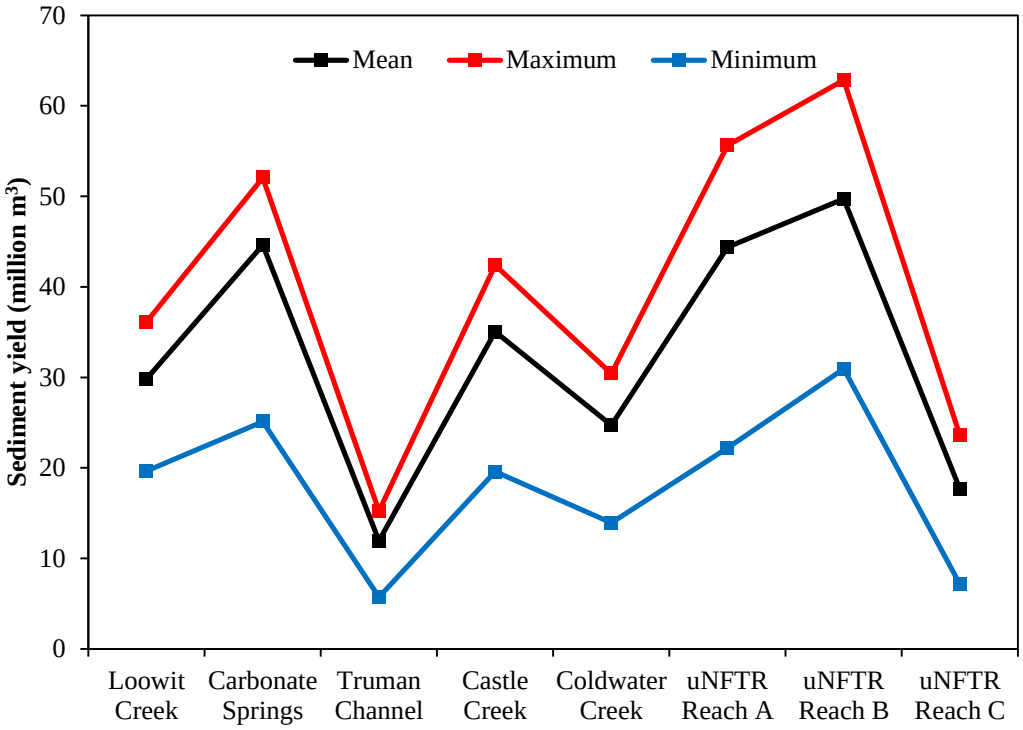

Figure 6.14 Maximum, minimum and mean values of sediment yield from the eight sub-catchments for the 36-model ensemble.

It is evident from Figure 6.14 that each sub-catchment is a net source of sediment in all of the 36 simulations during the 91-year forecasting period. Furthermore, the pattern of sub-catchment sediment yield is broadly the same as that produced by the two selected model configurations during hindcasting (see Figure 5.19). Specifically, uNFTR Reach B generally exports the greatest volume of sediment, while Truman Channel and uNFTR Reach C export the least.

6.4.3 In-channel sources of future sediment yield

It has been argued in a number of previous studies that future long-term sediment yields from the upper North Fork Toutle River catchment are likely to be driven by lateral erosion and bank collapse (e.g. Meyer and Martinson, 1989; Simon and Thorne, 1996; Simon, 1999; Major et al., 2000; Simon and Klimetz, 2012). To assess whether C-L simulations support this contention, and to understand how geomorphic evolution represented in C-L drives predicted volumes of sediment yield, it is necessary to examine how fluvial processes (erosion, transport and deposition) relate to changes in channel geometry (vertical degradation and/or aggradation, lateral erosion and/or accretion) within the model. These relationships were investigated based on channel changes modelled at the ten cross-sections that were selected for use in model evaluation in Chapter 5, to identify the relative contributions of bed scour/fill and bank retreat/advance to overall changes in cross-sectional area.

The results of these investigations are illustrated using the results of the models that predicted the lowest (Model 17) and highest (Model 24) cumulative catchment sediment yields in 2100 (see Tables 6.11 and 6.13). The results of simulations run using these two models bracket all the other outcomes predicted by C-L and so cover the range of possible sediment futures envisaged in all combinations of model set up and climate change scenario. Model 17 has the lower value of the lateral erosion parameter (Λ) and is driven by discharge forecasts generated by the ECHO-G GCM, while Model 24 has the higher value of the lateral erosion parameter and is driven by discharge forecasts generated by the CGCM3.1(T47) GCM (Table 6.11).

The relative contributions of vertical and lateral adjustments to overall change in cross-sectional area between 2009 and 2100 are shown for both models in Figure 6.15. It is clear in these plots that lateral adjustments through bank erosion are the dominant source of sediment according to both models and that this is the case for all but one of the sampled locations (the exception being cross-section CA225 for Model 17). On average, bank erosion is modelled as

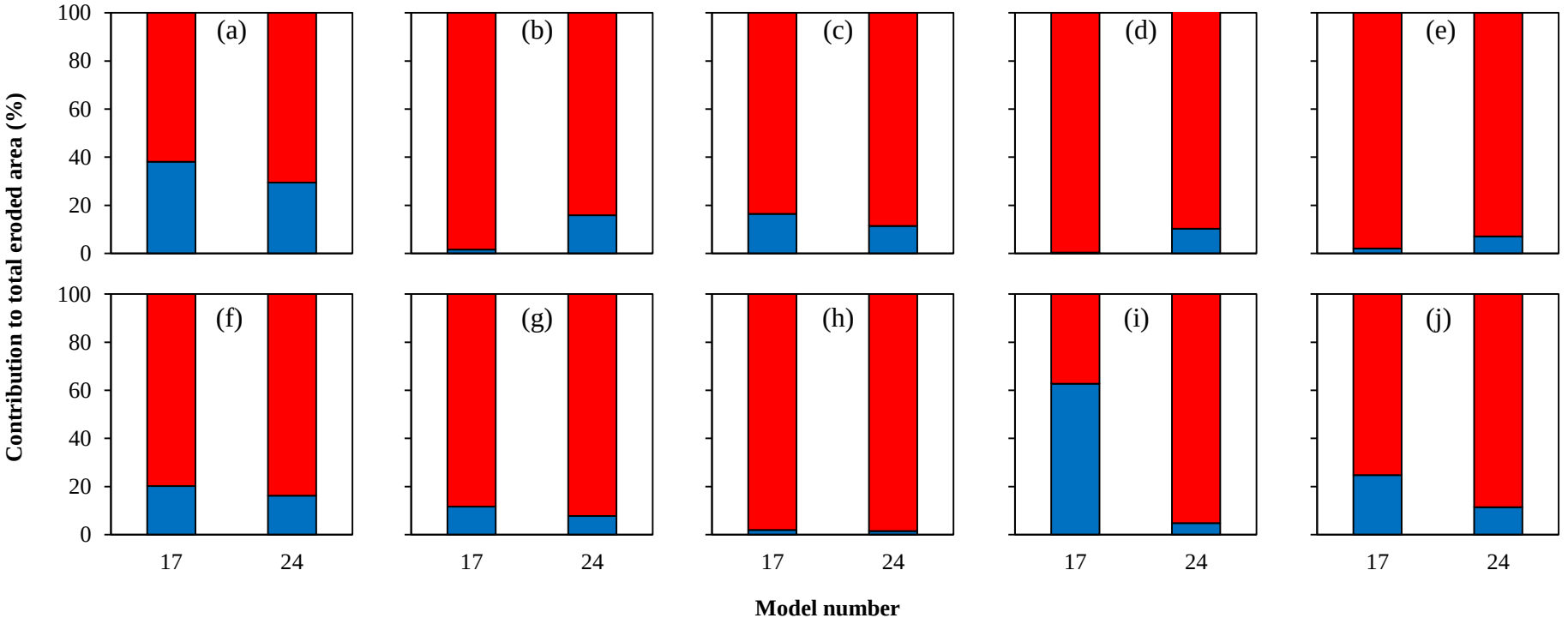

Figure 6.15 Relative contributions of bed (blue) and bank (red) adjustments to overall changes in cross-sectional area at ten selected locations. (a) LO030; (b) LO040; (c) NF100; (d) NF120; (e) NF300; (f) NF320; (g) NF350; (h) NF375; (i) CA225; (j) CW245.

being responsible for over 80% of the increase in cross-sectional area according to Model 17, rising to nearly 90% according to Model 24. This analysis therefore shows that C-L predictions support the hypothesis that future sediment yields will be driven by continuous bank instability.

6.5 PROCESS-RESPONSE MECHANSIMS AND TEMPORAL TRENDS IN PREDICTED LONG-TERM SEDIMENT YIELDS FROM THE UPPER NORTH FORK TOUTLE RIVER CATCHMENT

6.5.1 Trends in future annual sediment yields and in-channel sources

Although the volume of sediment delivered from the upper North Fork Toutle River catchment over the next 91 years is clearly important, knowledge of potential changes in the rate of sediment delivery is also critical for designing appropriate sediment management strategies. Moreover, as discussed in Chapter 3 and shown in Figure 6.12, past predictions of how annual sediment yield will change through time have varied substantially. Specifically, two studies (WEST, 2002; Simon and Klimetz, 2012) have predicted a decay in the rate at which cumulative sediment yield increases with time, while a third (Biedenharn Group, 2010) predicted that annual sediment yield will remain constant. These differences are the result of different interpretations of historical empirically-derived trends of sediment yield, together with different conceptualisations of the processes driving channel change and evolution (Chapter 3).

The predictions made by WEST (2002) and Simon and Klimetz (2012) – that annual sediment yield has declined in the years following the 1980 eruption of Mount St Helens and that this trend will continue – are consistent with a recent study into the morphological evolution of the upper North Fork Toutle River conducted by Zheng et al. (2014). This study analysed vertical channel adjustments by quantifying changes in thalweg elevation at sixteen cross-sections between 1980 and 2009. The analysis revealed a marked reduction in the rate of degradation in upstream reaches and that the channel long profile has therefore begun to stabilise. Moreover, as in Simon and Klimetz (2012), it

was found that time series of thalweg elevation in upstream degrading reaches could be described by non-linear decay functions similar to the rate law model introduced by Graf (1977). The rate law, which is discussed in more detail in Chapter 7, suggests that rates of river channel cross-sectional change reduce through time due to opposing trends of a range of variables including, for instance, boundary and critical shear stress (e.g. Simon and Thorne, 1996).

The application of the rate law to the upper North Fork Toutle River proposed by Zheng et al. (2014) therefore provides a physical explanation for the decay in annual sediment yield predicted by WEST (2002) and Simon and Klimetz (2012). However, by predicting that annual sediment yield would remain constant up to 2035, the Biedenharn Group (2010) implicitly rejected the concept of the rate law and suggested that processes of sediment production would not diminish in accordance with the rate law theory. It is therefore necessary to analyse in greater detail the trends in both sediment yields predicted by C-L and the relative contributions of bed and bank erosion in order to assess whether C-L predictions support or oppose the application of the rate law to the morphological evolution of the upper North Fork Toutle River. It is important to note that the study of Zheng et al. (2014) relates to vertical channel adjustments only, while Section 6.4 has shown that channel widening is the process dominating contemporary channel response.

C-L modelling suggests that while the total volume of sediment output is somewhat unpredictable (Table 6.12), the overall trend in the cumulative sediment yield from the upper North Fork Toutle River catchment is broadly linear throughout the remainder of the 21st century (Figure 6.12). As the data listed in Table 6.14 confirm, average annual sediment yields predicted using C-L do not decline significantly between the 2010s and 2090s. In fact, the ensemble mean rate of sediment production predicted using C-L during the 2090s is only 2% lower than that predicted for the 2010s. Moreover, that small net reduction is not the product of a consistent trend that persists over decades; the highest maximum, mean and minimum annual sediment yields are actually predicted to occur during the 2050s or 2060s (Table 6.14).

To assess whether this broad linearity masks any significant multi-decadal trends, the data for individual model configurations were assessed more closely. This was achieved by plotting the cumulative sediment yield for each model and joining the first and last data points with a straight line. Residuals were then calculated between this straight line and the observed values, and time series of these residuals were plotted for selected models (Figure 6.16 and Figure 6.17).

Table 6.14 Decade-averaged maximum, mean and minimum annual sediment yields for all models between 2009 and 2100. †2010s covers 2009 to 2020.

	Average annual sediment yield (million m^3)		
	Max.	Min.	Mean
2010s†	3.32	2.27	2.92
2020s	3.40	2.36	2.85
2030s	3.13	2.21	2.72
2040s	3.60	2.40	3.09
2050s	4.41	2.31	3.24
2060s	3.51	2.44	2.97
2070s	3.26	2.20	2.81
2080s	3.25	1.96	2.60
2090s	3.47	2.10	2.86

Figure 6.18 presents idealised and exaggerated trends of cumulative sediment yield that might be expected during the 91-year C-L simulations. The corresponding residual plots of these trends are also shown in Figure 6.18 to facilitate comparison and interpretation of the patterns evident in Figure 6.16 and Figure 6.17. Modelled patterns similar to those shown in Figure 6.18 (b), (d) and (f) would suggest that the rates of erosion decline in some fashion at some point during the simulation, while patterns similar to those shown in

Figure 6.18 (c) and (e) would provide evidence that erosion rates increase with time in varying ways at some point during the simulation.

It is evident from Figure 6.16 and Figure 6.17 that all model configurations exhibit a degree of nonlinearity in their temporal trends of sediment yield, and two distinct patterns of nonlinearity can be identified. The first pattern corresponds most closely to the idealised decay trends represented by the residual plots shown in Figure 6.18 (b) and (d). This pattern is most notable in models run with the lower rates of lateral erosion (i.e. Model 60 in Figure 6.16). It indicates that annual sediment yield declines through time. However, the fact that the maximum residual value generally occurs after the midpoint on the time-axis suggests that sediment production is initially linear but then declines towards the end of the century.

The second pattern that can be discerned is generally associated with models in which lateral erosion is simulated to occur at a higher rate (i.e. Model 75 in Figure 6.17). This corresponds to the idealised sinusoidal trend presented in Figure 6.18 (f). In this case, increasingly negative residuals appear during the initial part of the simulation, until a minimum value is approached, after which residuals increase towards zero. Residuals then become positive in the latter part of the simulation and increase to a maximum before declining towards the end of simulation. This pattern indicates that annual sediment yield increases during the first half of the 21st century but then decreases during the second half.

Temporal trends in channel geometry changes (vertical degradation and/or aggradation, lateral erosion and/or accretion) were also analysed to evaluate the mechanisms responsible for the trends identified in Figures 6.16 and 6.17. As in sub-section 6.4.3, this analysis was based on channel changes at the ten previously selected cross-sections, and illustrated using Models 17 and 24, which predicted the lowest and highest cumulative catchment sediment yields in 2100, respectively. These trends are plotted in Figures 6.19 and 6.20, while sequential changes at each cross-section are shown in Figure 6.21.

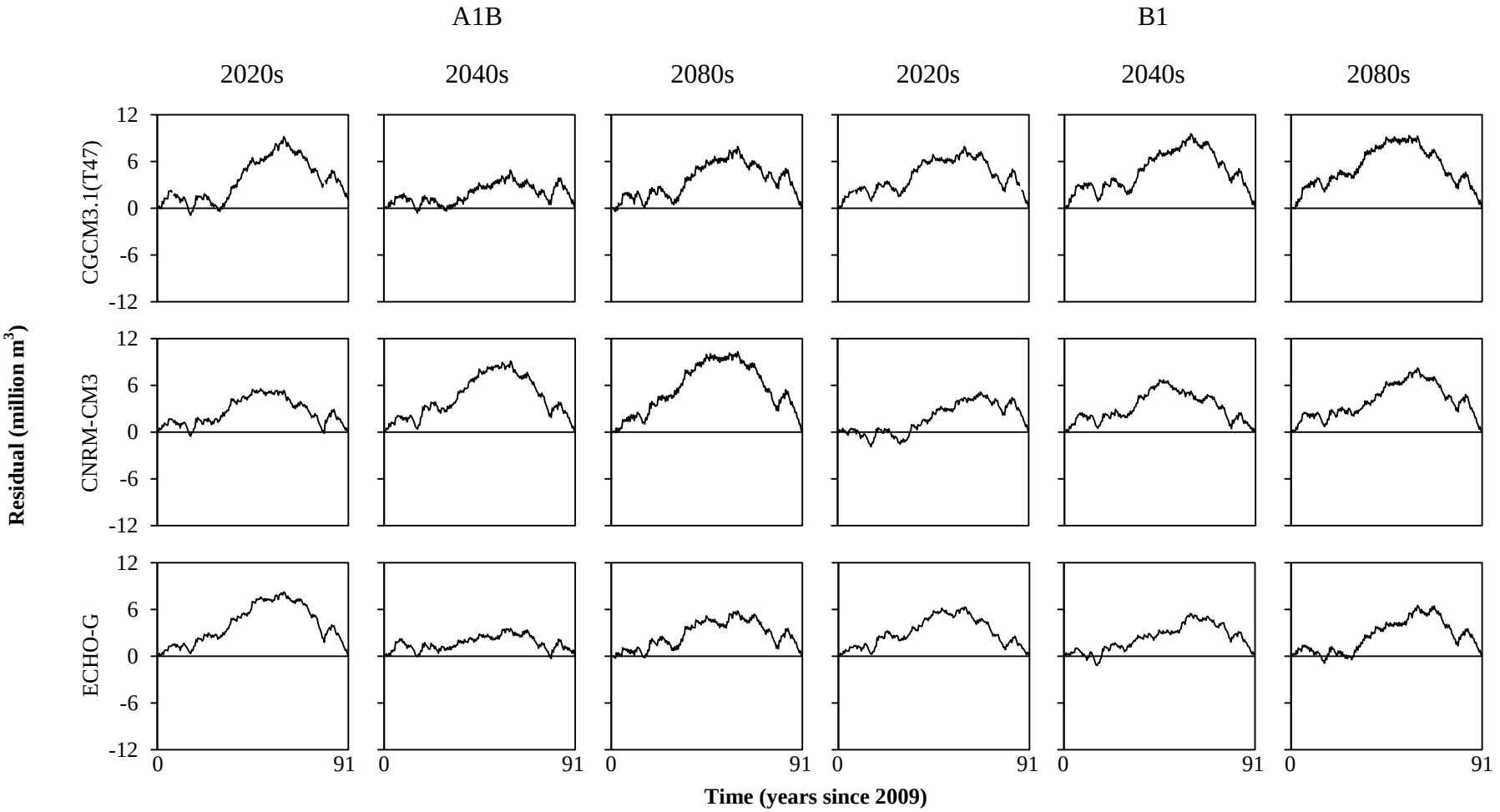

Figure 6.16 Time series plots of residuals calculated between the modelled erosion volumes and those predicted by a straight line. Model 60.

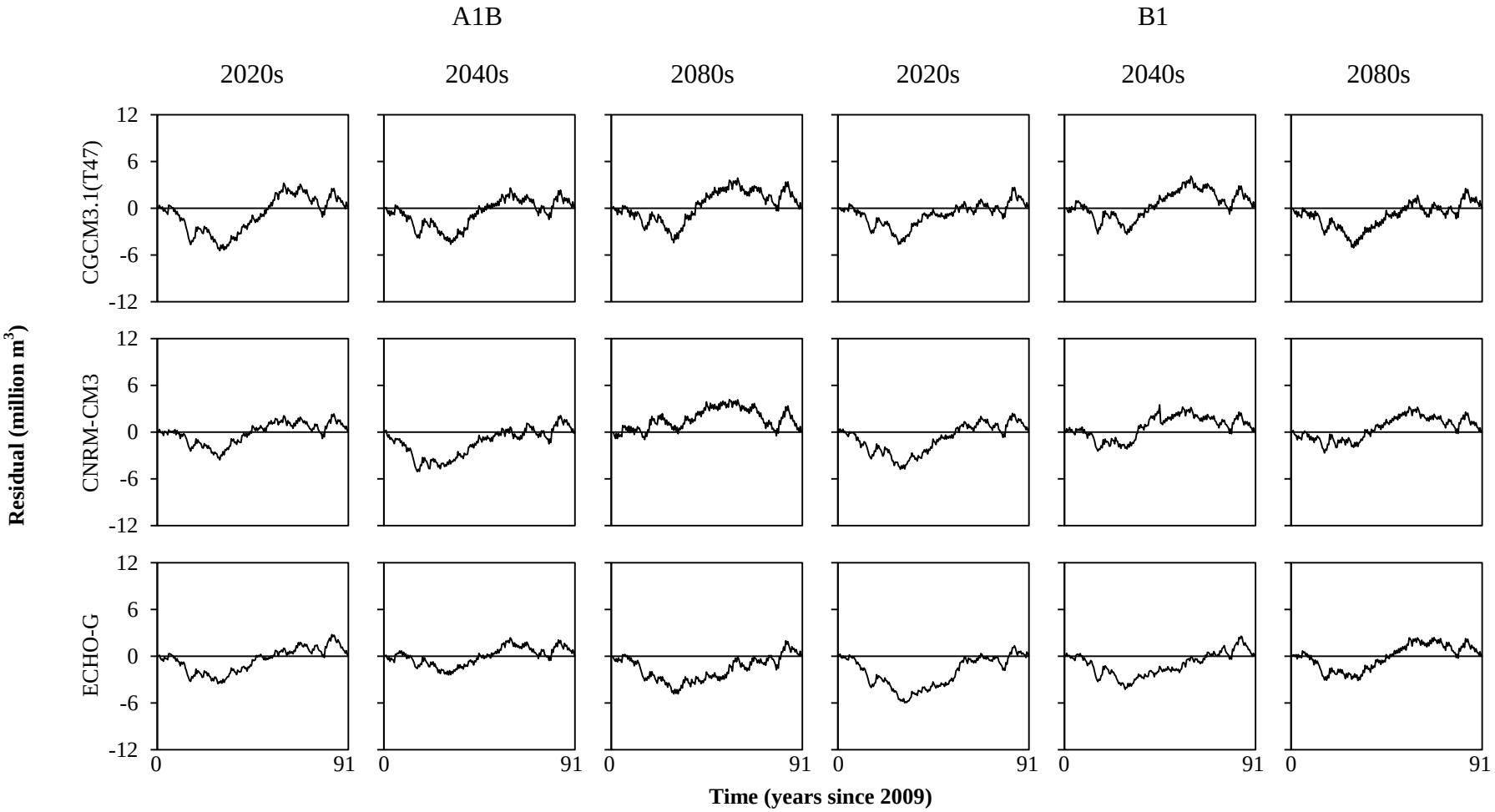

Figure 6.17 Time series plots of residuals calculated between the modelled erosion volumes and those predicted by a straight line. Model 75.

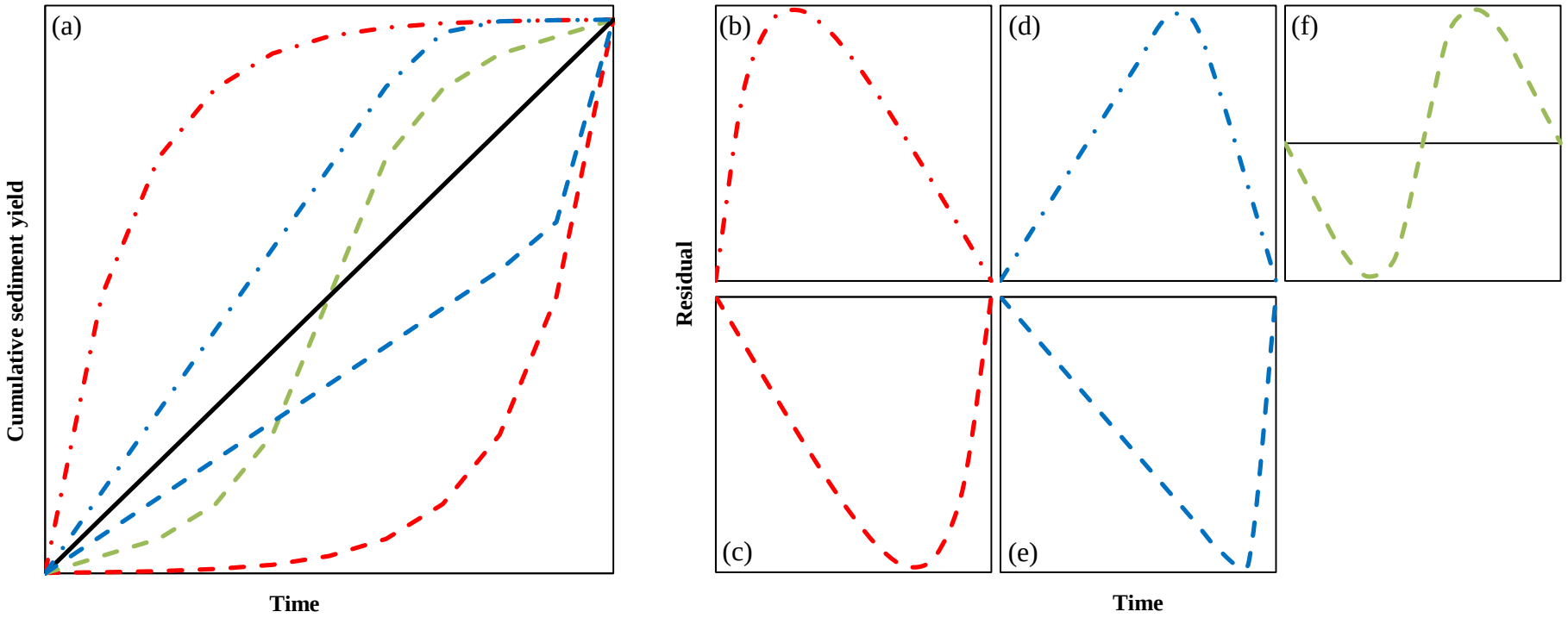

Figure 6.18 Schematic diagram showing the patterns of residuals that would result from different trends of cumulative sediment yield.

(a) Idealised cumulative sediment yield plots for each trend. (b) – (f) show resulting residual plots: (b) = nonlinear decay; (c) = exponential increase; (d) = linear increase followed by decay; (e) linear increase followed by rapid increase; (f) exponential increase followed by nonlinear decay.

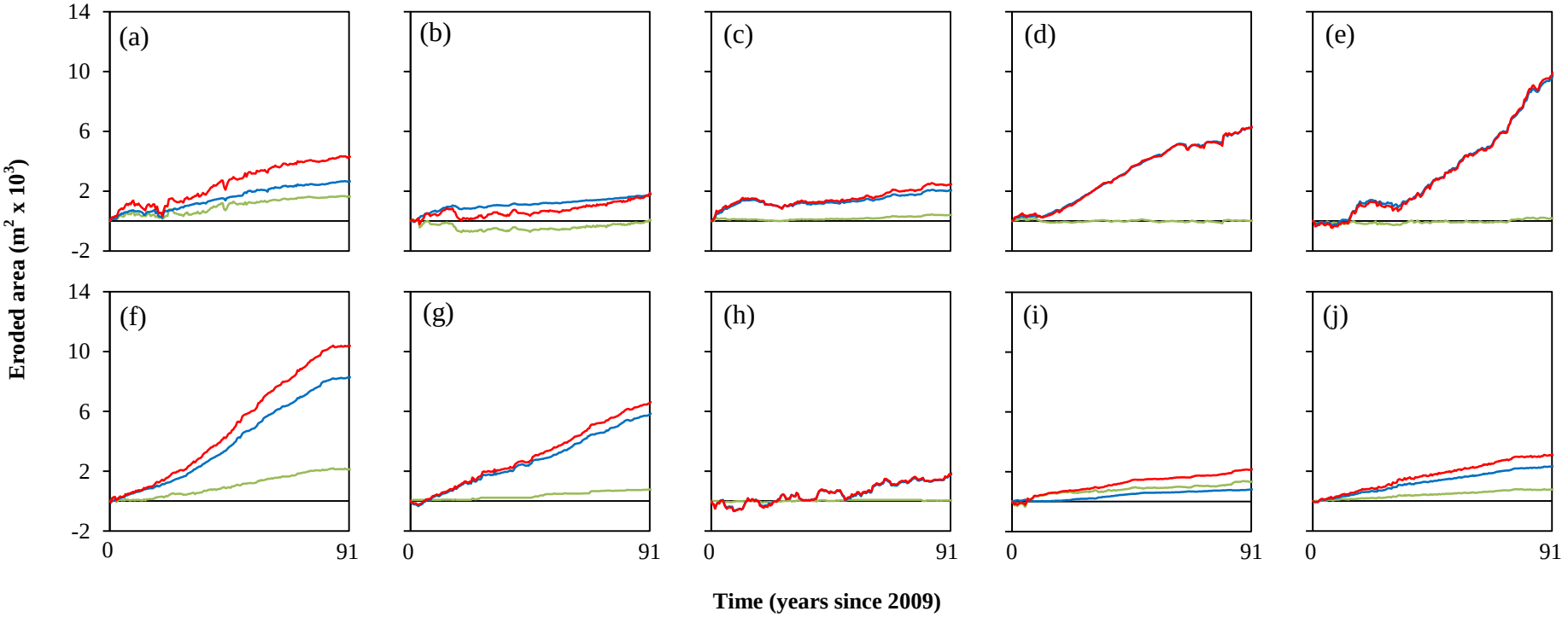

Figure 6.19 Cumulative eroded area at the ten cross-section locations for Model 17, showing total (red), bed (green) and bank (blue) erosion. (a) LO030; (b) LO040; (c) NF100; (d) NF120; (e) NF300; (f) NF320; (g) NF350; (h) NF375; (i) CA225; (j) CW245.

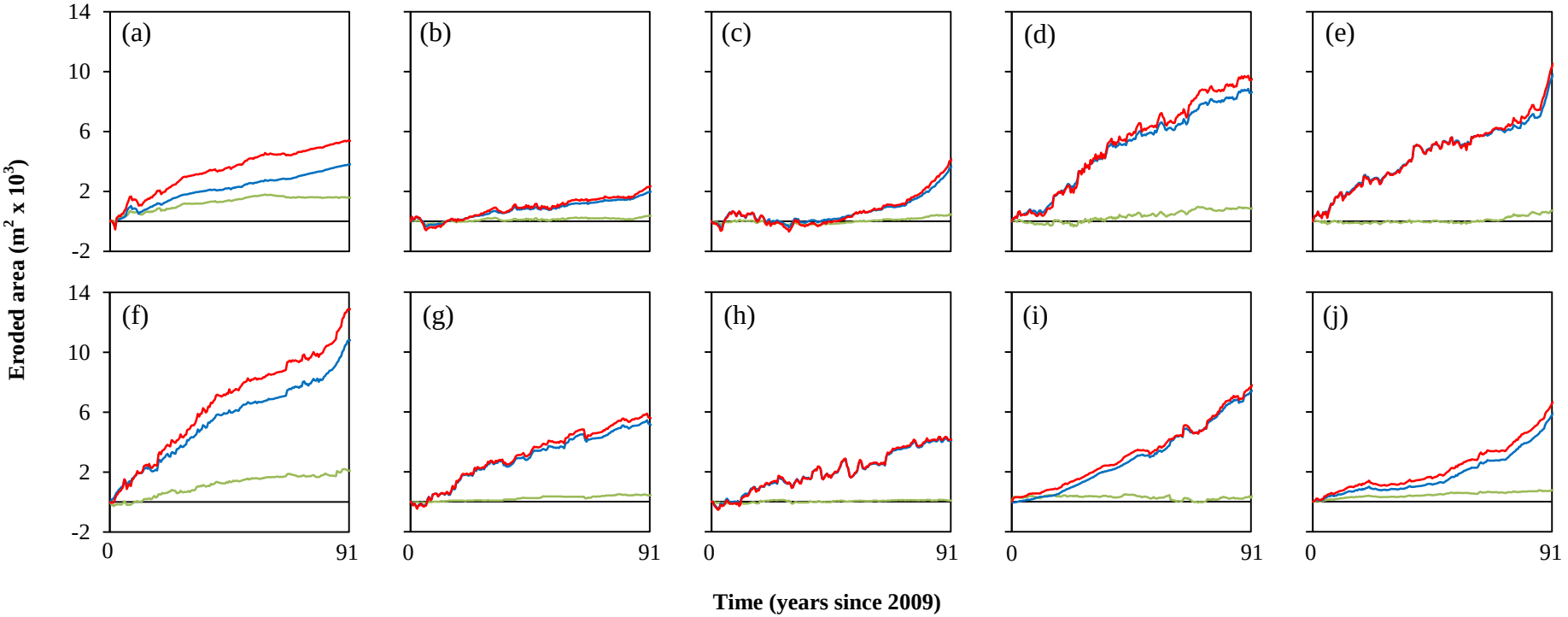

Figure 6.20 Cumulative eroded area at the ten cross-section locations for Model 24, showing total (red), bed (green) and bank (blue) erosion. (a) LO030; (b) LO040; (c) NF100; (d) NF120; (e) NF300; (f) NF320; (g) NF350; (h) NF375; (i) CA225; (j) CW245.

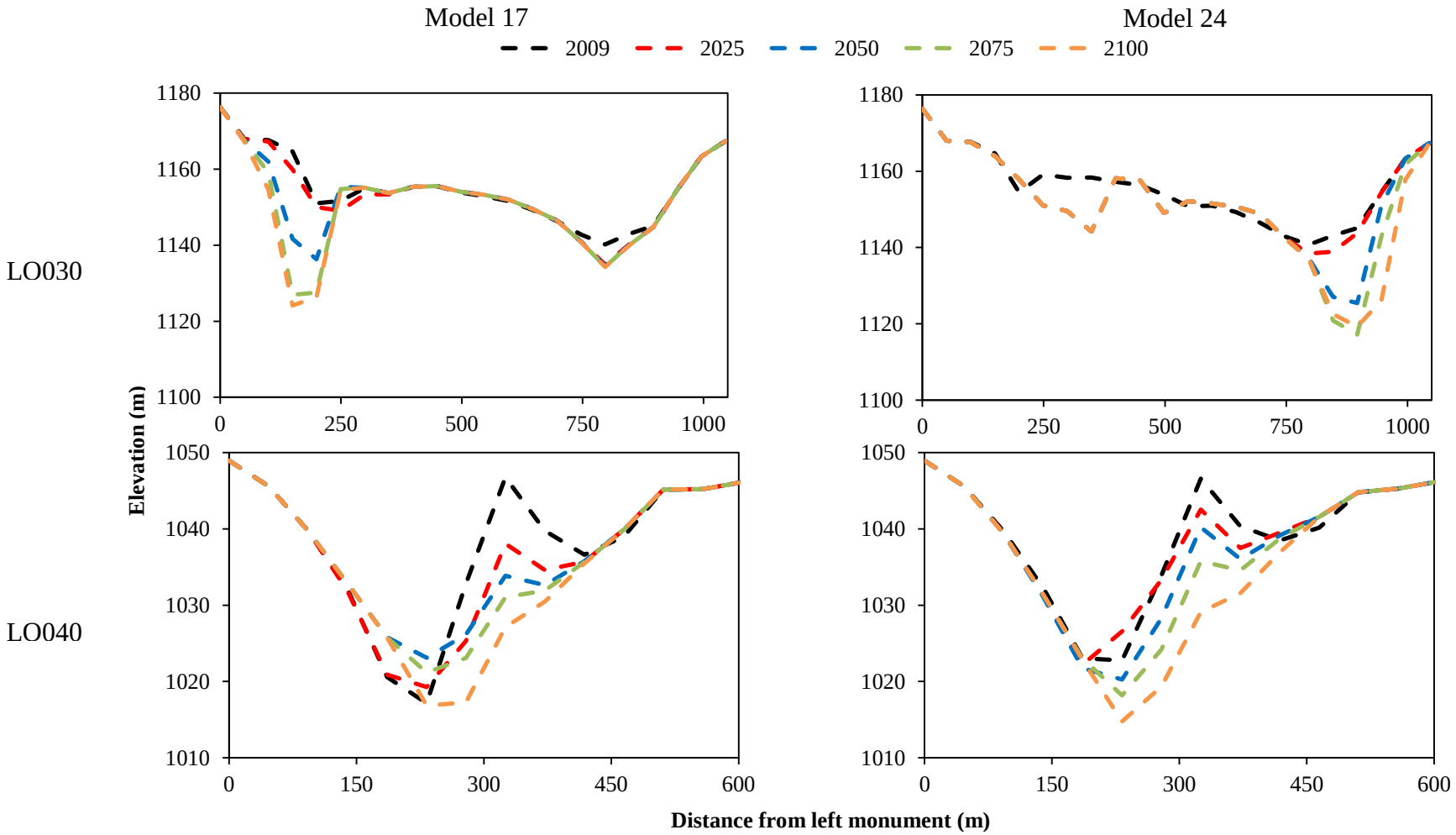

Figure 6.21 Profiles modelled at the ten cross-sections by Models 17 and 24 in 2009, 2025, 2050, 2075 and 2100.

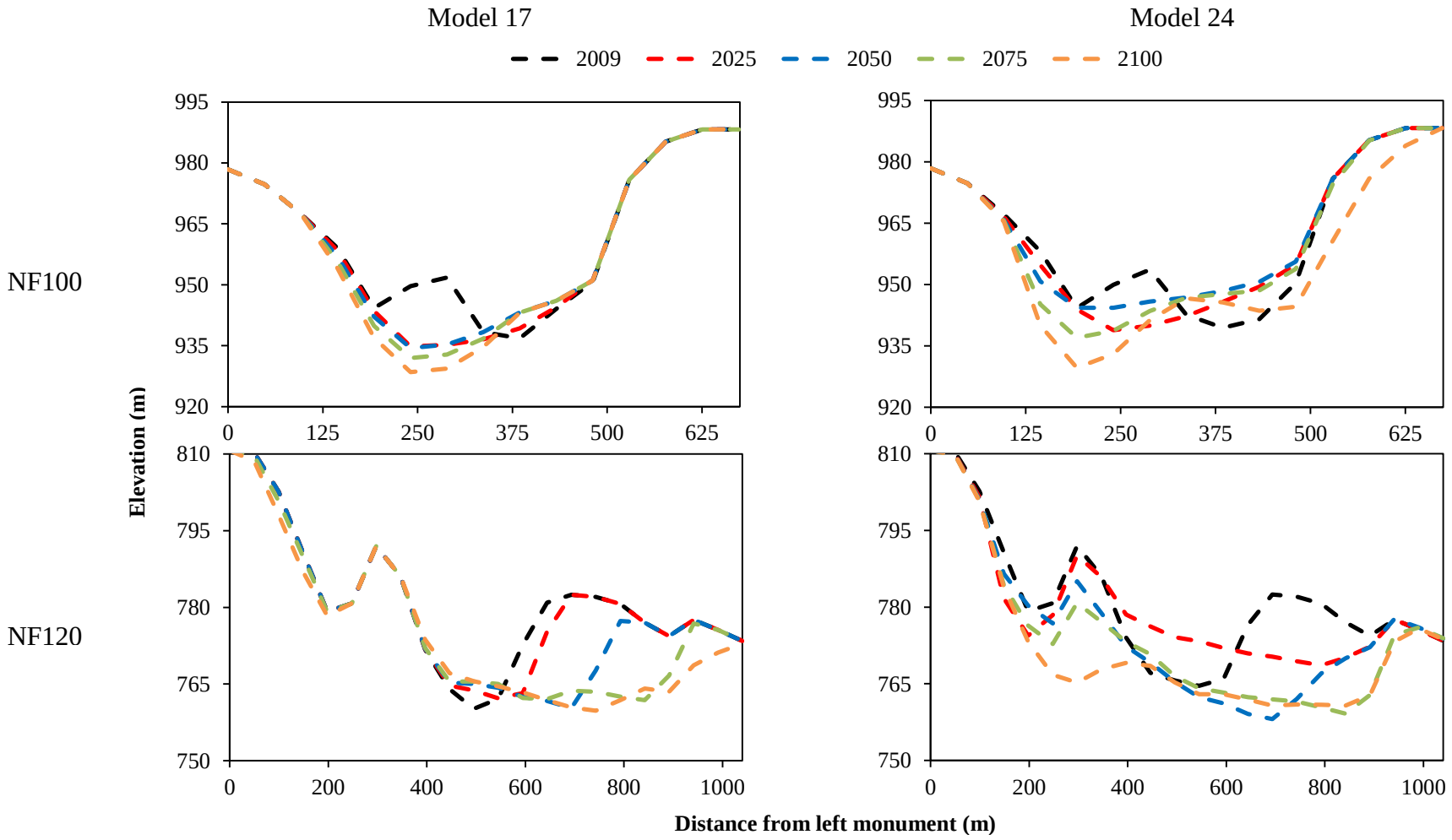

Figure 6.21(cont.) Profiles modelled at the ten cross-sections by Models 17 and 24 in 2009, 2025, 2050, 2075 and 2100.

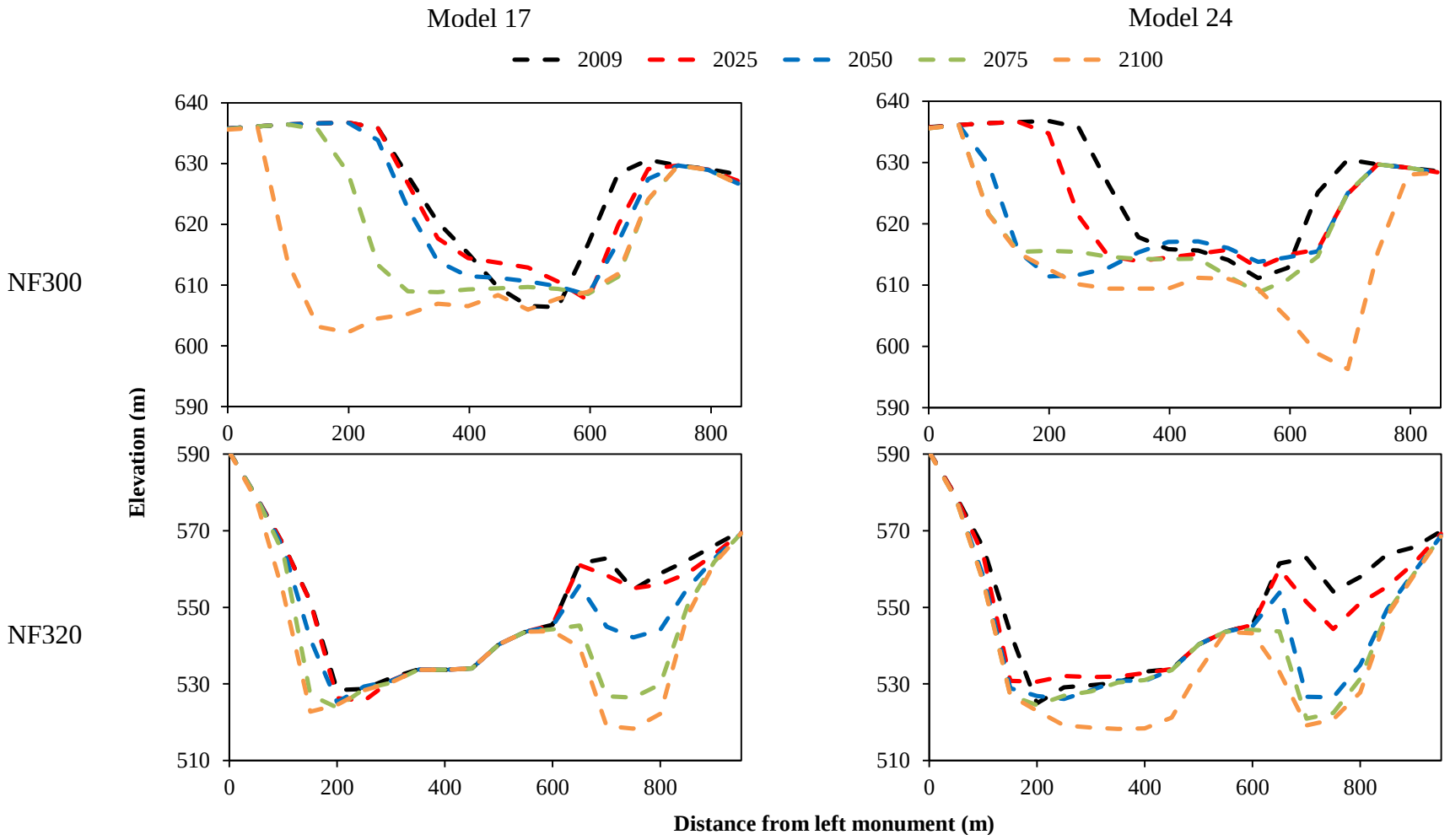

Figure 6.21(cont.) Profiles modelled at the ten cross-sections by Models 17 and 24 in 2009, 2025, 2050, 2075 and 2100.

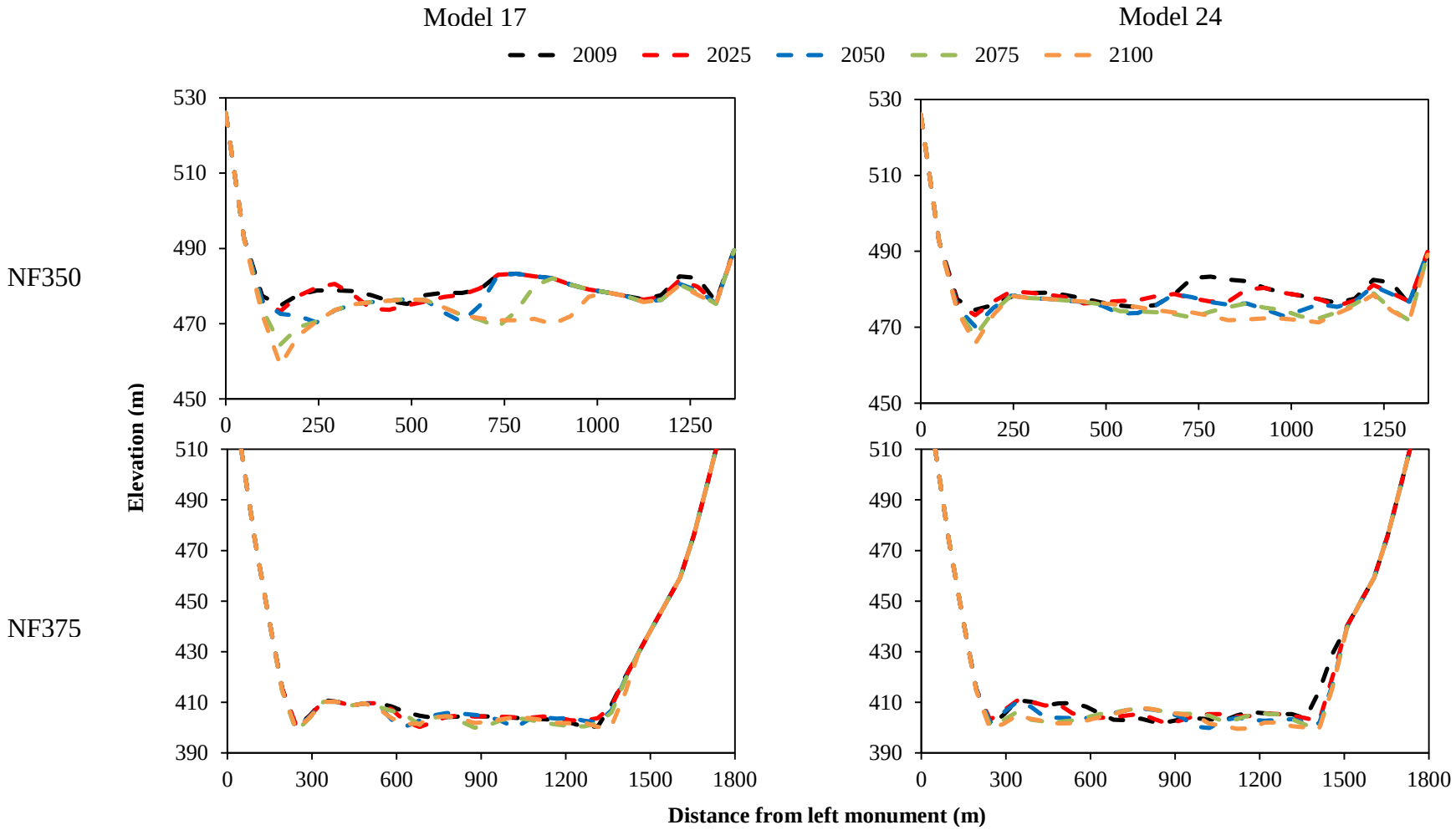

Figure 6.21(cont.) Profiles modelled at the ten cross-sections by forecasting runs 17 and 24 in 2009, 2025, 2050, 2075 and 2100.

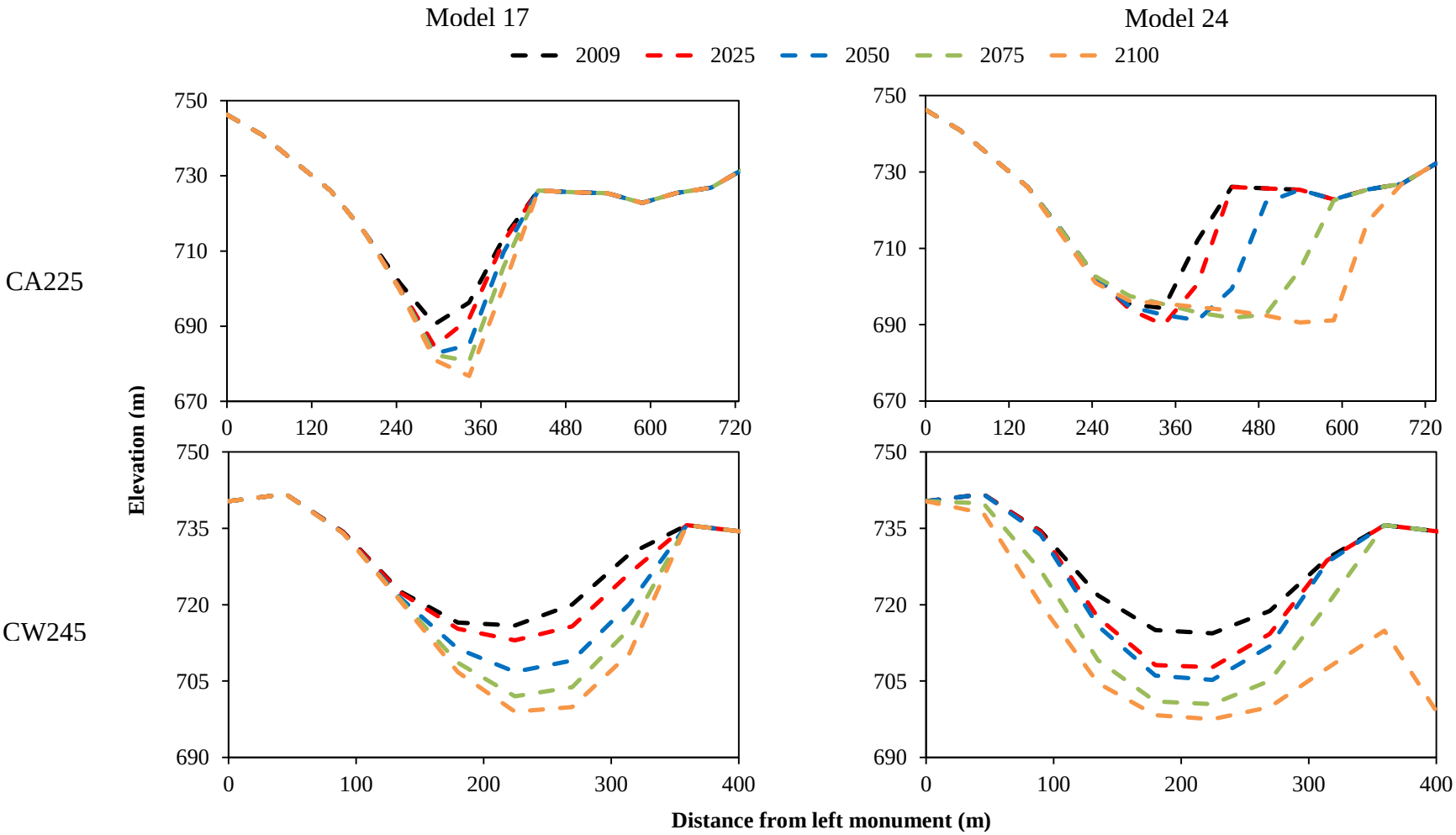

Figure 6.21(cont.) Profiles modelled at the ten cross-sections by forecasting runs 17 and 24 in 2009, 2025, 2050, 2075 and 2100.

Figures 6.19 and 6.20 show that the contribution of lateral erosion to sediment production exceeds that of bed lowering throughout the course of the 91-year simulations, with the difference between them generally increasing through time. This is the case because supplies of sediment from bed scour are predicted to decline asymptotically as bed elevations stabilise at most cross-sections, while rates of sediment production from bank sources decrease less markedly, if at all. This is particularly apparent in the simulation produced using Model 24 (Figure 6.20) which has the higher value of the lateral erosion coefficient. In this simulation, contributions from bed sources decay to negligible levels towards the end of century at most cross-sections.

In Model 17 (Figure 6.19), however, the supply of sediment from bed lowering is more persistent, although rates still decay and cumulative curves flatten towards the end of the simulation. Moreover, while rates of sediment production from channel widening decline at most cross-sections in Model 17 (which has the lower value of the lateral erosion coefficient) (Figure 6.19), such a decline is not apparent in Model 24 and rates of widening remain constant or increase towards the end of the simulation in this case (Figure 6.20).

The nonlinearities in total catchment sediment yield identified in Figures 6.16 and 6.17, together with those evident in Figures 6.19 and 6.20 for channel geometry changes, are not pronounced and may also be linked to the hydrological variability described above in sub-section 6.3.4 (a possibility which is considered further in sub-section 6.5.2, below). Nonetheless, this analysis demonstrates that for both C-L configurations used here, modelled rates of sediment output from the upper North Fork Toutle River catchment are not as linear as a brief inspection of Figure 6.12 would suggest. As such, it is evident that annual sediment yields are not predicted to remain constant and that they may, in fact, decline and/or increase during the course of the 21st century. Moreover, it is apparent that the timing, sequencing and degree of this decline depend predominantly on the modelled rate of lateral erosion. Specifically, when lateral erosion rates are low (exemplified using Model 17), annual sediment yield declines persistently during the remainder of the century

(Figure 6.16). Conversely, when the modelled rate of lateral erosion is high (exemplified using Model 24), annual sediment yield initially increases, before declining slightly towards the end of the century (Figure 6.17).

Given the fact that nonlinearities in cumulative sediment yield have been identified, the results presented here support, to an extent, the conclusion reached in the WEST (2002) and Simon and Klimetz (2012) reports that sediment yields are likely to decline at some point in the future. Having said that, based on the results of C-L modelling, it is apparent that the rate and overall degree of decay in annual sediment yield from the upper North Fork Toutle River between now and 2100 seems likely to be substantially lower than that forecast by either WEST (2002) or Simon and Klimetz (2012). In this regard, the linear trend identified by the Biedenharn Group (2010) may be a better approximation.

The broadly linear trend identified in C-L predictions of cumulative sediment yield, which implies that yields are likely to remain elevated above post-eruption levels for at least a century, is supported by a number of other studies that have documented the long-term response of fluvial systems disturbed by large, explosive volcanic eruptions. For instance, Pierson et al. (2011) found that post-eruption recovery of the Sandy River to a well-armoured single-thread channel following the Old Maid eruption of Mount Hood, Oregon, USA, in the late 18^{th} century took 50 to 100 years. Moreover, the massive 26.5 ka Oruanui eruption, New Zealand, triggered a period of fluvial instability that lasted more than 10,000 years (Manville and Wilson, 2004).

C-L predictions should also be put in the context of documented recovery trajectories following other natural and anthropogenic disturbances. Examples include the 1923 Kanto earthquake, Japan, which is known to have affected sediment discharge for over 80 years (Koi et al., 2008). Similarly, large coseismic landslides in South Westland, New Zealand (Korup, 2005), and the input of hydraulic mining debris in the Sierra Nevada, USA (e.g. James, 1989) have resulted in elevated sediment yields from affected river basins that have persisted for at least a century. These studies therefore illustrate that the

prolonged recovery period modelled by C-L in this study is by no means unprecedented.

6.5.2 Accounting for hydrological non-stationarity in discharge projections

The analyses reported above reveal that cumulative sediment yields from the upper North Fork Toutle River catchment were generally predicted in C-L simulations to increase as a linear function of time elapsed since 2009. However, deeper analysis of trends in data generated from two selected model runs provided evidence of nonlinear behaviour in both simulations. The apparent decay in annual sediment yield evident for simulations in which the modelled rate of lateral erosion is lower may, in part, be explained by stabilisation of channel bed elevations. However, the drivers of nonlinearities apparent for simulations in which the modelled lateral erosion rate is higher are less clear.

As such, the possibility remains that nonlinearity in catchment erosion is being masked or driven by the hydrologic non-stationarity associated with discharge projections obtained from the CBCCSP that is evident in Figure 6.11 (and which has been described in sub-section 6.3.4) in both simulations. As discussed in sub-section 6.3.1, it must be noted that the times series behaviour of the 18 future mean daily discharge simulations used to drive the C-L models was derived by the CBCCSP from historical data obtained between 1915 and 2006. As such, although the magnitude and intensity of individual events, such as floods and low flows, are driven by signals in the monthly GCM simulations, decadal scale variations in discharge reflect those observed during the 20th century (Hamlet et al., 2010; Tohver et al., 2014).

To investigate the potential influence of hydrological non-stationarity, annual sediment yields predicted by each model were divided by annual runoff to generate time series of mean annual sediment concentration. When the results of these analyses are plotted separately for the two C-L model configurations (Figure 6.22 and Figure 6.23) differences between the way sediment concentrations simulated by the two set ups vary through the course of the

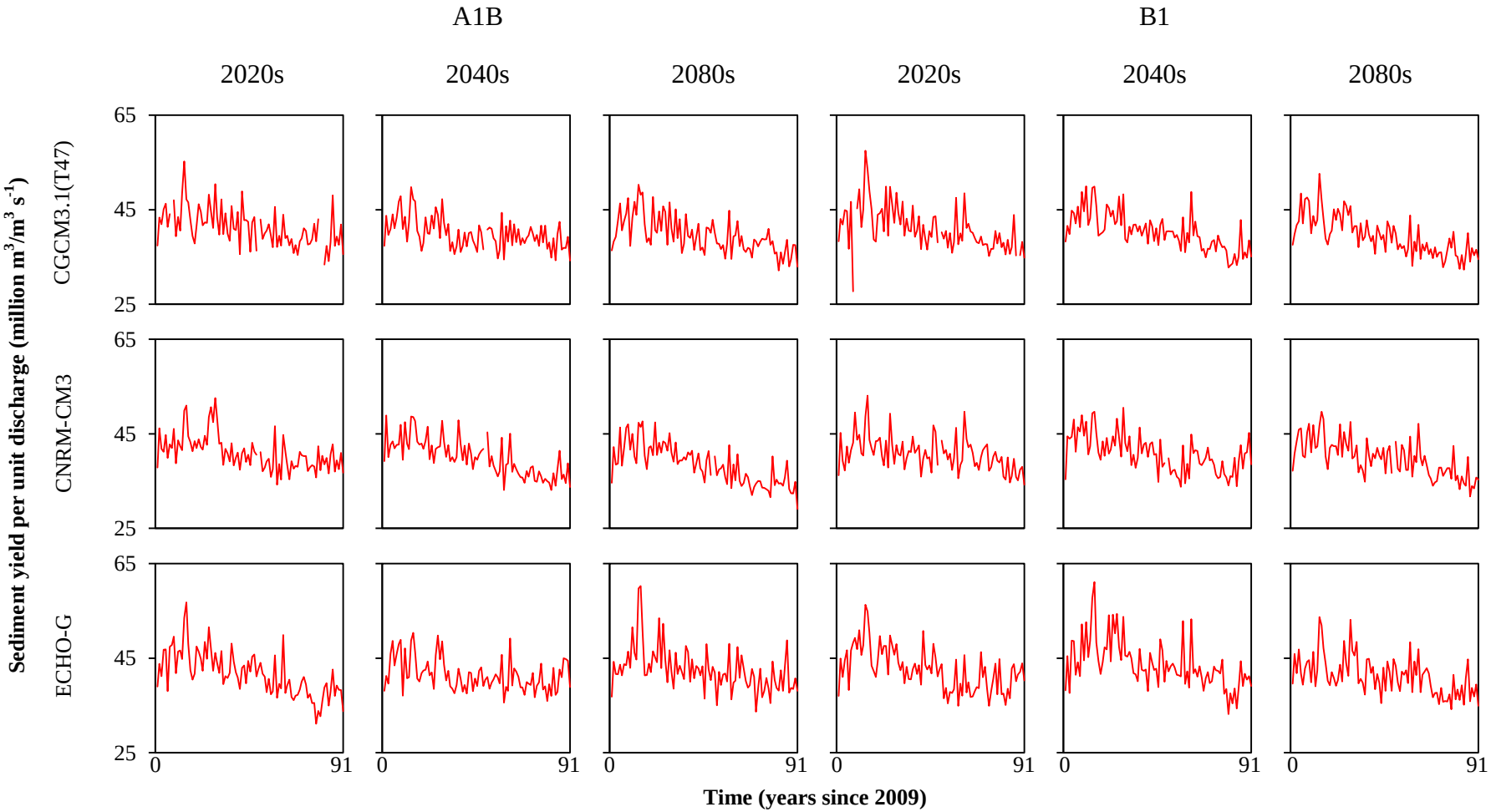

Figure 6.22 Time series of annual average sediment concentrations in runs with the lower rate of lateral erosion (i.e. Model 60 from hindcasting).

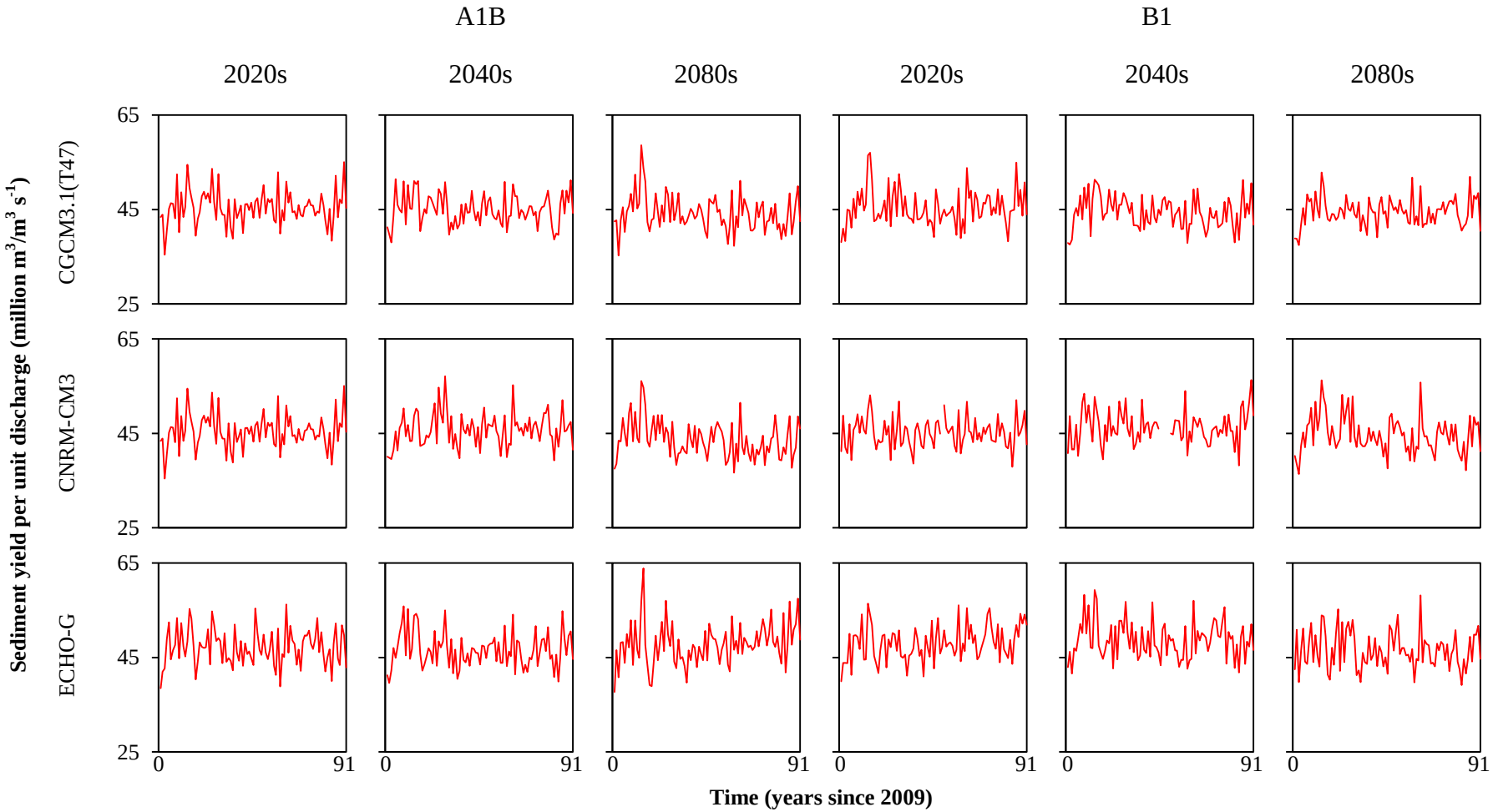

Figure 6.23 Time series of annual average sediment concentrations in runs with the higher rate of lateral erosion (i.e. Model 75 from hindcasting).

simulations are immediately apparent. Figure 6.22 shows that sediment concentrations decrease throughout the 91-year simulation for the majority of runs that used the configuration of Model 60 from the hindcasting period and therefore feature the lower rate of lateral erosion. This indicates that when channel lateral mobility is lower and sediment yield is more dependent on bed scour and channel degradation, yields decline through time, but that the impact of this decay on annual sediment yields is effectively masked by increases in annual runoff that occur in the second half of the 21st century. Conversely, Figure 6.23 shows that for runs using the higher lateral erosion rate (based on the configuration of Model 75 from hindcasting), sediment concentrations are maintained throughout the simulations, so that changes in annual runoff produce commensurate increases in sediment yields. It emerges, therefore, that trends in sediment yield noted in Section 6.5.1 for this model set up (see Figure 6.17) result from hydrological non-stationarity and that there is no evidence that catchment sediment yield is decaying in this scenario.

In summary, sediment yield in all simulations is dominated by lateral erosion and channel widening throughout the 21st century, and the overall trend in the cumulative sediment yield from the upper North Fork Toutle River is predominantly linear. However, rates of widening and therefore annual sediment yield are predicted to decline at some point by each model configuration. In low lateral erosion runs, the decline begins approximately midway through the century, and is thought to be associated with stabilisation of both the channel long profile and valley bottom width. The magnitude of this decline is masked, however, by increases in annual runoff in the second half of the 21st century, and is therefore more evident in plots of annual sediment concentration (Figure 6.22). On the other hand, stabilisation of the channel long-profile that results from a reduction in bed scour during the middle of the century has a less significant impact on annual sediment yield in high lateral erosion runs because lateral erosion increases with increased runoff. As such, annual sediment yield increases during the first half of the 21st century in these runs due to an increase in annual runoff. The rate at which cumulative sediment yield increases with time then declines towards the end of the century, potentially as a result of increased valley width which reduces the

efficacy of lateral erosion processes, but also due to a reduction in annual runoff. Temporal trends in sediment yields for higher lateral erosion runs are therefore predominantly driven by hydrological non-stationarity.

6.6 FORECASTING BEYOND 2100: SEDIMENT YIELDS AND TRENDS DURING THE 22ND CENTURY

Analyses presented above in Section 6.5 indicate that although cumulative sediment yields display a predominantly linear trend during the 21st century, there is some evidence for decay in rates of sediment production, particularly when lateral erosion rates are lower. To further investigate this and provide an indication if, and when, future sediment yields might be expected to decline significantly, Models 17 and 24 (which were used for analysis in sub-sections 6.4.3 and 6.5.1) were run for an additional 91 years. These runs were effectively continuations of those discussed previously, with these particular models again selected in order to encompass the range of likely possible sediment futures.

The models were driven using the same input flow series that were used for the initial (2009 to 2100) simulations (see sub-section 6.3.4 for details). Extending the modelling period by doubling its duration is speculative as uncertainties in model outcomes grow with run time, but the results may nevertheless provide some idea of how the catchment may evolve over the longer-term. Models 17 and 24 predict that an additional 175 to 275 million m^3 of sediment may be exported from the upper North Fork Toutle River catchment between 2100 and 2091, which is 10 to 15% less than that predicted using the same models for the period between 2009 and 2100 (205 to 307 million m^3).

Figure 6.24 presents cumulative sediment yield curves for the 22nd century produced using both models, together with time series plots of the residuals between the predicted annual sediment yields and a straight line connecting the first and last data points (repeating the investigation of shorter-term trends in the prediction undertaken for the 21st century in sub-section 6.5.2). Decade-average annual sediment yields are listed in Table 6.15.The results suggest that

the predominantly linear trends in cumulative sediment yields displayed during the 21st century will continue in the 22nd century. As a result, the annual sediment yield in the 2180s is predicted to be only 12 to 13% lower than that in the 2110s (see Table 6.15 and compare with Table 6.14).

However, residual plots (Figure 6.24(b) and (c)) reveal a greater degree of nonlinearity in annual yields than that detected in the 21st century (compare Figure 6.24 with Figure 6.16 and Figure 6.17). In Figure 6.24(c) the distribution of residuals for Run 24 (higher lateral erosion coefficient) exhibits a pattern that is clearly similar to the idealised distribution represented in Figure 6.18(d), which contrasts with the 21st century results plotted in Figure 6.17. This finding provides evidence that annual sediment yields may decline significantly after 2100 rather than varying in response to non-stationarity and variability in annual runoff, as was inferred during the 21st century. Decay in sediment yields predicted during the 21st century using Model 17 (lower lateral erosion coefficient) is projected to continue throughout the 22nd century, although sediment production remains stubbornly high in the 2180s.

Time series of sediment concentration plotted in Figure 6.24(d) and (e) provide further evidence to suggest that sediment production will decline during the 22nd century, albeit slowly. Sediment concentrations predicted using both models clearly display downward trends throughout the simulation. This trend is strongest for Model 17 (Figure 6.24(d)), which is consistent with the lower lateral erosion rate in that model set up. The downward trend evident for Model 24 (Figure 6.24(e)) is less marked but still contrasts sharply with the equivalent graph plotted using the results of Model 24 for the 21st Century (Figure 6.23). This suggests that sediment yield is predicted to decay during the next century even using the higher lateral erosion rate. That would indicate that valley bottom width may start to stabilise before the 2180s even if the high values of bank and slope erodibility associated with the higher lateral erosion rate are representative of current and future conditions in the upper North Fork Toutle River catchment.

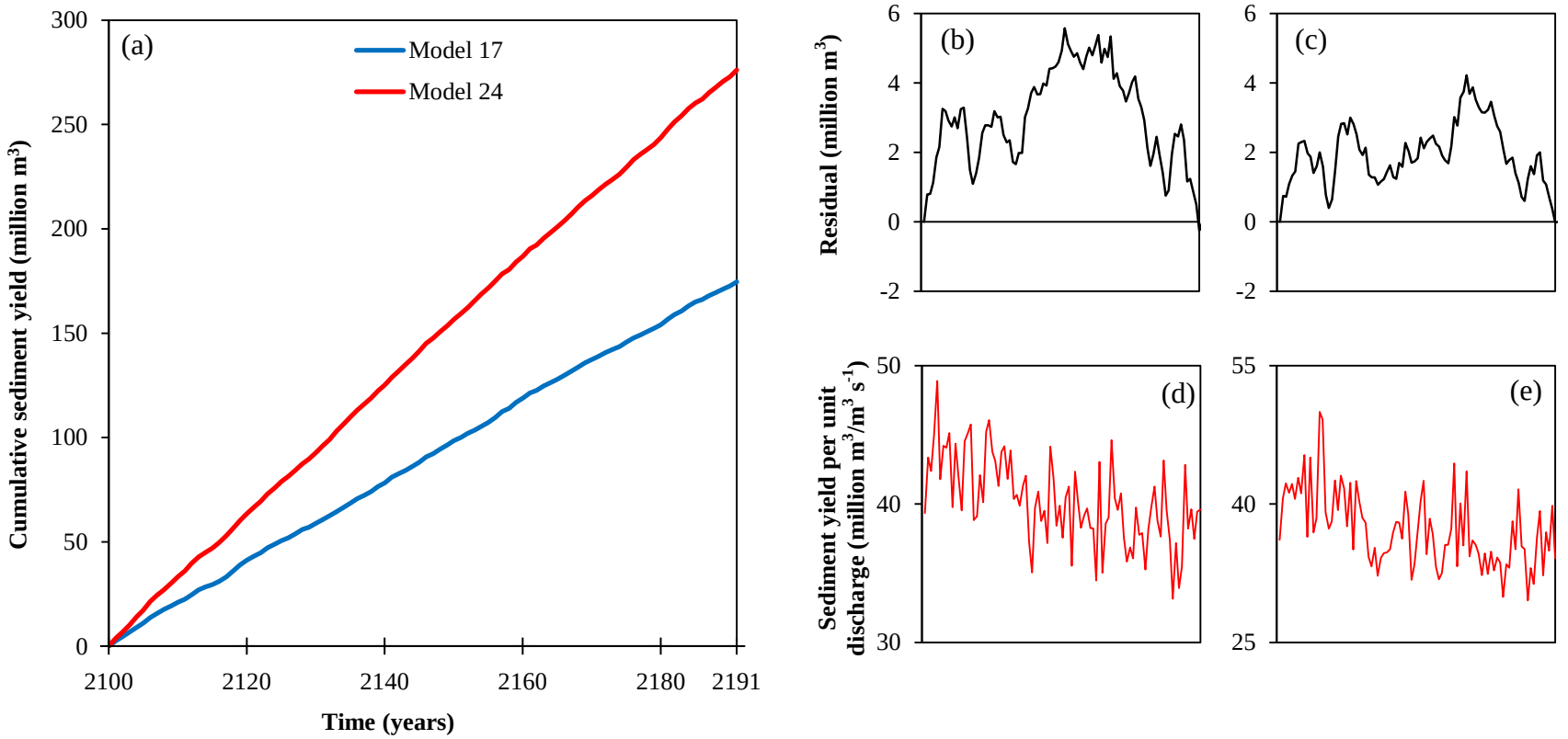

Figure 6.24 (a) cumulative sediment yields for Models 17 and 24; (b) and (c) residuals calculated between the modelled erosion volumes and those predicted by a straight line for Models 17 and 24 respectively; (d) and (e) sediment yield per unit volume of discharge for Models 17 and 24 respectively.

Table 6.15 Decade-averaged annual sediment yields between 2100 and 2191 for Models 17 and 24. †2180s covers the period 2180 to 2191.

	Average annual sediment yield (million m^3)	
Decade	Run 17	Run 24
2100s	2.10	3.35
2110s	2.01	3.02
2120s	1.78	2.93
2130s	1.93	3.26
2140s	1.98	3.11
2150s	2.03	3.01
2160s	1.83	2.91
2170s	1.67	2.78
2180s†	1.85	2.92

6.7 SUMMARY

This Chapter began by noting the lack of studies which have attempted to make quantitative, chronological predictions in fluvial geomorphology using numerical models to inform decision-making. It was argued that this research gap is the result of widespread and understandable caution amongst modellers regarding the capability of their models in this context. This caution is thought to stem from the significant challenges associated with prediction, which were outlined in detail in Section 6.1. These include: qualitative and quantitative model uncertainties; the difficulty in defining initial conditions; historical path dependency; and the complex nonlinear behaviour of disturbed fluvial systems. Although it was acknowledged that this research can neither avoid nor entirely resolve these issues, they form the context in which the predictions made in this Chapter should be evaluated and assessed.

A further significant challenge to developing predictions in fluvial geomorphology is the incorporation of climate change information into hydrological driving data sets to reflect its expected impact on flow regimes. Recent studies have indicated that future climate change could lead to significant changes in average annual runoff, both positive and negative, across more than 80% of the global land surface. However, representations of climate change in past applications of C-L's predecessor CAESAR, for instance, have been highly simplistic and involved increasing and/or decreasing the magnitude of rainfall events in the historical record. The work presented in this Chapter attempted to improve upon this by using state-of-the-art climate projections specific to the Pacific Northwest region developed by the Columbia Basin Climate Change Scenarios Project (CBCCSP).

The CBCCSP produced a comprehensive and up-to-date database of simulated hydrological data in the Columbia River basin that incorporates climate change information from the IPCC Fourth Assessment Report. The processing procedure used in the CBCCSP, which was summarised in Section 6.2, involved downscaling raw GCM outputs and implementing a macro-scale hydrologic model to develop a suite of outputs, including runoff, precipitation, SWE and temperature, for 297 streamflow locations throughout the Columbia River basin. One of these locations was on the Toutle River at the USGS Tower Road gauge meaning that hydrological variables, specifically daily streamflow, archived at this location could be used in future long-term C-L simulations of the upper North Fork Toutle River catchment.

In total, 76 possible realisations of future hydrological variables for the Columbia River basin were available at Tower Road. These include two GHG emissions scenarios (A1B and B1), 10 GCMs, three downscaling techniques (CD, BCSD and HD) and, for the CD and HD downscaling techniques, three future time periods (2020s, 2040s and 2080s). An analysis of the advantages and disadvantages of the three downscaling procedures in Section 6.3, however, indicated that only the HD technique was appropriate for the current application. This is because it is the only method that preserves the temporal structure of the observed (historical) data, while allowing for the effects of

changing probability distributions of temperature and precipitation on climatic extremes to be represented.

Moreover, it was not necessary to use each of the 10 GCM projections because a number of them were found to forecast similar future hydrologic regimes. As such, three GCM projections were selected (Section 6.3) which represented contrasting futures for runoff and hydrological characteristics of the upper North Fork Toutle River catchment. The selected GCMs therefore encapsulated the range of all available scenarios employed by the CBCCSP so that the uncertainty associated with these forecasts was represented to as great an extent as possible. In total, 18 different runoff projections, consisting of three GCMs, three future time periods and two GHG emissions scenarios, were implemented within the two C-L model configurations that had previously been identified in Chapter 5 so that 36 separate forecasts of future catchment sediment yield from the upper North Fork Toutle River catchment were produced. Each forecast spanned a 91-year period from 2009 to 2100.

C-L forecasts of cumulative catchment sediment yield in 2100 presented in Section 6.4 fell between those projected from relationships reported by the Biedenharn Group (2010) and Simon and Klimetz (2012). Cumulative yields were, however, similar to those reported by WEST (2002). Despite the fact that C-L configurations and future hydrologic scenarios were selected to encapsulate as much of the uncertainty associated with these two factors as possible, the range of sediment yields forecast by C-L was surprisingly well-constrained in that the difference between the maximum and minimum C-L predictions was approximately +/- 20% of the mean predicted value. Intuitively, higher predictions of cumulative sediment yield were found to be associated with models that used the higher rate of lateral erosion, and those that used hydrological forecasts derived from the CGCM3.1(T47) climate model which projects the greatest increase in annual runoff relative to historic observations.

One of the most important uncertainties associated with previous forecasts of long-term sediment yield from the upper North Fork Toutle River was whether

annual sediment yields would decay through time or not. Initial visual assessments of C-L forecasts indicated that the projected temporal trend was broadly linear through to 2100. Although this supports the prediction made by the Biedenharn Group (2010), it contradicts the conclusions of WEST (2002) and Simon and Klimetz (2012), together with the well-established theory of the rate law. As such, it was necessary to undertake further, in-depth analyses of the temporal patterns of sediment yield predicted by C-L to assess whether this broad linearity masked any significant multi-decadal trends. This included an investigation of the influence of hydrologic non-stationarity on annual sediment yield variations.

The results of this analysis, which are presented in sub-sections 6.5.1 and 6.5.2, indicated that all models showed a degree of nonlinearity (albeit unpronounced), the pattern of which varied between C-L configurations. Specifically, in low lateral erosion runs annual sediment yields appear to decay consistently and probably as a result of stabilisation of the long profile over time. This decay was seen to be independent of variations in runoff volume as higher flows towards the middle of the century were seemingly insufficient to counteract the reduction in slope and mobility of the bed material. Nonetheless, hydrological variations were found to mask this decay to a certain extent.

In high lateral erosion runs, however, sediment yields increase towards the middle of the century as the reduction in bed scour has a less significant impact on lateral erosion in this scenario. The rate at which cumulative sediment yield increases with time then declines towards the end of the century potentially as a result of increased valley width which reduces the efficacy of lateral erosion processes. However, analyses of the influence of hydrological non-stationarity in sub-section 6.5.2 revealed that the trends in sediment yield for this scenario are predominantly driven by variations in runoff volume and that there is no evidence that erosion rates declined in these runs.

Given the lack of significant decay identified during the 21st century, two speculative model runs were undertaken in order to provide an indication of if, and when, future sediment yields may be expected to decline substantially.

These runs suggested that the predominantly linear trend will continue beyond 2100, although deeper analysis revealed a greater degree of nonlinearity in annual yields than that detected in the 21st century. Furthermore, annual sediment concentrations were shown to decline in both the high and low lateral erosion scenarios, indicating that valley bottom widths may begin to stabilise before the end of the 22nd century, even if high values of bank and slope erodibility associated with the higher lateral erosion rate are representative of current and future conditions in the upper North Fork Toutle River catchment.

CHAPTER 7 DISCUSSION

7.1 UNDERSTANDING MODELLED FORECASTS OF LONG-TERM SEDIMENT YIELD FROM THE UPPER NORTH FORK TOUTLE RIVER CATCHMENT

The results presented in Chapter 6 potentially have significant implications for long-term sediment management in the Toutle-Cowlitz River system, and these implications are discussed in more detail in Section 7.3. However, before model projections generated by C-L can be considered for use in planning and management, it is necessary to assess the extent to which these results can be explained on the basis of a physical understanding of the upper North Fork Toutle River catchment and the processes operating within it. A qualitative assessment of model results in the context of the contemporary landscape is therefore essential, and evidence obtained during field reconnaissance can be used as the basis for such an assessment.

It was noted in Chapter 6 that the predominantly linear trends of future long-term sediment yield from the upper North Fork Toutle River projected by C-L are driven by lateral shifting and channel widening. Four key features of the channel and hillslope morphology observed in the catchment support the results of C-L and suggest that widening is indeed likely to dominate future sediment production. These are:

1. Channels in upstream reaches have incised to form deep canyons with near-vertical walls;
2. These headwater canyons are generally narrow with no distinct floodplain; consequently, close coupling exists between the channel and valley walls;
3. Both the channel banks and canyon walls are composed of debris avalanche material which is mostly in situ and which contains a high proportion of fine-grained sediment;

4. Channels in downstream reaches are unconstrained, wide and braided at high flows; consequently they continue to interact with the valley sides, despite the greater width of the valley floors in these reaches.

Figure 7.1 and Figure 7.2 illustrate the first three features listed above. As discussed in Chapter 2, early channel adjustments were dominated by incision, particularly in upstream reaches, as a result of drainage reintegration on the debris avalanche by processes of lake filling-and-spilling. The outcome was that at the end of this period of incision the majority of streams had developed deep, steep-sided channels surrounded by narrow floodplains, such as that evident in Figure 7.1. In many of the upstream reaches, channel bank heights are of the order of tens of metres. Undercutting and gravity failures of these banks, as illustrated in Figure 7.2, therefore result in large volumes of sediment being mobilised during a single flood event. The resistance of banks to lateral erosion is also low because they are commonly composed of poorly sorted, noncohesive debris avalanche material, the characteristics of which were described in detail in Chapter 4.

In downstream reaches, channel planform and valley floor morphology are also indicative of high lateral mobility. Specifically, the channels are predominantly multi-thread (wandering or braided at high flows), with the traces of numerous channels that would be active during higher flows evident in the floodplain (Figure 7.3). Wandering and braided streams are characterised by frequent shifts in channel pattern and position, leading to them reworking alluvial deposits frequently and repeatedly (Knighton, 1998), maintaining high rates of sediment transport, exchange and production.

If abundant bedload is supplied from the narrow canyons upstream, as C-L forecasts it will, the wandering/braided planform farther downstream in the upper North Fork Toutle will persist and the elevated yield of sediment to the sediment plain, SRS and beyond would be expected to continue unabated. This situation would be expected to prevail until the planform pattern of the North Fork Toutle evolves from braided to single-threaded, which is unlikely without a significant reduction in the sediment supply from upstream. As the mainstem

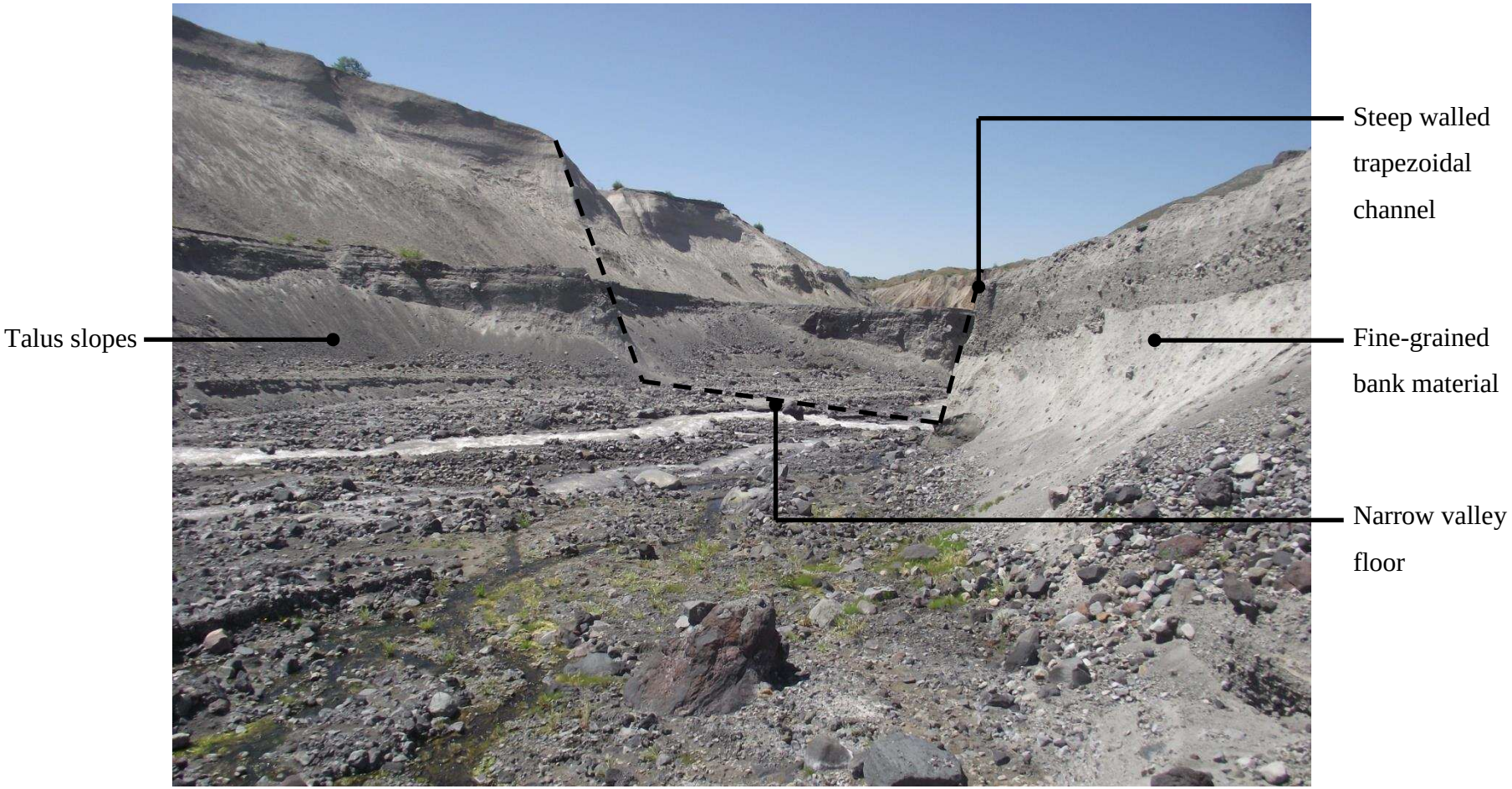

Figure 7.1 Upper North Fork Toutle River near NF100 exemplifying the key features identified as being responsible for continued lateral erosion in upstream reaches. Photograph by author (2011). Direction of flow is left to right.

Figure 7.2 Upper North Fork Toutle River near NF120 showing the channel impinging on the toe of its very high and steep bank. Photograph by Colin Thorne (2011). View upstream.

Figure 7.3 Upper North Fork Toutle River near NF350 showing lateral reworking of floodplain and terraces by the multi-thread, wandering/braided planform in downstream reaches. Photograph by Colin Thorne (2009). View upstream.

and tributaries show no evidence of stabilising, the extended duration of lateral shifting, widening and elevated sediment loads to date is not only explicable, it is likely to persist. Contemporary form and process in the upper North Fork Toutle River therefore provide ample evidence to support the outputs of C-L modelling, which predict that the sediment yield, driven predominantly by lateral erosion and widening, is likely to remain high and that, consequently, C-L projections of long-term sediment yield are realistic.

7.2 RELEVANCE OF MODELLED EROSION PROCESSES AND TRENDS TO UNDERSTANDING CHANNEL ADJUSTMENTS IN SEVERELY DISTURBED FLUVIAL SYSTEMS

The dominant role of lateral erosion in extending elevated production of sediment from the upper catchment of the North Fork Toutle River has been alluded to in a number of previous studies (e.g. Meyer and Martinson, 1989; Simon and Thorne, 1996; Simon, 1999; Major et al., 2000; Simon and Klimetz, 2012). Simon and Klimetz (2012, p. 84), for instance, found that bank erosion contributes "an estimated 80% of the material being eroded from channel boundaries" while Major et al. (2000, p. 821) remark that "sediment entrainment relies primarily on bank collapse during trench widening, rather than bed scour" and, "if bank instability persists, high sediment yield persists".

These and other such statements further support the evidence gained from field reconnaissance presented above. However, the outcomes of modelling performed in the present study contrast with predictions reported in Simon and Klimetz (2012) in that C-L predictions indicate that rates of lateral erosion will not decay substantially during the remainder of this century and that, consequently, sediment yield from the catchment will persist to 2100 and beyond. This discrepancy deserves consideration and explanation.

The Simon and Klimetz (2012) forecast is based on application of the rate law, which was first proposed by Graf (1977) (see also Chapter 5). The rate law takes the form of a negative, exponential decay function and reflects the observation that in many disturbed fluvial systems the rate of relaxation or

adjustment to a new equilibrium condition begins rapidly but slows nonlinearly, both through time and with distance from the point of maximum disturbance (Graf, 1977). Although initially introduced in the context of gully network development (Graf, 1977), the concept has been successfully applied to describe post-disturbance channel response in a variety of contexts (e.g. Williams and Wolman, 1984; Simon, 1992; Hooke, 1995; Simon and Thorne, 1996; Prosser and Soufi, 1998; Simon, 1998; Surian and Rinaldi, 2003; Leon et al., 2009; Wu et al., 2012; Zheng et al., 2014).

The negative, exponential form of the rate law implies that a negative feedback loop is operating to dampen the effects of disruption and so cause a reduction in the rate of change through time (Graf, 1977). In the context of bed elevation change, this negative feedback is thought to result from opposing trends of change in boundary and critical shear stresses through time (Simon and Thorne, 1996). Boundary shear stress decreases as channel evolution progresses due to channel widening and reduction in channel gradient. Simultaneously, critical shear stress increases due to bed armouring, and these trends combine to dampen vertical channel adjustments over time (Simon and Thorne, 1996).

The theoretical basis for the rate law and nonlinear decay is well-established and it has been demonstrated empirically in a number of studies, examples of which are cited above. While its validity in many situations is accepted, the results of C-L simulations presented in Chapter 5 question the applicability of the rate law to prediction of long-term trends in sediment yield from the upper North Fork Toutle River.

To explore this further, the data provided by Simon and Klimetz (2012) to support the use of negative exponential decay functions were re-examined, taking into account not only the model outcomes reported here but also the evidence provided recently by Zheng et al. (2014). While Zheng et al. (2014) provide examples of how rates of change of bed elevation have decayed through time at multiple sections distributed along the length of the upper North Fork Toutle River, the Simon and Klimetz (2012) report presents data

from just three cross-sections: NF300, NF310 and LO033. The data used to derive these graphs were not provided in the Simon and Klimetz (2012) report and so, in this study, the points plotted on their graphs were digitised to facilitate data extraction and support the further analysis reported here (Figure 7.4).

Coefficients of determination (r^2 values) for the exponential regression models for cumulative bed, bank and total erosion at the selected cross-sections were reported in Simon and Klimetz (2012) as a means of quantifying the fit of the model to the data (Table 7.1). Seven of the nine listed r^2 values are greater than 0.9, indicating that change in the x-variable (that is, the passage of time) explains over 90% of the change in the y-variable (cumulative bed, bank or total erosion). While these r^2 values certainly indicate a strong correlation between cumulative change and time, the Simon and Klimetz (2012) study does not indicate whether any other regression models were tested alongside the exponential decay model that is associated with the rate law. Consequently, linear regression was performed on the digitised data and the resulting r^2 values (also listed in Table 7.1) indicate that a linear model actually fits the trend in the data about as well as a nonlinear decay model. With respect to bank erosion at NF300 and NF310, and bed and total erosion at LO033, the linear model is actually a better fit.

NF300 and NF310 are close together on the North Fork Toutle River and therefore show similar trends (Figure 7.4). The rate of bed erosion at these two locations does appear to be slowing and the exponential decay is clearly the best fit. However, the rate of lateral erosion is not reducing and a linear regression model appears to be best. At LO033, the contribution from bed scour is minimal and shows a slight declining trend after the first 10 year. However, lateral erosion dominates cross-sectional change at this location, the rate of which does not appear to be reducing through time (Figure 7.4).

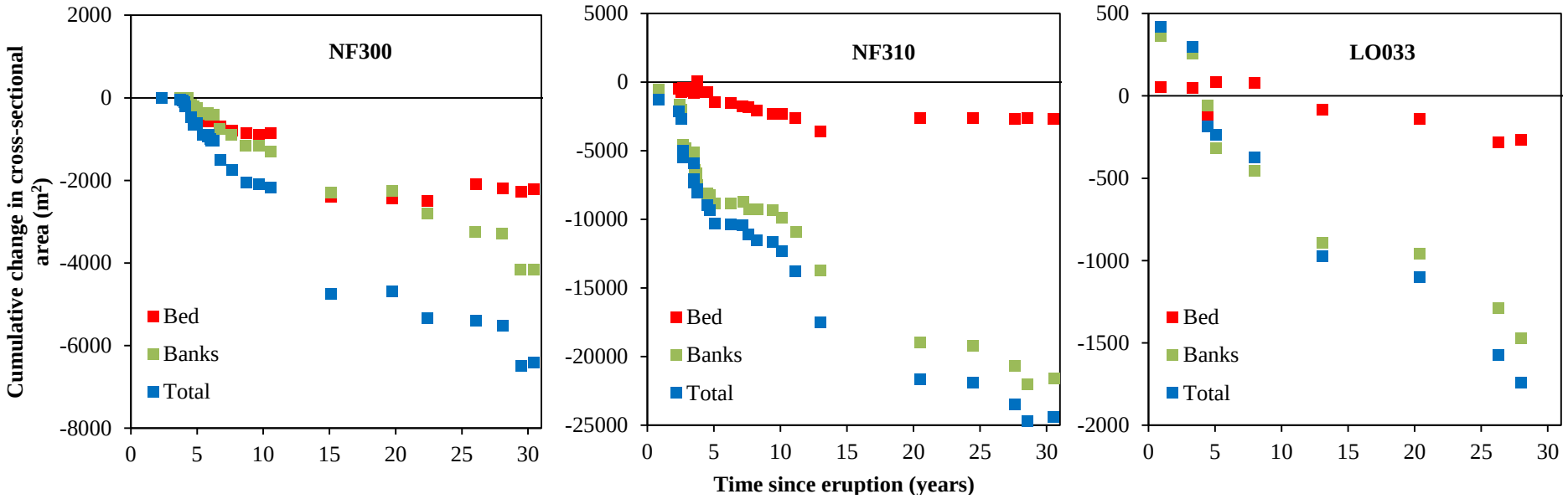

Figure 7.4 Cumulative change in cross-sectional area due to bed, bank and total erosion at NF300, NF310 and LO033, based on figures presented in Simon and Klimetz (2012) and re-assessment herein. Note that the scale on the y-axis at NF310 is an order of magnitude larger than at the other two sites.

Table 7.1 Coefficients of determination (r^2 values) for logarithmic and linear regression models of cumulative bed, bank and total erosion at NF300, NF310 and LO033. The highest r^2 value for each site and variable is in bold. Note: 'ARS' = r^2 value reported in Simon and Klimetz (2012); 'Calculated' = r^2 values calculated in this study. Differences between 'ARS' and 'Calculated' r^2 values indicate errors in digitising.

Cross-section		ARS (nonlinear)	Calculated (nonlinear)	Calculated (linear)
NF300	Bed	**0.9189**	0.9154	0.8543
	Banks	0.9395	0.9392	**0.9791**
	Total	**0.9598**	0.9589	0.9596
NF310	Bed	**0.7553**	0.7475	0.6096
	Banks	0.9273	0.9188	**0.9307**
	Total	**0.9530**	0.9414	0.9265
LO033	Bed	0.5594	0.5742	**0.7642**
	Banks	**0.9228**	0.9186	0.9157
	Total	0.9105	0.9068	**0.9460**

This re-analysis reveals that simple, linear regression performs about as well as a nonlinear regression in characterising historically observed trends of erosion in the upper North Fork Toutle River since the 1980 eruption. While there is evidence that rates of bed erosion at NF300 and NF310 have declined since the first decade following the eruption, it may be the case that rapid erosion early in the adjustment sequence is masking the fact that cumulative bed erosion has been increasing linearly for about the last 15 years. There is no empirical evidence for this at LO033, where the bed was stable for the first few years, but has been eroding slowly since then (Figure 7.4).

Bank sources dominate sediment production at all three of these cross-sections and, indeed, throughout the catchment. As a result, rates and trends of bank and total erosion are similar. It is therefore significant that there is as much

justification for describing the trend in bank erosion as linear as there is for describing it as declining.

When considered in conjunction with the results of C-L simulations outlined in Chapter 6, this re-analysis reveals that while the rate law may be applicable to describing the historical record of bed lowering in the upper North Fork Toutle River (as demonstrated by Zheng et al. (2014)) it appears that its extension to the record of bank erosion is inappropriate in this specific context. As bank sources dominate the sediment yield from the upper North Fork Toutle Basin, this explains why the Simon and Klimetz (2012) prediction of long-term, future sediment yield differs so markedly from that based on C-L simulations.

Historically, the rate law has most frequently been used to describe adjustments in channel bed elevation (Williams and Wolman, 1984; Simon, 1992; Hooke, 1995; Simon and Thorne, 1996; Simon, 1998; Prosser et al., 2001; Surian and Rinaldi, 2003; Wu et al., 2012; Zheng et al., 2014) and the headward expansion of gully networks (Graf, 1977; Prosser and Soufi, 1998). It is fair to say that its suitability for describing changes in channel width has yet to be established.

In the case of the upper North Fork Toutle River, the results of this study indicate that in situations where lateral erosion dominates sediment production as a result of abundant bed loads, high stream gradients and easily erodible channel boundaries, rates of sediment production and channel adjustment do not necessarily follow trends that can be represented by a negative exponential regression model. Moreover, although rates of bed degradation are much lower than rates of widening and arguably show some evidence of decay, it is clear that they are sufficiently large to maintain a time-averaged condition of ‘unimpeded removal’ at the base of many banks that are high, steep and toe-scoured (Thorne, 1978), thereby facilitating parallel retreat and the persistence of bank erosion as a primary and abundant source of sediment (Thorne, 1982).

The importance of lateral erosion in maintaining high annual sediment yields is confirmed by differences in the trends of both cumulative sediment yield and

sediment yield per unit discharge between the two C-L model configurations described in Chapter 6. Specifically, it is apparent that the rate of cumulative sediment yield decays more slowly in the model within which lateral erosion is more dominant (see Figures 6.16 and 6.17). Where stream channels are highly mobile laterally, such as the upper North Fork Toutle River, bank erosion can persist as channels continues to shift laterally by undercutting banks and steep slopes of adjacent terraces.

In light of the results presented here, it cannot be assumed a priori that fluvial adjustment will follow a nonlinear asymptotic pattern (c.f. Simon and Rinaldi, 2003) in the aftermath of severe disturbance. Although the debris avalanche generated by the 1980 eruption of Mount St Helens introduced an exceptional volume of sediment into the upper North Fork Toutle River catchment, the problem of sediment inundation to upland rivers is not unique and the results of this study may have significant implications for predicting post-disturbance sediment yields in a range of other geographical settings. As discussed in Chapter 6, the results of C-L forecasting presented in this thesis add to the body of evidence that suggests that fluvial system recovery following large-scale sediment loading can take several decades, centuries or even millennia (e.g. James, 1989; Manville and Wilson, 2004; Gran and Montgomery, 2005; Korup, 2005; Koi et al., 2008; Manville et al., 2009; Pierson et al., 2011; Pierson and Major, 2014).

7.3 IMPLICATIONS OF PROJECTED TRENDS AND VOLUMES OF SEDIMENT YIELD FOR FLOOD RISK MANAGEMENT IN THE TOUTLE-COWLITZ RIVER SYSTEM

The projections of sediment yield from the upper North Fork Toutle River developed using C-L in Chapter 6 raise a number of significant points regarding long-term sediment management for flood risk mitigation in the Toutle-Cowlitz River system. Perhaps most importantly, they suggest that rates of sediment production from the debris avalanche are unlikely to decline significantly below their current level during this century, while more

speculative, longer-term simulations suggest that an annual sediment yield of between 1.92 and 3.02 million $m^3 yr^{-1}$ may persist throughout the 22nd century.

These projections raise the possibility that measures to control sediment-related flood risks will be required for one or two centuries, rather than the next few decades (c.f. Major et al., 2000). Although the lack of definitive evidence makes it difficult to confirm whether these projections are consistent with recovery of the Toutle River system following historic eruptions, the findings of Scott (1989) suggest that fluvial instability following previous eruptive periods may have lasted for several centuries (see Section 3.1).

With respect to previous investigations of sediment loads in the North Fork Toutle River, the results obtained in this study are consistent in terms of quantum with the projections made by WEST and, in terms of trend they support the work of the Biedenharn Group (2010) who concluded that there was no evidence of significant decay in debris avalanche erosion rates between 1984 and 2007 and, therefore, predicted that future yields will remain constant at a rate of about 4.5 million $m^3 yr^{-1}$ at least until 2035 (see Figure 6.12 and Table 6.12).

Although the projections of catchment sediment yield reported in this thesis have been determined as the difference in net erosion across the terrain, rather than as a simulated output transport rate, it is unlikely that this represents a significant error source. As discussed in Section 5.2, consolidation and change in bulk density of eroded material is not an important consideration in the study catchment because the source debris avalanche material has a similar density to typical fluvial deposits.

This study adds weight to the argument that future trends of long-term sediment yield are more likely to be linear and that, while the nonlinear trend postulated by Simon and Klimetz (2012) is valid for the rate of bed lowering, that finding cannot be extended to either lateral erosion or, most significantly, total sediment production in the upper North Fork Toutle River (see Section 7.2). If this finding, which is specific to the upper North Fork Toutle River

catchment, is accepted, the effect is to markedly reduce the uncertainty that currently clouds projections of both volumes of sediment delivered to the sediment plain upstream of the SRS and future trends in sediment yield, evident in the reports issued by WEST (2002), Biedenharn Group (2010) and Simon and Klimetz (2012), which were discussed in detail in Chapter 3.

With regard to uncertainty in projections made herein using C-L, the methodological approach employed in Chapters 5 and 6 instils some confidence that these projections not only encapsulate the full range of potential model outcomes, but also span the range of possible sediment futures. Confidence in the projections stems first from the way the two C-L configurations described in detail in Chapter 5 were selected to capture uncertainty regarding the lateral mobility of the channel of the upper North Fork Toutle River, using carefully chosen values of the relevant model parameter (Λ) and, second, from the locally-derived climate change scenarios used to represent uncertainty in the catchment's future hydrologic regime (Chapter 6).

Allowing for these uncertainties, the difference between the upper and lower bound C-L projections for cumulative sediment yield in 2100 was less than 40%. This compares with a difference of 124% between the yields predicted by the extrapolated Simon and Klimetz (2012) and Biedenharn Group (2010) relationships. Differences between C-L projections employing high and low parameter values for lateral erosion, considered alongside uncertainty in the hydrological impacts of climate change, hint at the underlying reasons for future trends in cumulative sediment yield being predominantly linear in all C-L simulations. These reasons fall into two categories, related to lateral erosion and catchment hydrology.

First, future trends in sediment yield are sensitive to the relative dominance of bank sources relative to bed sources in driving sediment production. Essentially, as the dominance of bank sources increases, decay in the rate of sediment production decreases and the trend in future sediment yields becomes increasingly linear. The effect is to delay the onset of that decay, which can be

described by a rate law, until such time that the width of the floodplain is sufficient to decouple the channel from failures of the high, easily destabilised canyon and terrace slopes that bound it. Once this happens, sediment loads in the upper North Fork Toutle River will decrease, the channel planform will metamorphose from its current wandering/braided pattern to a single-thread, meandering configuration, and the extent and rate of bank erosion and lateral channel shifting across the floodplain will decrease. This geomorphic development will further reduce sediment production, and only then will substantive decay of sediment yield become evident. The two sets of model runs reported in Chapter 6, which adopt different rates of lateral erosion, simulate this process-response mechanism, but suggest that it will not be effective in causing future sediment yields to decay until well into the next century.

Second, the sensitivity of sediment production to catchment hydrology means that future trends in catchment sediment yield are affected by the scenarios selected for climate change. Most of the climate futures generated by the CBCCSP anticipate increases in rainfall towards the middle of the century, which translate into commensurate increases in runoff and sediment production that offset any tendencies for future sediment yields to decay. The outcome is for expected declines in future annual sediment yields to be further postponed until later in the 22nd century. However, it is again important to note that the decadal scale variations evident in future discharge projections have been derived from the observed climate record obtained between 1915 and 2006. Discharge patterns are therefore driven by winter storms and summer dry spells that have the same timing and duration as their counterparts in the observed record, although the magnitude of such events is scaled by signals in the GCM simulations (Hamlet et al., 2010; Tohver et al., 2014).

It is therefore conceivable that the actual decadal scale discharge variability observed in the remainder of the 21st century will be different from that projected by the CBCCSP. However, the sensitivity of modelled sediment yield to catchment hydrology remains a relevant and important finding as it implies that future climate will play a pivotal role in controlling long-term sediment

yields from the upper North Fork Toutle River. Moreover, fundamental climate change signals in the GCM simulations, including warming, increasing precipitation and increasing seasonal variability, are preserved by the downscaling technique used by the CBCCSP (see Section 6.2) (Tohver et al., 2014) and are therefore incorporated into the discharge time series implemented in C-L. As such, systematic changes in future climate, and their impacts on the geomorphological evolution of the study catchment, are well-represented by the datasets and methods used in the current study.

Nonetheless, the inherent uncertainty associated with GCM simulations should also be recognised. Visser et al. (2000), for instance, identified four key sources of uncertainty relating to projections of climate change: greenhouse gas emissions; greenhouse gas cycle; radiative forcing; and climate sensitivity. The use of a projected range, as in the CBCCSP, reduces this uncertainty as a range of projections will always be more likely than a single scenario (Jones, 2000). However, unquantifiable uncertainty will still exist outside this range, meaning that climate surprises, such as rapid climate changes, nonlinear forcings, and nonlinear responses to stochastic processes that may not be captured by GCM projections, should be expected (Jones, 2000; Tohver et al., 2014).

In summary, it is important to recognise that uncertainty in projections of future sediment yields is not only unavoidable, but also that this uncertainty is, to a degree, irreducible. Accepting that some uncertainty will continue to surround estimates of future sediment yields, the results derived in this study increase confidence in the veracity of the projections compared with knowledge derived from the three previous studies (WEST, 2002; Biedenharn Group, 2010; Simon and Klimetz, 2012). This should clearly be of benefit to engineers and scientists charged with planning and implementing measures to manage sediment and related flood risks in the Toutle-Cowlitz River system.

The Portland District's Progress Report (USACE, 2010) and the report of the SRS Spillway Raise Project (USACE, 2012) identified a number of measures which might be implemented to provide long-term flood risk reduction benefits on the lower Cowlitz River. These have now been reduced to three primary

alternatives (Paul Sclafani, USACE Portland District, personal communication, 2014):

1. dredging the lower Cowlitz River;
2. a single 13 m raise of the entire SRS structure (dam and spillway);
3. an adaptive approach involving three 3 m raises of the SRS spillway (the first of which was undertaken in summer 2012) followed by construction of grade-building structures on the SRS sediment plain (based on experience gained from a 2010 pilot project);

It is anticipated that options 2 and 3 would increase sediment storage capacity upstream of the SRS to approximately 79 and 74 million m^3, respectively. Based on estimates of future long-term sediment yield developed in Chapter 6, the additional capacity provided by option 2 would therefore be exceeded between 2034 and 2044, while that provided by option 3 would be exceeded between 2032 and 2042. Option 3 is the current preferred alternative given the potentially significant adverse environmental consequences associated with options 1 and 2, as outlined below.

As discussed in Chapter 2, undertaking continual dredging operations along the lower Cowlitz River (option 1) throughout the 21st century and beyond will be difficult due to high and escalating costs and cumulative impacts of repeated and recurrent dredging on the environment and ecology of the river. These include impacts to species listed under the Endangered Species Act (ESA; Title 16 United States Code, Sections 1531-1544), the designation of which also means that dredging will continue to be stringently regulated (USACE, 2012). Notwithstanding this, dredging has the benefit of addressing flood risk directly and in the area at risk and it allows for flexibility in adapting the programme in response to actual sediment accumulation rates as the future unfolds, so avoiding the need to allow for irreducible uncertainties in future sediment yields (USACE, 2010).

However, the annual cost of dredging is estimated to be \$2.5 – \$13 million depending on the volume of sediment that it is required to be removed. The

results derived in this study (Chapter 6) suggest that without further measures to trap sediment upstream, the cumulative volume of sediment delivered to the Toutle-Cowlitz River system from the upper North Fork Toutle River in 2100 is likely to be of the order of between 205.45 and 306.54 million m^3. This would require dredging operations to continue until at least the end of the century, with costs near the upper end of the predicted range. Using dredging along the lower Cowlitz River as the primary means of delivering flood risk reduction benefits to authorised communities would therefore be an expensive option, and as such it is likely that dredging will only be undertaken when necessary and in response to significant peaks in sediment delivery.

Raising the SRS by 13 m (option 2) is the least preferred alternative. The existing SRS prevents volitional upstream migration of anadromous fish species and inhibits access to an estimated 80 km of previously high-quality spawning habitat (USACE, 2012). This problem has been partly mitigated by a trap-and-haul fish collection facility (FCF), funded and constructed by the USACE and currently operated and owned by the Washington Department of Fish and Wildlife (WDFW). However, there are regional concerns regarding the effectiveness of this facility in producing a sustainable fish population in the Toutle-Cowlitz River system. Furthermore, the sediment plain itself presents a formidable challenge to downstream migration of juvenile fish and this problem will only be exacerbated if the height of the structure is increased.

Although the operation of the FCF is not affected by a potential raise of the SRS, issues arise concerning potential loss of connectivity between the North Fork Toutle River and its tributaries upstream of the SRS due to burial of the lower courses of these tributaries as a result of continued sediment accumulation behind the structure. This fate has in fact already befallen two branches of Pullen Creek that enter the sediment plain about 1 km upstream of the SRS (Figure 7.5), which have already been impacted by sediment accumulation (Figure 7.6) to the extent that they are no longer connected to the

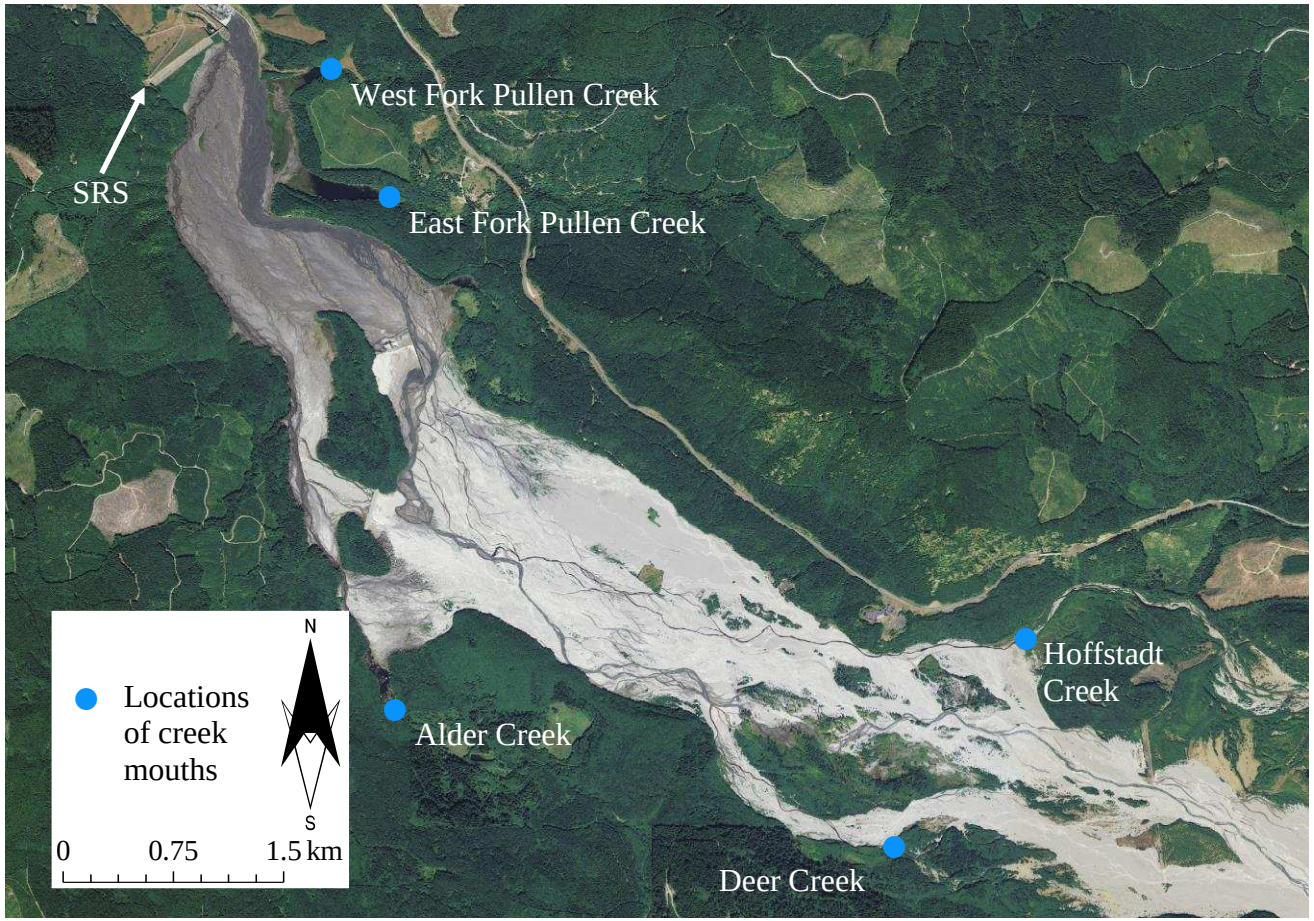

Figure 7.5 Locations of the mouths of East and West Pullen, Alder, Deer and Hoffstadt Creeks. Aerial imagery from National Agricultural Inventory Project (2011).

Figure 7.6 Sediment accumulation at the mouth of East Pullen Creek caused by construction of the SRS. The SRS is visible in the middle distance. Photograph by Colin Thorne (2013).

North Fork Toutle River and can therefore no longer provide passage for anadromous fish (USACE, 2007).

Excellent spawning habitat is currently provided primarily by Alder, Deer and Hoffstadt Creeks (Figure 7.5), and it is possible that these tributaries could be impacted over the next century if the SRS were raised substantially. As such, maintaining fish passage across the sediment plain to facilitate the downstream migration of juveniles is a significant challenge that would result from a large increase in the elevation of the SRS and one that would require a viable solution before such a raise could be permitted by the NOAA National Marine Fisheries Service and US Fish and Wildlife Service.

In this sense, option 3 (incremental raises of the spillway and the construction of grade-building structures) is preferable, not only because it can be adapted based on actual future sediment yields, but also because downstream fish passage can be maintained. This is the case for two reasons. First, the structure remains run-of-the-river. Second, the raised spillway is notched and constructed with staged elevations rather than a single crest level meaning that the structure can successfully trap sediment while maintaining a coherent channel across the sediment plain that can facilitate fish passage (Thorne et al., 2014).

Regardless of the measure chosen, the current study implies that sediment storage in the upper North Fork Toutle River catchment will cease to be effective before the middle of this century. Moreover, C-L modelling results indicate that sediment yields will not decline significantly before the end of the century, meaning that the proposed options represent only temporary solutions. It must therefore be concluded that alternative strategies and ones capable of managing sediment-related flood risk in the Toutle-Cowlitz River system into the next century in ways that are economically, environmentally and ecologically sustainable must be sought.

It may be necessary, for instance, to relocate and/or raise vulnerable communities such as Castle Rock, where risks to life and property posed by

flooding are particularly high due to its position close to the mouth of the Toutle River (Figure 2.1) and location on the floodplain at the inside of a tight meander bend (Figure 7.7). Incremental relocation of the city (or at least its essential utilities and services) to nearby, higher ground over a period of years or decades would not only move people and property permanently out of harm's way, but would also provide new spaces for sediment and flood water storage on the floodplain, thereby reducing flood risk to downstream communities at the same time.

In considering sediment projections based on the C-L simulations presented in Chapter 6, and searching for sustainable approaches to sediment management, it is important to remember that these simulations do not include any representation of vegetation or the effects that colonisation of the catchment and sediment plain by vegetation might have on sediment production and retention. Catchment, riparian and aquatic vegetation is known to exert powerful influences on the hydrological regime, roughness, hydraulics, sediment dynamics and channel-floodplain morphology of a river (McKenney et al., 1995; Gran and Paola, 2001; Gurnell and Petts, 2006; Tal and Paola, 2007; Bertoldi et al., 2011; Gurnell et al., 2012; Polvi and Wohl, 2013). In the upper North Fork Toutle River within the National Monument, natural revegetation will increasingly act to intercept precipitation, increase evapo-transpiration, protect soils, slow surface erosion rates, and stabilise slopes. In theory, this could reduce runoff, sediment loads and rates of lateral erosion sufficiently to produce decay in the trend of cumulative sediment yield commensurate with what would be expected based on a rate law.

Although it is possible to account for vegetation in runs of C-L (as described in Chapter 4), this would require significant further development of the model and collection of base data necessary to represent the effects of vegetation on hydrology, soil strength, hydraulics, sediment transport and slope stability – a not inconsiderable undertaking, but one with potential to alter the outcomes of simulations from those presented in Chapter 6. However, as discussed in Chapter 4, it is unlikely that revegetation will have a tangible impact on

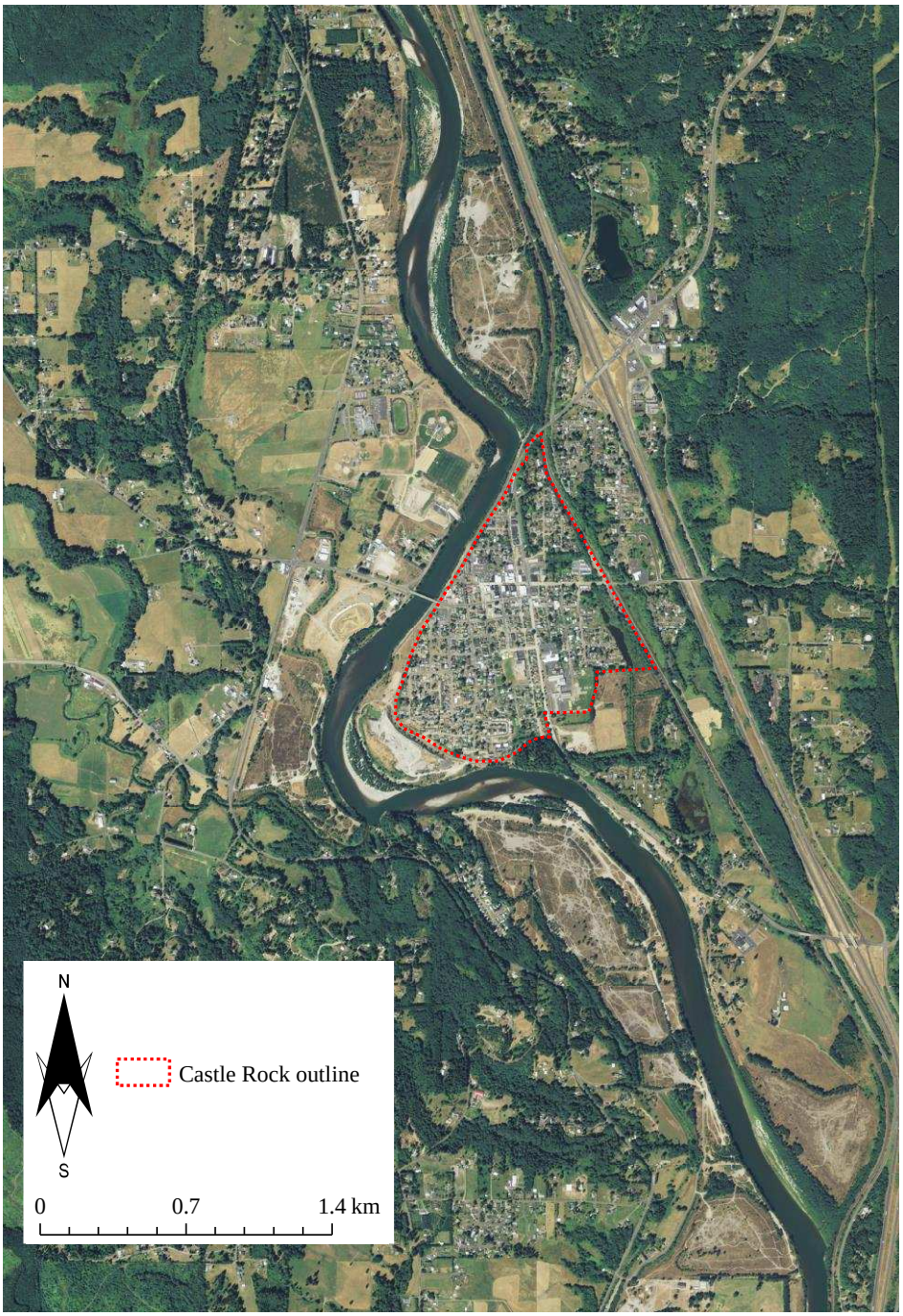

Figure 7.7 Aerial photograph of Castle Rock showing its location on the inside of a tight meander bend. Imagery from National Agricultural Inventory Project (2011).

channel evolution and, therefore, sediment yields until rates of widening reduce substantially and banks become more stable.

Moreover, it is clear from modelling outcomes and field reconnaissance that the geomorphic process primarily responsible for sediment production now and in the future is toe scour that generates mass instability in banks and terrace slopes and it cannot be assumed that vegetation will be effective in slowing this processes given the high velocities and excessive stream power available to the North Fork Toutle River and its headwater tributaries. Given how active channels of the upper North Fork Toutle River are currently, and considering that model results provide no evidence that this activity will decline, it may be argued that fluvial and other geomorphic processes will continue to severely limit colonisation of the river floodplain and riparian corridor for decades. In that case, vegetation would continue to be controlled by the river, rather than vice versa.

This argument is supported by Hupp (1992), who stated that a considerable shift in dominant channel process, such as from degradation to aggradation, is often necessary to trigger significant shifts in vegetation patterns. This implies that disturbed geomorphic systems must achieve a critical level of stability before vegetation can establish sufficiently to limit the rate of further erosion (Swanson and Major, 2005). C-L modelling results presented in Chapter 6, however, suggest that high rates of lateral erosion will persist in the upper North Fork Toutle River catchment and act to preclude substantial vegetation establishment. The dominance of fluvial processes, and in particular rates of bank widening, over riparian vegetation growth has also been shown in the studies of Simon and Hupp (1987), Hupp (1992), and Gran and Montgomery (2005) to support this contention, as discussed in Chapter 4.

The potential for planting vegetation for sediment trapping and retention on the sediment plain upstream of the SRS is also unknown, but could be significant. Recent monitoring and evaluation of engineered log jams and grade-building structures built as part of the 2010 pilot project (Chapter 2) demonstrates how

quickly vegetation can colonise the sediment plain in areas sheltered from fluvial processes, but also reveals how easily it can be removed or buried in situ by the North Fork Toutle River as its wandering/braided channel shifts laterally (Thorne et al., 2014). The results of the study of Thorne et al. provide further evidence to suggest that revegetation is likely to be too slow to reduce erosion in the medium term.

Nonetheless, post-project appraisal of the 2010 pilot project hints at the potential for encouraging vegetation to colonise the sediment plain through the use of further grade-building structures and engineered log jams, but it will take continued effort to learn how this might be done in practice and, most importantly, to gauge whether the additional quantities and calibres of sediment trapped and retained by a vegetated sediment plain would make any meaningful and cost-effective contribution to managing flood risks in communities along the lower Cowlitz River.

The situation outside the National Monument is different in that the major land-owner (Weyerhauser) has already revegetated much of the blast zone, albeit with tree-farms. Comparison of satellite images captured shortly after the eruption with those taken recently reveals the extent to which the upper basin is greening and this trend looks set to accelerate. However, the extent to which tree-farms reduce runoff and sediment yield to the upper North Fork Toutle River is unclear, although this could be investigated during future studies.

7.4 UTILITY OF REDUCED COMPLEXITY MODELLING FOR FORECASTING LONG-TERM SEDIMENT YIELDS

The results presented in Chapters 5 and 6 demonstrate that C-L can be used to make quantitative forecasts of landscape evolution in a complex fluvial geomorphological setting. Specifically, it was evident that the two calibrated models selected in Chapter 5 were able to provide a good approximation of catchment and sub-catchment sediment yield as well as changes in channel cross-sectional characteristics observed between 2003 and 2009. These models were then applied in Chapter 6 to generate forecasts of sediment yield for up to

182 years and provided information regarding trends and mechanisms of future long-term sediment production. These results can and should be used to inform the development of sediment management measures, as outlined in Section 7.3.

The forecasts presented in Chapter 6, together with discussions earlier in this Chapter (Sections 7.1 and 7.2), highlight two key benefits of the modelling approach used in this study. Firstly, forecasts have been generated in the absence of any a priori assumptions regarding the behaviour of the system, and have not relied on a subjective interpretation of historical observed data. This is a clear advantage over previous modelling studies that have been based on curve-extrapolation to predict sediment yield from the upper North Fork Toutle River catchment.

The prediction of Simon and Klimetz (2012), for instance, was based on the assumption that the rate law could be used to describe channel adjustments. As such, negative exponential decay functions were fitted to time series of erosion volumes, while linear functions were apparently not tested. Analysis undertaken in Section 7.2 questions this assumption and C-L model results confirm these doubts. Similarly, the linear trend predicted by the Biedenharn Group (2010) was based on a very subjective interpretation of the influence of hydrological variations on DEM-derived sediment yields during the period of observed data (see Chapter 3; sub-section 3.2.2). The proposed linear trend is now supported, for the most part, by C-L model results, but the subjectivity associated with the Biedenharn Group forecast had previously limited the confidence with which this linearity could be accepted and heightened uncertainty surrounding predictions.

The second benefit of modelling using C-L is the ability to interrogate model outcomes in terms of the processes and mechanisms responsible for the projected sediment yields. Not only is this useful in terms of assessing the physical realism of the model and therefore how much trust can reasonably be placed in its projections, but it can also inform the development of management and mitigation plans. For instance, it is evident from modelling results that the erosion of channel banks is primarily responsible for

maintaining high sediment yields in the study catchment, and that stabilising channel banks would be an effective means of controlling sediment production.

The current designation of the upper North Fork Toutle River catchment as part of the Mount St Helens National Volcanic Monument (see Chapter 2; sub-section 2.4.2) prevents the implementation of any in-stream erosion control measures. However, the ability to identify mechanisms of sediment production in this way could prove valuable in other contexts where channel management is not inhibited by legislation and/or the spatial scale and magnitude of the erosion problem is not as great as that presented at Mount St Helens. Such information, which is not provided by curve-extrapolation or reductionist modelling techniques, makes C-L a very useful predictive tool.

Despite the benefits identified above, a number of problems associated with the application of C-L for generating meaningful forecasts of long-term sediment yield were identified during the course of this research. Firstly, the computational efficiency and consequent short run times of reduced complexity models such as C-L are often cited as key advantages of this modelling approach (e.g. Brasington and Richards, 2007; Coulthard et al., 2007). However, run times experienced during the current study were considered to be rather long (Table 7.2) given that the modelled catchment area was not particularly large (approximately 161 km^2). Models were run on a variety of standard desktop computers with varying processors ranging from an Intel Core 2 Duo to an AMD Six-Core Opteron (housed at the University of Hull), although the majority of simulations were carried out on machines with Intel Core 2 Quad processors at the University of Nottingham.

The long run times evident in Table 7.2 probably reflect the large volume of erosion (and subsequent transport and deposition) that the models had to simulate, and it is likely that simulations undertaken in less dynamic catchments will be shorter. Nonetheless, run times of this length place a significant demand on computational resources, especially given the need to carry out multiple simulations for both model hindcasting and forecasting. The run times presented in Table 7.2 should therefore be taken as a note of caution

for researchers planning future applications of C-L in highly dynamic fluvial geomorphological settings regarding the potential scope of their study and/or the computational resources that will be required. Moreover, they emphasise the need to develop a version of C-L that can run on high performance computing clusters. Although this is by no means a trivial task and would require rewriting the model code (Tom Coulthard, University of Hull, personal communication, 2011), it would significantly reduce run times and enhance the applicability of the model considerably.

Table 7.2 Summary of model run times.

	Run time (hours)		
	Maximum	Minimum	Mean
Spin-up (3 years)	25.42	7.12	14.04
Hindcasting (2003 – 2009)	68.08	19.35	34.63
Forecasting (2009 – 2100)	471.73	219.96	326.78

The calibration of model parameters and the evaluation of model outcomes undertaken during hindcasting (Chapters 4 and 5) also raised a number of issues regarding the application of C-L to real-world problems and more generally. Firstly, there is a clear shortcoming in previous publications that have applied C-L in that they fail to sufficiently document or justify the parameter values that have been used. This is problematic and clearly restricts the development of knowledge and thus inhibits model development and limits its applicability. Although the model author provides a good online resource (Coulthard, 2013) that explains each model parameter and gives recommended ranges, these recommendations are understandably generic and can span several orders of magnitude (e.g. for the lateral erosion parameter Λ). It would be far more useful if published examples of C-L applications were available in which parameter settings had been fully presented and their selection explained.

This lack of documentation of parameter settings, in combination with the lack of examples in which C-L has been quantitatively evaluated in the context of empirical data, is particularly concerning given the results of the model hindcasting presented in Chapter 4. Specifically, it was evident that variations to five model parameters (Λ, λ, N_{smooth}, N_{shift} and Q_{max}) across a feasible range of values resulted in significant differences between model outputs and, in some cases, very poor agreement between modelled and observed geomorphological change during the six-year hindcasting runs. It is claimed in Table 1 of Hancock et al. (2011) that C-L does not required calibration, but this statement is clearly misleading. This study has shown that the process of parameter calibration and evaluation is vital in selecting a model on which reliable forecasts could be based, and that forecasts made by studies which do not implement a similar calibration procedure should be questioned. In light of this, there is a clear need for more rigorous testing of the influence of parameter settings on C-L results in the context of observed data, and to develop appropriate evaluation and model selection procedures.

This study, and in particular Chapters 4 and 5, goes some way toward addressing these problems. Chapter 4 presents an extensive documentation and justification of model parameters (which are further tested in Chapter 5), and this may be a useful reference for future studies. Moreover, the selection of two best-fit models in Chapter 5 required the development of a novel approach to model evaluation and selection which provides an objective and transparent means of identifying a subset of model configurations on the basis of physically justified criteria. In combination with recent work such as that of Ziliani et al. (2013), which focused on the assessment of C-L model performance in a braided river system, the approach developed in this study is an important starting point in the development of rigorous procedures for testing the performance of reduced complexity geomorphic models in the context of real case studies.

Nonetheless, the evaluation procedure outlined in Chapter 5, as well as that used by Ziliani et al. (2013), is dependent upon high quality, spatially extensive field and remotely sensed data that has, ideally, been collected over

an extended period of time. Although such data sets are becoming more readily available, this requirement means that reduced complexity modelling can be highly data-intensive and arguably limits its applicability to catchments that have been subject to extensive long-term monitoring such as the upper North Fork Toutle River. The need for calibration and evaluation in the context of high quality empirical data is compounded by the large number of parameters that require specification in models such as C-L, many of which are conceptual rather than physically-based and cannot be defined a priori. It is apparent from this study, therefore, that the application of reduced complexity models is more complex than the name suggests.

However, this study has also shown that, following parameter calibration, model outputs can provide a good fit to observed data. This is demonstrated by the similarity between modelled and observed estimates of catchment and sub-catchment sediment yield and simulated patterns of channel change at selected cross-sections for the two best-fit models selected in Chapter 5. This provides evidence to suggest that, despite the simplified representation of processes within C-L, the model is able to simulate the key geomorphological changes that took place in the upper North Fork Toutle River catchment between 2003 and 2009 reasonably well. Such a finding contradicts, to an extent, the studies of Doeschl-Wilson and Ashmore (2005), Doeschl et al. (2006) and Nicholas and Quine (2007) who all concluded that channel morphology simulated by reduced-complexity models can be highly unrealistic.

The general realism of results presented in this thesis is, of course, not without exception. For instance, the consistent underestimation of erosion from the Loowit Creek sub-catchment reported in Chapter 5 may indicate that some aspects of catchment dynamics are not fully represented by the model, or, similarly, that spring and glacial water inputs to this part of the catchment are more important than had been realised previously. Similarly, large errors were apparent for modelled changes in channel thalweg elevation and cross-sectional area (Chapter 5). Although there was good agreement when modelled and observed cross-sectional change were compared qualitatively, some discrepancies, for instance at NF350 (see Figure 4.22(g)), indicate scope for

improving the representation of in-channel processes within C-L. However, differences at individual cross-section could equally be attributed to DEM error or the reduction in DEM resolution that was undertaken in Chapter 4.

Furthermore, it must be noted that the general agreement between modelled outputs and observations during evaluation could be slightly exaggerated. As stated by Nicholas and Quine (2007), when models are implemented using real world DEMs possible inadequacies in process representation may be masked by the driving influence of imposed initial topographic conditions, particularly in the short-term. However, although the hindcasting period used in the present study was only 6 years, the dynamic nature of the catchment and the considerable geomorphological change that occurred during this period arguably negated, or at least minimised, the influence of topographic forcing on model outcomes.

The value of model calibration has also been questioned by Beven (1993, p. 43), who argues that when models contain free parameters that must be calibrated, it is "usually not difficult to obtain predictions that mimic the behaviour of observed variables to a reasonable degree". Similarly, Oreskes (2003, p. 23) contends that unconstrained calibration ensures that a model is "refutation-proof" in that any flaws in the model will be hidden such that the model cannot fail. The calibration undertaken in Chapter 5 of this thesis was not, however, unconstrained and such criticisms are therefore less applicable to the results presented therein. Importantly, values for only five key parameters were varied across a well-constrained and feasible range following a period of initial testing. Moreover, parameters that could be defined or justified physically, including the Froude number, Manning's n and the threshold for slope failure, together with the key input data sets of discharge and sediment size, were not altered.

Although this study identified a number of shortcomings of C-L that are thought to be applicable to reduced-complexity modelling more generally, resolution of these issues is by no means an insurmountable task and the work presented in this thesis has gone some way to beginning this process.

Moreover, significant benefits afforded by this modelling approach have been revealed during the course of this research and useful predictions of long-term sediment yield from the upper North Fork Toutle River have been generated. As such, it is important that this modelling approach is pursued and developments to models such as C-L continue to be made so that their full potential to inform river basin management planning over long timescales can be realised.

CHAPTER 8 CONCLUSIONS

8.1 SUMMARY, CONCLUSIONS AND KEY CONTRIBUTIONS

The aim of the work presented in this thesis, as specified in Chapter 1, was to answer the following question:

To what extent can reduced complexity, landscape evolution modelling be used to support quantitative, long-term forecasting of sediment yields generated in a complex fluvial geomorphological setting?

The research was set in the context of the upper North Fork Toutle River catchment, Washington State, USA, which was severely disturbed by the May 18, 1980 eruption of Mount St Helens. This Section summarises the principal conclusions and contributions of this research with respect to the eight research objectives detailed in Chapter 1, while recommendations for further research are made in Section 8.2.

Objective 1: To explain the practical need to forecast future long-term sediment yield from the upper North Fork Toutle River catchment.

The events and processes of the May 18, 1980 eruption of Mount St Helens, together with the impacts that the eruption had on the Toutle-Cowlitz River system were outlined in Chapter 2. It was explained that all catchments draining the volcano were severely disturbed by the eruption, although the deposition of a 2.5 km^3 debris avalanche into the upper 64 km^2 of the North Fork Toutle River catchment had the greatest impact on fluvial geomorphological processes.

Post-disturbance channel response in the catchment and its fluvial system has resulted in elevated annual sediment yields that have persisted for over three decades since the eruption and which have increased flood risks to communities situated along downstream depositional reaches in the Cowlitz River. Predictions of long-term sediment yield from the catchment are

therefore needed to inform decision-making with respect to development and implementation of sediment management measures for sustainable, long-term flood risk mitigation along the lower Cowlitz. As explained in Chapter 3, this need has been heightened by the fact that previous estimates reported in three separate studies commissioned by the US Army Corps of Engineers, which were based on extrapolation of post-eruption trends in sediment yield and channel network evolution, have varied widely.

Objective 2: To establish the feasibility of modelling of geomorphological change at large space and timescales as an approach to predicting future sediment yields.

It was determined in Chapter 3 that the application of a reduced complexity model, which uses simplified rules to represent complex flow and sediment dynamics, was the most appropriate approach for developing such predictions. Although the simplifications associated with such reduced complexity models can have negative consequences for process representation, the benefits afforded in terms of computational efficiency make them suitable to catchment scale modelling over extended time periods, giving them distinct advantages over, for example, reductionist numerical modelling techniques that attempt to represent physical processes and are described as being 'physics-based'. Reduced complexity models also have advantages over empirical curve-fitting and extrapolation approaches, like those employed in previous attempts to predict long-term trends in the sediment yield from the upper North Fork Toutle River catchment, which eschew representation of geomorphological processes and morphological responses entirely, relying instead on expert-interpretation and simple statistical treatments of observed historical trends.

Objective 3: To identify the most appropriate model available for modelling geomorphological change at large space and timescales.

Following the review of contemporary, reduced complexity landscape evolution models reported in Chapter 3, CAESAR-Lisflood (C-L) was selected as being the most suitable model for use within the context of the upper North

Fork Toutle River. This model was selected for a number of reasons which were summarised Table 2.8. An important consideration in the selection process was incorporation into C-L of the LISFLOOD-FP hydrodynamic flow code developed by Bates et al. (2010). This facilitates a far more sophisticated representation of fluvial hydraulics, including conservation of mass and fluid momentum, which has consequent benefits for the simulation of sediment transport by fluvial processes. Incorporation of a lateral erosion algorithm into C-L's cellular automaton framework (Coulthard and Van De Wiel, 2006) also enables bank erosion in channels with both meandering and braided planforms to be modelled simultaneously; a capability that is not provided by any other contemporary reduced complexity model. Additional features that distinguish C-L from otherwise similar models is its inclusion of multi-size sediment transport using nine grain size fractions and either the complete Einstein (1950) or Wilcock and Crowe (2003) transport equations, as well as its representation of climate using an hourly time series for rainfall.

Objective 4: To assess data requirements for model set-up and parameterisation, and assemble the data sets for the study catchment necessary to apply the most appropriate landscape evolution model.

Chapter 4 considered how C-L operates, in order to explain in detail how flow, sediment dynamics, hillslope erosion/failure and vegetation growth are represented in the model. Model parameters were defined and described, their meanings explained and their initial values selected. The definition of model parameters was based, as far as was possible, on physical reasoning and recommended values. However, the process of parameter specification was hindered by a lack of documentation reporting parameter values used in previous applications of C-L, let alone any justification or explanation of how parameter values were selected in these studies. This is a significant gap in the current literature that may slow the development and reduce the uptake of C-L. The documentation of models parameters in Chapter 4 therefore represents an important contribution that could be used to inform future applications of the model.

Chapter 4 also identified the key data sets to be used to run C-L in the upper North Fork Toutle River catchment, including a digital elevation model (DEM), a sediment size distribution and an input hydrological driver. Despite the fact that the catchment has been the subject of intensive monitoring since the eruption of Mount St Helens in 1980, appropriate data sets proved difficult to obtain and implement within the model. For instance, DEMs with sufficient spatial coverage were available only after 2002, while implementing a local precipitation time series was found to be impossible and so a time series of discharges based on gauging station records had to be used instead. Appropriately describing the grain size distribution of sediment throughout the catchment was also found to be challenging, and few adequate datasets were found to be available. Given the heavy data demands for model set-up identified in this thesis, the extent to which reduced complexity models such as C-L can be applied to data-sparse catchments must be questioned.

Objective 5: To evaluate model outputs by comparison to observed data during a data-rich period through model hindcasting.

It was identified in Chapter 5 that few studies have attempted to assess the performance of reduced complexity models, either in general or specifically related to C-L, using observed data from quantified case studies. Hence, once the necessary data sets and parameters had been assembled, model hindcasting was undertaken as reported in Chapter 5, the objectives being to:

1. evaluate the performance of the model by investigating its capacity to replicate the behaviour of the system and resulting sediment yield as evidenced by data collected between 2003 and 2009;
2. test and refine appropriate values for those parameters that could not be defined empirically or on the basis of relevant literature in Chapter 4, and;
3. assess the utility of C-L and reduced complexity modelling more generally.

Furthermore, the model evaluation undertaken during the hindcasting period was necessary in order to facilitate selection of a sub-set of best fit models to be used for forecasting in Chapter 6. A novel model evaluation and selection technique was developed for this purpose and used to identify two model configurations that provided a good fit to the observed records while also acknowledging and capturing model uncertainty with respect to the appropriate value of the parameter for lateral erosion rate, which had been demonstrated in the hindcasting exercise to be crucial to model performance.

The results of the model hindcasting revealed that the two selected models were able to provide a good fit to the observed data for four evaluation criteria (total catchment sediment yield, sub-catchment sediment yield, change in cross-sectional area and change in channel thalweg elevation), suggesting that these models could reasonably be used for forecasting. However, it was also evident that significant differences in model outcomes could be obtained with small variations in a small number of parameters across a well-constrained and feasible range. This finding further emphasises the need for greater documentation of parameter settings and more rigorous testing of model outcomes in the context of observed data. In this context, the development of a novel model evaluation and selection procedure in Chapter 5 therefore represents an important contribution and goes some way toward addressing this issue. However, the procedure required multiple, high quality digital elevation datasets which are unlikely to be available for many catchments. Heavy data demands for model evaluation and calibration, as well as set-up, further hinder the application of C-L to data-sparse settings.

Objective 6: To use the calibrated models to make ensemble predictions of long-term sediment yield in the upper North Fork Toutle River catchment, explicitly accounting for the main sources of model uncertainty and incorporating potential changes in climate during the forecast period.

Use of the two models selected in Chapter 5 to forecast future long-term sediment yields from the upper North Fork Toutle River catchment is reported in Chapter 6. These models were implemented in ensembles with runoff

forecasts developed as part of the Columbia Basin Climate Change Scenarios Project (CBCCSP) undertaken by the Climate Impacts Group (CIG) at the University of Washington. The runoff forecasts selected from the CBCCSP incorporated three different global climate model (GCM) simulations and two greenhouse gas (GHG) emissions scenarios and, therefore, encapsulate the majority of variation associated with uncertainties in predictions of the future hydrological regime of the catchment. A total of 36, 91-year forecasting runs were undertaken, along with two, more speculative, 182-year simulations extending forecasts to the late 22nd century.

Objective 7: To assess trends in future sediment yields forecast by the model, compare them with the results of predictions made in previous studies, and relate the forecast trends to changes in the climatic and geomorphic drivers of sediment production, so gaining insights into modelled processes responsible for long-term, post-disturbance relaxation in the fluvial system.

The assessment and analysis of model outcomes in terms of projected volumes, trends and mechanisms of sediment production were reported in Chapter 6. It was shown that all 36 C-L predictions of cumulative sediment yield in 2100 fell between previous predictions that were based on expert interpretation and curve-extrapolation. However, the difference between the maximum and minimum C-L predictions was only +/- 20% of the mean predicted value. This range is very well constrained despite conscious efforts being made throughout the study to maximise the difference between selected model configurations (Chapter 5) and future hydrological scenarios (Chapter 6).

The results and analysis presented in Chapter 6 also suggest that the trend in cumulative sediment yield is predominantly linear, and the rate of sediment delivery from the catchment is therefore not expected to decline significantly from its current value during the remainder of this century. Moreover, speculative simulations suggest that elevated rates of sediment production may persist well into the 22nd century. Current sediment production in the catchment is dominated by lateral erosion and channel widening, and this situation is predicted to continue for the foreseeable future due to the high lateral channel

mobility and the impacts of climate change on the upper North Fork Toutle River.

The forecasts generated by C-L in this thesis have therefore contributed to understanding of long-term channel evolution and resultant sediment yield in fluvial systems disturbed by massive sedimentation. Specifically, the predominantly linear trend in cumulative sediment yield modelled by C-L suggests that negative exponential decay functions based on a rate law are not appropriate for predicting sediment yields from the upper North Fork Toutle River catchment, and as such it may also be inferred that this is likely to be the case in other rivers disturbed by volcanic eruptions or landslides that bury catchments in significant thicknesses of erodible sediment. Although the rate law can be used to describe changes in bed elevation and adjustments to the channel long profile, C-L model results reveal that it is lateral erosion caused by fluvial undercutting and slumping of high, steep banks, that drives long-term trends in sediment yield, rather than bed scour. The concepts that underpin the rate law, including how opposing trends in boundary and critical shear stress act through time to reduce excess bed shear stress (Simon and Thorne, 1996), are less applicable to bank stresses and materials, and so these concepts cannot be used to predict sediment yields when and where channel adjustments are dominated by lateral shifting.

Objective 8: To interpret the research findings in terms of the applicability of reduced complexity modelling and the implications for sediment management in the Toutle-Cowlitz River system.

The research reported in this thesis has demonstrated the utility of a reduced complexity model for long-term forecasting of catchment-scale sediment yield. Although modelling based on cellular automata has often been criticised by proponents of reductionist, 'physics-based' models, in the context of the upper North Fork Toutle River it has been shown to be a powerful tool that can and should be used to explore landscape evolution and response to disturbance. It also has the potential to help inform long-term, catchment-scale planning and sustainable management of environmental hazards associated with, for

example, elevated sediment yields. It would not have been possible to implement a reductionist model at the spatial and temporal scales studied in this thesis, or to extract information regarding geomorphic process-response mechanisms crucial to understanding system behaviour and, hence, long-term trends in sediment yield.

Moreover, two key benefits of using C-L over expert interpretation and curve-extrapolation were identified:

1. The capability to make long-term forecasts without a priori, unsupported assumptions or subjective interpretations of observed historical data and trends;
2. The capacity to interrogate model outputs in order to assess the physical realism of the forecasts and inform decision-making with respect to alternative sediment management strategies.

In short, it is apparent that reduced complexity modelling can occupy an important niche left vacant by hydraulic models and curve-extrapolation techniques with the capacity to simulate erosion, sediment transport and deposition, and that their continued development is, therefore, worth pursuing.

The implications of the forecasts developed in this thesis for long-term sediment management in the Toutle-Cowlitz River system were discussed in Chapter 7. Importantly, C-L forecasts have reduced the uncertainty associated with previous predictions of long-term sediment yield from the upper North Fork Toutle River catchment. This has been achieved in two ways. First, it has been shown that a rate law-based prediction, which was significantly lower than other estimates, can probably be discounted. Second, the difference between C-L predictions of the probable maximum and minimum cumulative sediment yield in 2100 is only +/-20% of the mean predicted value, despite the incorporated uncertainties. The substantive point here is that, while none of the individual forecasts will be what actually happens (the future sediment yields are not uncertain, they are unknowable), it is probable that the actual future

cumulative sediment yield will follow a trajectory contained within the envelope predicted by C-L.

Of course, the possibility exists that the cumulative load might follow a different trajectory, and that the cumulative total in 2100 could fall outside the predicted range. This could happen if climate change is more or less extreme than envisaged, if catchment hydrology is more sensitive to climate change than expected, or if lateral shifting and slope failures are constrained by rapid colonisation of stabilising vegetation. It must, therefore, be borne in mind that cumulative sediment yields outside the bounds of those predicted by C-L are possible, but that there is a high probability that observed cumulative yield up to 2100 will lie within the predicted range.

Moreover, persistence of elevated annual sediment yields predicted by C-L modelling suggests that it may be difficult to maintain flood risk reduction benefits to vulnerable communities on the lower Cowlitz River solely by artificially trapping sediment upstream of the SRS. For example, it was reported in Chapter 7 that the two methods of improving the trap efficiency of the SRS proposed by the USACE (a 13 m dam raise or incremental raises of the spillway combined with grade-building structures) would be effective only until the 2040s if C-L predictions were realised.

Although an adaptive strategy based on incremental spillways raises would potentially have less severe adverse environmental consequences than a raise of the entire SRS, both options would require persistent monitoring and maintenance and would result in the storage of a large volume of sediment behind a structure that could be vulnerable should a further major eruption occur at Mount St Helens. Given these issues, alternative and additional options for sediment management should be considered, and these may need to include permanent relocation of vulnerable communities downstream on the lower Cowlitz River. If continued lateral shifting of the upper North Fork Toutle River does continue in the manner suggested by C-L modelling, it will be necessary to make some hard choices concerning flood and sediment management in the Toutle-Cowlitz River system.

8.2 RECOMMENDATIONS FOR FURTHER RESEARCH

A number of the issues that emerged during the course of this study should be addressed as part of further research on landscape evolution modelling and long-term sediment prediction and management in the Toutle-Cowlitz River system. These are summarised in the following sub-sections.

8.2.1 Reduced complexity modelling

1. It is necessary to build upon the model evaluation and calibration methodology outlined in Chapter 5, together with recent studies such as that by Ziliani et al. (2013), to develop a consistent approach for assessment of the performance of reduced complexity landscape evolution models based on hindcasting in catchments which have good records of observed data.
2. Given the apparent sensitivity of model outputs to parameter specification (demonstrated in Chapter 5), there is a clear need for more rigorous testing of C-L parameters in order to inform the future applications of the model. Moreover, such testing will improve understanding of model operation and, in turn, facilitate its continued technical development.
3. Continued application of C-L in the upper North Fork Toutle River could build on the results reported here by, for instance:
    i. incorporating vegetation growth into forecasting simulations;
    ii. improving the understanding and representation of hydrological inputs in the catchment headwaters (e.g. glacier melt and spring-fed inputs in the Loowit Creek sub-catchment) through detailed, field-based investigation and measurement.
4. There is a need to develop a version of C-L that can be implemented on high performance computing clusters to increase the number of simulations that can be conducted for both hindcasting and forecasting in highly dynamic fluvial geomorphological settings, such as the upper North Fork Toutle.

8.2.2 Sediment management in the Toutle-Cowlitz River system

1. Continued monitoring at Mount St Helens is essential to provide the data needed to assess the accuracy of the C-L projections using observed data sets other than those used during calibration, and test the utility of the selected models in informing decision-making with respect to sustainable, long-term sediment management.
2. Long-term monitoring is also necessary to understand and explain past, present and future trends in sediment yield from the upper North Fork Toutle River catchment which, for the reasons set out in Chapter 2, is of undisputed importance to advancing knowledge of recovery and relaxation processes and pathways in fluvial systems perturbed by massive disturbances such as volcanic eruptions like that at Mount St Helens on May 18, 1980. Specifically, quantification of the rates and mechanisms of bank erosion is required in order to test the contention that the rate law is not applicable to lateral channel adjustments.
3. Analysis of a range of sediment management options should continue to be pursued. However, given the magnitude and longevity of sediment yields predicted from the upper North Fork Toutle River by C-L, sediment storage behind the SRS may not be a sustainable long-term solution. As such, it may be necessary to investigate land management options on the lower Cowlitz River instead. Similarly, efforts to improve sediment capture and retention on the sediment plain (e.g. using engineered log jams and grade-building structures) should continue in parallel with staged, incremental raises of the SRS spillway in order to learn how to optimise the long-term performance of the structure.

REFERENCES

Abbott, M.B., Bathurst, J.C., Cunge, J.A., O'Connell, P.E. and Rasmussen, J. (1986a). An introduction to the European Hydrological System - Système Hydrologique Europeén, "SHE", 1: History and philosophy of a physically-based, distributed modelling system. Journal of Hydrology 87(1-2), 45-59.

Abbott, M.B., Bathurst, J.C., Cunge, J.A., O'Connell, P.E. and Rasmussen, J. (1986b). An introduction to the European Hydrological System - Système Hydrologique Europeén, "SHE", 2: Structure of a physically-based, distributed modelling system. Journal of Hydrology 87(1-2), 61-77.

Ahnert, F. (1976). Brief description of a comprehensive three-dimensional model of landform development. Zeitschrift fur Geomorphologie Supplement Band 25, 29-49.

Aksoy, H. and Kavvas, M.L. (2005). A review of hillslope and watershed scale erosion and sediment transport models. Catena 64, 247-271.

Armstrong, J.S. and Collopy, F. (1992). Error measures for generalizing about forecast methods: empirical comparisons. International Journal of Forecasting 8, 69-80.

Arnell, N.W. and Gosling, S.N. (2013). The impacts of climate change on river flow regimes at the global scale. Journal of Hydrology 486, 351-364.

Banks, N.G. and Hoblitt, R.P. (1981). Summary of temperature studies of 1980 deposits. In: Lipman, P.W. and Mullineaux, D.R. (Eds.) The 1980 eruptions of Mount St Helens, Washington: US Geological Survey Professional Paper 1250. Washington, DC: US Government Printing Office, pp. 295-314.

Bates, P.D. and De Roo, A.P.J. (2000). A simple raster-based model for flood inundation simulation. Journal of Hydrology 236(1), 54-77.

Bates, P.D., Horritt, M.S., Smith, C.N. and Mason, D. (1997). Integrating remote sensing observations of flood hydrology and hydraulic modelling. Hydrological Processes 11(14), 1777-1795.

Bates, P.D., Horritt, M.S. and Fewtrell, T.J. (2010). A simple inertial formulation of the shallow water equations for efficient two-dimensional flood inundation modelling. Journal of Hydrology 387(1), 33-45.

Bathurst, J.C. (1986). Physically-based distributed modelling of an upland catchment using the Système Hydrologique Européen. Journal of Hydrology 87(1), 79-102.

Bathurst, J.C. (2002). Physically-based erosion and sediment yield modelling: the SHETRAN concept. In: Summer, W. and Walling, D. (Eds.) Modelling erosion, sediment transport and sediment yield. Paris, France: UNESCO, pp. 47-67.

Bathurst, J.C., Hubbard, L., Leeks, G.J.L., Newson, M.D. and Thorne, C.R. (1990). Sediment yield in the aftermath of a dambreak flood in a mountain stream. Hydrology of Mountainous Regions. II - Artificial Reservoirs; Water and Slopes (Proceedings of two Lausanne Symposia, August 1990). IAHS Publ. no. 194.

Bathurst, J.C., Kilsby, C. and White, S. (1996). Modelling the impacts of climate and land-use change on basin hydrology and soil erosion in Mediterranean Europe. In: Brandt, C. and Thornes, J. (Eds.) Mediterranean desertification and land use. Chichester, UK: John Wiley and Sons Ltd, pp. 355-387.

Bathurst, J.C., Ewen, J., Parkin, G., O'Connell, P.E. and Cooper, J.D. (2004). Validation of catchment models for predicting land-use and climate change impacts. 3. Blind validation for internal and outlet responses. Journal of Hydrology 287, 74-94.

Bathurst, J.C., Burton, A., Clarke, B.G. and Gallart, F. (2006). Application of the SHETRAN basin-scale, landslide sediment yield model to the Llobregat basin, Spanish Pyrenees. Hydrological Processes 20(14), 3119-3138.

Bathurst, J.C., Moretti, G., El-Hames, A., Beguería, S. and García-Ruiz, J.M. (2007). Modelling the impact of forest loss on shallow landslide sediment yield, Ijuez river catchment, Spanish Pyrenees. Hydrology and Earth System Sciences 11(1), 569-583.

Bennett, N.D., Croke, B.F., Guariso, G., Guillaume, J.H., Hamilton, S.H., Jakeman, A.J., Marsili-Libelli, S., Newham, L.T., Norton, J.P. and Perrin, C. (2013). Characterising performance of environmental models. Environmental Modelling and Software 40, 1-20.

Bertoldi, W., Drake, N. and Gurnell, A. (2011). Interactions between river flows and colonizing vegetation on a braided river: exploring spatial and temporal dynamics in riparian vegetation cover using satellite data. Earth Surface Processes and Landforms 36(11), 1474-1486.

Beven, K.J. (1989). Changing ideas in hydrology - the case of physically-based models. Journal of Hydrology 105, 157-172.

Beven, K.J. (1993). Prophecy, reality and uncertainty in distributed hydrological modelling. Advances in Water Resources 16(1), 41-51.

Beven, K.J. (1996). Equifinality and uncertainty in geomorphological modelling. In: Rhodes, B.L. and Thorn, C.E. (Eds.) The Scientific Nature of Geomorphology. Proceedings of the 27th Binghampton Symposium in Geomorphology, 27-29 September, 1996, pp. 289-315.

Beven, K.J. (2001). On explanatory depth and predictive power. Hydrological Processes 15, 3069-3072.

Beven, K.J. (2002). Towards a coherent philosophy for modelling the environment. Proceedings of the Royal Society A: Mathematical, Physical and Engineering Sciences 458, 2465-2484.

Beven, K.J. (2006). A manifesto for the equifinality thesis. Journal of Hydrology 320, 18-36.

Beven, K.J. (2009). Environmental modelling: an uncertain future? Abingdon, UK: Routledge.

Beven, K.J. and Kirkby, M.J. (1979). A physically based, variable contributing area model of basin hydrology. Hydrological Sciences Journal 24, 43-69.

Beven, K.J. and Binley, A. (1992). The future of distributed models: model calibration and uncertainty prediction. Hydrological Processes 6, 279-298.

Beven, K.J. and Freer, J. (2001). Equifinality, data assimilation, and uncertainty estimation in mechanistic modelling of complex environmental systems using the GLUE methodology. Journal of Hydrology 249, 11-29.

Biedenharn Group (2010). Toutle-Cowlitz River sediment budget. Portland, OR: US Army Corps of Engineers Portland District.

Bras, R.L., Tucker, G.E. and Teles, V. (2003). Six myths about mathematical modelling in geomorphology. In: Wilcock, P.R. and Iverson, R.M. (Eds.) Prediction in Geomorphology. Geophysical Monograph 135. Washington, DC: American Geophysical Union, pp. 63-79.

Brasington, J. and Richards, K. (2007). Reduced-complexity, physically-based geomorphological modelling for catchment and river management. Geomorphology 90, 171-177.

Braun, J. and Sambridge, M. (1997). Modelling landscape evolution on geological time scales: a new method based on irregular spatial discretization. Basin Research 9, 27-52.

Bray, M.J. and Hooke, J.M. (1997). Prediction of soft-cliff retreat with accelerating sea-level rise. Journal of Coastal Research 13(2), 453-467.

Bryan, R.B. (2000). Soil erodibility and processes of water erosion on hillslope. Geomorphology 32, 385-415.

Carson, M.A. and Kirkby, M.J. (1972). Hillslope form and process. Cambridge, UK: Cambridge University Press.

Chow, V.T. (1959). Open Channel Hydraulics. New York, NY: McGraw-Hill.

Christensen, N.S., Wood, A.W., Voisin, N., Lettenmaier, D.P. and Palmer, R.N. (2004). The effects of climate change on the hydrology and water resources of the Colorado River basin. Climatic Change 62(1-3), 337-363.

Christiansen, R.L. and Peterson, D.W. (1981). Chronology of the 1980 eruptive activity. In: Lipman, P.W. and Mullineaux, D.R. (Eds.) The 1980 eruptions of Mount St Helens, Washington: US Geological Survey Professional Paper 1250. Washington, DC: US Government Printing Office, pp. 17-30.

Cigizoglu, H.K. (2003). Estimation, forecasting and extrapolation of river flows by artificial neural networks. Hydrological Sciences Journal 48(3), 349-361.

Clynne, M.A., Ramsey, D.W. and Wolfe, E.W. (2005). The pre-1980 eruptive history of Mount St Helens, Washington: US Geological Survey Fact Sheet 2005-3045.

Clynne, M.A., Calvert, A.T., Wolfe, E.W., Evarts, R.C., Fleck, R.J. and Lanphere, M.A. (2008). The Pleistocene eruptive history of Mount St Helens, Washington, from 300,000 to 12,800 years before present: US Geological Survey Professional Paper 1750. Washington, DC: US Government Printing Office.

Codilean, A.T., Bishop, P. and Hoey, T.B. (2006). Surface process models and the links between tectonics and topography. Progress in Physical Geography 30, 307-333.

Collins, B.D. and Dunne, T. (1986). Erosion of tephra from the 1980 eruption of Mount St Helens. Geological Society of America Bulletin 97, 896-905.

Costa-Cabral, M., Roy, S.B., Maurer, E.P., Mills, W.B. and Chen, L. (2013). Snowpack and runoff response to climate change in Owens Valley and Mono Lake watersheds. Climatic Change 116(1), 97-109.

Coulthard, T.J. (1999). Modelling upland catchment response to Holocene environmental change. PhD Thesis, University of Leeds.

Coulthard, T.J. (2001). Landscape evolution models: a software review. Hydrological Processes 15, 165-173.

Coulthard, T.J. (2013). CAESAR-Lisflood landscape evolution and flow model. [Online]. [Last accessed December 5, 2013]. Available from: http://code.google.com/p/caesar-lisflood/.

Coulthard, T.J. and Macklin, M.G. (2001). How sensitive are river systems to climate and land-use changes? A model-based evaluation. Journal of Quaternary Science 16, 347-351.

Coulthard, T.J. and Van De Wiel, M.J. (2006). A cellular model of river meandering. Earth Surface Processes and Landforms 31, 123-132.

Coulthard, T.J. and Van De Wiel, M.J. (2007). Quantifying fluvial non linearity and finding self organized criticality? Insights from simulations of river basin evolution. Geomorphology 91, 216-235.

Coulthard, T.J. and Van De Wiel, M.J. (2012). Modelling river history and evolution. Philosophical Transactions of the Royal Society A: Mathematical, Physical and Engineering Sciences 370(1966), 2123-2142.

Coulthard, T.J., Kirkby, M.J. and Macklin, M.G. (1998). Non-linearity and spatial resolution in a cellular automaton model of a small upland basin. Hydrology and Earth System Sciences 2(2-3), 257-264.

Coulthard, T.J., Kirkby, M.J. and Macklin, M.G. (2000). Modelling geomorphic response to environmental change in an upland catchment. Hydrological Processes 14, 2031-2045.

Coulthard, T.J., Macklin, M.G. and Kirkby, M.J. (2002). A cellular model of Holocene upland river basin and alluvial fan evolution. Earth Surface Processes and Landforms 27, 269-288.

Coulthard, T.J., Lewin, J. and Macklin, M.G. (2005). Modelling differential catchment response to environmental change. Geomorphology 69, 222-241.

Coulthard, T.J., Hicks, D. and Van De Wiel, M.J. (2007). Cellular modelling of river catchments and reaches: Advantages, limitations and prospects. Geomorphology 90, 192-207.

Coulthard, T.J., Ramirez, J., Fowler, H.J. and Glenis, V. (2012). Using the UKCP09 probabilistic scenarios to model the amplified impact of climate change on drainage basin sediment yield. Hydrology and Earth System Sciences 16(11), 4401-4416.

Coulthard, T.J., Neal, J.C., Bates, P.D., Ramirez, J., Almeida, G.A. and Hancock, G.R. (2013). Integrating the LISFLOOD-FP 2D hydrodynamic model with the CAESAR model: implications for modelling landscape evolution. Earth Surface Processes and Landforms 38, 1897-1906.

Cox, C., Brasington, J. and Richards, K. (2005). Predicting reach-scale flow patterns using reduced complexity cellular schemes. Geophysical Research Abstracts 7, 01646.

Crandell, D.R. (1971). Postglacial lahars from Mount Rainier Volcano, Washington: US Geological Survey Professional Paper 677. Washington, DC: US Government Printing Office.

Crandell, D.R. (1987). Deposits of the pre-1980 pyroclastic flows and lahars from Mount St Helens volcano, Washington: US Geological Survey Professional Paper 1444. Washington, DC: US Government Printing Office.

Cui, Y. and Parker, G. (2005). Numerical model of sediment pulses and sediment-supply disturbances in mountain rivers. Journal of Hydraulic Engineering 131(8), 646-656.

Dale, V.H. and Adams, W.M. (2003). Plant reestablishment 15 years after the debris avalanche at Mount St Helens, Washington. Science of the Total Environment 313, 101-113.

Dale, V.H., Crisafulli, C.M. and Swanson, F.J. (2005). 25 years of ecological change at Mount St Helens. Science 308, 961-962.

Darby, S.E. and Van De Wiel, M.J. (2003). Models in fluvial geomorphology. In: Kondolf, G.M. and Piegay, H. (Eds.) Tools in Fluvial Geomorphology. Chichester, UK: John Wiley and Sons Ltd, pp. 501-537.

Dawson, C.W., Abrahart, R.J. and See, L.M. (2007). HydroTest: a web-based toolbox of evaluation metrics for the standardised assessment of hydrological forecasts. Environmental Modelling and Software 22(7), 1034-1052.

Dawson, C.W., Mount, N.J., Abrahart, R.J. and Shamseldin, A.Y. (2012). Ideal point error for model assessment in data-driven river flow forecasting. Hydrology and Earth System Sciences 16(8), 3049-3060.

De Roo, A.P.J., Wesseling, C.G. and Ritsema, C.J. (1996). LISEM: a single-event physically based hydrological and soil erosion model for drainage basins. I: Theory, input and output. Hydrological Processes 10(8), 1107-1117.

Dearing, J.A., Richmond, N., Plater, A.J., Wolf, J., Prandle, D. and Coulthard, T.J. (2006). Modelling approaches for coastal simulation based on cellular automata: the need and potential. Philosophical Transactions of the Royal Society A: Mathematical, Physical and Engineering Sciences 364, 1051-1071.

del Moral, R. and Lacher, I.L. (2005). Vegetation patterns 25 years after the eruption of Mount St Helens, Washington, USA. American Journal of Botany 92(12), 1948-1956.

Dinehart, R.L. (1998). Sediment transport at gaging stations near Mount St Helens, Washington, 1980-1990. Data collection and analysis: U.S. Geological Survey Professional Paper 1573. Richmond, VA: US Geological Survey.

Dinehart, R.L., Ritter, J.R. and Knott, J.M. (1981). Sediment data for streams near Mount St Helens, Washington - Volume 1: US Geological Survey Open-File Report 81-822. Tacoma, WA: US Geological Survey.

Doeschl-Wilson, A.B. and Ashmore, P.E. (2005). Assessing a numerical cellular braided-stream model with a physical model. Earth Surface Processes and Landforms 30(5), 519-540.

Doeschl, A.B., Ashmore, P.E. and Davison, M. (2006). Methods for assessing exploratory computational models of braided rivers. In: Sambrook Smith, G.H., Best, J.L., Bristow, C.S. and Petts, G.E. (Eds.) Braided Rivers: Process, Deposits, Ecology and Management (Special Publication 36 of the International Association of Sedimentologists). Oxford, UK: Wiley-Blackwell, pp. 177-197.

Döll, P. and Zhang, J. (2010). Impact of climate change on freshwater ecosystems: a global-scale analysis of ecologically relevant river flow alterations. Hydrology and Earth System Sciences Discussions 7, 1305-1342.

Dottori, F. and Todini, E. (2011). Developments of a flood inundation model based on the cellular automata approach: Testing different methods to improve model performance. Physics and Chemistry of the Earth, Parts A/B/C 36(7), 266-280.

Downs, P.W. and Thorne, C.R. (1996). A geomorphological justification of river channel reconnaissance surveys. Transactions of the Institute of British Geographers 21(3), 455-468.

Einstein, H.A. (1950). The bed-load function for sediment transportation in open channel flows: Technical Bulletin 1026. Washington, DC: US Department of Agriculture.

Elsner, M.M., Cuo, L., Voisin, N., Deems, J.S., Hamlet, A.F., Vano, J.A., Mickelson, K.E., Lee, S.-Y. and Lettenmaier, D.P. (2010). Implications of 21st century climate change for the hydrology of Washington State. Climatic Change 102(1-2), 225-260.

ESRI. (2013). Using the ArcGIS Spatial Analyst toolbar to calculate slope. [Online]. [Last accessed November 28, 2013]. Available from: www.webhelp.esri.com/arcgisdesktop/9.3/.

Ewen, J. and Parkin, G. (1996). Validation of catchment models for predicting land-use and climate change impacts. 1. Method. Journal of Hydrology 175, 583-594.

Ewen, J., Parkin, G. and O'Connell, P.E. (2000). SHETRAN: distributed river basin flow and transport modeling system. Journal of Hydrologic Engineering 5(3), 250-258.

Fischer, G.R., Costa, M.H., Murta, F.Z., Malhado, A., Aguiar, L.J. and Ladle, R.J. (2013). Multi-site land surface model optimization: An exploration of objective functions. Agricultural and Forest Meteorology 182, 168-176.

Fleurant, C., Tucker, G.E. and Viles, H.A. (2008). Modelling cockpit karst landforms. Geological Society, London, Special Publications 296(1), 47-62.

Forman, E.H. and Gass, S.I. (2001). The Analytic Hierarchy Process - an exposition. Operations Research 49(4), 469-486.

Formann, E., Habersack, H. and Schober, S. (2007). Morphodynamic river processes and techniques for assessment of channel evolution in Alpine gravel bed rivers. Geomorphology 90(3), 340-355.

Franklin, J.F., Frenzen, P.M. and Swanson, F.J. (1988). Re-creation of ecosystems at Mount St Helens: contrasts in artificial and natural approaches. In: Cairns Jr., J. (Eds.) Rehabilitating damaged ecosystems. Boca Raton, FL: CRC Press, pp. 1-37.

Gaillard, M.-J., Dearing, J.A., El-Daoushy, F., Enell, M. and Håkansson, H. (1991). A multidisciplinary study of the lake Bjäresjösjön (S Sweden): land-use history, soil erosion, lake trophy and lake-level fluctuations during the last 3000 years. Hydrobiologia 214, 107-114.

Gilbert, G.K. (1917). Hydraulic-mining debris in the Sierra Nevada: US Geological Survey Professional Paper 105. Washington, DC: US Government Printing Office.

Glade, T. (2003). Landslide occurrence as a response to land use change: a review of evidence from New Zealand. Catena 51(3), 297-314.

Glicken, H. (1996). Rockslide-debris avalanche of May 18, 1980, Mount St Helens volcano: US Geological Survey Open File Report 96-677. Vancouver, WA: US Geological Survey.

Goderniaux, P., Brouyère, S., Fowler, H.J., Blenkinsop, S., Therrien, R., Orban, P. and Dassargues, A. (2009). Large scale surface–subsurface hydrological model to assess climate change impacts on groundwater reserves. Journal of Hydrology 373(1), 122-138.

Goepel, K.D. (2013). BPMSG AHP Excel template with multiple inputs, version 08-02-13. [Online]. [Last accessed February 16, 2013]. Available from: www.bpmsg.com.

Gomez, B. and Church, M. (1989). An assessment of bed load sediment transport formulae for gravel bed rivers. Water Resources Research 25(6), 1161-1186.

Goudie, A.S. (2006). Global warming and fluvial geomorphology. Geomorphology 79(3), 384-394.

Graf, W.L. (1977). The rate law in fluvial geomorphology. American Journal of Science 277(2), 178-191.

Gran, K.B. (2012). Strong seasonality in sand loading and resulting feedbacks on sediment transport, bed texture, and channel planform at Mount Pinatubo, Philippines. Earth Surface Processes and Landforms 37(9), 1012-1022.

Gran, K.B. and Paola, C. (2001). Riparian vegetation controls on braided stream dynamics. Water Resources Research 37(12), 3275-3283.

Gran, K.B. and Montgomery, D.R. (2005). Spatial and temporal patterns in fluvial recovery following volcanic eruptions: Channel response to basin-wide sediment loading at Mount Pinatubo, Philippines. Geological Society of America Bulletin 117, 195.

Gran, K.B., Montgomery, D.R. and Halbur, J.C. (2011). Long-term elevated post-eruption sedimentation at Mount Pinatubo, Philippines. Geology 39(4), 367-370.

Grant, G.E. (1997). Critical flow constrains flow hydraulics in mobile-bed streams: A new hypothesis. Water Resources Research 33(2), 349-358.

Gurnell, A.M. and Petts, G. (2006). Trees as riparian engineers: the Tagliamento River, Italy. Earth Surface Processes and Landforms 31(12), 1558-1574.

Gurnell, A.M., Bertoldi, W. and Corenblit, D. (2012). Changing river channels: The roles of hydrological processes, plants and pioneer fluvial landforms in humid temperate, mixed load, gravel bed rivers. Earth-Science Reviews 111(1-2), 129-141.

Hamlet, A.F., Carrasco, J., Deems, J., Elsner, M.M., Kamstra, T., Lee, C., Lee, S.-Y., Mauger, G., Salathe, I., Tohver, I.M. and Whitely Binder, L. (2010). Final project report for the Columbia Basin Climate Change Scenarios Project.

Hamlet, A.F., Elsner, M.M., Mauger, G., Lee, S.-Y. and Tohver, I.M. (2013). An overview of the Columbia Basin Climate Change Scenarios Project: approach, methods and summary of key results. Atmosphere-Ocean 51(4), 392-415.

Hancock, G.R. and Willgoose, G.R. (2002). The use of a landscape simulator in the validation of the SIBERIA landscape evolution model: transient landforms. Earth Surface Processes and Landforms 27, 1321-1334.

Hancock, G.R. and Coulthard, T.J. (2012). Channel movement and erosion response to rainfall variability in southeast Australia. Hydrological Processes 26(5), 663-673.

Hancock, G.R., Lowry, J.B.C., Coulthard, T.J., Evans, K.G. and Moliere, D.R. (2010). A catchment scale evaluation of the SIBERIA and CAESAR landscape evolution models. Earth Surface Processes and Landforms 35, 863-875.

Hancock, G.R., Coulthard, T.J., Martinez, C. and Kalma, J.D. (2011). An evaluation of landscape evolution models to simulate decadal and centennial scale soil erosion in grassland catchments. Journal of Hydrology 398(3), 171-183.

Harvey, C.L., Dixon, H. and Hannaford, J. (2010). Developing best practice for infilling daily river flow data. In: Kirby, C. (Eds.) Role of Hydrology in Managing Consequences of a Changing Global Environment. Proceedings of the BHS Third International Symposium: British Hydrological Society, pp. 816-823.

Hayes, S. (2002). Fluvial sediment transport and deposition following the 1991 eruption of Mount Pinatubo. Geomorphology 45, 211-224.

Henderson, F. (1966). Open Channel Flow. New York, NY: McMillan.

Hicks, D.M., Gomez, B. and Trustrum, N.A. (2000). Erosion thresholds and suspended sediment yields, Waipaoa River Basin, New Zealand. Water Resources Research 36(4), 1129-1142.

Hirsch, R.M. (1979). An evaluation of some record reconstruction techniques. Water Resources Research 15(6), 1781-1790.

Hirsch, R.M. (1982). A comparison of four streamflow record extension techniques. Water Resources Research 18(4), 1081-1088.

Hoblitt, R.P., Miller, C.D. and Vallance, J.W. (1981). Origin and stratigraphy of the deposit produced by the May 18 directed blast. In: Lipman, P.W. and Mullineaux, D.R. (Eds.) The 1980 eruptions of Mount St Helens, Washington:

US Geological Survey Professional Paper 1250. Washington, DC: US Government Printing Office, pp. 401-420.

Hooke, J.M. (1995). River channel adjustment to meander cutoffs on the River Bollin and River Dane, northwest England. Geomorphology 14(3), 235-253.

Horritt, M.S. and Bates, P.D. (2001). Predicting floodplain inundation: raster-based modelling versus the finite-element approach. Hydrological Processes 15(5), 825-842.

Horritt, M.S. and Bates, P.D. (2002). Evaluation of 1D and 2D numerical models for predicting river flood inundation. Journal of Hydrology 268(1), 87-99.

Horritt, M.S., Di Baldassarre, G., Bates, P.D. and Brath, A. (2007). Comparing the performance of a 2D finite element and a 2D finite volume model of floodplain inundation using airborne SAR imagery. Hydrological Processes 21(20), 2745-2759.

Hunter, N.M., Bates, P.D., Neelz, S., Pender, G., Villanueva, I., Wright, N.G., Liang, D., Falconer, R.A., Lin, B. and Waller, S. (2008). Benchmarking 2D hydraulic models for urban flooding. Proceedings of the ICE-Water Management 161(1), 13-30.

Hupp, C.R. (1992). Riparian vegetation recovery patterns following stream channelization: a geomorphic perspective. Ecology, 1209-1226.

Hyndman, R.J. and Koehler, A.B. (2005). Another look at measures of forecast accuracy. International Journal of Forecasting 22, 679-688.

Iverson, R.M. (2003). How should mathematical models of geomorphic processes be judged? In: Wilcock, P.R. and Iverson, R.M. (Eds.) Prediction in Geomorphology. Geophysical Monograph 135. Washington, DC: American Geophysical Union, pp. 1-12.

James, L.A. (1989). Sustained storage and transport of hydraulic gold mining sediment in the Bear River, California. Annals of the Association of American Geographers 79(4), 570-592.

James, L.A. (1997). Channel incision on the lower American River, California, from streamflow gage records. Water Resources Research 33(3), 485-490.

James, L.A. (1999). Time and the persistence of alluvium: River engineering, fluvial geomorphology, and mining sediment in California. Geomorphology 31(1), 265-290.

Janda, R.J., Scott, K.M., Nolan, K.M. and Martinson, H.A. (1981). Lahar movements, effects and deposits. In: Lipman, P.W. and Mullineaux, D.R. (Eds.) The 1980 eruptions of Mount St Helens, Washington: US Geological Survey Professional Paper 1250. Washington, DC: US Government Printing Office, pp. 461-478.

Janssen, P.H.M. and Heuberger, P.S.C. (1995). Calibration of process-oriented models. Ecological Modelling 83, 55-66.

Jones, R.N. (2000). Managing uncertainty in climate change projections – issues for impact assessment. Climatic Change 45, 403-419.

Keylock, C. (2007). Identifying linear and non-linear behaviour in reduced complexity modelling output using surrogate data methods. Geomorphology 90, 356-366.

Kinnell, P.I.A. (2005). Raindrop-impact-induced erosion processes and prediction: a review. Hydrological Processes 19, 2815-2844.

Kirkby, M.J. (1971). Hillslope process-response models based on the continuity equation. In: Brunsden, D. (Eds.) Slopes - form and process. Institute of British Geographers Special Publication 3, pp. 15-30.

Kirkby, M.J. (1984). Modeling cliff development in South Wales Savigear re-viewed. Zeitschrift für Geomorphologie 28, 405-426.

Knighton, D. (1998). Fluvial Forms and Processes: A New Perspective. London, UK: Hodder Arnold.

Koi, T., Hotta, N., Ishigaki, I., Matuzaki, N., Uchiyama, Y. and Suzuki, M. (2008). Prolonged impact of earthquake-induced landslides on sediment yield in a mountain watershed: the Tanzawa region, Japan. Geomorphology 101(4), 692-702.

Korup, O. (2005). Large landslides and their effect on sediment flux in South Westland, New Zealand. Earth Surface Processes and Landforms 30(3), 305-323.

Korup, O. (2012). Earth's portfolio of extreme sediment transport events. Earth-Science Reviews 112(3), 115-125.

Krause, P., Boyle, D. and Bäse, F. (2005). Comparison of different efficiency criteria for hydrological model assessment. Advances in Geosciences 5(5), 89-97.

Lancaster, S.T. and Grant, G.E. (2003). You want me to predict what? In: Wilcock, P.R. and Iverson, R.M. (Eds.) Prediction in Geomorphology.

Geophysical Monograph 135. Washington, DC: American Geophysical Union, pp. 1-10.

Lane, S.N. (1998). Hydraulic modelling in hydrology and geomorphology: a review of high resolution approaches. Hydrological Processes 12(8), 1131-1150.

Lane, S.N. and Richards, K.S. (1997). Linking river channel form and process: time, space and causality revisited. Earth Surface Processes and Landforms 22(3), 249-260.

Lane, S.N. and Richards, K.S. (2001). The validation of hydrodynamic models: some critical perspectives. In: Anderson, M.G. and Bates, P.D. (Eds.) Model Validation: Perspectives in Hydrological Science. Chichester, UK: John Wiley and Sons, pp. 413-438.

Lane, S.N., Hardy, R.J., Ingham, D.B. and Elliott, L. (2004). Numerical modelling of flow processes over gravelly-surfaces using structured grids and a numerical porosity treatment. Water Resources Research 40, W01302.

Lawrence, R. (2005). Remote sensing of vegetation responses during the first 20 years following the 1980 eruption of Mount St Helens: A spatially and temporally stratified analysis. In: Dale, V.H., Swanson, F.J. and Crisafulli, C.M. (Eds.) Ecological Responses to the 1980 Eruption of Mount St Helens. New York, NY: Springer, pp. 111-123.

Legates, D.R. and McCabe Jr., G.J. (1999). Evaluating the use of "goodness-of-fit" measures in hydrologic and hydroclimatic model validation. Water Resources Research 35(1), 233-241.

Lehre, A.K., Collins, B.D. and Dunne, T. (1983). Post-eruption sediment budget for the North Fork Toutle River drainage, June 1980 - June 1981. Zeitschrift für Geomorphologie, Neue Folge, Supplementband 46, 143-165.

Leon, C., Julien, P.Y. and Baird, D.C. (2009). Case Study: Equivalent Widths of the Middle Rio Grande, New Mexico. Journal of Hydraulic Engineering 135(4), 306-315.

Leopold, L.B. (1994). A View of the River. Cambridge, MA: Harvard University Press.

Liang, X., Lettenmaier, D.P., Wood, E.F. and Burges, S.J. (1994). A simple hydrologically based model of land surface water and energy fluxes for general circulation models. Journal of Geophysical Research 99(D7), 14415-14428.

Lipman, P.W. and Mullineaux, D.R. (Eds.) (1981). The 1980 Eruptions of Mount St Helens, Washington: US Geological Survey Professional Paper 1250. Washington, D.C.: US Government Printing Office.

Lipman, P.W., Moore, J.G. and Swanson, D. (1981). Bulging of the north flank before the May 18 eruption: geodetic data. In: Lipman, P.W. and Mullineaux, D.R. (Eds.) The 1980 eruptions of Mount St Helens, Washington: US Geological Survey Professional Paper 1250. Washington, DC: US Government Printing Office, pp. 143-156.

Lombard, R., Miles, M., Nelson, L., Kresh, D. and Carpenter, P. (1981). The impact of mudflows of May 18 on the lower Toutle and Cowlitz Rivers. In: Lipman, P.W. and Mullineaux, D.R. (Eds.) The 1980 eruptions of Mount St Helens, Washington: US Geological Survey Professional Paper 1250. Washington, DC: US Government Printing Office, pp. 693-699.

Lukey, B.T., Sheffield, J., Bathurst, J.C., Hiley, R.A. and Mathys, N. (2000). Test of the SHETRAN technology for modelling the impact of reforestation on badlands runoff and sediment yield at Draix, France. Journal of Hydrology 235, 44-62.

Major, J.J. (2004). Posteruption suspended sediment transport at Mount St Helens: Decadal-scale relationships with landscape adjustments and river discharges. Journal of Geophysical Research 109, 1-22.

Major, J.J. and Mark, L.E. (2006). Peak flow responses to landscape disturbances caused by the cataclysmic 1980 eruption of Mount St Helens, Washington. Geological Society of America Bulletin 118, 938-958.

Major, J.J., Pierson, T.C., Dinehart, R.L. and Costa, J.E. (2000). Sediment yield following severe volcanic disturbance - a two-decade perspective from Mount St Helens. Geology 28, 819-822.

Major, J.J., Pierson, T.C. and Scott, K.M. (2005). Debris flows at Mount St Helens, Washington, USA. In: Jakob, M. and Hungr, O. (Eds.) Debris Flow Hazards and Related Phenomena. Berlin, Germany: Springer-Praxis, pp. 685-731.

Major, J.J., Crisafulli, C.M., Frenzen, P.M. and Bishop, J. (2009). After the disaster: The hydrogeomorphic, ecological, and biological responses to the 1980 eruption of Mount St Helens, Washington. Field Guides 15, 111-134.

Major, J.J., O'Connor, J.E., Podolak, C.J., Keith, M.K., Grant, G.E., Spicer, K.R., Pittman, S., Bragg, H.M., Wallick, J.R. and Tanner, D.Q. (2012). Geomorphic response of the Sandy River, Oregon, to removal of Marmot Dam: US Geological Survey Professional Paper 1792. Washington, DC: US Government Printing Office.

Makridakis, S. (1993). Accuracy measures: theoretical and practical concerns. International Journal of Forecasting 9(4), 527-529.

Mantua, N.J., Hare, S.R., Zhang, Y., Wallace, J.M. and Francis, R.C. (1997). A Pacific interdecadal climate oscillation with impacts on salmon production. Bulletin of the American Meteorological Society 78(6), 1069-1079.

Manville, V. and Wilson, C.J. (2004). The 26.5 ka Oruanui eruption, New Zealand: A review of the roles of volcanism and climate in the post-eruptive sedimentary response. New Zealand Journal of Geology and Geophysics 47(3), 525-547.

Manville, V., Segschneider, B., Newton, E., White, J., Houghton, B. and Wilson, C. (2009). Environmental impact of the 1.8 ka Taupo eruption, New Zealand: Landscape responses to a large-scale explosive rhyolite eruption. Sedimentary Geology 220(3), 318-336.

Martin, Y. and Church, M. (2004). Numerical modelling of landscape evolution: geomorphological perspectives. Progress in Physical Geography 28, 317-339.

Maurer, E.P. and Hidalgo, H.G. (2008). Utility of daily vs. monthly large-scale climate data: an intercomparison of two statistical downscaling methods. Hydrology and Earth System Sciences 12(2), 551-563.

Mayer, D.G. and Butler, D.G. (1993). Statistical validation. Ecological Modelling 68, 21-32.

McCuen, R.H., Knight, Z. and Cutter, A.G. (2006). Evaluation of the Nash–Sutcliffe efficiency index. Journal of Hydrologic Engineering 11(6), 597-602.

McKenney, R., Jacobson, R.B. and Wertheimer, R.C. (1995). Woody vegetation and channel morphogenesis in low-gradient, gravel-bed streams in the Ozark Plateaus, Missouri and Arkansas. Geomorphology 13, 175-198.

Meier, M., Carpenter, P. and Janda, R. (1981). Hydrologic effects of Mount St Helens' 1980 eruptions. Eos, Transactions American Geophysical Union 62(33), 625-626.

Meyer, D. and Dodge, J.E. (1987). Post-eruption changes in channel geometry of streams in the Toutle River drainage basin, 1983-85, Mount St Helens, Washington: US Geological Survey Open-File Report 87-549. Vancouver, WA: US Geological Survey.

Meyer, D. and Martinson, H. (1989). Rates and processes of channel development and recovery following the 1980 eruption of Mount St Helens, Washington. Hydrological Sciences Journal 34, 115-127.

Montgomery, D.C., Peck, E.A. and Vining, G.G. (2001). Introduction to linear regression analysis. New York, NY: John Wiley and Sons.

Moog, D.B., Whiting, P.J. and Thomas, R.B. (1999). Streamflow record extension using power transformations and application to sediment transport. Water Resources Research 35(1), 243-254.

Moore, J.G. and Albee, W.C. (1981). Topographic and structural changes, March-July 1980 — photogrammetric data. In: Lipman, P.W. and Mullineaux, D.R. (Eds.) The 1980 eruptions of Mount St Helens, Washington: US Geological Survey Professional Paper 1250. Washington, DC: US Government Printing Office, pp. 123-134.

Moore, J.G. and Sisson, T.W. (1981). Deposits and effects of the May 18 pyroclastic surge. In: Lipman, P.W. and Mullineaux, D.R. (Eds.) The 1980 eruptions of Mount St Helens, Washington: US Geological Survey Professional Paper 1250. Washington, DC: US Government Printing Office, pp. 421-438.

Morgan, R.P.C., Quinton, J.N., Smith, R.E., Govers, G., Poesen, J.W.A., Auerswald, K., Chisci, G., Torri, D. and Styczen, M.E. (1998). The European Soil Erosion Model (EUROSEM): a dynamic approach for predicting sediment transport from fields and small catchments. Earth Surface Processes and Landforms 23(6), 527-544.

Mote, P.W. and Salathé Jr., E.P. (2010). Future climate in the Pacific Northwest. Climatic Change 102(1-2), 29-50.

Mullineaux, D.R. and Crandell, D.R. (1981). The eruptive history of Mount St Helens. In: Lipman, P.W. and Mullineaux, D.R. (Eds.) The 1980 eruptions of Mount St Helens, Washington: US Geological Survey Professional Paper 1250. Washington, DC: US Government Printing Office, pp. 3-15.

Murray, A.B. (2003). Contrasting the goals, strategies, and predictions associated with simplified numerical models and detailed simulations. In: Wilcock, P.R. and Iverson, R.M. (Eds.) Prediction in Geomorphology, Geophysical Monograph 135. Washington, DC: American Geophysical Union, pp. 151-165.

Murray, A.B. (2007). Reducing model complexity for explanation and prediction. Geomorphology 90, 178-191.

Murray, A.B. and Paola, C. (1994). A cellular model of braided rivers. Nature 371(6492), 54-57.

Nachtergaele, J., Poesen, J., Steegen, A., Takken, I., Beuselinck, L., Vandekerckhove, L. and Govers, G. (2001). The value of a physically based

model versus an empirical approach in the prediction of ephemeral gully erosion for loess-derived soils. Geomorphology 40(3), 237-252.

Nakićenović, N. and Swart, R. (Eds.) (2000). Special report on emissions scenarios. A special report of working group III of the Intergovernmental Panel on Climate Change. Cambridge, UK: Cambridge University Press.

Nearing, M., Foster, G., Lane, L. and Finkner, S. (1989). A process-based soil erosion model for USDA - Water Erosion Prediction Project technology. Transactions of the American Society of Agricultural Engineers 32(5), 1587-1593.

Nelson, J.M., Bennett, J.P. and Wiele, S.M. (2003). Flow and sediment-transport modeling. In: Kondolf, G.M. and Piegay, H. (Eds.) Tools in Fluvial Geomorphology. Chichester, UK: John Wiley and Sons Ltd, pp. 539-576.

Newson, M. (1980). The geomorphological effectiveness of floods - a contribution stimulated by two recent events in mid-Wales. Earth Surface Processes 5, 1-16.

Nicholas, A.P. (2005). Cellular modelling in fluvial geomorphology. Earth Surface Processes and Landforms 30, 645-649.

Nicholas, A.P. (2009). Reduced-complexity flow routing models for sinuous single-thread channels: intercomparison with a physically-based shallow-water equation model. Earth Surface Processes and Landforms 34, 641-653.

Nicholas, A.P. and Quine, T. (2007). Crossing the divide: Representation of channels and processes in reduced-complexity river models at reach and landscape scales. Geomorphology 90, 318-339.

Nijssen, B., O'Donnell, G.M., Lettenmaier, D.P., Lohmann, D. and Wood, E.F. (2001). Predicting the discharge of global rivers. Journal of Climate 14(15), 3307-3323.

Oreskes, N. (1998). Evaluation (not validation) of quantitative models. Environmental Health Perspectives 106, 1453-1460.

Oreskes, N. (2003). The role of quantitative models in science. In: Canham, C.D., Cole, J.J. and Lauenroth, W.K. (Eds.) Models in Ecosystem Science. Princeton, NJ: Princeton University Press, pp. 13-31.

Oreskes, N. and Belitz, K. (2001). Philosophical issues in model assessment. In: Anderson, M.G. and Bates, P.D. (Eds.) Model Validation: Perspectives in Hydrological Science: John Wiley and Sons, Ltd., pp. 23-41.

Oreskes, N., Shrader-Frechette, K. and Belitz, K. (1994). Verification, validation, and confirmation of numerical models in the earth sciences. Science 263, 641-646.

Paola, C. (2001). Modelling stream braiding over a range of scales. In: Mosley, M.P. (Eds.) Gravel-Bed Rivers V. Wellington, NZ: New Zealand Hydrological Society, pp. 11-38.

Paola, C. and Seal, R. (1995). Grain size patchiness as a cause of selective deposition and downstream fining. Water Resources Research 31, 1395-1407.

Parkin, G., O'Donnell, G., Ewen, J., Bathurst, J.C., O'Connell, P.E. and Lavabre, J. (1996). Validation of catchment models for predicting land-use and climate change impacts. 2. Case study for a Mediterranean catchment. Journal of Hydrology 175, 595-613.

Payne, J.T., Wood, A.W., Hamlet, A.F., Palmer, R.N. and Lettenmaier, D.P. (2004). Mitigating the effects of climate change on the water resources of the Columbia River basin. Climatic Change 62(1-3), 233-256.

Pazzaglia, F. (2003). Landscape evolution models. Developments in Quaternary Science 1, 247-274.

Pearson, M.L. (1984). Geomorphological analysis of the North Fork, Toutle River Washington: 1980-1984. US Army Corps of Engineers Technical Report GL-94-7. Vicksburg, MS: US Army Corps of Engineers.

Phillips, J.D. (2006). Evolutionary geomorphology: thresholds and nonlinearity in landform response to environmental change. Hydrology and Earth System Sciences Discussions 3(2), 365-394.

Pierce, D.W., Westerling, A.L. and Oyler, J. (2013). Future humidity trends over the western United States in the CMIP5 global climate models and variable infiltration capacity hydrological modeling system. Hydrology and Earth System Sciences 17(5), 1833-1850.

Pierson, T.C. and Major, J.J. (2014). Hydrogeomorphic effects of explosive volcanic eruptions on drainage basins. Annual Review of Earth and Planetary Sciences 42, 469-507.

Pierson, T.C., Janda, R.J., Umbal, J.V. and Daag, A.S. (1992). Immediate and long-term hazards from lahars and excess sedimentation in rivers draining Mt. Pinatubo, Philippines: US Geological Survey Water-Resources Investigations Report 92-4039.

Pierson, T.C., Pringle, P.T. and Cameron, K.A. (2011). Magnitude and timing of downstream channel aggradation and degradation in response to a dome-

building eruption at Mount Hood, Oregon. Geological Society of America Bulletin 123(1-2), 3-20.

Pitlick, J. (1993). Response and recovery of a subalpine stream following a catastrophic flood. Geological Society of America Bulletin 105(5), 657-670.

Pizzuto, J.E. (2003). Numerical modeling of alluvial landforms. In: Kondolf, G.M. and Piegay, H. (Eds.) Tools in Fluvial Geomorphology. Chichester, UK: Jon Wiley and Sons Ltd, pp. 577-595.

Polvi, L.E. and Wohl, E. (2013). Biotic drivers of stream planform: implications for understanding the past and restoring the future. BioScience 63(6), 439-452.

Prosser, I.P. and Soufi, M. (1998). Controls on gully formation following forest clearing in a humid temperate environment. Water Resources Research 34(12), 3661-3671.

Prosser, I.P., Rutherfurd, I.D., Olley, J.M., Young, W.J., Wallbrink, P.J. and Moran, C.J. (2001). Large-scale patterns of erosion and sediment transport in river networks, with examples from Australia. Marine and Freshwater Research 52(1), 81-99.

Randall, D.A., Wood, R.A., Bony, S., Colman, R., Fichefet, T., Fyfe, J., Kattsov, V., Pitman, A., Shuckla, J., Srinivasan, J., Stouffer, R.J., Sumi, A. and Taylor, K.E. (2007). Climate models and their evaluation. In: Solomon, S., Qin, D., Manning, M., Chen, Z., Marquis, M., Averyt, K.B., Tignor, M. and Miller, H.L. (Eds.) Climate Change 2007: The Physical Science Basis. Contribution of Working Group I to the Fourth Assessment Report of the Intergovernmental Panel on Climate Change. Cambridge, UK: Cambridge University Press, pp. 589-662.

Rathburn, S.L., Rubin, Z.K. and Wohl, E.E. (2013). Evaluating channel response to an extreme sedimentation event in the context of historical range of variability: Upper Colorado River, USA. Earth Surface Processes and Landforms 38(4), 391-406.

Refsgaard, J.C. and Storm, B. (1995). MIKE SHE. In: Singh, V.P. (Eds.) Computer Models of Watershed Hydrology. Colorado, USA: Water Resources Publications, pp. 809-846.

Renard, K.G., Foster, G.R., Weesies, G.A. and Porter, J.P. (1991). RUSLE: Revised universal soil loss equation. Journal of Soil and Water Conservation 46(1), 30-33.

Rowley, P., Kuntz, M. and MacLeod, N. (1981). Pyroclastic-flow deposits. In: Lipman, P.W. and Mullineaux, D.R. (Eds.) The 1980 eruptions of Mount St

Helens, Washington: US Geological Survey Professional Paper 1250. Washington, DC: US Government Printing Office, pp. 489-512.

Saaty, R.W. (1987). The analytic hierarchy process - what it is and how it is used. Mathematical Modelling 9(3-5), 161-176.

Saaty, T.L. (1980). The Analytic Hierarchy Process. New York, NY: McGraw Hill.

Saaty, T.L. (1986). Axiomatic foundation of the analytic hierarchy process. Management Science 32(7), 841-855.

Saaty, T.L. (1994a). How to make a decision: the Analytic Hierarchy Process. Interfaces 24(6), 19-43.

Saaty, T.L. (1994b). Highlights and critical points in the theory and application of the Analytic Hierarchy Process. European Journal of Operational Research 74(3), 426-447.

Saaty, T.L. (2008). Decision making with the Analytic Hierarchy Process. International Journal of Services Sciences 1(1), 83-98.

Salathé Jr., E.P. (2004). Methods for selecting and downscaling future global climate with application to hydrologic modelling. International Journal of Climatology 25, 419-436.

Salathé Jr., E.P. (2005). Downscaling simulations of future global climate with application to hydrologic modelling. International Journal of Climatology 25(4), 419-436.

Salathé Jr., E.P. (2006). Influences of a shift in North Pacific storm tracks on western North American precipitation under global warming. Geophysical Research Letters 33, L19820, doi:19810.11029/12006GL026882.

Salathé Jr., E.P., Mote, P.W. and Wiley, M.W. (2007). Review of scenario selection and downscaling methods for the assessment of climate change impacts on hydrology in the United States Pacific Northwest. International Journal of Climatology 27(12), 1611-1621.

Sarna-Wojcicki, A.M., Shipley, S., Waitt Jr, R.B., Dzurisin, D. and Wood, S.H. (1981). Areal distribution, thickness, mass, volume, and grain size of air-fall ash from the six major eruptions of 1980. In: Lipman, P.W. and Mullineaux, D.R. (Eds.) The 1980 eruptions of Mount St Helens, Washington: US Geological Survey Professional Paper 1250. Washinton, DC: US Government Printing Office, pp. 577-600.

Sayer, A. (1992). Method in social science: a realist approach. London, UK: Routledge.

Schumm, S.A. (1973). Geomorphic thresholds and complex response of drainage systems. In: Morisawa, M. (Eds.) Fluvial geomorphology. Binghampton, NY: New York State University Publications in Geomorphology, pp. 299-310.

Schumm, S.A. (1979). Geomorphic thresholds: the concept and its applications. Transactions of the Institute of British Geographers 4(4), 485-515.

Schumm, S.A. (1991). To interpret the Earth: ten ways to be wrong. Cambridge, UK: Cambridge University Press.

Scott, K.M. (1989). Magnitude and frequency of lahars and lahar-runout flows in the Toutle-Cowlitz River system: US Geological Survey Professional Paper 1447-B. Washington, DC: US Government Printing Office.

Silburn, D.M. and Connolly, R.D. (1995). Distributed parameter hydrology model (ANSWERS) applied to a range of catchment scales using rainfall simulator data I: Infiltration modelling and parameter measurement. Journal of Hydrology 172, 87-104.

Simon, A. (1992). Energy, time, and channel evolution in catastrophically disturbed fluvial systems. Geomorphology 5(3), 345-372.

Simon, A. (1998). Processes and forms of the Yalobusha River System: A detailed geomorphic evaluation. Vicksburg, MS: US Army Corps of Engineers Vicksburg District.

Simon, A. (1999). Channel and drainage-basin response of the Toutle River system in the aftermath of the 1980 eruption of Mount St Helens, Washington: US Geological Survey Open File Report 96-633. Vancouver, WA: US Geological Survey.

Simon, A. and Hupp, C.R. (1987). Geomorphic and vegetative recovery processes along modified Tennessee streams: an interdisciplinary approach to distributed fluvial systems. International Association of Hydrological Sciences Publication 167, 251-262.

Simon, A. and Thorne, C.R. (1996). Channel adjustment of an unstable coarse-grained stream: opposing trends of boundary and critical shear stress, and the applicability of extremal hypotheses. Earth Surface Processes and Landforms 21, 155-180.

Simon, A. and Klimetz, D. (2012). Analysis of long-term sediment loadings from the upper North Fork Toutle River system, Mount St Helens, Washington. US Department of Agriculture, Agricultural Research Service, National Sedimentation Laboratory Technical Report Number 77. Portland, OR.

Simon, A., Curini, A., Darby, S.E. and Langendoen, E.J. (2000). Bank and near-bank processes in an incised channel. Geomorphology 35, 193-217.

Stewart, M.D., Bates, P.D., Anderson, M.G., Price, D.A. and Burt, T.P. (1999). Modelling floods in hydrologically complex lowland river reaches. Journal of Hydrology 223, 85-106.

Surian, N. and Rinaldi, M. (2003). Morphological response to river engineering and management in alluvial channels in Italy. Geomorphology 50(4), 307-326.

Swanson, F.J. and Major, J.J. (2005). Physical events, environments, and geological—ecological interactions at Mount St. Helens: March 1980–2004. In: Dale, V.H., Swanson, F.J. and Crisafulli, C.M. (Eds.) Ecological responses to the 1980 eruption of Mount St. Helens. New York: Springer, pp. 27-44.

Swanson, F.J., Fredriksen, R.L. and McCorison, F.M. (1982). Material transfer in a western Oregon forested watershed. In: Edmonds, R.L. (Eds.) Analysis of coniferous forest ecosystems in the western United States. Stroudsburg, PA: Hutchison Ross Publishing, pp. 233-266.

Tabor, K. and Williams, J.W. (2010). Globally downscaled climate projections for assessing the conservation impacts of climate change. Ecological Applications 20(2), 554-565.

Takken, I., Beuselinck, L., Nachtergaele, J., Govers, G., Poesen, J. and Degraer, G. (1999). Spatial evaluation of a physically-based distributed erosion model (LISEM). Catena 37(3), 431-447.

Tal, M. and Paola, C. (2007). Dynamic single-thread channels maintained by the interaction of flow and vegetation. Geology 35(4), 347-350.

Temme, A.J.A.M., Claessens, L., Veldkamp, A. and Schoorl, J.M. (2011). Evaluating choices in multi-process landscape evolution models. Geomorphology 125, 271-281.

Thomas, R. and Nicholas, A.P. (2002). Simulation of braided river flow using a new cellular routing scheme. Geomorphology 43(3), 179-195.

Thomas, R., Nicholas, A.P. and Quine, T. (2007). Cellular modelling as a tool for interpreting historic braided river evolution. Geomorphology 90, 302-317.

Thorne, C.R. (1978). Processes of bank erosion in river channels. PhD Thesis, University of East Anglia.

Thorne, C.R. (1982). Processes and mechanisms of river bank erosion. In: Hey, R.D., Bathurst, J.C. and Thorne, C.R. (Eds.) Gravel-Bed Rivers. Chichester, UK: John Wiley and Sons, Ltd., pp. 227-271.

Thorne, C.R., Townsend, J. and Ashley, T. (2014). Geomorphic and ecological assessment and evaluation of grade building structure on the SRS sediment plain, North Fork Toutle River. Final report to the Portland District, US Army Corps of Engineers, under contract W9127N-13-P-0072. Portland, OR: US Army Corps of Engineers Portland District.

Tinkler, K. (1997). Critical flow in rockbed streams with estimated values for Manning's n. Geomorphology 20(1), 147-164.

Tohver, I.M., Hamlet, A.F. and Lee, S.Y. (2014). Impacts of 21st-Century Climate Change on Hydrologic Extreme in the Pacific Northwest Region of North America. Journal of the American Water Resources Association (JAWRA), 1-16. DOI: 10.1111/jawr.12199.

Trimble, S.W. (2009). Fluvial processes, morphology and sediment budgets in the Coon Creek Basin, WI, USA, 1975–1993. Geomorphology 108, 8-23.

Tucker, G.E. and Slingerland, R. (1994). Erosional dynamics, flexural isostasy, and long-lived escarpments: A numerical modeling study. Journal of Geophysical Research 99, 12229-12243.

Tucker, G.E. and Bras, R.L. (2000). A stochastic approach to modeling the role of rainfall variability in drainage basin evolution. Water Resources Research 36, 1953-1964.

Tucker, G.E. and Hancock, G.R. (2010). Modelling landscape evolution. Earth Surface Processes and Landforms 35, 28-50.

Tucker, G.E., Lancaster, S.T., Gasparini, N.M. and Bras, R.L. (2001). The Channel-Hillslope Integrated Landscape Development Model (CHILD). In: Harmon, R.S. and Dow III, W.W. (Eds.) Landscape Erosion and Evolution Modeling. Norwell, MA: Kluwer Academic Publishers, pp. 349-384.

Uhrich, M.A. (1990). Precipitation data for the Mount St Helens area, Washington - 1981-86: US Geological Survey Open-File Report 90-117. Vancouver, WA: US Geological Survey.

USACE (1982). Mount St Helens Cowlitz and Toutle Rivers sedimentation study 1980-1982. Portland, OR: US Army Corps of Engineers Portland District.

USACE (1983). A comprehensive plan for responding to the long-term threat created by the eruption of Mount St Helens, Washington. Portland, OR: US Army Corps of Engineers Portland District.

USACE (1984). Mount St Helens Toutle and Cowlitz Rivers sedimentation study 1984. Portland, OR: US Army Corps of Engineers Portland District.

USACE (1985). Mount St Helens, Washington Decision Document, Toutle, Cowlitz and Columbia Rivers. Portland, OR: US Army Corps of Engineers Portland District.

USACE (1988). Sediment Gradation Analysis Results. Portland, OR: US Army Corps of Engineers Portland District.

USACE (1989). Cowlitz River Basin Water Year 1989 Hydrologic Summary. Portland, OR: US Army Corps of Engineers Portland District.

USACE (1990). Cowlitz River Basin Water Year 1990 Hydrologic Summary. Portlnd, OR: US Army Corps of Engineers Portland District.

USACE (1991). Cowlitz River Basin Water Year 1991 Hydrologic Summary. Portland, OR: US Army Corps of Engineers Portland District.

USACE (1992). Cowlitz River Basin Water Year 1992 Hydrologic Summary. Portland, OR: US Army Corps of Engineers Portland District.

USACE (2002). Mount St Helens engineering reanalysis. Hydrologic, hydraulics, sedimentation and risk analysis. Design documentation report. Portland, OR: US Army Corps of Engineers Portland District.

USACE (2007). Mount St Helens ecosystem restoration reconnaissance report. Portland, OR: US Army Corps of Engineers Portland District.

USACE (2010). Mount St Helens long-term sediment management plan for flood risk reduction: progress report. Portland, OR: US Army Corps of Engineers Portland District.

USACE (2012). Sediment retention structure (SRS) spillway raise project. Mount St Helens sediment management for flood risk reduction. Final environmental assessment. Portland, OR: US Army Corps of Engineers Portland District.

Vaidya, O.S. and Kumar, S. (2006). Analytic hierarchy process: An overview of applications. European Journal of Operational Research 169, 1-29.

Van De Wiel, M.J. and Coulthard, T.J. (2010). Self-organized criticality in river basins: Challenging sedimentary records of environmental change. Geology 38(1), 87-90.

Van De Wiel, M.J., Coulthard, T.J., Macklin, M.G. and Lewin, J. (2007). Embedding reach-scale fluvial dynamics within the CAESAR cellular automaton landscape evolution model. Geomorphology 90, 283-301.

Van De Wiel, M.J., Coulthard, T.J., Macklin, M.G. and Lewin, J. (2011). Modelling the response of river systems to environmental change: progress, problems and prospects for palaeo-environmental reconstructions. Earth-Science Reviews 104(1), 167-185.

Vano, J.A., Scott, M.J., Voisin, N., Stöckle, C.o., Hamlet, A.F., Mickelson, K.E.B., Elsner, M.M. and Lettenmaier, D.P. (2010). Climate change impacts on water management and irrigated agriculture in the Yakima River Basin, Washington, USA. Climatic Change 102(1-2), 287-317.

Vargas, L.G. (1990). An overview of the Analytic Hierarchy Process and its applications. European Journal of Operational Research 48, 2-8.

Visser, H., Folkert, R.J.M., Hoekstra, J. and De Wolff, J.J. (2000). Identifying key sources of uncertainty in climate change projections. Climatic Change 45, 421-457.

Voight, B. (1981). Time scale for the first moments of the May 18 eruption. In: Lipman, P.W. and Mullineaux, D.R. (Eds.) The 1980 eruptions of Mount St Helens, Washington: US Geological Survey Professional Paper 1250. Washington, DC: US Government Printing Office, pp. 69-92.

Voight, B., Glicken, H., Janda, R.J. and Douglass, P.M. (1981). Catastrophic rockslide avalanche of May 18. In: Lipman, P.W. and Mullineaux, D.R. (Eds.) The 1980 eruptions of Mount St Helens, Washington: US Geological Survey Professional Paper 1250. Washington, DC: US Government Printing Office, pp. 347-379.

WADNR. (2011). Washington State Department of Natural Resources GIS Data Centre. [Online]. [Last accessed August 18, 2011]. Available from: http://www.dnr.wa.gov/BusinessPermits/Topics/Data/Pages/gis_data_center.aspx.

Waitt, R.B. (1981). Devastating pyroclastic density flow and attendant air fall of May 18 - stratigraphy and sedimentology of deposits. In: Lipman, P.W. and Mullineaux, D.R. (Eds.) The 1980 eruptions of Mount St Helens, Washington: US Geological Survey Professional Paper 1250. Washington, DC: US Government Printing Office, pp. 439-460.

Waitt, R.B. (1989). Swift snowmelt and floods (lahars) caused by great pyroclastic surge at Mount St Helens volcano, Washington, 18 May 1980. Bulletin of Volcanology 52, 138-157.

Waitt, R.B. and Dzurisin, D. (1981). Proximal air-fall deposits from the May 18 eruption - stratigraphy and field sedimentology. In: Lipman, P.W. and Mullineaux, D.R. (Eds.) The 1980 eruptions of Mount St Helens, Washington: US Geological Survey Professional Paper 1250. Washinton, DC: US Government Printing Office, pp. 601-616.

Walder, J.S., LaHusen, R.G., Vallance, J.W. and Schilling, S.P. (2007). Emplacement of a silicic lava dome through a crater glacier: Mount St Helens, 2004-06. Annals of Glaciology 45, 14-20.

Walder, J.S., Schilling, S.P., Sherrod, D.R. and Vallance, J.W. (2010). Photographic documentation of the evolution of Crater Glacier, Mount St Helens, Washington, September 2006 - November 2009: US Geological Survey Open-File Report 2010-1141. Reston, VA: US Geological Survey.

Welsh, K.E., Dearing, J.A., Chiverrell, R.C. and Coulthard, T.J. (2009). Testing a cellular modelling approach to simulating late-Holocene sediment and water transfer from catchment to lake in the French Alps since 1826. The Holocene 19(5), 785-798.

Werner, B.T. (1999). Complexity in natural landform patterns. Science 284(5411), 102-104.

WEST (2002). Mount St Helens engineering reanalysis. Hydrologic, hydraulic and sedimentation analysis. Volume 1: Technical report. Bellvue, WA.

Wicks, J.M. and Bathurst, J.C. (1996). SHESED: a physically based, distributed erosion and sediment yield component for the SHE hydrological modelling system. Journal of Hydrology 175, 213-238.

Wilcock, P.R. (1998). Two-fraction model of initial sediment motion in gravel-bed rivers. Science 280(5362), 410-412.

Wilcock, P.R. (2001). Toward a practical method for estimating sediment-transport rates in gravel-bed rivers. Earth Surface Processes and Landforms 26(13), 1395-1408.

Wilcock, P.R. and Crowe, J.C. (2003). Surface-based transport model for mixed-size sediment. Journal of Hydraulic Engineering 129(2), 120-128.

Willgoose, G. (2005). Mathematical Modeling of Whole Landscape Evolution. Annual Review of Earth and Planetary Sciences 33, 443-459.

Willgoose, G., Bras, R.L. and Rodriguez-Iturbe, I. (1991). A coupled channel network growth and hillslope evolution model: 1. Theory. Water Resources Research 27(7), 1671-1684.

Williams, G.P. and Wolman, M.G. (1984). Downstream effects of dams on alluvial rivers: US Geological Survey Professional Paper 1286. Washington, DC: US Government Printing Office.

Willmott, C.J. (1982). Some comments on the evalutation of model performance. Bulletin of the American Meteorological Society 63(11), 1309-1313.

Willmott, C.J. (1984). On the evaluation of model performance in physical geography. In: Gaile, G.L. and Willmott, C.J. (Eds.) Spatial Statistics and Models. Dordrecht, NL: D. Reidel.

Willmott, C.J. and Matsuura, K. (2005). Advantages of the mean absolute error (MAE) over the root mean square error (RMSE) in assessing average model performance. Climate Research 30, 79-82.

Wilson, C. (2001). The 26.5 ka Oruanui eruption, New Zealand: an introduction and overview. Journal of Volcanology and Geothermal Research 112(1), 133-174.

Winner, W.E. and Casadevall, T.J. (1981). Fir leaves as thermometers during the May 18 eruption. In: Lipman, P.W. and Mullineaux, D.R. (Eds.) The 1980 eruptions of Mount St Helens, Washington: US Geological Survey Professional Paper 1250. Washington, DC: US Government Printing Office, pp. 315-320.

Wischmeier, W.H. and Smith, D.D. (1978). Predicting rainfall erosion losses. USDA Agricultural Research Service Handbook 537. Washingon, DC: US Department of Agriculture.

Wolfram, S. (1984). Universality and complexity in cellular automata. Physica D: Nonlinear Phenomena 10(1), 1-35.

Wood, A.W., Leung, L.R., Sridhar, V. and Lettenmaier, D. (2004). Hydrologic implications of dynamical and statistical approaches to downscaling climate model outputs. Climatic Change 62(1-3), 189-216.

Wu, B., Zheng, S. and Thorne, C.R. (2012). A general framework for using the rate law to simulate morphological response to disturbance in the fluvial system. Progress in Physical Geography 36(5), 575-597.

Zheng, S., Wu, B., Thorne, C.R. and Simon, A. (2014). Morphological evolution of the North Fork Toutle River following the eruption of Mount St Helens, Washington. Geomorphology 208, 102-116.

Ziliani, L., Surian, N., Coulthard, T.J. and Tarantola, S. (2013). Reduced-complexity modeling of braided rivers: assessing model performance by sensitivity analysis, calibration, and validation. Journal of Geophysical Research: Earth Surface 18, 1-20.